UNIVERSITÀ DI PISA
Scuola di Dottorato in Ingegneria "Leonardo da Vinci"

Corso di Dottorato di Ricerca in
SICUREZZA NUCLEARE ED INDUSTRIALE

Tesi di Dottorato di Ricerca

NUCLEAR SAFETY OF RBMK REACTORS

Carlo Parisi

Anno 2008

UNIVERSITÀ DI PISA

Scuola di Dottorato in Ingegneria "Leonardo da Vinci"

Corso di Dottorato di Ricerca in
SICUREZZA NUCLEARE ED INDUSTRIALE

Tesi di Dottorato di Ricerca

NUCLEAR SAFETY OF RBMK REACTORS

Autore:

CARLO PARISI *Firma*_____

Relatori:

Prof. Francesco D'Auria (UNIPI) *Firma*_____

Dr. Gianni Petrangeli *Firma*_____

Prof. Eugenius Uspuras (LEI) *Firma*_____

Dr. Sergei L. Soloviev (NIKIET) *Firma*_____

Anno 2008

ACKNOWLEDGMENTS

This PhD thesis was developed at the San Piero a Grado Nuclear Research Group of the University of Pisa. So, my first thank is due to the leader of this Group and thesis supervisor, prof. F. D'Auria. He gave me the opportunity to perform this job in a fruitful and stimulating environment, and he always supported and encouraged the research activities. I appreciated also his example in looking at the RBMK technology without any prejudice.

I would like to give also special thanks to the other PhD thesis supervisors, Dr. G. Petrangeli, prof. E. Uspuras and Dr. S. L. Soloviev, for their collaboration, suggestions and for the trust they showed in my activities.

Dr. V. Malofeev from Kurchatov Institute and Prof. K. N. Ivanov from the Pennsylvania State Univeristy helped me a lot with their advises on the neutron transport calculations. I am very grateful to them.

A special mention is due to the NIKIET staff, led by Dr. B. Gabaraev, for their kind hospitality and assistance provided during my stays in Russia.

I would like to thank also Dr. B. Ivanov, from Westinghouse Electric and Dr. E. Vanagas, from the Lithuanian Safety Authority for the useful conversations I had with them on the RBMK HELIOS models.

This work would not be possible if I did not have the opportunity to work in the serious and at the same time friendly environment of the San Piero a Grado Nuclear Research Group. For this reason I am grateful to all my present colleagues and to the whole original team of persons that from 2004 to 2006 contributed with dedicated work to the unquestionable success of the TACIS Project R2.03/97, from which this PhD work originated.

My final thanks and dedication of this work should go to my parents, and especially to my father. During all these years he staunchly supported and encouraged me to perform and finalize the PhD activities, reminding, when difficulties seemed discouraging, that "..non est ad astra mollis e terra via".

SOMMARIO

La presente Tesi di Dottorato esamina il livello di sicurezza dei reattori di potenza raffreddati ad acqua bollente e moderati a grafite (reattori RBMK), mediante l'uso di codici di calcolo best-estimate termoidraulici e neutronici accoppiati. La disponibilità di tali sofisticati strumenti ha reso possibili, infatti, analisi dettagliate e realistiche anche per questo tipo di impianti nucleari, notoriamente complessi e comunemente denominati "reattori di tipo Chernobyl" (in riferimento al gravissimo incidente occorso ad uno di questi impianti nel 1986). Parte delle attività della presente Tesi di Dottorato, si sono svolte nell'ambito del Progetto TACIS R2.03/97 "Software development for the RBMK and WWER reactors", coordinato dal Gruppo di Ricerca Nucleare San Piero a Grado dell'Università di Pisa in collaborazione con i progettisti e gli esercenti russi di tali impianti (NIKIET, Kurchatov Institute, RosEnergoAtom, oggi EnergoAtom Concern OJSC).

Le attività di ricerca hanno contemplato lo sviluppo di una complessa nodalizzazione termoidraulica dell'unità 3 dell'impianto nucleare di Smolensk, la sua validazione ed il suo successivo accoppiamento con un modello di cinetica neutronica tridimensionale. Il codice utilizzato è il RELAP5-3D. I calcoli di neutronica hanno richiesto, preliminarmente, lo sviluppo di librerie di sezioni d'urto macroscopiche. Tale attività, è stata svolta in collaborazione con la Pennsylvania State University, ed ha comportato l'utilizzo del codice di trasporto deterministico HELIOS.

Dopo la validazione dei modelli sviluppatii, si sono eseguite analisi di transitori a piena potenza, focalizzandosi su quelli particolarmente critici per la sicurezza (per esempio, la rottura di un collettore dei canali di potenza o del sistema di raffreddamento delle barre di controllo). Una speciale enfasi è stata data, anche mediante l'uso del codice Montecarlo MCNP5, allo studio del transitorio contemplante il bloccaggio di un canale di potenza.

L'ultima parte delle attività di dottorato si sono concentrate sull'analisi di un transitorio a bassa potenza, ricostruendo uno scenario incidentale estremo come quello occorso a Chernobyl. Le sezioni d'urto di cella per lo Xeno sono state calcolate con il codice al trasporto deterministico DRAGON.

In conclusione, le analisi avanzate effettuate nell'ambito di questa Tesi di Dottorato, hanno confermato il migliorato grado di sicurezza di tali impianti, ottenuto grazie alle importanti modifiche effettuate a seguito dell'incidente di Chernobyl.

ABSTRACT

This PhD thesis is evaluating the safety level of the graphite-moderated boiling water cooled nuclear power reactors (RBMK reactors) by the use of best estimate three dimensional neutron kinetics coupled thermal-hydraulics codes. The availability of such sophisticated tools has allowed detailed and realistic analyses of these kind of reactors, also known as "Chernobyl-type" reactors. Chernobyl is the name of a RBMK reactor where, in 1986, a severe accident occurred, leading to the destruction of the plant and to a major release of radioactivity into the environment. Parts of the activities of this PhD thesis were developed in the framework of the European Union funded TACIS Project R2.03/97 "Software development for the RBMK and WWER reactors". This project was awarded to the "Gruppo di Ricerca Nucleare San Piero a Grado" of the University of Pisa and managed by it in collaboration with the RBMK designers (NIKIET, Kurchatov Insititute) and the licensee (RosEnergoAtom, now EnergoAtom Concern OJSC).

The research activities dealt with the development and the validation of a sophisticated thermal-hydraulic nodalization of the Smolensk-3 Nuclear Power Plant. This thermal-hydraulic model was then coupled with a three dimensional neutron kinetics model of the core. The code used was RELAP5-3D system code. Suitable RBMK cross sections libraries were developed in collaboration with the Pennsylvania State University, using the deterministic lattice physics code HELIOS.

After the validation of the developed models, the most relevant transients for the plant safety at full power were calculated, e.g. the group distribution header rupture, the break of the control and protection system cooling circuit. A special emphasis was put in the simulation of the single fuel channel transient, using also the Monte Carlo code MCNP5.

The last part of the PhD activities concerned the analysis of a low power transient. In particular, the Chernobyl extreme scenario was reconstructed. Xenon fuel cell cross sections were calculated using the deterministic transport code DRAGON.

Finally, all the analyses performed in the framework of this PhD confirmed the upgraded level of nuclear safety of the RBMK reactors, obtained also as a consequence of the relevant hardware modifications implemented in the aftermath of the Chernobyl accident.

CONTENTS

NOMENCLATURE

0D	Zero-dimensional
1D	One-dimensional
2D	Two-dimensional
3D	Three-dimensional
AA	Additional Absorber
ACC	Accumulator (part of the ECCS, also identified as hydro-accumulator)
ACRR	Annular Core Research Reactor (Sandia National Lab)
ADF	Assembly Discontinuity Factor
AECL	Atomic Energy of Canada Limited
AHTLM	Adaptive High-order Table Look-up Method
ALS	Accident Localization System
ALT	Accident Localization Tower
ANM	Analytical Nodal Method
ANS	American Nuclear Society
ANS	Advanced Neutron Source (Oak Ridge National Lab)
AOO	Anticipated Operational Occurrences
ATR	Advanced Test Reactor
ATWS	Anticipated transient without scram
AZ-1, AZ-3 to AZ-6	RBMK Emergency Protection Signals (Scram or Power reduction)
AZM	(Signal of) Emergency Protection by Power
BAZ	RBMK scram key (Fast functioned emergency protection)
BDBA	Beyond Design Basis Accident
BE	Best Estimate
BIC	Boundary and Initial Conditions
BPLU	Border Profile Lower Upper (Matrix Solver)
BRU-K, -D, -TK	Safety Valves on Steam Lines
BWR	Boiling Water Reactor
CHF	Critical Heat Flux
ChNPP	Chernobyl Nuclear Power Plant
CMFD	Coarse Mesh Finite Difference
CAMP	Code Assessment and Maintenance Program
CANDU	Canadian deuterium uranium (reactor)
CCPM;	Current-Coupling Collision Probability Method
CPM	Collision Probability Method
CPS	Control and Protection System
CPU	Central Processing Unit
CR	Control Rod
CRCC	Control Rod Cooling Circuit
CTV	Control Throttling Valve
DBA	Design basis accident
DC	Down-Comer
DF	Discontinuity Factor
DOE	Department of Energy (U.S.A.)

DREG	Diagnostic Parameter Recording Program
DS	Drum Separator, see also SD or Steam Drum
EC	The European Commission
ECCS	Emergency Core Cooling System
ENDL	Evaluated Nuclear Data Library
ENDF	Evaluated Nuclear Data File -
ESF	Engineered Safety Features
FASS	Fast Acting Scram System
FDM	Finite Difference Method
FLOP	Floating Operation
GDH	Group Distribution Header
GRNSPG	The San Piero a Grado Nuclear Research Group of the University of Pisa, Italy
DBA	Design Basis Accident
DIMNP	Department of Mechanical, Nuclear and Production Engineering of the University of Pisa, Italy
DS	Drum separator
ECCS	Emergency Core Cooling System
EPS	Emergency Protection Signal
EREC	Electrogorsk Research and Engineering Center
ET	Equivalent Channel
FASS	Fast Acting Scram System
FC	Fuel Channel
FDM	Finite Difference Method
FLOP	Floating Point Operation
FP	Fission Product
FSP	Fixed Source Problem
GAN	Gosatomnadzor, the former Russian Nuclear Safety Authority, now Rostechnadzor
KI	The Russian Research Center “Kurchatov Institute” or see RRC KI
HFBR	High Flux Beam Reactor
HFIR	High Flux Isotope Reactor
IAEA	International Atomic Energy Agency
ICAP	International Code Assessment and Applications Programme
ICV	Isolated control valve
IGR	Impulse Graphite Reactor
INL	Idaho National Laboratory
LAC	Local Automatic Control
LANL	Los Alamos National Laboratory
LAP	Local Automatic Protection
LAR	Local Power Control
LEI	Lithuanian Energy Institute
LOCA	Loss of coolant accident
LOFT	Loss of Fluid Test Reactor
LNPP	Leningrad Nuclear Power Plant
LTC	Leak-Tight Compartment
LWL	Lower Water Line
LWR	Light Water Reactor

MCC	Main circulation circuit
MCP	Main circulation pump
MCR	Manual Control Rod
MFCC	Multipass Forced Circulation Circuit
MPTR	Multiple Pressure Tube Rupture
MSV	Main Safety Valve
NEM	Nodal Expansion Method
NIKIET	“N. A. Dollenzhal” Institute for Power Engineering (RBMK designer)
NK	Neutron Kinetics
NPR	New Production Reactor
NRC	Nuclear Regulatory Commission (U.S.A.)
NRU	National Research Universal Reactor (Chalk River Lab)
NPP	Nuclear Power Plant
ORM	Operating Reactivity Margin
ORNL	Oak Ridge National Laboratory
PDDMS	Power Density Distribution Monitoring System
PDMS-A	Power Density Sensors of the Axial Monitoring
PH	Pressure Header
PHWR	Pressurized heavy water reactor
PSA	Probabilistic Safety Analysis
PSP	Pressure Suppression Pool
PSU	The Pennsylvania State University
PT	Pressure Tube
PWR	Pressurized Water Reactor
RBMK	Reactor Bolsoi Mochnosti Kipyashiy (Large Power Boiling Reactor)
RC	Reactor Cavity
RCPS	see MCR
RCSRV	Reactor Cavity Steam Relief Valve
RCVS	Reactor Cavity Venting System
RDFMG	The Reactor Dynamics and Fuel Management Group
RIA	Reactivity Initiated Accident
RRCC	Radial Reflector Cooling Channels
RRC KI	The Russian Research Center “Kurchatov Institute”
SA	Severe Accident
SCS	Sprinkler Cooling System
SCV	Stop-control valve
SD	Steam Drum
SDC	Steam Corridor Distribution
SHR	Shortened Control Rod
SL	Steam Line
SOR	Successive Over Relaxation
SPTR	Single Pressure Tube Rupture
SR	Safety Control Rod (components of FASS)
SRV	Steam Relief Valve
SS	Steady State
SV	Stop Valve
SWL	Steam Water Line

TACIS	Technical Aid to the Commonwealth of the Independent States
TH	Thermal-Hydraulic
TPEN	Triangle-based Polynomial Expansion Nodal Method
URC	Under Reactor Compartments
UNIPI	The University of Pisa
VATESI	Lithuanian Nuclear Power Safety Inspectorate
VVER	see WWER
XSEC	Cross-section (for 3D Neutron Kinetics calculations)
WWER	Water Cooled Water Moderated Energy Reactor

LIST OF SYMBOLS

Greek Symbols

α_{φ}	Void Reactivity Coefficient (pcm/% void)
α_{w}	Power Reactivity Coefficient (pcm/MW_{th})
α_{t}	Doppler Reactivity Coefficient (pcm/°C)
α_{c}	Graphite Temperature Reactivity Coefficient (pcm/°C)
α_{cool}	Coolant Temperature Reactivity Coefficient (pcm/°C)
β	Delayed Neutron Fraction
ϕ	Neutron flux (n/cm^2*s)
ε	Fast Fission Factor
ε_R	Error in the neutron flux calculation
γ	Gamma Particle
η	Fission Neutron per Neutron Absorption into the Fuel
ν	Number of Fission Neutrons
μ	Cosine of the direction angle for neutrons
ρ	Reactivity
ρ_w	Material Density (Kg/m^3)
ξ	Average Logarithmic Energy Loss
σ_i	Stress Intensity (MPa)
σ_{Xe}	Microscopic Xenon Absorption Cross Section (*10^6 barn)
Σ_a	Macroscopic Absorption Cross Section (cm^{-1})
Σ_f	Macroscopic Fission Cross Section (cm^{-1})
$\Sigma s_{g'g}$	Macroscopic Group-to-Group Scattering Cross Section (cm^{-1})
$\nu \Sigma_f$	Macroscopic Neutron Generation Cross Section (neutron* cm^{-1})
τ_{th}	Fermi age (cm^2)
ζ_i	Strain Rate Intensity

Roman Symbols

$	Reactivity (1$ = 1 β)
B	Neutron Flux Distribution Buckling (cm^{-1})
$^{(12)}C_{(6)}$	Graphite (Nuclear Grade)
D	Diffusion Coefficient (cm)
f	Thermal Utilization Factor
eV	Electron Volt
k	Multiplication factor (eigenvalue)
j	Neutron current
j_i	Rupture Strain Power (W/Kg)
L	Diffusion Length (cm)
L_{gi}^{l}	Average i-directed leakage for group *g* in node l
M	Migration Length (cm)
n	Neutron Particle

p	Resonance Escape Probability Factor
T_w	Pressure Tube Temperature (K)
u	Neutron Lethargy

LIST OF FIGURES

LIST OF TABLES

1. INTRODUCTION

1.1. State of the Art on the RBMK Safety Analyses

The Russian designed Water-Cooled Graphite-Moderated reactors RBMK were the subjected to an extensive campaign of studies, researches and upgrades in the aftermath of the Chernobyl disaster (26 April 1986).

In particular, immediate actions focused on plant modifications, and concerned about a complete review of the neutronic design (e.g., increase of Uranium enrichment, insertion of Additional Absorber (AA)), hardware modification (e.g., modification of Control Rods (CR) design, improvement of the core electronic calculator) and plant operating procedures [1], [2].

After the Soviet Union collapse (26 December 1991) and during the whole '90s, the European Commission (EC) and the United States Department of Energy (US-DOE) financed a series of international projects (e.g., the TACIS Projects from the European side), in collaboration with Russian Institutions, for a further improvement of the safety of RBMK Nuclear Power Plant (NPP) and for the uniformities of safety technology methods and understanding [3], [4], [5].

Objectives of these Projects were NPP hardware upgrading, personnel training, nuclear safety codes improvements, accident analyses and accident management procedures development.

The TACIS project R2.03/97 "Software Development for the WWER and RBMK reactors", managed by the Gruppo di Ricerca Nucleare San Piero a Grado (GRNSPG) of the University of Pisa (UNIPI) during 2005 and 2006, concerned the nuclear safety codes improvements and the accident management procedures developement. An important part of the work for this PhD thesis was developed in the framework of this Project, in collaboration with Russian RBMK designers (NIKIET), researchers (Russian Research Center "Kurchatov Institute") and licensee (RosEnergoAtom, Russian nuclear electric utility, now Energoatom Concern OJSC).

At the beginning of the present PhD thesis (January 2005), RBMK systems were thoroughly analyzed by a series of mainly thermal-hydraulic or stand-alone neutronic codes, e.g. [87], [88], [89]. Coupled codes analyses were also executed by few leading Western Institutions (e.g., Idaho National Laboratory, USA, or GRS, Germany, see [98], [99], [100]) and by Lithuanian Institutions (e.g., Lithuanian Energy Institute (LEI), see [26], [77], [78]).

Chernobyl-type events were anymore simulated and most of the analyses found in the literature, were executed in the aftermath of the Chernobyl disaster, with simplified (for the today's standards) numerical tools (see section 6.3).

1.2. Scope

The safety of nuclear power plants, understood as its capability to keep the radiation exposure of personal and population within specified limits, is ensured by maintaining the integrity of safety barriers, which are part of the plant defence in depth concept. A series of barriers prevents the release of radioactive fission products from their source beyond the reactor containment and into the environment. In analyzing the NPP safety, it is essential to assess the integrity of these barriers and to decide to what degree the response of the whole NPP and its systems to a certain initiating event is acceptable from the viewpoint of the plant safety. For the sake of simplicity and clarity, the integrity of the safety barriers is related to certain threshold values, which are referred to as acceptance criteria. Essentially these are the design limits for design basis accidents (DBA), adopted with a conservative margin so that the safety barrier integrity is guaranteed as long as the parameters do not exceed the relevant criteria.

Safety analysis for an RBMK NPP should assess the integrity of the following barriers in the path of radioactivity transport and release:

- Fuel matrix.
- Fuel cladding.
- Circulation circuit pressure boundary and, in particular, the components most susceptible to damage, namely fuel channel (pressure) tubes.
- Metal structures forming the reactor cavity.
- Structural components of the leak-tight Accident Localization System (ALS) compartments and other buildings of the NPP housing circulation circuit pipelines.

Should any safety barrier fail, thus opening the pathway for the release of radioactivity beyond the plant boundaries, the amount of radioactivity and the population exposure should be assessed. Beyond design basis accidents (BDBA) are analyzed for the following purposes:

a) To assess the degree of reactor protection and the time available for taking countermeasures.
b) To determine the emergency and other signals available to the operator for identifying the plant status and to devise appropriate accident management steps.
c) To develop a package of organizational and technical measures (management strategy) for prevention and mitigation of the accident consequences.
d) To assess the possible consequences of the BDBA as input information for planning protection of the population and personnel.

According to the requirements of the Russian nuclear regulatory authority RosTechnadzor (Russian Federal Ecological, Technological and Nuclear Inspectorate, the former Gosatomnadzor (GAN)), both deterministic and

probabilistic approaches for BDBA analysis should be used. According to requirements OPB-88/97:

- The estimated probability of an event with large release should be less than 10^{-7} within one reactor year.
- The estimated probability of severe reactor core degradation or melting should be less than 10^{-5} within one reactor year.

However, if some initiating events can lead to severe consequences and the inside features of reactor are not able to prevent this, accident mitigation means should be foreseen without drawing the attention to the probability of these events.

The deterministic approach for analysis BDBA is therefore also very important. According to the Russian nuclear regulatory authority RosTechnadzor the deterministic approach should be based on the method of postulating accidental conditions. This method is based on determination of connections between the plant conditions, level of severity of accident consequences (how many physical barriers are violated: fuel assembly including fuel pellet and fuel cladding, pressure tube, reactor cavity, main circulation circuit, accident localization system) and availability of critical safety functions.

Thus, according to requirements OPB-88/97 of the Russian nuclear regulatory authority RosTechnadzor, a list of BDBA scenarios for further detailed investigations should be developed. The analysis results will be the basis for the development of the accident management program for RBMK reactors.

1.3. Objectives

The key objective and the key products of the present PhD Thesis are:

1) the development of a set of advanced Best-Estimate (BE) computational models (i.e, codes input-decks) for the safety analyses of the RBMK, focusing on the core behavior;
2) the execution of safety analyses, investigating a broad spectrum of accidents, comprehensive of both DBA and BDBA

1.4. Structure

The road-map of the PhD activities is outlined in the Chapter 4 and hereafter the structure of this document is presented. Eight main chapters (including this one) constitute the PhD thesis report. The contents and the reasons for each main chapter are outlined in the following.

1) Chapter 2. This chapter deals with the description of the RBMK system focusing on the safety features. The description essentially duplicates information available in the literature. However, the self-standing nature of the PhD thesis report and the need to avoid repeating NPP data in the other chapters suggested the consideration of this chapter. Some basic

considerations about the neutronics characteristics were derived during the PhD activities and are reported here.

2) Chapter 3. The status of RBMK safety technology and the related needs are discussed in this chapter. The outcomes contributed to finalizing the research and development activities. Namely, accident scenarios were selected whose expected phenomena are envisaged to encompass the relevant RBMK safety technology areas for the core. The list of transients by itself constitutes a result from the PhD Thesis.
3) Chapter 4. This Chapter deals with the presentation of the chain of codes used and the methodologies for codes application. A short description of codes used is also given. Then, the description of the developed codes input decks and their qualification according to GRNSPG/UNIPI criteria are reported.
4) Chapter 5. This Chapter reports the results for some Hot Full Power (HFP) realistic transient analyses. Calculations results for CR and CR group withdrawal, Group Distribution Header (GDH) Loss of Coolant Accident (LOCA) and GDH Blockage, Control and Protection System (CPS) LOCA and Fuel Channel (FC) blockage accident are given. Results were obtained mainly by the use of 3D Neutron Kinetics (NK) coupled thermal-hydraulics (TH) system code RELAP5-3D©. In the case of the FC Blockage scenario, calculations were supported by the use of Monte Carlo MCNP5 code.
5) Chapter 6. The Chapter deals with the results of the accident analyses performed at low power conditions, in order to simulate a “Chernobyl-type” event (Loss of Main Circulation Pumps (MCP) at low power with Xenon poisoned reactor). Calculations were performed using RELAP5-3D 3D NK TH code. DRAGON lattice physics code was used in order to derive Xenon cell nuclear Cross Sections (XSecs).
6) Chapter 7. The Chapter reports the list of the main results achieved during the execution of the PhD activities.
7) References. The list of documents mentioned in the main body of this report is given.

2. THE DESCRIPTION OF THE RBMK

Twelve RBMK units are installed in Russia and Lithuania, [6]. In the case of Russia the RBMK contribute for about 50% of the electricity generated by the nuclear source. Information of general validity for the RBMK systems is provided below. However, specific information is related to the reference reactor for the PhD activities, i.e. Smolensk 3 NPP. This is a "3rd generation RBMK reactor" constructed in the Russian Federation about 400 Km Southwest of Moscow. The unit 3 was put into operation on January 17, 1990. Relevant information for the chapter is derived from refs. [7] and [9], the last one dealing with the Ignalina NPP. Additional details about RBMK generations can be found in section 3.2.1.5.

An overall sketch of the RBMK NPP can be seen in Fig. 1 and Fig. 2 and key system data are given in Tab. 1. Information is provided hereafter about system hardware relevant for safety technology.

1) Core
2) Water pipe
3) Reactor bottom plate
4) Group Distribution Header
5) Shield
6) Steam Drum
7) Steam Water Pipe
8) Reactor top plate
9) Refuelling machine
10) Reactor lid structure
11) Top reactor channel
12) Downcomers
13) Pressure Header
14) Suction header
15) Main Coolant Pump

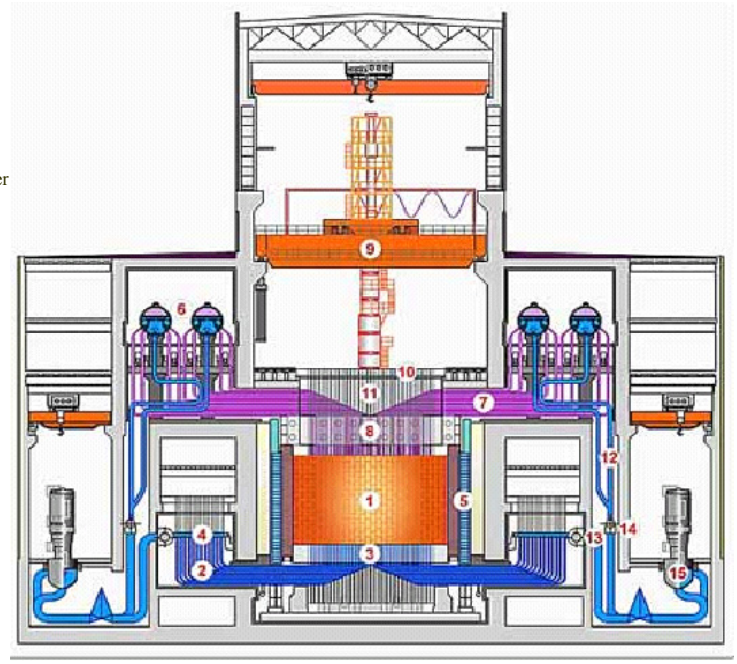

Fig. 1 – Overall view of the RBMK NPP system

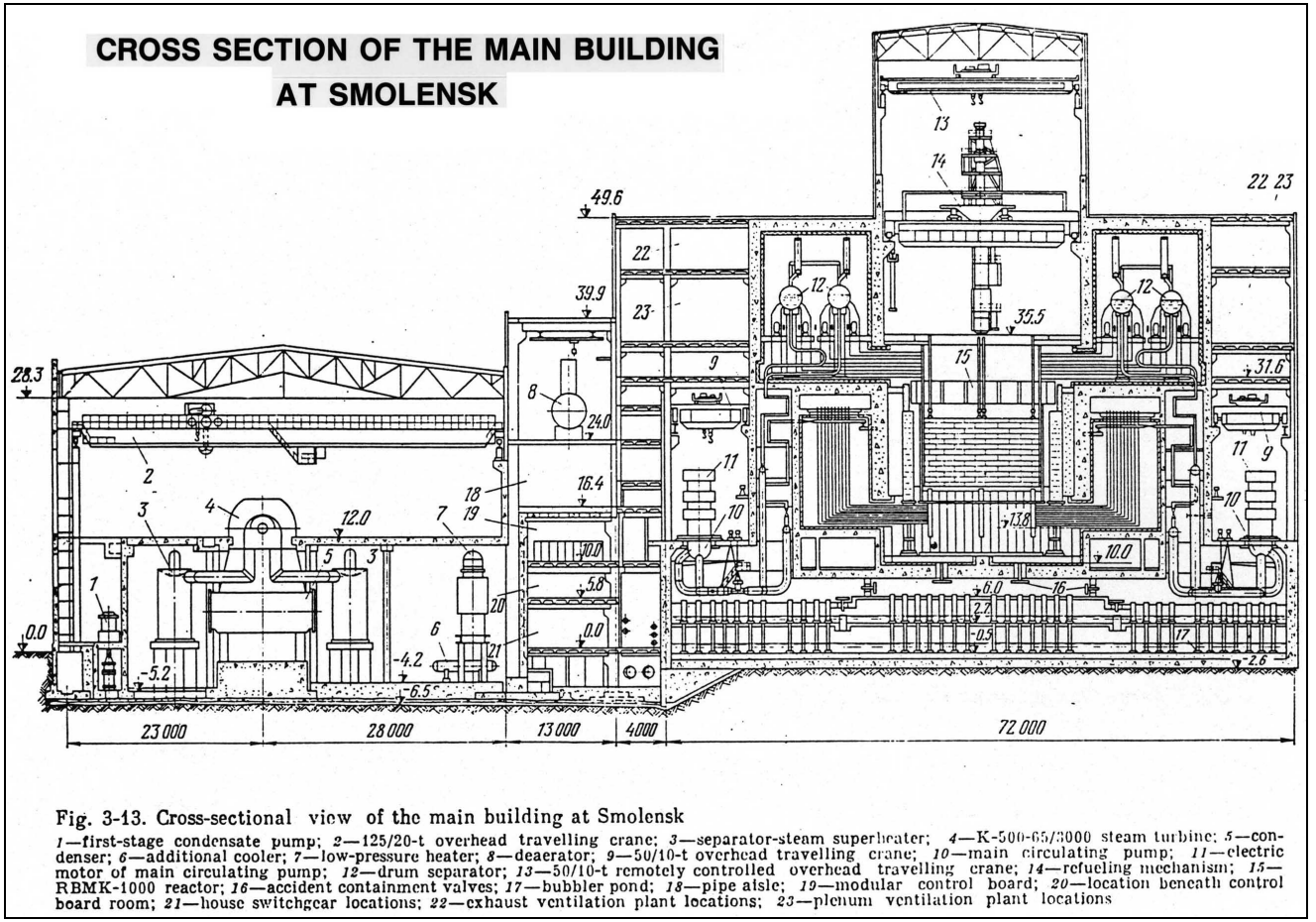

Fig. 3-13. Cross-sectional view of the main building at Smolensk

1—first-stage condensate pump; *2*—125/20-t overhead travelling crane; *3*—separator-steam superheater; *4*—K-500-65/3000 steam turbine; *5*—condenser; *6*—additional cooler; *7*—low-pressure heater; *8*—deaerator; *9*—50/10-t overhead travelling crane; *10*—main circulating pump; *11*—electric motor of main circulating pump; *12*—drum separator; *13*—50/10-t remotely controlled overhead travelling crane; *14*—refueling mechanism; *15*—RBMK-1000 reactor; *16*—accident containment valves; *17*—bubbler pond; *18*—pipe aisle; *19*—modular control board; *20*—location beneath control board room; *21*—house switchgear locations; *22*—exhaust ventilation plant locations; *23*—plenum ventilation plant locations

Fig. 2 – Smolensk-3 NPP view

Tab. 1 – Key parameters of the Smolensk-3 RBMK-1000

Key-parameters of core			
Power, MW_{th}	**Total**	**Left Part**	**Right Part**
	3213	1629	1583
Flow rate Kg/s	10118	5158	5104
Number of FC	1568	794	774
Number FC with AA	90	45	45
Fuel Channel parameters			
Full length, mm		18325	
Number of channels		1660	
Upper part diameter, mm and thickness, mm		95x5	
Middle part diameter, mm and thickness, mm		88x4	
Lower part diameter, mm and thickness, mm		60x5.5	
Fuel rod overall length, m		3.46	
Active core length, m		6.92	
Spacer/support grids		20 per FC	
Key dimensions of the down-comers			
Diameter, mm and thickness, mm		325 x 15	
Average length, m		29.15	
Total volume, m^3		47.7	
Key dimensions of the Steam Header			
Diameter, mm and thickness, mm		1020x60	
Length, mm		21 080	
Volume m^3		17.3	
Volume cylindrical part, m^3		13.4	
Key MCP thermal-hydraulic parameters (at 265 ^oC)			
Q, m^3/h (Kg/s)		8000±200 (2.22)	
Head, m		200±20	
P inlet, bars		70.5	
Power, MW		4.3±0.3	
Speed, rpm		1000	
Torque, N-m		39400	
Key-parameters of Group Distribution Header			
Diameter, mm and thickness, mm		325x15	
Length, mm		5400	
Design pressure, bar		100	
Design flow, t/h		1700	
Total volume of GDH, m^3		16.5	
Key-parameters of steam lines			
Diameter, mm and thickness, mm		76x4	
Average length, m		32	
Design flow, t/h		40	
Design pressure, bar		75	
Key-parameters of Drum Separators			
Number per reactor		4	
DS length, m		30.98	
DS internal diameter, m		2.6	
DS volume, m^3		150.2	
Operation pressure, bar		68.9	
Design pressure, bar		73.5	
Nominal water level (above the central axis) mm		380±50	

2.1. The Primary System

2.1.1. The pressure boundary

The MCC consists of two loops, whose components are arranged symmetrically with respect to the vertical axis of the reactor. Each loop has two separator drums (1) (number in parenthesis refers to legend of Fig. 3, which separate the steam from the steam-water mixture exiting from the core block. The separator drums are horizontal cylindrical vessels interconnected both at the lower liquid level and at the upper steam level.

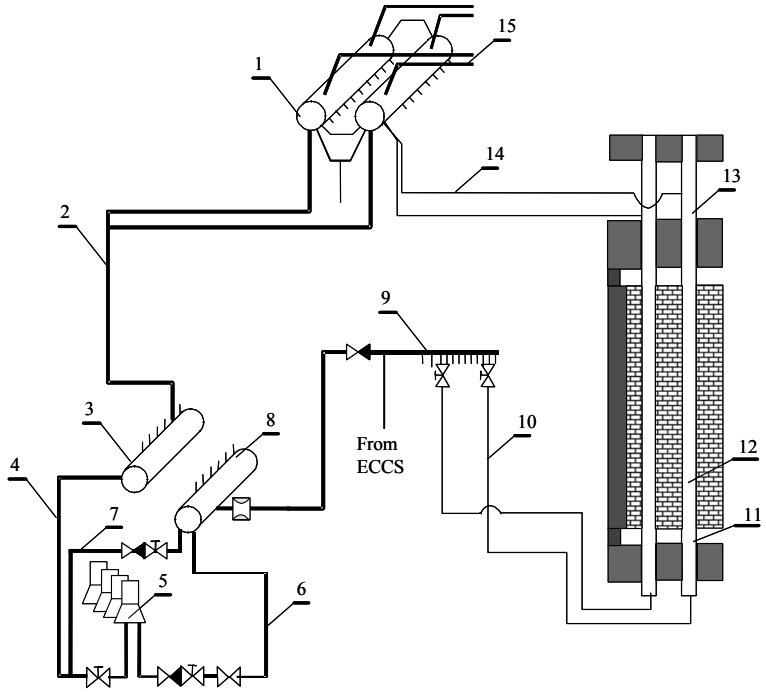

1-separator drum, 2-downcomers, 3-suction header, 4-suction piping of the MCP, 5-MCP, 6-pressure piping of the MCP, 7-bypass between headers, 8-pressure header, 9-group distribution header with flow limiter, check valve and mixer, 10-water bottom piping, 11-fuel channel before the core, 12-fuel channel within the core, 13-fuel channel above the core, 14-steam water pipes, 15-steam pipelines.

Fig. 3 – RBMK Main Circulation Circuit (MCC) flow diagram

In the bottom section of each separator drum (SD) a feed-water header is installed which provides through special mixers feed-water to the down-comer pipes. The separated water mixed with the feed-water reaches the suction header (3) through 24 down-comer pipes per each loop (2). The flow path continues through four suction pipes (4) connected to the four Main Circulation pumps (MCP). During normal reactor operation, only three pumps are operating in each loop, the fourth is a reserve. They are single stage vertical and centrifugal type.

From the MCP, water flows through pressure header pipes (6) to the pressure header, PH, (8). The suction and pressure headers are connected by bypass lines (7), provided with a gate and a check valve. The bypass ensures that natural circulation of the coolant takes place in case of main circulation pumps shut-off. From the pressure header (8) water continues through twenty two pipes to twenty two group distribution headers (GDH) (9). Mechanical filters are provided inside the pressure header while at GDH exit there are a flow limiter, a check valve and a mixer to which ECCS are connected.

Each GDH is connected to liquid pipes (10) leading to an average of forty-five fuel channels (12). The flow in each pipe, and therefore in each fuel channel (12), is set by isolation and control valves and is measured by a ball flow-meter. The steam-water mixture generated in the fuel channel flows through the steam-water pipes (14) to the separator drums (1).

The elevations for the most important components of the MCC are presented schematically in Fig. 4. The total, top-to-bottom elevation of the primary system is over 30 m. The elevation driving the natural circulation loop, measured from the bottom of the core to the bottom of the separator drums, is ~ 21m. These large elevation heads determine the flow parameters of the system under natural circulation conditions.

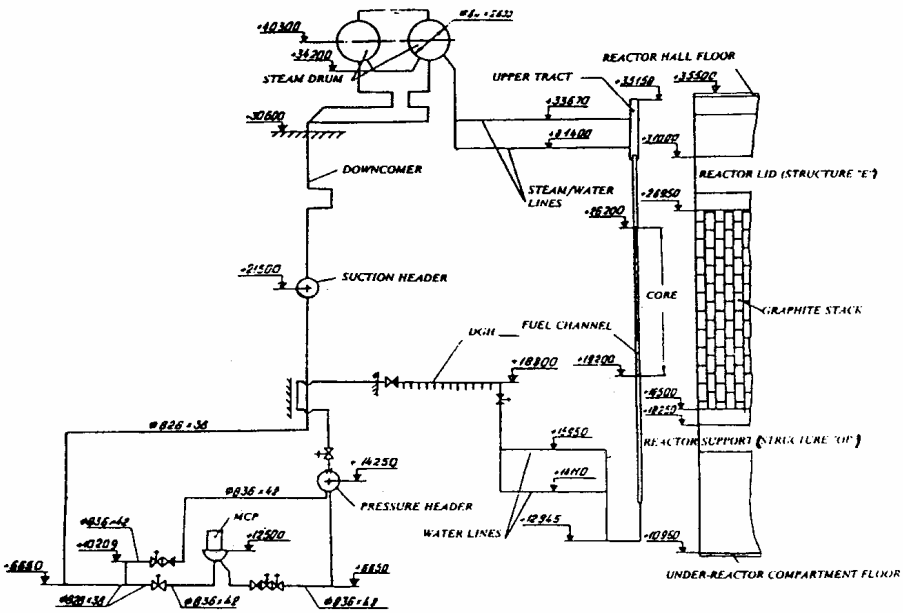

Fig. 4 – Key elevations in the MCC of the RBMK system (Smolensk 3)

From the separator drums the generated steam is directed to the turbines. Discharge steam from the turbines is accumulated in condensers, from there the condensate flows down through filters, heaters and deaerators to the main feed water pump and is finally returned to the separator drums.

The purification and the cooling of the primary cooling circuit water is performed by the Purification and Cooling System (PCS) which is an equivalent of the Chemical and Volume Control System (CVCS) in Western LWR. Part of the water is taken from the MCC, cooled down and filtered by a mechanical filter and by an ion-exchanger in the purification bypass. The treated water then joins the feed-water flow. The reactor also contains a number of channels for control rods and metering devices. These are cooled by a separate circulation system, which is called the Control Rod Cooling Circuit (CRCC).

The twelve down-comer pipes direct the water from the separator drums to the suction header, thus each of the two circulation loops contains twenty-four down-comers. The geometrical dimensions of each down-comer are given in Tab. 1. The suction headers collect water from the down-comers and supply coolant to four suction pipes in such a way a mixing of the water from the drum separator occurs. The geometrical dimensions of the suction headers are also given in Tab. 1.

For the forced circulation of cooling water through the RBMK reactor type CVN-8 ('wet stator' type) MCP are employed, Fig. 5. The CVN-8 type is centrifugal, vertical, single-stage pump with a sealed shaft. Four pumps are installed per each loop, three of them are normally in operation, and the fourth is kept as a reserve. The basic parameter of the pump at nominal conditions are reported in Tab. 1 and the pump curves for hot and cold water are given in Fig. 6, left and right sides, respectively.

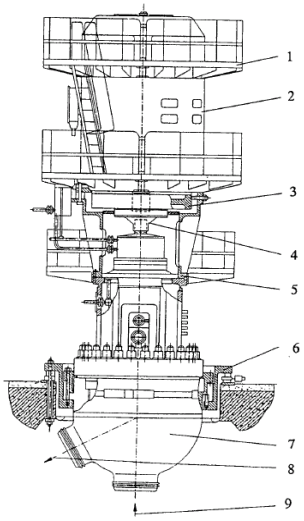

1-service platform, 2-flywheel, 3- electric motor, 4- junction coupling, 5-support of electric motor, 6- foundation frame, 7-tank of the pump, 8- water outlet, 9- water inlet

Fig. 5 – The MCP for RBMK NPP.

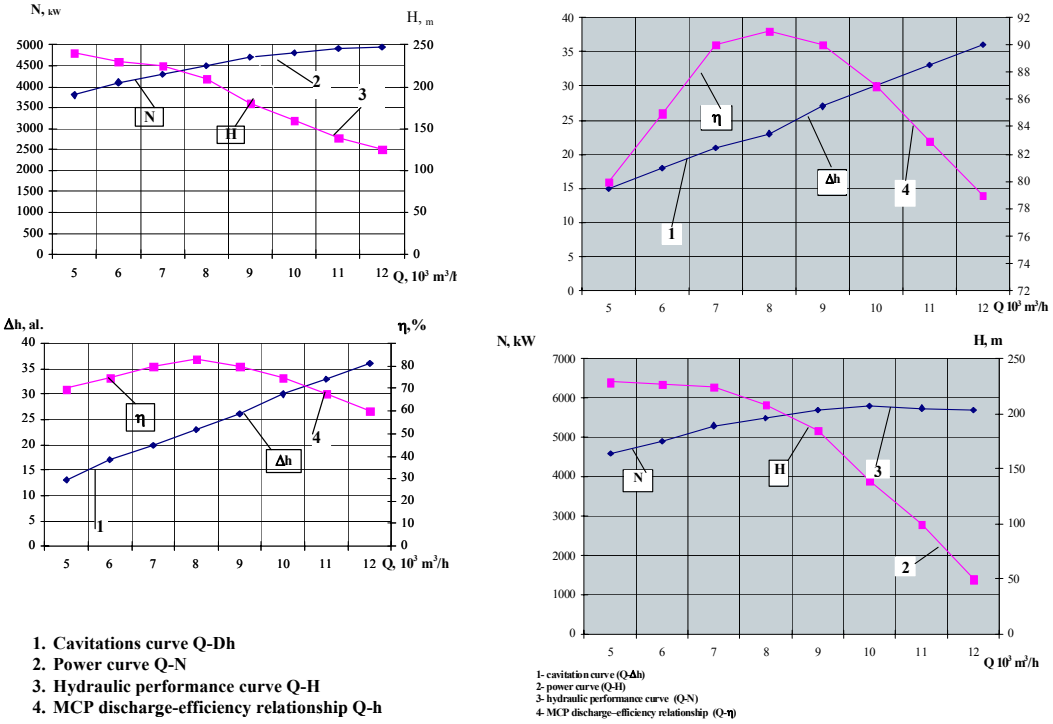

Fig. 6 – RBMK MCP (CVN-8) performance data (left: high temperature conditions, 265 ºC; right: low temperature conditions, 90 °C)

The main function of each PH is to collect the water that comes from the pressure pipes connected to all main pumps exit and supply the coolant to the twenty-two GDH through twenty-two pipes. The pressure header has 1040 mm outside diameter and 70 mm thick walls.

The coolant is distributed to individual GDH by means of twenty-two pipes 325x15 mm. Each pipe has a manual control gate valve, a check valve and a mixer to mix (in case of accident) the cold water from the Emergency Core Cooling System (ECCS) and the hot water from the MCC. The check valve prevents back-flow from the fuel channels in case of failure of the pressure header. Mixers protect the MCC from thermal or hydraulic shocks. Flanges designed to prevent pipe whip in the event of a pressure surge are fixed to the structural beams of the plant and to a special framework

The coolant is supplied to the individual fuel channels via group distribution header, Fig. 2.6 which are horizontal cylinders, Tab. 3.1 The GDH are securely fastened to support structures to prevent any sliding in case of failure. Each header distributes coolant to 40-43 bottom water pipes. These pipes are provided with isolation and

control valves between the GDH outlet and the fuel channel inlet. Isolation and control valves are used to adjust channel flow on the basis of channel power. Flow rates can be controlled by varying the flow-area of the valves. This is achieved by manual operation from a separate room in the vicinity of the reactor block. The bottom water pipes leading into the reactor block drive the water into the fuel channels that remove the heat generated in the fuel assemblies. The liquid water starts to boil and the steam-water mixture flows from the top of the fuel channels by way of individual steam - water pipe to the separator drums. The exiting steam-water pipes include several bends. This aids in reducing gamma streaming.

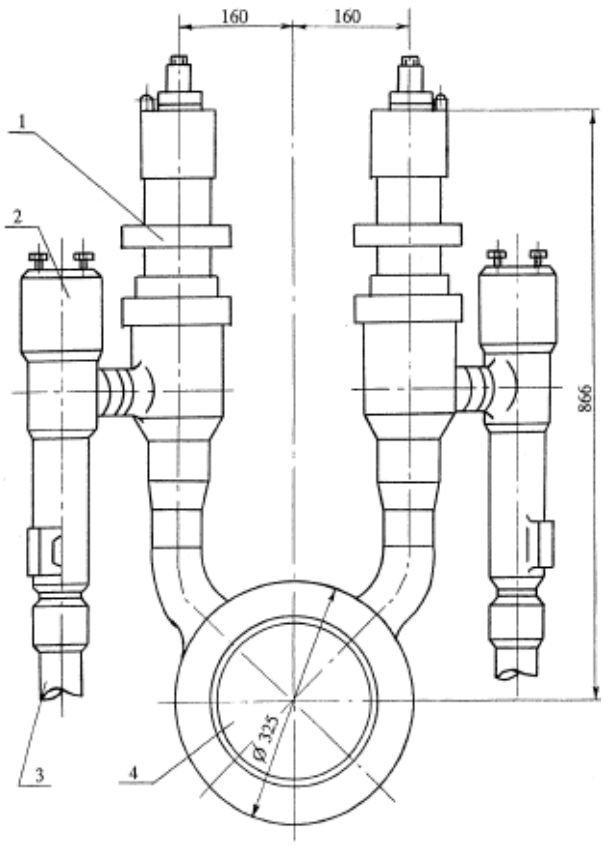

1 – isolation and control valve, 2 – ball type flow-rate meter, 3 – coolant water pipe leading to the fuel channel, 4 – group distribution header

Fig. 7 – Geometrical configuration of RBMK GDH

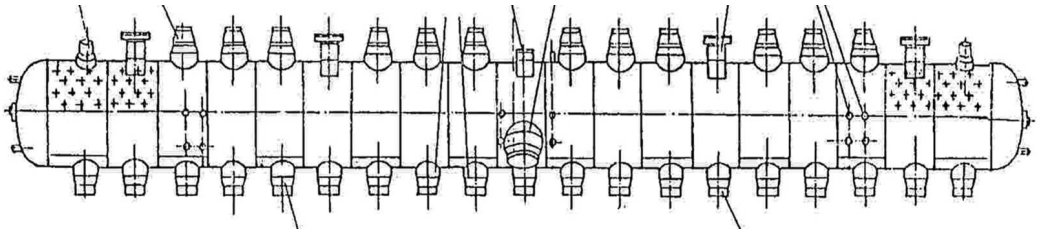

a)

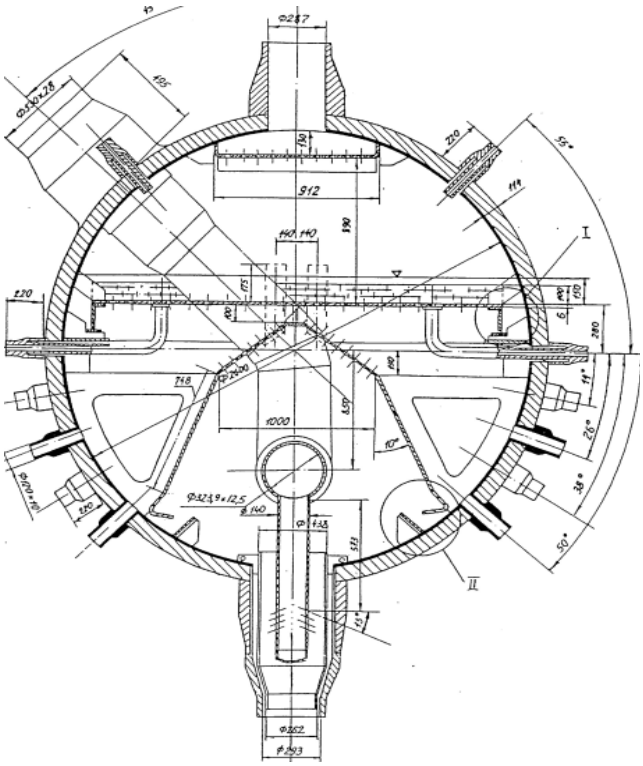

b)

Fig. 8 – Geometrical configuration of RBMK SD: a) overall view; b) cross section

The separator drum has the following functions:

- separation of steam from the steam-water mixture flowing from the fuel channels,
- mixing of the separated water with feed-water,
- storing of coolant for the MCC.

The steam water mixture arrives at the separator drum, through inlet pipes (9), (see Fig. 9 for numbering). A part of the steam is separated in the distribution compartments because the flow looses its kinetic energy in impact to the special plates (3).

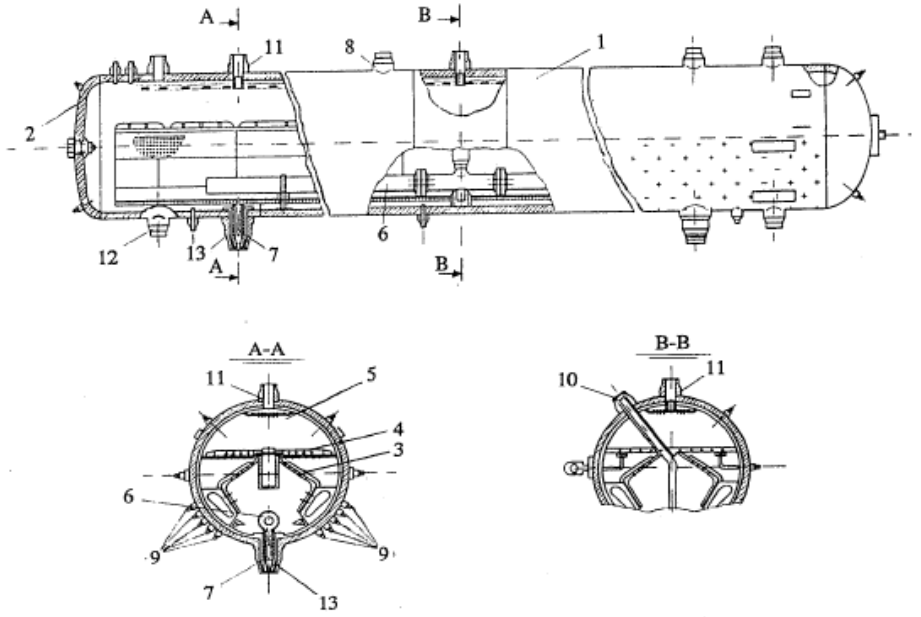

Fig. 9 – Steam Drum – Component Specifications

This steam then penetrates the submerged perforated sheet (4) and the "barbotage" layer above it. Final separation occurs because of gravity force.
The separated steam goes through the perforations of the upper shields (5) into the steam-flow piping, the separated liquid flows downward from pipes at the bottom (13). The feed-water line has a nominal diameter of 500 mm (10). It enters into the separator drum at a 45 degree angle, and extends to a distribution header in the lower part of the drum. The feed-water is injected from the header (6) (7) to the down-comer (13) via jet spray nozzle in order to cool the water to be supplied to the MCP. Both the steam and liquid containing regions of the two separator drums are connected by number of pipes. The non uniform generation of power in fuel channels can lead to a non homogeneous steam-water distribution in the steam drum. This requires design features which serve to reduce both transverse and longitudinal variations of the steam content. This is accomplished by a submerged perforated sheet (4) with a 150 mm thick downward frame. A down-flow passages is provided between the frame and the drum wall for the part of the water, which penetrates the perforations together with steam. The down flow passages functions as a hydraulic lock against any penetrations of steam at the side of the perforated sheet. The sink is covered by safety plates spaced at 75 mm from the frame. Traverse and circumferential variations of pressure at the entrance of the steam pipes are reduced by a similar perforated shield in the upper part of the drum (5) and by inside diameter bushing installed in the steam outlet pipes.

The two separator drums within each loop are interconnected both in the liquid and steam region, Fig. 10. There are five connecting (300x15) mm pipes in the steam

zone and four pipes (300x15) mm in the water zone. The total length of the pipes is 19.8m in the water zone and 16.2m in the steam zone. These connections ensure that equal water levels and steam pressures are maintained in both drums.

1 – separator drums, 2 – connecting pipes at the water level, 3 – connecting pipes at the steam level, 4 – submerged perforated sheet

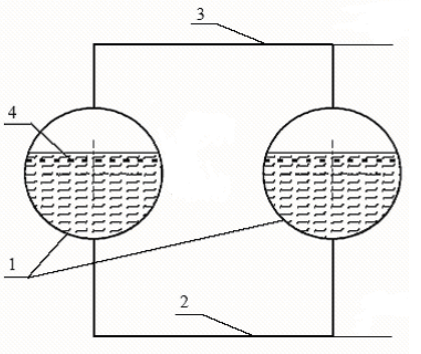

Fig. 10 – Layout of the two DS and related connection

2.1.2. The core

2.1.2.1. The fuel

The RBMK core is mounted in a graphite stack with a lattice of vertical channels loaded by fuel assemblies, additional absorbers and regulators. A ring of periphery channels forms a radial reflector. Top and bottom reflectors are core-wide and are 0.5 m width each one. The graphite stack is enclosed in a space, named reactor cavity, formed by lower and upper metal constructions and ringed by a steel cylindrical structure, see section 2.2.1. The graphite stack of the RBMK-1000 reactors serves several functions. The primary one is the neutron moderation and reflection, but it also provides structural integrity and in the event of a temporary cooling malfunction, a relatively large heat capacity. A general view of the core region and of a portion of the graphite stack are given in Fig. 11. More details in Tab. 1.

The FC together with the fuel rod is reported in Fig. 12. A key feature for the RBMK is the FC housed by graphite blocks. The core contains 1570 fuelled channels separated from its nearest neighbors by the wall of the pressure tube and graphite blocks. Each pressure tube has considerable autonomy. For example the coolant flow rate of each tube is controlled online by an individual isolation and control valve. In such a way any pressure tube can be isolated from the rest of the primary cooling system while the reactor remains under operation. This peculiarity makes possible to change fuel clusters online and also has a significant impact on the potential consequences of loss-of-coolant accidents.

A fuel assembly consists of an upper and a lower fuel bundle, symmetrically placed around the core middle plane. Each section is formed by 18 active rods and a central steel rod that ensures structural rigidity together with 11 spacer grids equally distributed along the section. Each fuel rod has a zirconium alloy clad that recovers the fuel pins, see Fig. 12. The top, centre and bottom segments of a typical reactor fuel channel are shown schematically in Fig. 13. The central

segment usually called Pressure Tube (PT) is made of a zirconium-niobium alloy (Zr+2.5% Nb). The top (3) and bottom (11) segments are stainless steel. The choice of zirconium-niobium for the centre part was made because of the relatively low thermal neutron absorption cross section of the material and its adequate mechanical and anticorrosive properties at high temperature (up to 350 ^{o}C).

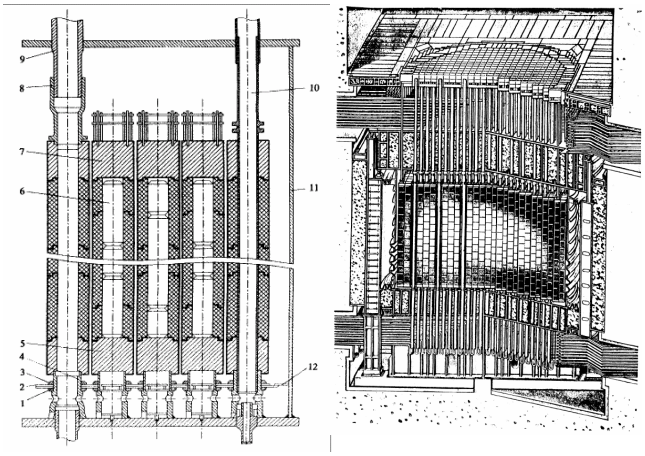

1 – top ring,
2 – diaphragm,
3 – bottom ring,
4 – bushing,
5 – steel support plates,
6 – graphite rods,
7 – shield plates,
8 – standpipe,
9 – guide pipe,
10 – reinforcing tube (reflector cooling),
11 – outer steel shell,
12 – ring plate

Fig. 11 – Geometrical configuration of RBMK core: a) detail of active region; b) overall view

The interaction of fast neutrons can lead to dimensional changes in various materials. For example, in graphite moderated reactors, initial accumulation of the fast neutron dose produces a gradual shrinkage of the graphite blocks. For the RBMK reactors this results in a decrease of the bore diameter through which the fuel channel passes. For the pressure tube made of a Zr+2.5% alloy, the effect is opposite, due to thermal and irradiation effects the tube diameter increases. As a result, the gap between the pressure tube and the graphite, which has a nominal thickness of 1.5 mm is gradually diminished leading to an eventual closure of the gap itself.

Referring to the Smolensk 3 plant data, [7], the reactor core is composed by 2488 graphite columns, of which 1570 are fuel channel columns and 314 are non-fuel channels columns. The non-fuel channel columns are subdivided as follows: 211 Control and Protection System (CPS) channels, 12 ADC, 90 AAC and 1 water column. In addition, 604 are Radial Reflector Channels (RRC). The reference height for FC is 8.0 m, however the core active region is 7.0 m and the graphite top and bottom reflector have 0.3 m width.

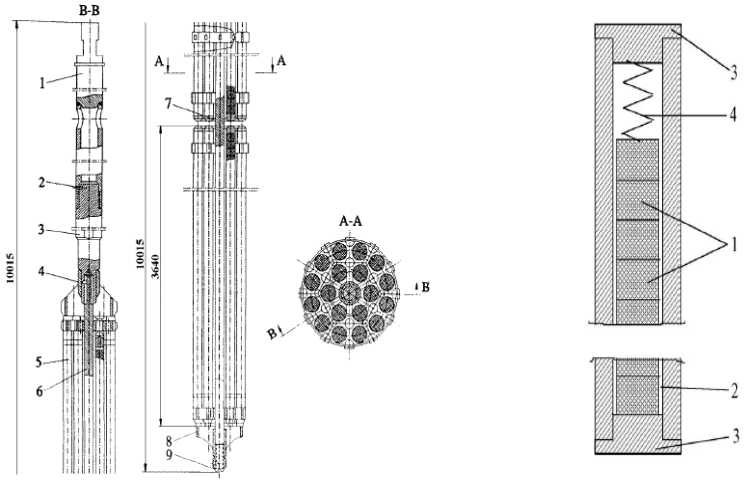

1 – suspension bracket, 2 – top plug, 3 – adapter, 4 – connecting rod, 5 – fuel element, 6 – carrier rod, 7 – end sleeve, 8 – end cap, 9 – retaining nut.

a) *b)*

Fig. 12 – Geometrical configuration of a) RBMK fuel bundle, b) fuel rod

1 – steel biological shield plug, 2,10 – top and bottom metal structures, respectively, 3 – top part of the fuel channel, 4 – welding-support ledge, 5 – fuel assembly support bracket, 6 – encasement cylinder, 7 – seal plug, 8 – graphite cylinder, 9 – central part of the channel, 11 – bottom part of the channel, 12 – thermal expansion bellows compensator, 13 – stuffing box

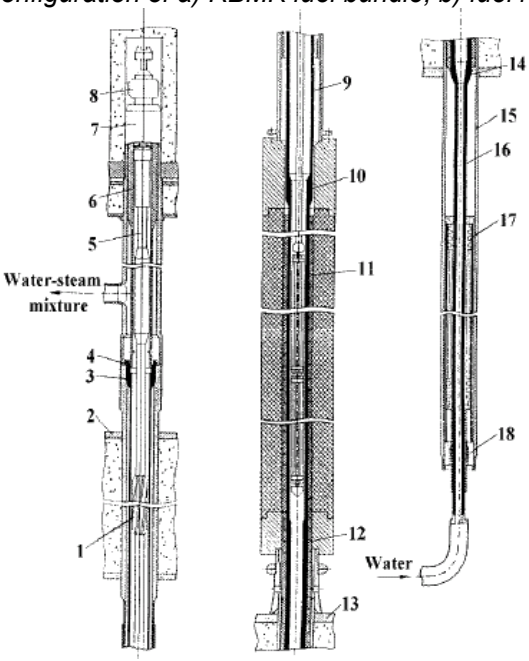

Fig. 13 – Geometrical and material configuration of RBMK FC

2.1.2.2. The Absorbers and the Power Control System

AAC are located symmetrically around core midline. 90 AAC are placed inside the core in order to increase the Operative Reactivity Margin (ORM). Regular AAC and cluster AAC (two FC) shall be distinguished that have the configuration (cross section) depicted in Fig. 14. Namely the cluster-type additional absorber consists of two bundles, where inner displacer is surrounded by 18 small-size, stainless-steel tubes, 2 tubes are empty while 16 tubes are filled with boron carbide (density 1678 Kg/m^3). The height of the column is 3.50 m and the distance between boron columns of two bundles in the middle of the core is 0.044m. The displacer is a tube with a graphite block inside.

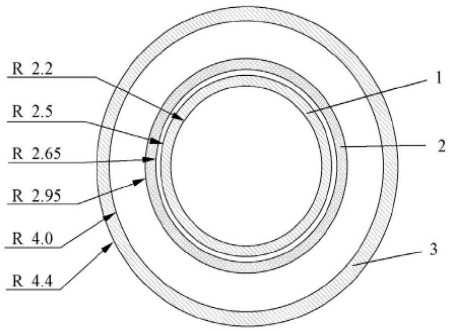

1 – support tube, 2 – absorbing sleeves, 3 – channel tube

a) regular

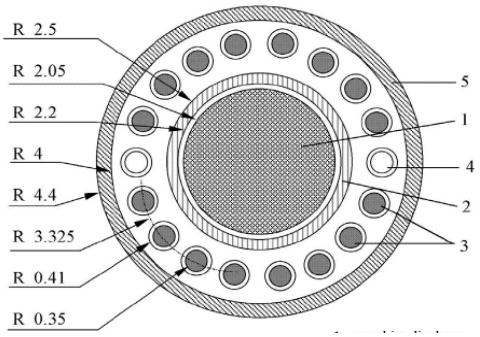

1 – graphite displacer, 2 – support tube, 3 – absorbing pins, 4 – empty tube, 5 – channel tube

b) cluster

Fig. 14 – Geometrical and material configuration of regular and cluster type AAC of RBMK core

Control rods are inserted in special channels of the CPS that is hydraulically independent from the fuel channel system. The CPS can be kept in operation in case of emergency when the FC fail. There are three types of control rods: a) 32 short CR (SHR), b) 24 safety or fast scram CR (SR), c) 155 manual CR (MCR). SHR move upward from the bottom when inserted, all others move downward from the core top. A sketch of the three CR types is given in Fig. 15 and a cross section (for regular CR) in Fig. 16.

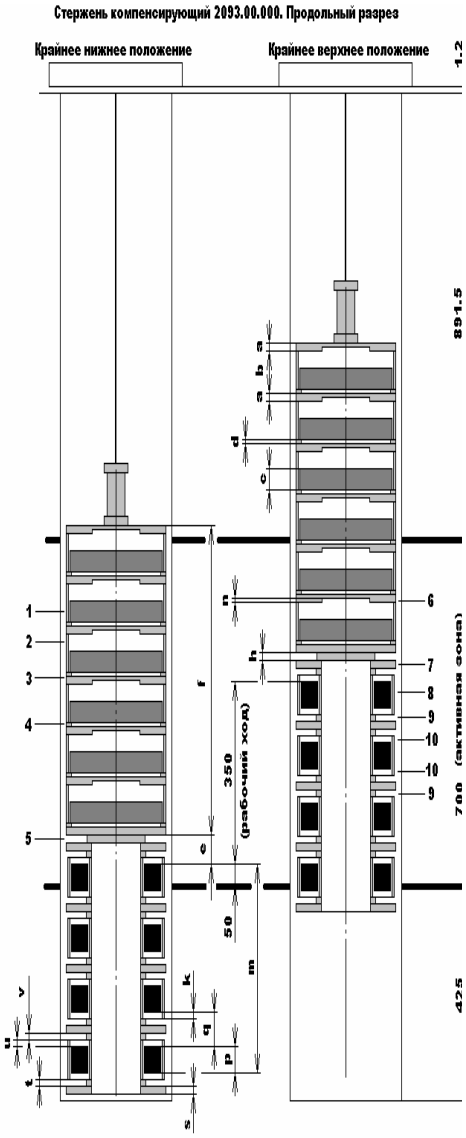

a) Short CR

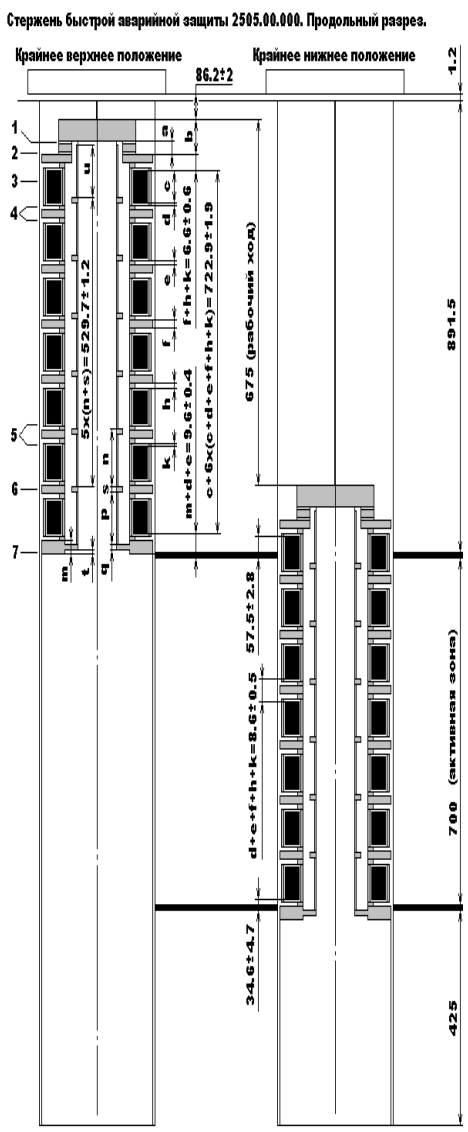

b) Safety CR

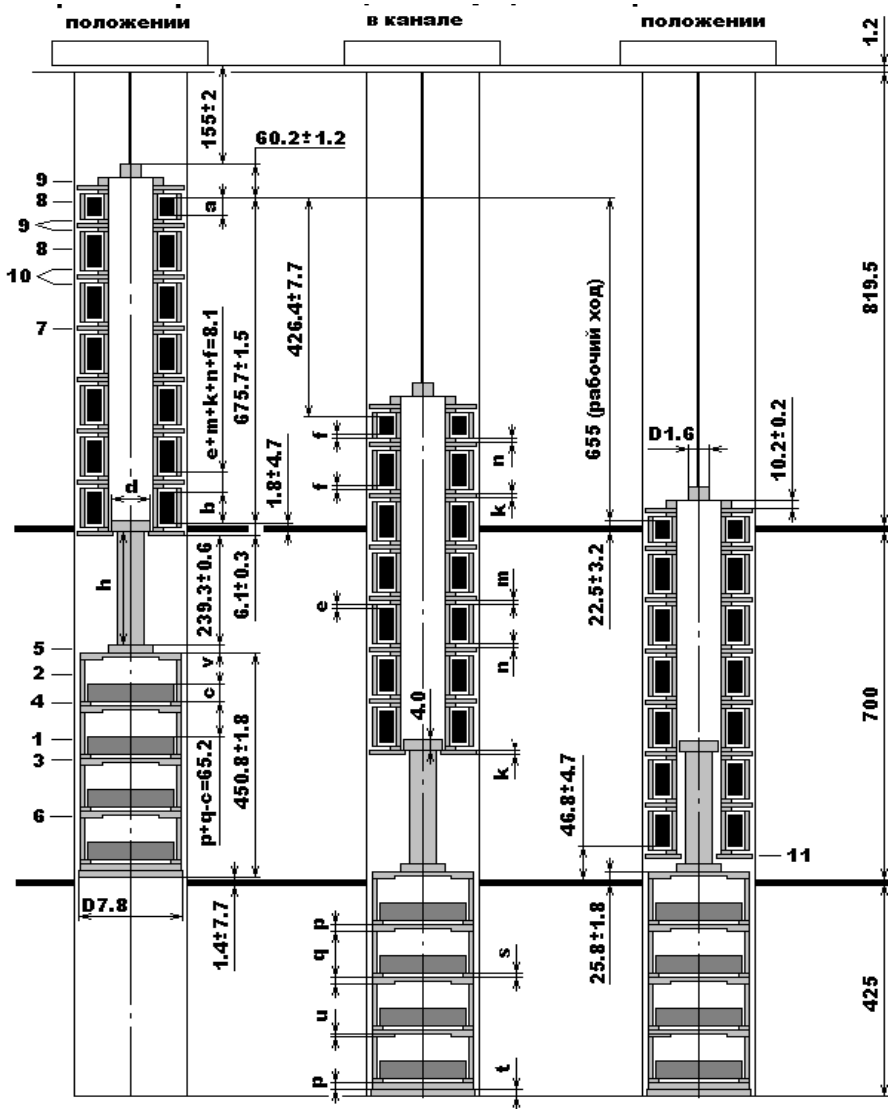

c) Manual CR

Fig. 15 – Longitudinal view of RBMK CRs (Short, Safety and Manual types)

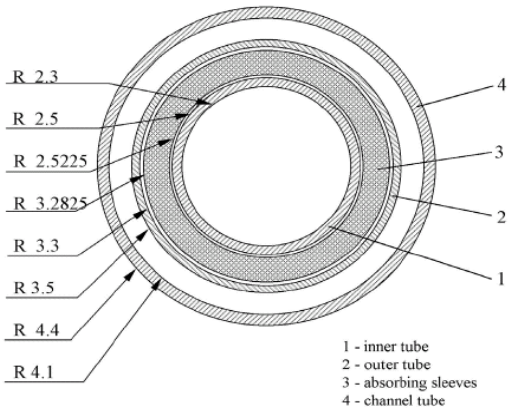

Fig. 16 – Cross sectional view of RBMK regular CR

Control rods are placed in an independent cooling loop, as already mentioned, with its own pumps and heat carrier (see Fig. 17).

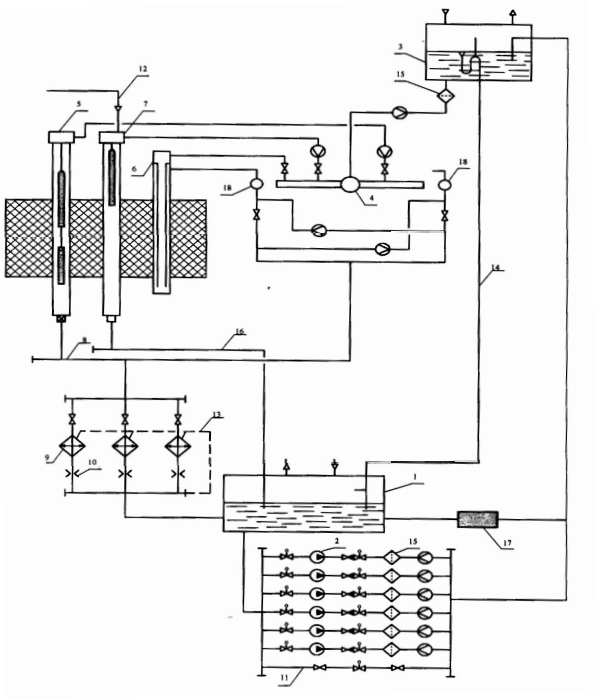

1 – top storage tank circulation tank; 2 – Circulation pump (CPS-P); 3 – Emergency tanks; 4 – Distribution header; 5 – CPS channel, 6 Reflector cooling channel , 7 – Scram channel, 8 – CPS discharge collector, 9 – CPS heat exchanger, 10 – Supporting device, 11 – CPS-P bypass with valves for flow-rate regulation, 12 – channel (train) for insertion of nitrogen in the scram channel, 13 – line for de-aeration, 14 – excess water sink overflow pipe, 15 – mechanical filter, 16 – Distribution header, 17 – purification bypass, 18 – Reflector cooling channel distribution header.

Fig. 17 – Flow diagram of the CPS cooling system

The piping of Control Rod Cooling Circuit (CRCC) cools the channels of the CPS rods, fission chambers, Power Density Distribution Monitoring System (PDDMS)

sensor and Radial Reflector Cooling Channels (RRCC). The coolant must be distributed in the circuit to ensure that proper temperature fields prevail in the channels of the control meters and of the graphite moderator. The cooling in this circuit is gravity driven, see Fig. 17. The cooling circuit includes: a) 211 CPS channels containing rods and safety instrumentation, b) 12 channels containing the in-core Power Density Sensors of the Axial Monitoring (PDMS-A), c) 604 channels of RRCC.

2.1.2.3. The scram signals

Several modes of scram operation are possible for the Smolensk-3 NPP and are summarized in Tab. 2. The BAZ mode is initiated from both neutronic signals (excess power and reduced period), two process trips (increase of pressure in selected rooms and increase of reactor cavity pressure) and by manual action. The more normal shutdown mode of AZ-1 is initiated by 16 process parameters and by failure of more than 3 local protection zones to reduce power satisfactorily. The other modes are initiated by a variety of upset conditions (see [8] for more info).

Tab. 2 – CPS Modes of Operation

Name	Rods Used / Insertion Times	Conditions	Power reduction
BAZ	24 SR + All CRs <2.5s 12-14 s	5 initiating signals	Operating power to zero
AZ-1	24 SR + All CRs 7s 12-14 s	17 initiating signals	Operating power to zero
AZ-3	LAC CR 0.4 m/s insertion 0.2 M/s withdrawal	3 initiating signals power deviation <1% (LAR) power deviation <5% (LAP)	From 100% to 50 % at 2%/s
AZ-4	LAC CRs	6 initiating signals	From 100% to 60% at 1%/s
AZ-5		NOT USED	
AZ-6	LAC CRs	Local Protection 1 initiating signal	Operates until LAP signal disappears (up to 50% power)

The following should be noted concerning the CPS CR grouping:

- 24 SR belong to the fast active scram system (FASS)
- 9 MCR are automatically moved for controlling the local power (LAR)
- 32 ShR (inserted from the bottom)
- 146 MCR including 18 CR of the Local Automatic Protection (LAP)
- 27 rods are provided for the local automatic control (LAC) which consists of 18 LAP CR and 9 LAR CR (LAC= LAP + LAR)
- 4 of the peripheral LARs are used for automatic control of the power level under 10% of nominal power.

This information gives an idea of the complexity of the power control for RBMK system.

2.1.2.4. The fuel cell neutronic characteristics

Several considerations on the RBMK lattice design can help in obtaining the core neutronics characteristics. The use of graphite as moderator gives the opportunity to use natural or (in the case of RBMK) slightly enriched uranium as fuel thanks to its low Capture Cross Section (Σ_c = 2.4*10^{-4} cm^{-1}). On the other hand, the weaker slowing down power of graphite ($\xi\Sigma_s$ of C is 400 smaller than $\xi\Sigma_s$ of H_2O) implies a greater neutron thermalization length, resulting in the use of large lattice pitch (25 cm for the RBMK). The relevant neutronics characteristics of the graphite, compared to the light and heavy water are given in Tab. 3.

Tab. 3 – Comparison between diffusion parameters of Graphite, Light Water and Heavy Water

Moderator	Density (g/cm3)	D (cm)	$\xi\Sigma_s$	$\xi\Sigma_s/\Sigma_a$	Σ_a (cm^{-1})	L (cm)	$\tau_{th}^{1/2}$ (cm)	M (cm)
Graphite	1.6	0.84	0.06	175	2.4*10^{-4}	59	19	62
D_2O	1.1	0.87	0.18	6670	2.9*10^{-5}	170	11.4	170
H_2O	1.0	0.16	1.5	70	2.9*10^{-2}	2.9	5.1	5.8

Therefore, for the graphite, the mean-squared distance that a neutron travels from birth as fast fission until the "death" by capture as a thermal neutron is:

$$\bar{r}^2 = 6(\tau_{th} + L^2) \equiv 6M^2 = 173400\,\text{cm}^2,$$

resulting in an average distance of $\bar{r} = 416$ cm.

Hence, considering the reactor lattice main parameters, diffusion parameters can be recalculated obtaining representative values for the whole reactor core. In Tab. 4, the diffusion parameters for RBMK and LWR cores are given.

Tab. 4 – Comparison of diffusion parameters for RBMK and LWRs

Reactor	L (cm)	$\tau_{th}^{1/2}$ (cm)	M (cm)	Diameter (L)	Diameter (M)
RBMK	14.1	14.4	20.2	100	69
BWR	2.2	7.1	7.3	180	50
PWR	1.8	6.3	6.6	190	56

From Tab. 4, it is clearly evident the reasons of the greater geometrical dimensions of RBMK reactors compared with those of LWR of comparable thermal power. Neutronic characteristics have some immediate consequences in the MCC hardware design (e.g., no such large reactor pressure vessel can be constructed) and in the containment feature (e.g., no full pressure containment). The safety considerations about these issues are reported later in this document.

Coming back to the RBMK neutron cell characteristics, other relevant neutronics parameters can be easily calculated considering the elementary fuel element (FA and graphite) reproduced in Fig. 18.

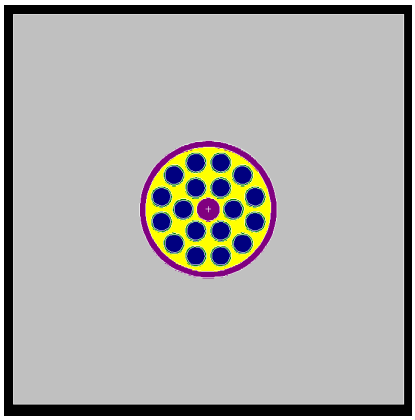

Fig. 18 – Fuel Cell basic model

Monte Carlo analyses of the Fuel Cell (see section 4.5.5 of this report), showed the following interesting characteristics reported in Tab. 5.

Tab. 5 – Neutronic characteristics of a RBMK fuel cell

Neutronic characteristics of a RBMK fuel cell	
Percentages of fissions caused by neutrons for various energy ranges	thermal range (E<0.625 eV): 91.67% intermediate range (0.625 eV< E < 100 KeV): 5.39% fast range (E>100 KeV): 2.94%
Average number of neutrons produced per fissions (ν)	2.44
Average fission neutrons produced per neutron absorbed in the fuel (η)	1.57
Energy corresponding to the average neutron lethargy causing fission	0.0933 eV

Monte Carlo calculations shows also the distribution of the thermal, fast and total flux into the fuel cell, see *Fig. 19*, *Fig. 20* and *Fig. 21*.

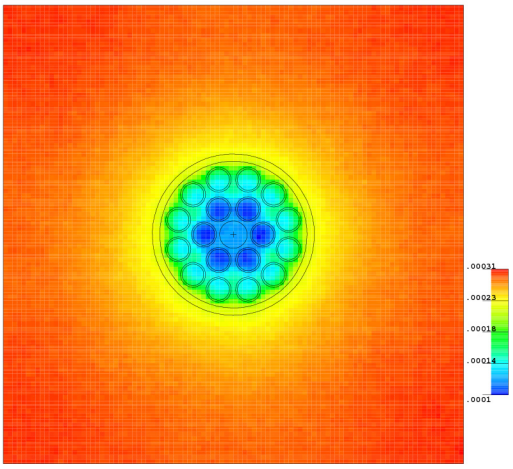

Fig. 19 – Thermal neutron flux distribution

It is clear in Fig. 19 the neutron thermalization and accumulation in the graphite brick. In Fig. 20 it is instead clear the born of the fast neutrons into the fuel rods and their loss of energy into the zone of graphite close to the pressure tube.

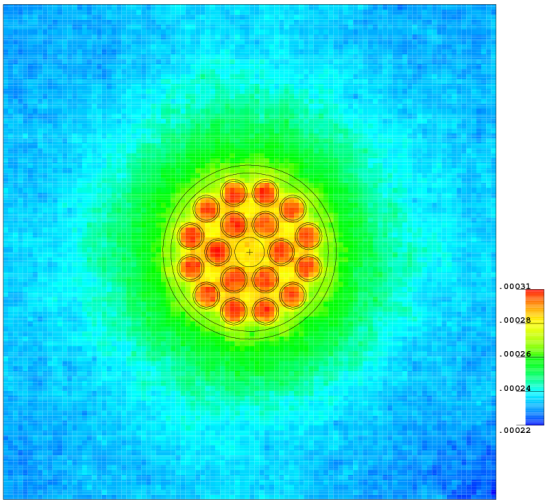

Fig. 20 – Fast neutron flux

Total flux distribution is showed in the Fig. 21. The accumulation of the neutron flux in the graphite is also here very clear.

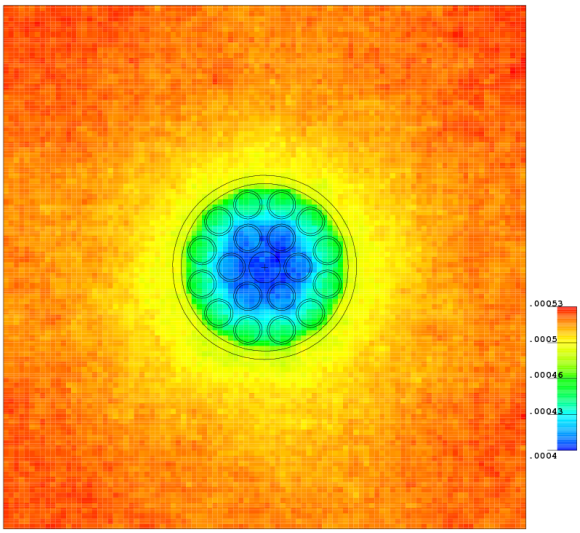

Fig. 21 – Neutron flux distribution

Tab. 6 is finally summarizing the fuel performance and the core power density, comparing it with those of a 900 MWe BWR.

Tab. 6 – Comparison between BWR and RBMK core parameters

Reactor Type	Thermal Power (MW)	Power Density (KW/l)	FA Average Linear Power (KW/m)	FA Maximum Linear Power (KW/m)	Maximum Burnup (GWd/tonHM)
RBMK (Smolensk-3)	3159	2.9 (56 considering only the coolant volume)	14.8	31	22
BWR-6	2894	56	19.8	44	~54

2.1.2.5. Reactivity Control

The dynamic analysis of large and strongly heterogeneous cores like those of the RBMK reactors is quite complex. In the following sections, the most relevant peculiarities and parameters affecting RBMK neutron kinetics are reported and discussed.

2.1.2.5.1. Fuel Cell Overmoderation

RBMK fuel cell neutronic design is based on a slightly over-moderated lattice. This is clearly evident in the Fig. 22, where the k_{inf} versus the ratio of the moderator are on fuel area is given. The k_{inf} values were obtained performing Monte Carlo

MCNP5 calculations for a RBMK and for a BWR typical fuel cell, changing the pitch of the lattice.

Operating conditions of the BWR are in the under-moderated zone while the RBMK are slightly in the over-moderated zone. This over-moderation has, as a consequence, that a lack of water in the RBMK FCs is causing an increase of reactivity, with all the obvious consequences for the reactor control and safety.

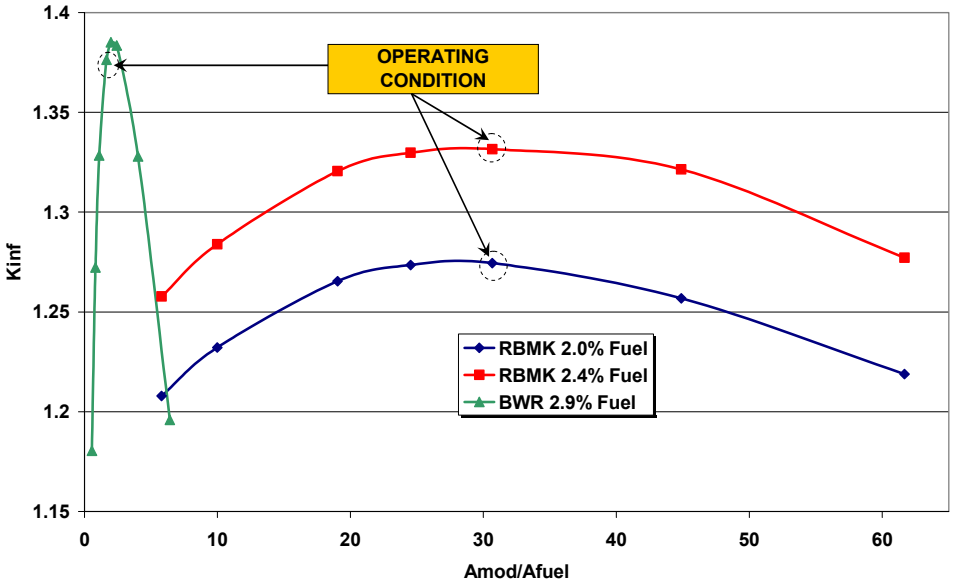

Fig. 22 – k_{inf} versus moderation ratio of Moderator area on Fuel area

The last generation of RBMK reactor, the Kursk-5 NPP (currently under construction), is addressing this issue, using a new design for the fuel cell graphite brick that removes the overmoderation [2].

2.1.2.5.2. The Operating Reactivity Margin

All reactors require an ORM in order to provide reactivity control as fuel burnup increases and to allow power maneuvering. In most reactors this reactivity reserve is provided by either CRs or by soluble or burnable poison (e.g., boron in the moderator or Gadolium in the fuel pins). In the case of power reduction, sufficient ORM is also required in order to compensate the loss of reactivity caused by the Xenon build up.

In the case of channel reactors with on-power fuelling (like the CANDU or the RBMK), a sufficient ORM is also necessary in order to provide with the CRs the suppression of power peaks in the vicinity of the newly fuelled channel. Removal of CRs can also provide reactivity for continued reactor operation in the event that the refuelling machine is unavailable.

Therefore the ORM has a multi purpose function and the choice of its magnitude during the reactor core design phase has an important consequence on the fuel burnup and consequently on the economy of the plant.

In the RBMK the magnitude of the ORM has added safety significance. The presence of absorbers in the core reduces the relative importance of neutron absorption in the water in the FC. In the event of loss of that water during an accident, the reactivity addition is smaller than would be the case with no in-core absorbers. Thus the CRs used to provide the ORM, in conjunction with the permanent in-core absorbers (the AAs) added to RBMK cores since the Chernobyl accident, reduce the magnitude of the void reactivity effect. The upper magnitude of the ORM, while specified as an operating limit, has safety implications in that enough CRs must remain available out-of-core to provide the appropriate sub-criticality margin to ensure the reactor can be shut down for the most reactive core configuration possible.

Consideration of the above effects has resulted in an ORM of between 43 and 48 rods for Smolensk-3 [8]. A lower safety limit of 30 rods has been established so that the shutdown system can overcome the positive void effect. Summarizing, the four main reasons for being within these two bounding limits are:

- reactor dynamics are improved by reducing the reactivity void coefficient (in conjunction with the added fixed AA);
- there must be enough CRs in the core to control the radial and axial power distribution;
- there must be sufficient reactivity holdup within the inserted rods to compensate for Xenon buildup during power maneuvering;
- the upper limit is required to ensure there is enough negative reactivity available to provide guaranteed cold shutdown, in most reactive core condition, upon insertion of all CRs.

If the ORM margin drops below 30 rods, the operator must manually scram the reactor.

2.1.2.5.3. The Reactivity Coefficients

Measurement of reactivity coefficients is a complex task for RBMK reactors. They strongly depend by the particular reactor conditions (e.g., average fuel burnup, CR positions, number of AAs, etc.) and some of them (e.g., the core total voiding coefficient) can never be practically measured. Therefore, some of the values given in Tab. 7 were derived from a posteriori calculations or simply extrapolated by small perturbations operated at the plant. They should be considered as representative (especially the void coefficient) of the Smolensk-3 configuration during the ‘90s.

Tab. 7 – Typical Reactivity coefficient for the Smolensk-3 NPP [8].

Reactivity Coefficient	Value (pcm)	Notes
Power ($\alpha_{\mathbf{w}}$)	-0.23/MWth	
Doppler ($\alpha_{\mathbf{t}}$)	-1.2/°C	
Coolant Temperature ($\alpha_{\mathbf{cool}}$)	~0 /°C	
Graphite Temperature ($\alpha_{\mathbf{t}}$)	4-5/°C	Measured at cold conditions
Void ($\alpha_{\boldsymbol{\varphi}}$)	1.65/%	or +0.3 β±0.2 β for full core voiding (assuming β = 0.0055) ±0.2 β is the allowed systematic and statistical error

The most important parameter monitored and controlled in regard ot neutronic effects is generally the void reactivity coefficient. As a result of the safety modifications made at Smolensk 3 following the Chernobyl accident, the void reactivity coefficient with an ORM of between 43 to 48 rods at HFP SS conditions, with 97 AAs, is maintained at a value < 0.3 β.

The void coefficient is an integral reactor parameter and it is generally done the assumption that it remains constant throughout the whole range of void fraction. In order to calculate the void reactivity effect this constant value is used assuming total core voiding (0 to 100%). This explains why the total core voiding and the void coefficient are both quoted frequently with the same value.

2.1.3. The Balance of Plant

An overall sketch of the RBMK BOP can be found in Fig. 23. Separated steam flows from each of the 14 SD outlet nozzles, passes through 300 mm nominal diameter pipes with 198 mm diameter flow restrictors to two 400 mm nominal diameter steam headers situated parallel to the drum separator axis. Connections to each header are from alternate nozzles along the separator length to provide uniform steam extraction from the separators and uniform steam supply to each header. For each reactor half, outlet pipes from the midpoints of each of the four steam headers are connected in pairs, one steam header from each drum separator, to form 600 mm nominal diameter main steam lines, as shown in Fig. 24.

The 600 mm nominal diameter main steam lines downstream of the drum separator are each fitted with four 250 mm internal diameter branch connections, pairs of which lead to main safety valves.

The four main steam lines therefore provide a total of 8 main safety valves, two per line. These eight main safety valves each open and close at one of three pressure set-points, two opening at 7.45 MPa and closing at 7.15 MPa, four opening at 7.55 MPa and closing at 7.25 MPa and two opening at 7.64 MPa and closing at 7.35

MPa, relieving steam through discharge pipes with hydrolocks into the pressure suppression pool.

Downstream the branch connections to the main safety valves, two of the 600 mm diameter main steam lines, from different halves of the reactor, are linked by a pipe of 300 mm nominal diameter, Fig. 25. This link is provided to promote uniformity of steam flow and pressure between the main steam lines from the reactor halves.

Additional smoothing of the steam pressure and flow is provided by the leveling header of, where all four main steam lines are interconnected through flow limiters. In this area, branch connections are made to four pressure reducing turbine bypass valves (BRU-K) each with capacity of 725 t/h which relieve excess steam to the turbine condenser during steam pressure transients, to avoid unnecessary opening of the main safety valves.

The opening set points of the BRU-K valves is 7.1 MPa, with an opening/closing time of 10 s, but once open are operated in a controlled mode to reduce drum separator pressure back to 6.86 MPa.

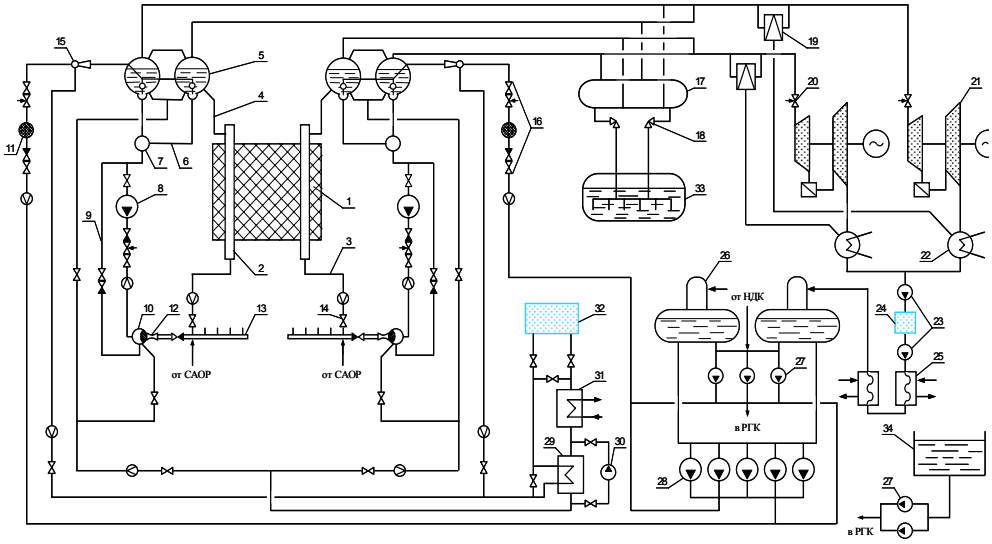

1 – reactor; 2 – fuel channel; 3 – feeding pipelines; 4 – steam-water pipelines; 5 – DS; 6 – DC; 7 – MCP suction header; 8 –MCP; 9 – bypass; 10 – MCP header; 11 – mechanical filter; 12 – flow limiter; 13 – GDH; 14 – control-throttling valve; 15 – mixer; 16 – feed-water valves; 17 – steam header; 18 – ГПК; 19 - BRU-K; 20 – SCV; 21 – turbo generator; 22 – condenser; 23 – condensate pumps; 24 – condensate polishing; 25 – heater; 26 – deaerator; 27 – AFWP; 28 – FWP; 29 – make up regenerator; 30 – cool down pump; 31 – make up cool down; 32 – bypass clearing; 33 – bubbler; 34 – water tank

Fig. 23 – Flow diagram of the BOP system of the RBMK core

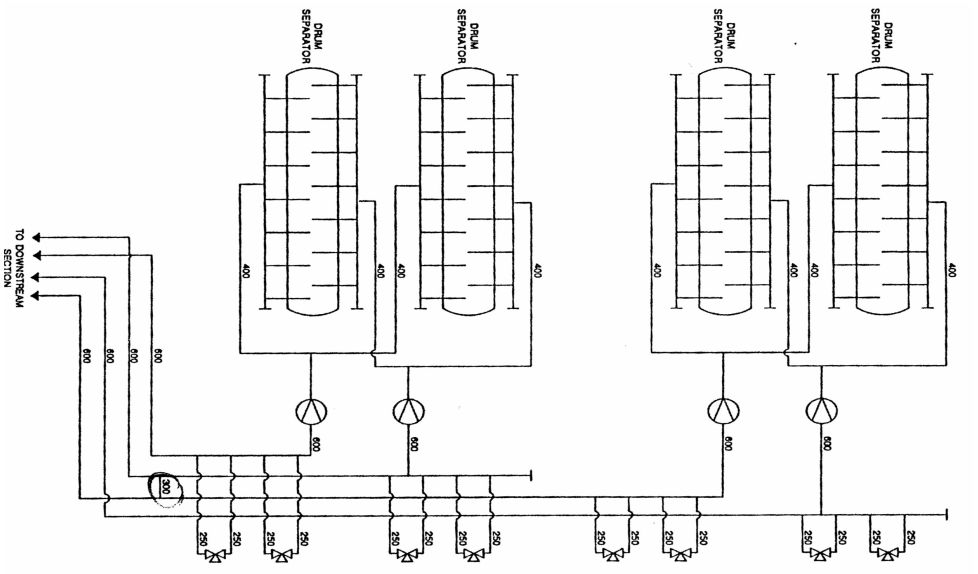

Fig. 24 – Flow diagram of SL from the SD region till the MSVs

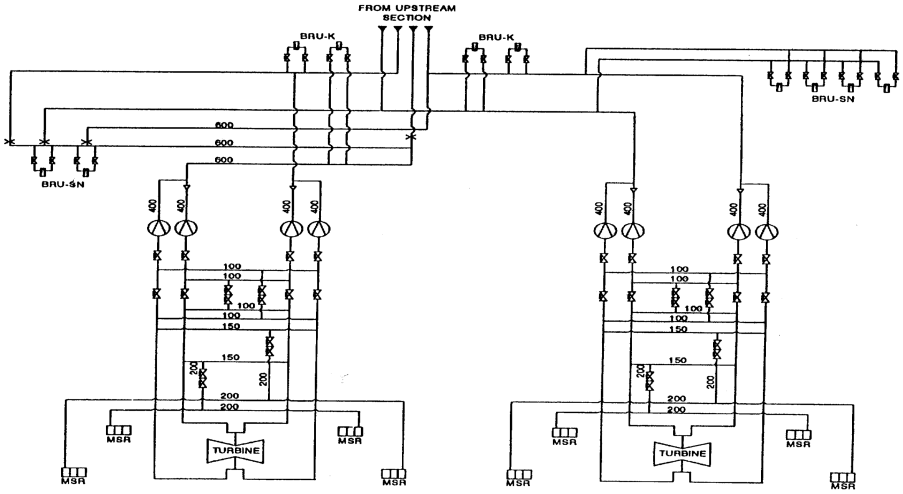

Fig. 25 – Flow diagram of RBMK SL from the MSIV till the turbines

When the load of either turbine is rejected, a signal to open both BRU-K valves associated with that turbine is generated by the AZ-3 signal, which reduces reactor power to 50%. This signal anticipates a subsequent pressure increase and controlled flow through the valves maintains the drum separator pressure close to

the nominal value. The same logic is used for load rejection by both turbines or a single operating turbine through the AZ-1 scram signal.

Branch connections are also provided to six pressure reducing valves (BRU-SN) with a capacity of 100 t/h each, supplying steam to the unit auxiliaries. These valves are used during depressurization and cool down to bleed steam through the technological condenser, cooled by service water, to maintain the deaerator level for use by the emergency feed-water pumps.

Downstream of the BRU-K and BRU-SN branch connections, the four 600 mm nominal diameters are routed in pairs to each turbine, each dividing into two of 400 mm nominal diameter. The 400 mm diameter pipes are each fitted with two turbine isolation valves. Of these, the upstream valve is closed for maintenance purposes only and the downstream valve is the main stream isolation and control valve during plant operation.

Pairs of main steam isolation and control valves are bypassed by linking pipes, each ling fitted a slide valve and control valve. This bypass line is intended for pre-operational testing and all bypass valves are closed during power operation. Downstream of the main steam isolation valves two turbines are connected. The exhaust steam is condensed, passes through the deaerators, the pre-heaters and finally it is pumped by the feed-water pump into the SD.

2.2. The Confinement System

The RBMK confinement constitutes a very complex system. The following main subsystems can be distinguished which contribute to mitigate or preventing possible radioactivity releases from the MCC, Fig. 26 and Fig. 27: a) the reactor cavity, b) the ALS, c) the reactor building, d) the fuel loading and unloading machine hall, e) the turbine hall.

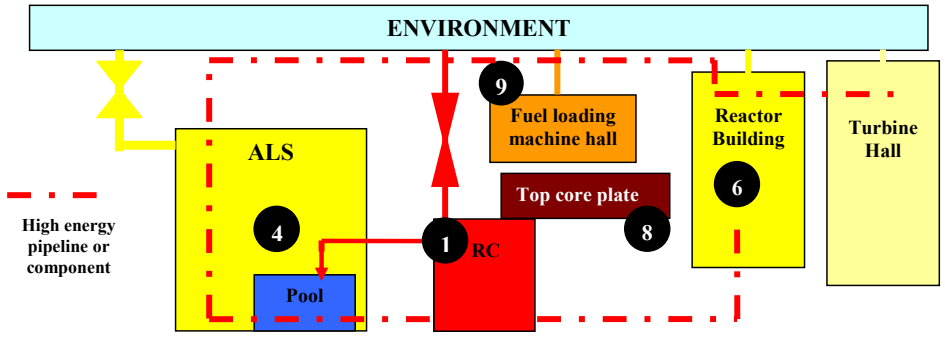

Fig. 26 – Sketch of the confinement system of the RBMK NPP with main sub-systems (numbers refer to components identified in Fig. 3.1, where applicable)

The RC is connected to the ALS through the pool suited for lowering the pressure in case of accident inside the RC itself. The RC is connected to the environment via valves that open in case of high pressure where high pressure is such to have the potential of lifting the upper core plate. After opening these valves do not close. The RC can be connected with the hall of the fuel loading and unloading machine only in case of lifting of the upper core plate.

The ALS is connected with the RC and the environment. This last connection occurs through valves that open at assigned pressure set-points. The ALS allows the characterization of the break location and the retention of the FP in case of mass and energy releases from the MCC. The connection via energized flow line (SL) between ALS, RB and Turbine Hall is depicted by a dotted line in Fig. 27. The zone of the fuel loading and un-loading machine is connected to environment by a bare line to show that there is not pressure boundary between this zone and the environment.

The RB and the Turbine Hall are characterized in Fig. 27 by bare lines connections with the environment for the same reason as above (no pressure boundary separation between each of these and the environment). However high energy flow lines or components are located in these regions as depicted by red dotted line in Fig. 26.

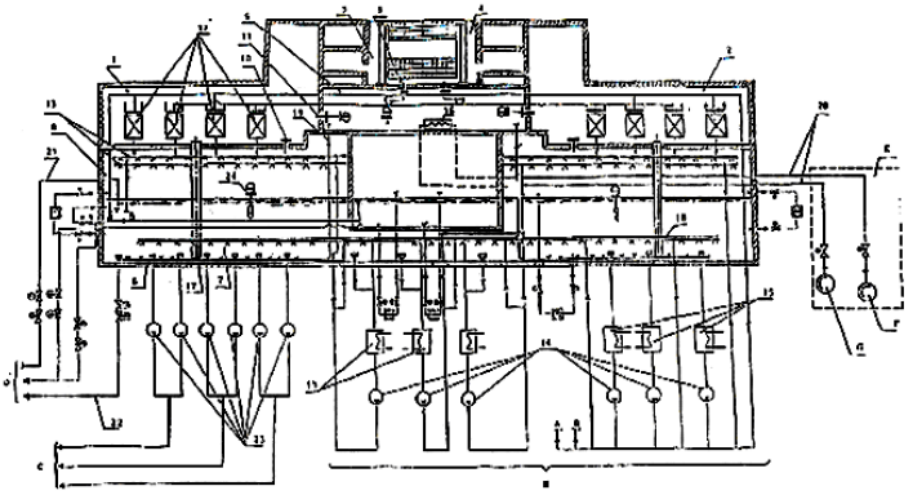

A – B Pipework of SCS; C Pressure pipelines of ECCS; D To the reactor auxiliary system; E Corridor "g – e"; F Service water dump header; G Service water pressure header; H Pump – heat exchanger - facility of SCS

1-2 Leaktight compartment
3-4 Under reactor and lower water line (LWL) compartments
5 Steam distribution corridor (SDC)
6 ALS leaktight guarding
7 Pressure suppression pool (PSP) water volume
8 PSP discharge valves
9 Under reactor compartment rupture membranes
10 PSP discharge valves
11 LC check valves
12 Ejector coolers of the sprinkler cooling system (SCS)
13 Sprinkler headers
14 SCS pumps
15 SCS heat exchangers
16 Surface condenser
17 Steam discharge tubes
18 Pool heater (perforated)
19 Condensate discharge pipes from SDC
20 Service water supply to the condensers
21 System for filling the PSP
22 System for draining the PSP
23 ECCS pumps
24 Measuring point

Fig. 27 – Cross sectional view of the RBMK confinement system

2.2.1. The Reactor Cavity

The cavity is a metal structure made up of a lateral cylindrical shroud a top and a bottom metal structures, Fig. 28. The lateral shroud is fitted with a lenticular compensator to compensate for longitudinal heat expansion. The pipes that are connected with the reactor cavity (e.g. fuel channels integrity monitoring system) are also defined as part of the reactor cavity, up to the first isolation valve.

The core with its graphite stack are enclosed into the reactor cavity that has a free volume of about 750 m^3. All the penetrations through the top (named E) and bottom (named OR) metal structures (e.g. pressure tubes) are welded and sealed. To avoid overpressure of the cavity in case of accident a set tubes are located at the top and bottom of the cavity to drain water and/or steam to the Pressure Suppression Pool.

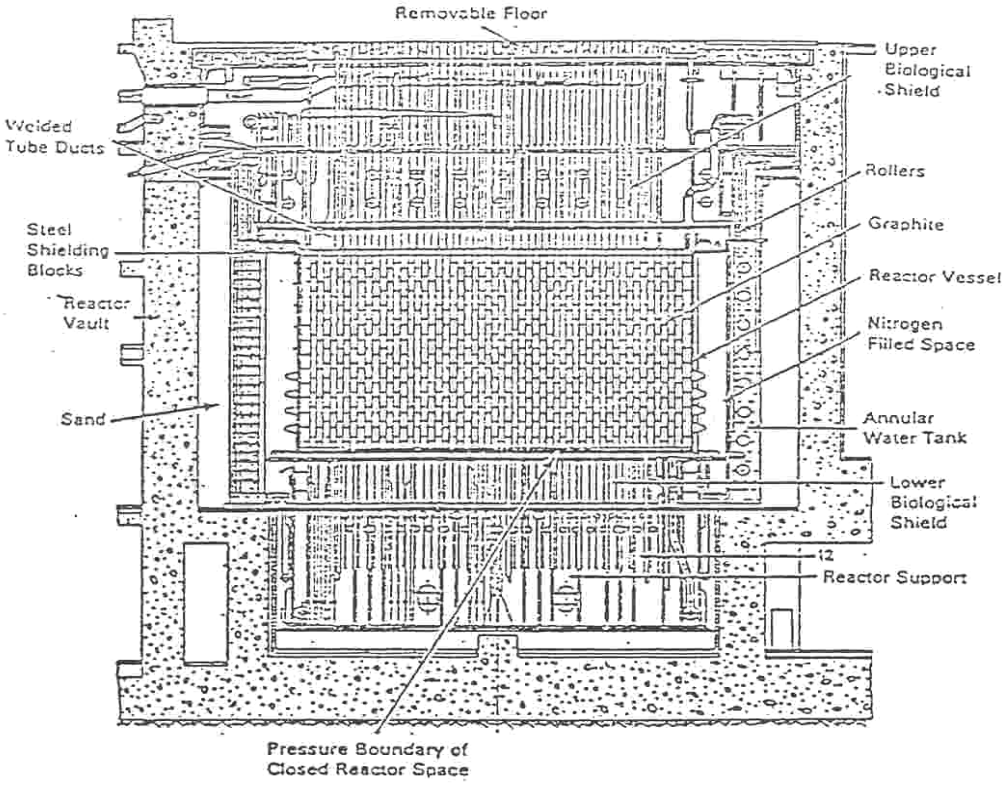

Fig. 28 – Longitudinal view of the RC of a RBMK NPP

A He-N mixture (coming from the pressure tube integrity monitoring system) continuously flows in the reactor cavity (flow ranging from 200 to 400 m^3/h at normal conditions). Maximum gas flow is 900 m^3/h.

The gas circuit system, Fig. 29, has the function to extract the gases from the reactor cavity which are product from the steam-graphite reaction or from leaking

pressure tubes and to lead them through different technical devices for their drainage and purification.

In order to avoid leaks of the gases, all the volumes surrounding reactor cavity (e.g. between the shroud and the lateral water shield) are filled with pure Nitrogen at higher pressure (2-5 KPa gauge), part of which flows into the reactor cavity. The residual flow of about 10-20 m^3/h of nitrogen coming from the outer structure is finally discharged to the high stack after having passed through filters for Iodine, delay tanks and particulate filters.

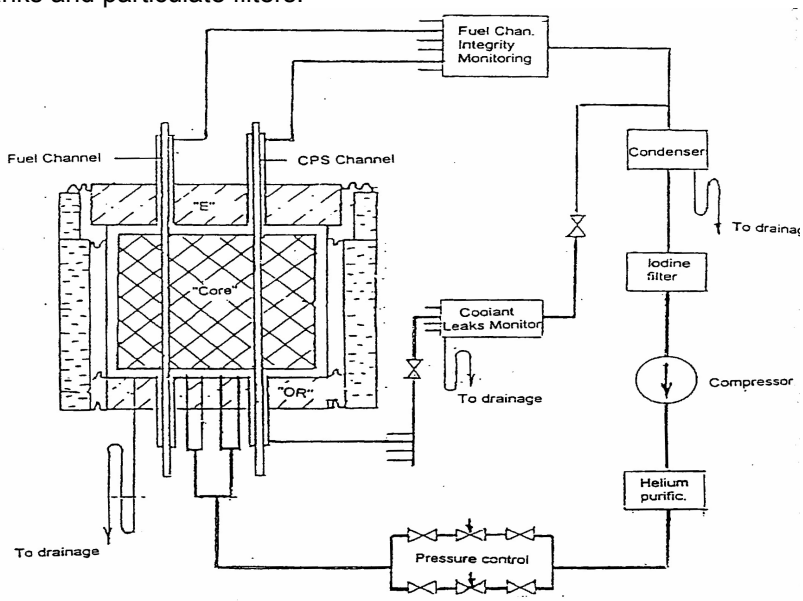

Fig. 29 – Gas removal system of the RC of a RBMK NPP

The pressure tube (fuel channel) integrity monitoring system is designed to continuously monitor temperature and humidity around each fuel channel. In addition, during plant outages, ultrasonic, visual and geometry measurements checks are performed on the pressure tubes.

2.2.2. The Accident Localization System

The Accident Localization System (ALS) is designed to avoid environment contamination as a consequence of a LOCA in the Main Circulation Circuit (MCC). The ALS is a seal space including the lower part of the down-comers from the Steam Drum (SD), the inlet and the outlet headers of the Main Coolant Pumps (MCP) and all the piping system downstream the MCP up to the cavity inlet. The ALS does not cover some relevant parts of the plant as SD, feed-water system and steam lines.

Another relevant function of the ALS is to make possible to recognize the damage side of the core by the pressure increase in the different compartments constituting the ALS. The main compartments of the system are:

- Leak-tight compartment (LTC): two compartments, one for each side of the core; these compartments include lower down-comers from the SD and the inlet header to the MCP.
- Pressure suppression pool (PSP): this part of the ALS is subdivided in three parts connected together; the main function is condensating the steam discharged from the break in a LOCA
- Steam corridor distribution (SDC): this part receive the steam released into the URC.
- Under reactor compartments (URC): these compartments include the piping down stream the MCP up to the cavity inlet.

LTC and SDC are connected with the PSP by discharge tubes in order to condensate the steam flowing from a break in the MCC covered by the ALS compartments. Other connections exists between the different compartments; these connections are constituted by valves and are designed to avoid any dangerous increase of the pressure inside a single compartment as a consequence of a large LOCA.

Some systems capable to reduce the pressure inside the ALS are part of the ALS itself. The main systems are:

- Sprinkler system: this system injects cold water in the pool water and in the atmosphere of the PSP. The system is composed two identical subsystems; each system includes pumps taking water from the pool, coolers and distribution headers injecting in the PSP. This system works in emergency conditions and in normal conditions to control the pressure and the temperature in the PSP compartment.
- Surface coolers: they are located in the SDS and are actuated by ECCS intervention signal.
- Ejector coolers: they are located in the LTC; these coolers are used to control pressure and temperature in the LTC. The ejectors coolers are also used in emergency conditions.
- Hydrogen removal system: this system remove the hydrogen from the atmosphere of the ALS and provide a purification of the air of the ALS. This system works during normal operation; in emergency condition is isolate to realize the sealing of the ALS, but it can be put in to operation by the operator.

The sketch of the ALS of Ignalina NPP is provided in Fig. 30, [10].

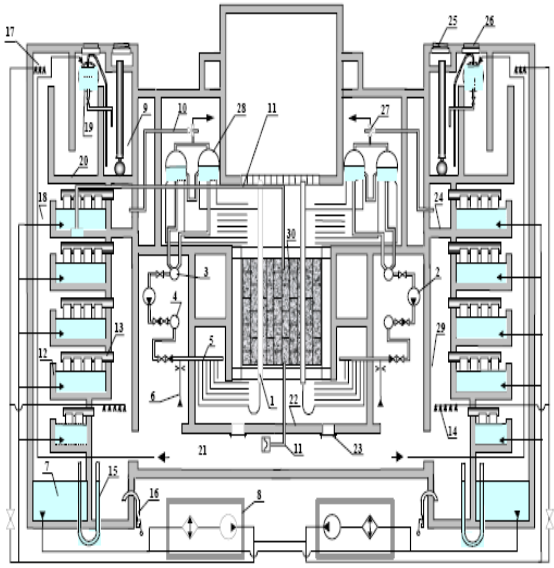

1. fuel channel 2. main circulation pumps 3. MCP suction header 4. MCP pressure header 5. group distribution header 6. ECCS headers 7. hot condensate chamber (HCC) 8. CTCS pumps and heat exchangers 9. discharge pipes section 10. pipe from the steam relief valves 11. steam gas mixture from the reactor cavity 12. condensing pools 13. steam distribution headers 14. bottom steam reception chamber (BSRC) sprays. 15. water seals/S traps between HCC and BSRC 16. BSRC vacuum breakers 17. air removal corridor sprays 18. air venting channel 19. gas delay chamber tank 20. gas delay chamber 21. reinforced leaktight compartments 22. Lower Water Piping compartments 23. steam relief valves from LWP compartments to RLC 24. top steam reception chamber 25. tip up hatches 26. knock down hatches 27. main safety valve and fast acting steam discharge valve 28. drum separators 29. Bottom Steam Reception Chamber 30. Reactor Cavity.

Fig. 30 – Sketch of the Ignalina ALS

2.2.3. The Reactor Building and the Turbine Hall

The reactor building and the turbine hall bound high energy lines and pressurized components. As such they are possible location of piping break. No pressure resistant wall are provided. Therefore, steam water releases to the environment are predicted in case of break occurrence. This does not imply significant radioactivity release because significant part of possible FP releases can be trapped in these confinement zones.

2.2.4. The fuel loading machine hall

The fuel loading machine hall is sketched in Fig. 1 (i.e. zone No. 9) and Fig. 2 (i.e., component No. 14). It has not a direct (or immediate) confinement role. However, in case of displacement of the top reactor plate, steam water mixture and FP from the reactor cavity may enter this zone.

In addition, during the (frequent) process of fuel loading and un-loading, accidents may happen that cause releases of high pressure two-phase mixture and eventually FP in this zone. Refueling-events were not considered during this PhD activities.

2.3. The Engineered Safety Features and the Emergency System

The Engineered Safety Features (ESF) include all components relevant to safety (therefore ECCS are part of ESF). The ECCS are characterized by suitable quality in the design and maintenance and are mostly addressed in the section below.

The pipes of ECCS trains, shown in Fig. 31, are 300 mm nominal diameter. Each of these terminated in ECCS headers, three per core region. From each header a pipe of 75 mm nominal leads through a 24.5 mm minimal diameter flow limiter and a check valve to each GDH. In addition a special connecting pipe of 75 mm nominal diameter is installed between the MCP pressure header and all the ECCS headers per each core side.

Delivery of the cooling water to the ECCS trains is provided by three subsystems, each of which is divided into three trains, namely: a) main (or short-term) subsystems, b) long term subsystems, further divided into the damaged core side and undamaged core side systems.

Flow from each train of each subsystem is delivered by a single pipe of either 200 or 300 mm nominal diameter. This pipe branches into two, and one of the branches is connected to each core side pipe of the corresponding train. Cooling water is delivered to the appropriate core side by an electrically powered fast-acting gate valve situated in each branch pipe, at inlet to the ECCS train.

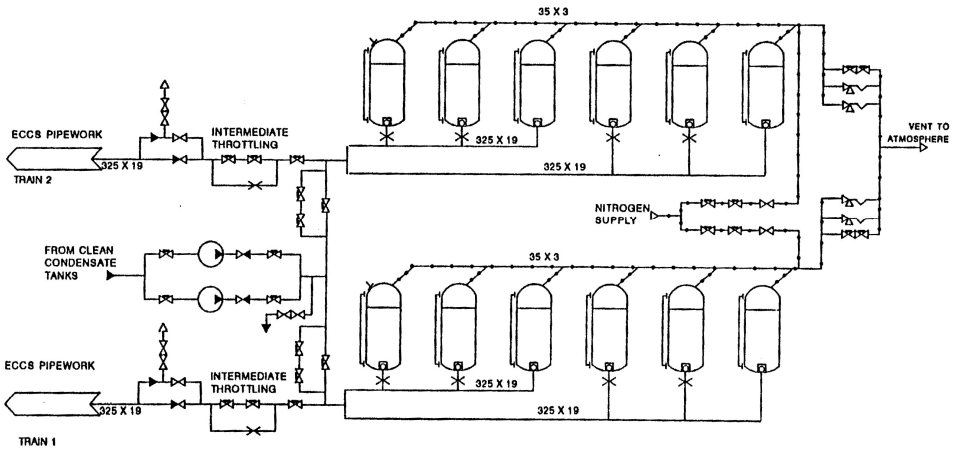

Fig. 31 – Main (or Short-term) ECCS subsystem, RBMK damaged core side delivery system

The main delivery subsystem consists of three separate trains, to deliver water to the trains. Trains 1 and 2 are identical, Fig. 31, each consisting of six pressurized accumulator tanks containing a total of 80 m^3 of water and 70 m^3 of nitrogen at 9.8 MPa pressure, per train. Each accumulator tank is fitted with water level indication.

A low water level signal automatically closes the isolation valve downstream the tank outlets of each train, but in addition, a float type cut-off valve avoids gas ingress to the trains following water discharge. One tank of each train has a pressure relief valve. The six tanks of each train deliver water at up to 40^{o}C through a single 300 mm nominal diameter pipe to the corresponding ECCS train.

Prior to the actuation of the two trains of the main subsystems, all valves in the flow path downstream the tank outlets leading to the trains are open. Two valves in each flow path, bypassed by a line fitted with a flow restrictor, are open on actuation of the accumulator tank trains. These are closed by a signal of 27 seconds after reactor trip, to provide intermediate throttling of the water flow, matching the reduction in decay heat of the reactor core and extending the total flow duration to at least 2 minutes.

Train 3 of the main subsystem delivers emergency cooling through a 400 mm nominal diameter connection from the main feed-water header. After any actuation of this train in an emergency without loss of offsite power, water at 165 ^{o}C is drawn from the deaerators by the main feed-water pumps for at least 10 minutes before the deaerators are emptied. Following loss of offsite power (LOOP) the main feed-water pumps stop. The coast-down time is approximately 55 s. In this period the pumps are powered by the running down TG.

The long-term subsystem is divided in two parts, one for delivery to the damaged core side and the other to the undamaged core side, Fig. 32 and Fig. 33, respectively.

The damaged core side delivery is constituted by three trains, each consisting of two damaged core side cooling pumps (DCSCP) operating in parallel, drawing suction from the Pressure Suppression Pool (PSP) which has a capacity of 3200 m^3. The six pumps of the three trains are each capable to provide 250 m^3/h of water at 7.8 MPa pressure. This system is required to operate within 2 minutes of the main subsystem actuation signal, before the main subsystem water tanks are exhausted.

The undamaged core side delivery is constituted by three trains, with one undamaged core side cooling pump (UCSCP) per train drawing suction through a common inlet line from the clean condensate tanks. There are three clean condensate tanks (1000 m^3 each) backed up by three makeup tanks, each of 750 m^3 in the makeup tanks is available for ECCS use. Other systems can use this same water source, but overridden by the ECCS actuation signal.

The three pumps of the three trains are identical to those of the damaged core side system, delivering 250 m^3/h at 7.8 MPa pressure. Water to the undamaged core side is provided by the main circulation pumps in coast down for at least one minute after any fault considered. The undamaged core side system is therefore required to initiate flow within one minute of the emergency.

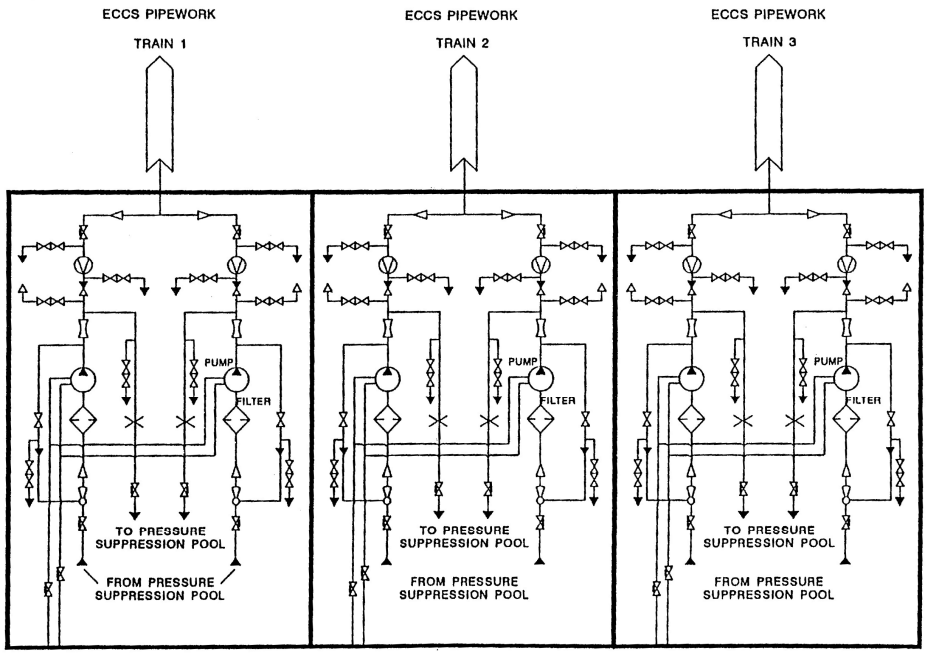

Fig. 32 – Long-term ECCS subsystem, RBMK damaged core side delivery system

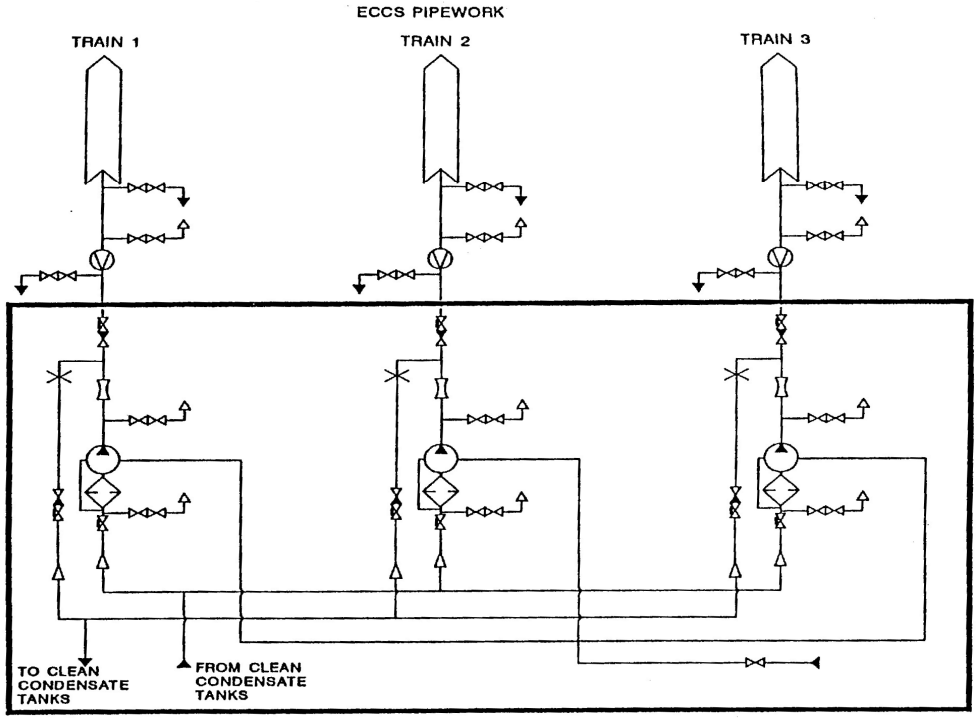

Fig. 33 – Long-term ECCS subsystem, RBMK un-damaged core side delivery system

In case of loss of offsite power, each train of power supplies is provided by a separate diesel generator, with power available 25 s after diesel start to the DCSCP and 35 s after diesel start to the UCSCP. Each pump can reach its rated flow rate within 1.0 to 1.5 s from the signal.

The special connection between the pressure header and the three ECCS headers per each core side is installed to provide a short term cooling to the affected GDH in case of MCC break between pressure header and GDH upstream the check valve at GDH inlet. In this emergency situation the signal for ECCS activation comes from differential pressure between pressure header and drum separator.

2.4. The reference plant and the reference conditions: Smolensk-3, 16 October 1996

2.4.1. Reference fuel load map

The map of the fuel load of the Smolensk NPP Unit-3 referring to the core status at October 16 1996 is represented in the Fig. 34 [11].

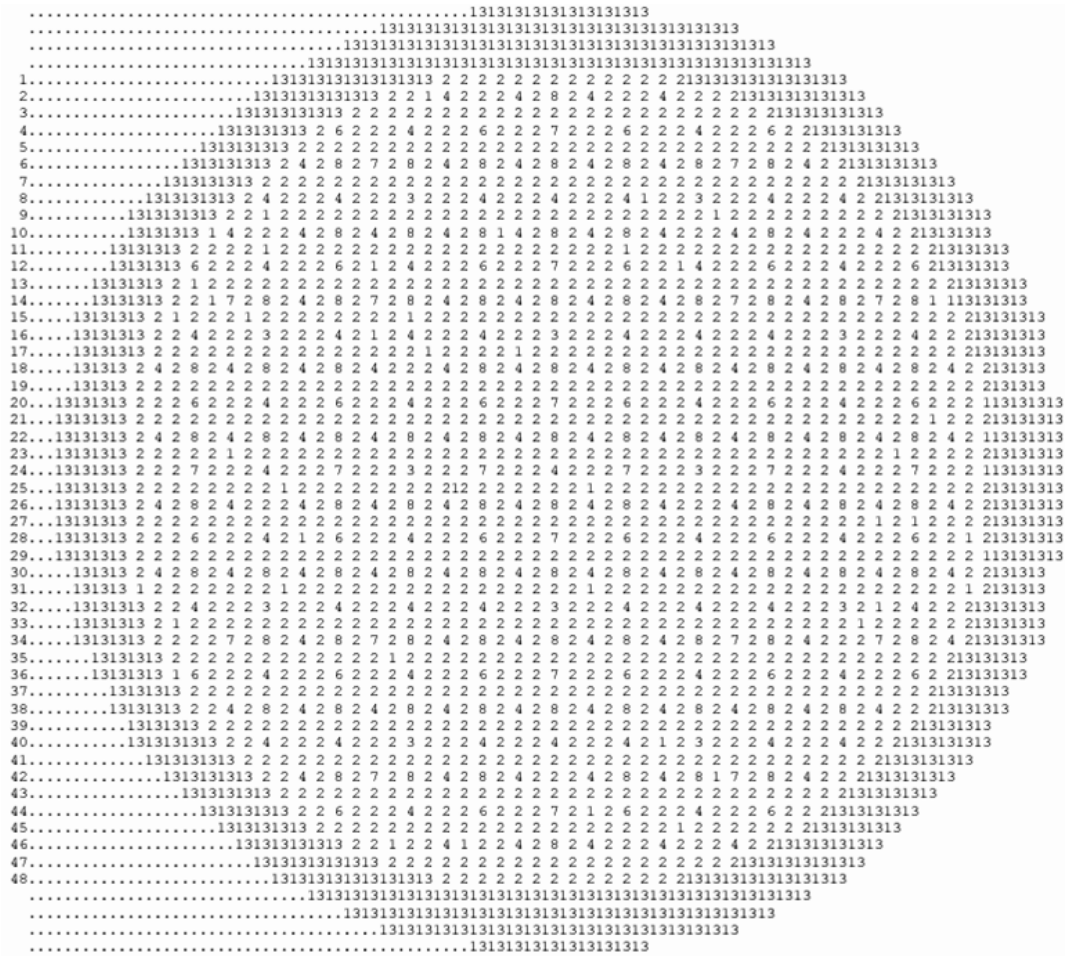

Fig. 34 – The reference map of fuel load of the Unit-3 of Smolensk NPP (16.10.96)

In Tab. 8 is reported the legend for the Fig. 34, listing the different type of channels present in the core, and their number.

Tab. 8 – Characteristics of FC and control rods

ID on Fig. 34	***Description***	***Quantity***
1	Fuel rod bundle with enrichment of 2% U^{235}	48
2	Fuel rod bundle with enrichment of 2.4% U^{235}	1552
3	High-altitude power gauge	12
4	Control rod (design 2091)	155
6	Shortened control rod (design 2093)	32
7	Fast Acting Safety System Rod (design 2505)	24
8	Rod with additional absorber (design 1814)	90
12	Water column in the channel	1
13	Graphite reflector	604

As it can be seen from the table, 211 control rods of various design and purposes are present in the core. The cartogram of the different type of control rods, with their arrangement in the core is reported in Fig. 35. A detailed geometrical description of the different control rods type can be found in the section 2.1.2 of this document.

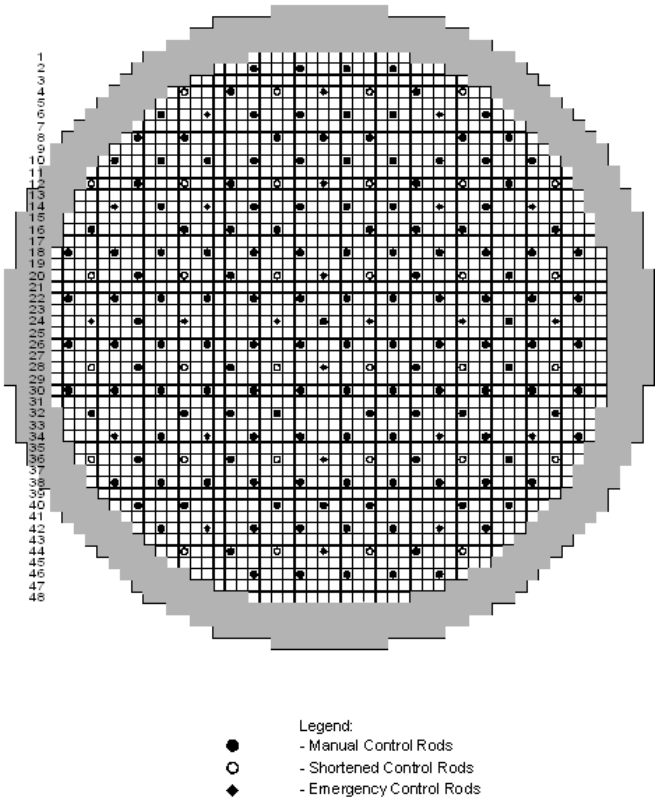

Fig. 35 – Control Rods Cartogram

In Tab. 9 is reported the initial condition of the tip of the control rods. It has to be noted that the numeration of the control rods was done according to their arrangement in the core reported in the cartogram of Fig. 35 and according to the rule "*from left to right, from top to bottom*". The insertion depth is measured in centimeters (cm) and it reports the distance between the tip of the control rod and the upper part of the top reflector. It has to be remarked that the insertion depth of the shortened control rods is negative because they move from the bottom to the top of the reactor core.

In Fig. 36, it is reported the map of the coolant mass flow in each of the core channels, except for the radial reflector channels.
It is important to remark that in all of these kinds of maps here reported the colors have always the following meaning:

- yellow is indicating a MCR channel;
- green a SR channel;
- orange a SHR channel;
- blue an Additional Absorber channel;
- grey an Axial Detector channel;
- dark blue the Water Column.

All the other colors used in such a kind of maps are indicating Radial Reflector Channels or FC grouping.

Tab. 9 – CR Standard Position

CR #	Insert. depth, cm (*)	CR Type	CR #	Insert. depth, cm (*)	CR Type	CR #	Insert. depth, cm (*)	CR Type	CR #	Insert. depth, cm (*)	CR Type
1	30	*MCR*	**55**	30	*SR*	**109**	30	*SR*	**163**	20	*MCR*
2	220	*MCR*	**56**	30	*MCR*	**110**	30	*MCR*	**164**	-270	*SHR*
3	60	*MCR*	**57**	30	*SR*	**111**	610	*MCR*	**165**	30	*MCR*
4	30	*MCR*	**58**	30	*MCR*	**112**	30	*MCR*	**166**	-290	*SHR*
5	-240	*SHR*	**59**	30	*MCR*	**113**	30	*MCR*	**167**	30	*MCR*
6	20	*MCR*	**60**	670	*MCR*	**114**	470	*MCR*	**168**	-270	*SHR*
7	-370	*SHR*	**61**	30	*MCR*	**115**	30	*MCR*	**169**	30	*SR*
8	30	*SR*	**62**	30	*MCR*	**116**	20	*MCR*	**170**	-280	*SHR*
9	-370	*SHR*	**63**	30	*MCR*	**117**	520	*MCR*	**171**	30	*MCR*
10	150	*MCR*	**64**	20	*MCR*	**118**	180	*MCR*	**172**	-310	*SHR*
11	-370	*SHR*	**65**	20	*MCR*	**119**	30	*MCR*	**173**	220	*MCR*
12	30	*MCR*	**66**	30	*MCR*	**120**	200	*MCR*	**174**	-260	*SHR*
13	30	*SR*	**67**	20	*MCR*	**121**	30	*MCR*	**175**	30	*MCR*
14	680	*MCR*	**68**	170	*MCR*	**122**	-310	*SHR*	**176**	30	*MCR*
15	170	*MCR*	**69**	20	*MCR*	**123**	30	*MCR*	**177**	20	*MCR*
16	30	*MCR*	**70**	30	*MCR*	**124**	-270	*SHR*	**178**	150	*MCR*
17	40	*MCR*	**71**	30	*MCR*	**125**	30	*MCR*	**179**	590	*MCR*
18	30	*SR*	**72**	520	*MCR*	**126**	-330	*SHR*	**180**	110	*MCR*
19	250	*MCR*	**73**	30	*MCR*	**127**	30	*SR*	**181**	340	*MCR*
20	20	*MCR*	**74**	30	*MCR*	**128**	-290	*SHR*	**182**	460	*MCR*

Tab. 9 (cont.) – CR Standard Position

CR #	Insert. depth, cm (*)	CR Type	CR #	Insert. depth, cm (*)	CR Type	CR #	Insert. depth, cm (*)	CR Type	CR #	Insert. depth, cm (*)	CR Type
21	20	*MCR*	**75**	90	*MCR*	**129**	30	*MCR*	**183**	360	*MCR*
22	30	*MCR*	**76**	210	*MCR*	**130**	-290	*SHR*	**184**	280	*MCR*
23	30	*MCR*	**77**	30	*MCR*	**131**	210	*MCR*	**185**	30	*MCR*
24	30	*MCR*	**78**	-370	*SHR*	**132**	-270	*SHR*	**186**	30	*MCR*
25	30	*MCR*	**79**	680	*MCR*	**133**	30	*MCR*	**187**	30	*MCR*
26	30	*MCR*	**80**	-340	*SHR*	**134**	80	*MCR*	**188**	30	*MCR*
27	30	*MCR*	**81**	120	*MCR*	**135**	260	*MCR*	**189**	30	*MCR*
28	210	*MCR*	**82**	-290	*SHR*	**136**	20	*MCR*	**190**	30	*MCR*
29	600	*MCR*	**83**	30	*SR*	**137**	30	*MCR*	**191**	30	*MCR*
30	110	*MCR*	**84**	-290	*SHR*	**138**	20	*MCR*	**192**	30	*MCR*
31	20	*MCR*	**85**	30	*MCR*	**139**	550	*MCR*	**193**	30	*SR*
32	30	*MCR*	**86**	-270	*SHR*	**140**	30	*MCR*	**194**	640	*MCR*
33	140	*MCR*	**87**	30	*MCR*	**141**	20	*MCR*	**195**	80	*MCR*
34	680	*MCR*	**88**	-310	*SHR*	**142**	100	*MCR*	**196**	550	*MCR*
35	30	*MCR*	**89**	130	*MCR*	**143**	30	*MCR*	**197**	30	*MCR*
36	20	*MCR*	**90**	170	*MCR*	**144**	20	*MCR*	**198**	30	*SR*
37	-270	*SHR*	**91**	30	*MCR*	**145**	30	*MCR*	**199**	220	*MCR*
38	680	*MCR*	**92**	30	*MCR*	**146**	650	*MCR*	**200**	-250	*SHR*
39	-270	*SHR*	**93**	30	*MCR*	**147**	60	*MCR*	**201**	30	*MCR*
40	30	*MCR*	**94**	30	*MCR*	**148**	30	*MCR*	**202**	-300	*SHR*
41	-270	*SHR*	**95**	20	*MCR*	**149**	30	*MCR*	**203**	30	*SR*
42	30	*SR*	**96**	80	*MCR*	**150**	80	*MCR*	**204**	-310	*SHR*
43	-290	*SHR*	**97**	30	*MCR*	**151**	30	*MCR*	**205**	60	*MCR*
44	20	*MCR*	**98**	100	*MCR*	**152**	660	*MCR*	**206**	-160	*SHR*
45	-280	*SHR*	**99**	30	*MCR*	**153**	30	*SR*	**207**	30	*MCR*
46	660	*MCR*	**100**	700	*MCR*	**154**	20	*MCR*	**208**	30	*MCR*
47	-230	*SHR*	**101**	30	*SR*	**155**	30	*SR*	**209**	20	*MCR*
48	30	*SR*	**102**	150	*MCR*	**156**	680	*MCR*	**210**	110	*MCR*
49	30	*MCR*	**103**	30	*SR*	**157**	30	*MCR*	**211**	30	*MCR*
50	30	*SR*	**104**	30	*SR*	**158**	20	*MCR*			
51	30	*MCR*	**105**	150	*MCR*	**159**	30	*MCR*			
52	670	*MCR*	**106**	30	*SR*	**160**	30	*SR*			
53	30	*MCR*	**107**	30	*SR*	**161**	30	*MCR*			
54	300	*MCR*	**108**	490	*MCR*	**162**	30	*SR*			

(*) Insertion Depth for MCR and SR is measured from the Upper Edge of the Top Reflector. Insertion Depth for SHR is measured from Bottom of Reactor Core (negative values because SHR are bottom to top inserted)

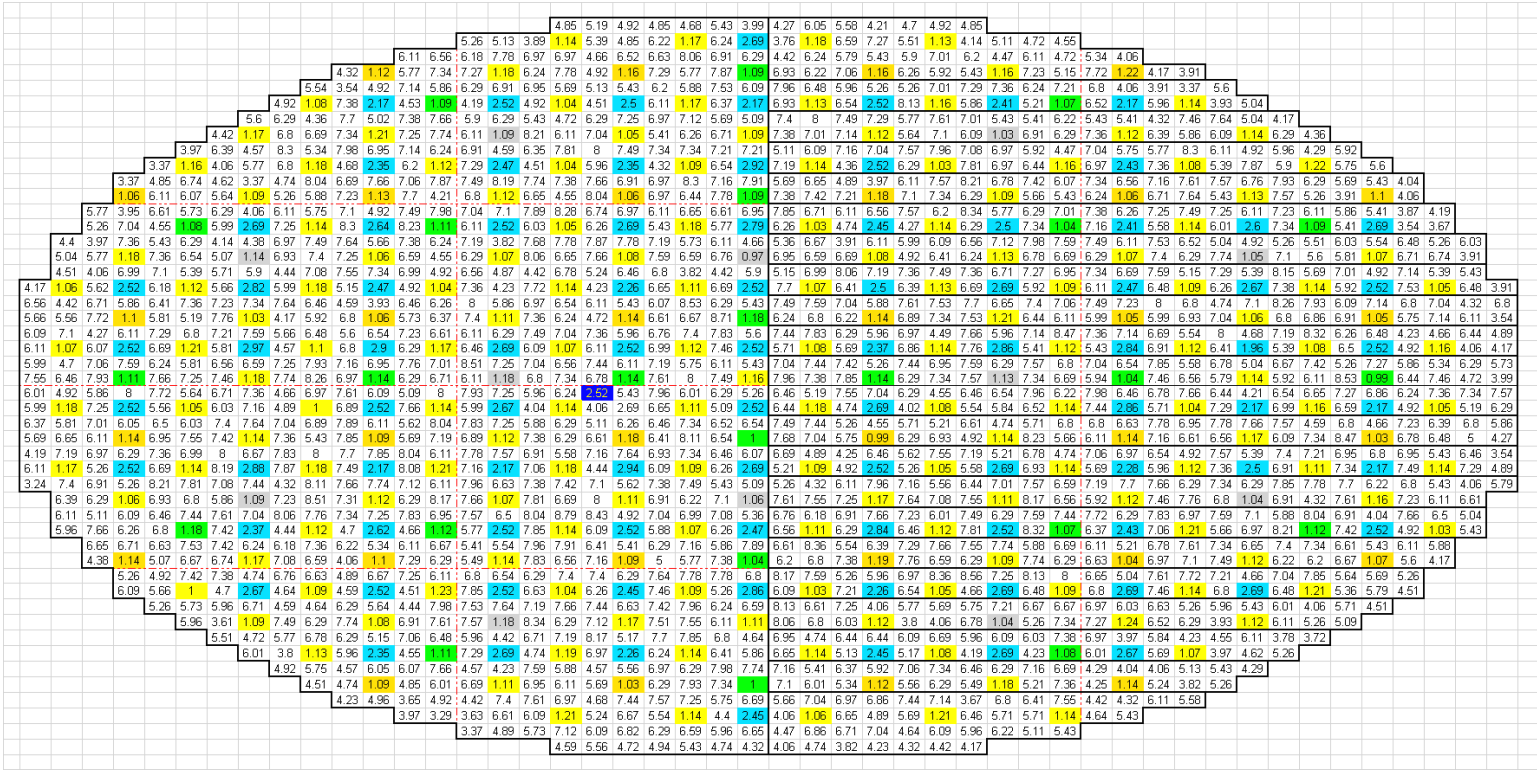

Fig. 36 – Core Channels Flow Map (Kg/s)

3. THE BACKGROUND FOR RBMK ACCIDENT ANALYSIS

One of the bases for the safety and the safety evaluations in NPP is constituted by the knowledge of phenomena that are envisaged following hypothetical transients and accidents. The present chapters introduces the safety of the RBMK starting from the expected phenomena.

Introductory general remarks are provided in section 3.1. The safety needs focused on the 'binding' acceptance criteria and the reasons for them are discussed in section 3.2. A more comprehensive description of expected physical phenomena and scenarios with connected relevant parameters is given in section 3.3.

3.1. The technological status for RBMK safety

3.1.1. The background

The safety of a nuclear power plant (NPP), understood as its capability to keep the radiation exposure of personnel and population within specified limits, is ensured by maintaining the integrity of safety barriers, which are part of the plant defense in depth concept. A series of barriers prevents the release of radioactive fission products from their source beyond the reactor containment and into the environment. In analyzing the NPP safety, it is essential to assess the integrity of these barriers and to decide to what degree the response of the whole NPP and its systems to a certain initiating event is acceptable from the viewpoint of the plant safety. For the sake of clarity, the integrity of the safety barriers is related to certain threshold values, which are referred to as acceptance criteria. Essentially these are the design limits for design basis accidents (DBA), adopted with a conservative margin so that the safety barrier integrity is guaranteed as long as the parameters do not exceed the relevant criteria.

Safety analysis for an RBMK NPP should assess the integrity of the following barriers in the path of radioactivity transport and release:

- Fuel matrix.
- Fuel cladding.
- Circulation circuit pressure boundary and, in particular, the components most susceptible to damage, namely fuel channel (pressure) tubes.
- Metal structures forming the reactor cavity.
- Structural components of the leaktight accident localization system (ALS) compartments and other compartments of the NPP housing circulation circuit pipelines.

Should any safety barrier fail, thus opening the pathway for the release of radioactivity beyond the plant boundaries, the amount of radioactivity and the population exposure should be assessed. Beyond Design Basis Accidents (BDBA) are analyzed for the following purposes:

- To assess the degree of reactor protection and the time available for taking countermeasures.
- To determine the emergency and other signals available to the operator for identifying the plant status and to devise appropriate accident management steps.
- To develop a package of organizational and technical measures (management strategy) for prevention and mitigation of the accident consequences.
- To assess the possible consequences as input information for planning protection of the population and personnel.

Related to BDBA analyses, according to the requirements of the Russian nuclear regulatory authority RosTechnadzor, both deterministic and probabilistic approaches should be used. Namely, according to requirements OPB-88/97:

- The estimated probability of an event with large release should be less than 10^{-7} within one reactor year.
- The estimated probability of severe reactor core degradation or melting should be less than 10^{-5} within one reactor year.

However, if some initiating events can lead to severe consequences and the inside features of reactor are not able to prevent this, accident mitigation means should be foreseen without drawing the attention to the probability of these events.

The deterministic approach for analysis BDBA is therefore also very important: this should be based on the method of postulating accidental conditions. The method is based on determination of connections between the plant conditions, level of severity of accident consequences, i.e. how many physical barriers are violated: fuel assembly including fuel pellet and fuel cladding, pressure tube, reactor cavity, Main Circulation Circuit (MCC), Accident Localization System (ALS) and availability of critical safety functions. According to the above requirements (OPB-88/97), a list of BDBA scenarios for further detailed investigations should be developed. The analysis results will be the basis for the development of the accident management program for RBMK reactors.

3.1.2. The relevant aspects

Because the RBMK comprises a pressure tube design with a number of unique features, the results of much Western work, mainly done for LWR on severe accidents, may not be directly applicable. Where work has been done on channel type reactors, there are always differences that make direct comparisons difficult. The main system characteristics can be summarized as follows (some of these also constitute differences between RBMK and other LWR systems):

1. The channel design; each fuel assembly is contained in a separate thermal-hydraulic environment.
2. The moderator is graphite; this has implications for structural performance and heat transfer. The graphite provides a very large heat sink and source and, as a result, slow core heating in case of hypothetical accidents

involving the loss of all heat removal systems and additional heat supply to pressure tubes following core cooling.

3. RBMK reactors have a large core, where local effects may have a significant role in safety analyses of the several initiating events (e.g. blockage of one hydraulic channel).
4. The MCC is divided into two symmetric loops; a pipe break in one of these directly affects the thermal-hydraulic and neutron kinetics behavior on one side of the core. The resulting asymmetry in reactivity and power has to be assessed by three-dimensional codes.
5. The accident localization system design has important implications for accident management and fission product retention under accident conditions involving radioactivity releases from the fuel.
6. Redundancy of safety system components gives very low probability of severe accidents.

Evaluating the unique features of RBMK reactors specific phenomena should be reflected in the modeling of transients. These phenomena are described below.

- The spatial feedback between the neutron intensity, the fuel temperature, the graphite temperature, and the coolant void fraction (coolant density) in the core and in separate fuel channels shall be considered. To fulfill this condition a 3D-space dynamic neutron kinetics code shall be coupled with a thermal-hydraulics code and properly qualified. The coupled code must also feature high computational speed and stability.
- The specific thermal-hydraulic processes in the primary circuit and the reactor core. At first, the thermal-hydraulic processes in the reactor channels (pressure drop, relative motion of phases, counter-current flow, reflood) should be considered. The abstract ‘reactor channels’ implies the fuel channels, channels in which the reactor control rods are placed and the instrumentation channels. The reactor core model should include the following types of processes (some of these are typical processes for a boiling channel in a BWR):
  - Heat transfer prior to the onset of critical heat flux (CHF). Heat transfer under steady state conditions and transients.
  - Critical heat flux. Sharp decrease of heat transfer from fuel elements to coolant (high L/D value typical of the RBMK channel, i.e. much higher than in the case of BWR).
  - Post-CHF heat transfer (heat transfer to coolant after the CHF onset, same note as above applies).
  - Radiation heat transfer. Radiant heat transfer through layer of the saturated steam–water mixture or superheated steam between fuel elements and fuel channel (FC) wall (the relevance of this process upon the overall scenario should be checked, at least by sensitivity studies).
  - The heat transfer in radial direction between the pressure tubes and the graphite stack through the gaps and bushes and the heat transfer between neighboring graphite columns should be considered.

- The specific natural circulation in the MCC that takes place after the main circulation pump (MCP) shut-off and coast-down should be considered, namely:
  - During transients, after reactor shutdown, natural circulation of the coolant provides adequate cooling of the reactor.
  - During loss of coolant accidents (LOCA) breakdown of natural circulation due to flashing in the down- comer piping may occur.
  - Analogously, during accidents involving the opening of the main safety valve, breakdown of natural circulation might occur due to failure of the valves to close.
- The specific phenomena in drum separators of RBMK should be considered:
  - The boiling and condensation in the drum separator (DS). The structure and dynamics of the coolant flow in the DS varies with changes of pressure and feed-water supply.
  - Separation and water entrainment from DS into steam lines. The phenomenon is typical for regimes with considerable level increase above submerged perforated plate.
  - Steam entrainment into down-comers. The phenomenon is typical for regimes with considerable decrease of total collapsed level and pressure in DS.
- During the analysis of LOCA-type accidents the modeling of the coolant discharge from the circulation loop break is important. Sub-cooled liquid, two-phase mixture and steam flows are involved. Modeling of possible internal critical sections (e.g. at the abrupt geometric discontinuities of the long pipelines connected with the FC) is also important.
- Occurrence of thermal-hydraulic instabilities following LOCA, connected with the (large) number of parallel channels and the (high) value of the L/D for individual channels, should be investigated.
- The flow instability in parallel steam generating channels is relevant in RBMK. This can take place both at forced and at natural circulation conditions. Under such oscillations the cladding temperatures can reach unsafe values.
- During the analysis of LOCA-type accidents the coolant through the break is discharged into the compartments of the Accident Localization System (ALS), unless the accident is constituted by the break of the FC (see below). In the former case, other than the modeling of pressure and temperature behavior inside the Reactor Cavity (RC) and the ALS, the generation-transport-accumulation-distribution of H2, fission products and products of the physical and chemical reaction between graphite and primary system coolant shall be considered.
- In case of fuel channel rupture, the steam–water mixture is discharged into the reactor cavity. The calculation of the venting capacity of a damaged core, including the local phenomena which may have an impact on the temperature and pressure transient in the reactor core cavity (mixing of He-N2 mixture with flashing steam, evaporation of discharged water, heat transfer from the graphite, liquid carry-over through the break, etc) shall be performed.

Overheating of pressure tube (PT) in the case of “fuel assembly power – coolant flow rate mismatch” at high pressure in the fuel channels is the most probable reason for fuel channel failure. Three known single FC failures in RBMK reactors (Leningrad NPP [LNPP] in 1975, Chernobyl NPP [ChNPP] in 1982, LNPP in 1992) occurred as a consequence of the pressure tube overheating mentioned. The assessment of PT rupture due to accidental overheating is the key element of RBMK safety analysis.

Combined calculations of fuel assembly, pressure tube, and graphite stack behavior under accident conditions with channel voiding show that, up to the moment of pressure tube rupture, the fuel rod cladding may reach a very high temperature, in some cases approaching the melting temperature (of the cladding). In such conditions fuel clad oxidation (H2 production), fuel melt and rod deformation can be expected. The PT rupture is possible owing to the combined effect of high temperature and pressure. Following PT rupture, hydrodynamic forces acting on the fuel assembly during the break and caused by the escaping steam–water mixture into the reactor cavity may lead to further fuel rod failure and to failure of the fuel assembly.

As an example of such a situation, the accident at unit 3 of LNPP in 1992 may be considered. The decrease of coolant flow through the individual control valve at nominal power happened and caused overheating of the channel, its rupture and graphite stack destruction. The accident investigation showed that the pressure tube rupture took place at the channel power of 1.94 MW, pressure about 7.0 MPa when temperature of the channel reached 650°C. Examination of the central stringer of the fuel assembly gave the evidence that the stringer material was heated up to 1200°C.

In the case of heating up of a FC thermal mechanical behavior of fuel assembly should be considered to wit elongation of fuel rods and hanger, inter action of fuel rods having pressed out claddings with stringers and hanger, possible bowing of assembly due to azimuthal temperature irregularity, steam-zirconium reaction, possible formation of low temperature eutectics.

On the basis of the results obtained in the experimental study of deformation and rupture of regular (i.e. full scale) PT and scaled PT mock-ups, as well as from inspection results after the incidents involving PT rupture at ChNPP and LNPP, it has been ascertained that the process of PT deformation from the start of accident heating to the moment of rupture can be subdivided into three stages:

Stage one: regular axial-symmetric ballooning of the tube up to the moment of closing all the gaps in the system PT – slit graphite rings – graphite blocks.

Stage two: the pressure load of the FC is partly released to the graphite rings and graphite blocks. Joint deformation of the tube, rings and blocks and tube material causes “pouring” into the slits of graphite rings. As a result, one or several radial cracks appear on the internal surface of the blocks under the influence of the ballooned PT. Their propagation results in graphite blocks destruction.

Stage three: the deformed PT comes in contact with fragments of the graphite rings and blocks and under the conditions of high temperature (caused by coolant overheating and possible contact between clad and FC walls) and high pressure (the system pressure is, typically, not affected by an event occurring in a single FC or limited to a small number of FC and keeps its nominal value) swells up to the tube rupture. Hydraulic loads cause fuel fragmentation and transport across the PT rupture. Under the influence of differential pressure loads the gap space between adjacent graphite stacks tends to increase.

When deriving the model of stress-strain state of a pressure tube, it is assumed that the deformation process at the first and third stages takes place with keeping of the axial symmetry. The deformation at the second stage is assumed to be close to zero, which is justified by the low plasticity of graphite blocks. The irradiation level of the graphite has a role at this stage.

Possible deformation of the pressure tubes in the RBMK core will occur in interaction with the graphite stacks. Analysis of tube ruptures taking into account the constraints provided by the graphite block and results of inspections after the channel rupture at LNPP and ChNPP suggest that under full pressure the graphite blocks cannot withstand the forces caused by PT ballooning and hence break.

For a pressure exceeding 4.0 MPa the failure criteria for tubes with graphite do not differ from the general pattern of data obtained under conditions of free-standing tubes. Therefore, the failure criteria of PT obtained largely in the experiments without graphite can be used for the evaluation of PT failure in case of accidental over heating under pressures exceeding 4.0 MPa. Under FC-pressures lower than 4.0 MPa the graphite blocks can prevent the PT rupture.

When the pressure tube ruptures, coolant discharges into graphite stack where it flashes and residual water evaporates on hot surfaces. The relationship between steam sources and sinks determines the reactor cavity (RC) pressure history in this case. Steam sources are steam–water mixture discharge from the ruptured FC and liquid phase evaporation on hot surfaces of graphite and metal in the reactor cavity. Steam sink is provided first of all by steam dumping via the reactor cavity venting system (RCVS) pipelines to the ALS and to the environment (RC-SRV). Some steam may condense on cold surfaces of pipes of the RCVS.

Large coolant discharge into the stack may cause essential displacement of core components under the influence of the forming pressure field, which produces complex deformations with gaps growth in some areas (e.g. around the broken PT) and reduction in others (neighboring FC). The following phenomena have to be analyzed for the pressure tube rupture accident:

- Flow regime and heat exchange in non-equilibrium two-phase flow conditions in the circulation loop (MCC), inside the graphite stacks and outside the stacks, before and after the PT rupture.
- Deformation and rupture of pressure tubes and fracture of graphite blocks due to overheating.
- Oxidation of fuel pins with H2 production and possible melting of the UO2.

- Deformation and destruction of fuel pins and fuel assembly owing to hydraulic and thermal loads.
- Release of fuel gap radioactive gases and fuel particles into the coolant (FP source term into the FC): FP transport and physical and chemical interactions between steam–water mixture and graphite.
- Displacement and deformation of graphite stack elements as a result of loads caused by PT rupture.
- PT zirconium and graphite oxidation leading to generation of hydrogen and hydrocarbons.
- Operation of the reactor cavity venting system and accident localization system.
- Transport of radioactive fission products from the FC to the RC (or gaps among the graphite stacks) and finally to the ALS.

The estimation of the possible evolution of a single FC failure (i.e. PT rupture) toward the Multiple Pressure Tube Rupture (MPTR) should be performed. This implies the evaluation of the structural-mechanics resistance of parallel stacks of graphite bricks and PT, following bending loads orthogonal to the PT axis, as a function of the PT position inside the core. The resulting 'resistance' loads shall be compared with differential pressure loads caused by the release (through the PT rupture) of MCC fluid and consequent thermal-hydraulic interactions with graphite.

3.2. The safety needs

Activity in the field of RBMK safety research including the identification of safety limits covers the entire history of RBMK design and operation. Obviously, one can split this activity into two parts: before 1986 and the post-Chernobyl era.

Parameters of steady state operation under nominal conditions were the main purposes of the work during the first twenty years of RBMK technology (i.e. in the pre-Chernobyl era). The steady state experiments concerning thermal-hydraulic problems of the core (FC) were accomplished mainly by the Kurchatov Institute on its KS facility (full-scale electrically heated 18-pin fuel channel model). Correlations for heat transfer in the bundle, pressure drop, CHF, post dry-out modes, critical discharge data, etc., were obtained at that time. Some aspects of these problems were then investigated at the reactor vendor organization (NIKIET) on its BM facility (seven-pin electrically heated model), including pressure drop and void fraction distribution. In the same period, phenomena of a dynamic nature were also addressed: experiments were performed concerning accident conditions, including ECCS injection and FC quenching and multiple channel stability (one- and six-channel loops of the facility #108 at EREC).

After the Chernobyl accident efforts were devoted to the investigation of the dynamic nature of RBMK: improved 3-D codes for neutron kinetics were developed, new facilities were constructed and instrumentation on existing ones was essentially enhanced to provide good conditions for fine dynamic experiments. Data were obtained related to the following problems: steam binding and counter-current flow limit (KS semi-scale facility), flow blockage in the channel and

overheating (KSB facility, RRC KI), low-pressure steam condensation in the outlet feeding pipe and FC ('PWK tube' facility at NIKIET) and some others. Interesting and informative experiments were accomplished at RBMK NPP sites. New facilities (e.g. PSB RBMK) have been constructed at EREC.

Thus the methods for accident analysis as well as the basis for acceptance criteria have been considerably improved during the last two decades due to a better insight into the physical phenomena through experimental research, enhancement of the computer codes and computational capabilities. These improvements have made it possible to switch from simplified codes to more sophisticated and mechanistic integral system codes. The ongoing improvements in computer capabilities have removed the main constraint of computational tools. In this context, the use of advanced coupled 3-D neutron kinetics and thermal-hydraulic codes is of utmost importance.

The accident analysis should demonstrate that parameters (acceptance criteria) defined by the designer and the regulatory authority must not be violated during accident events. Also the evaluation of the adequacy of the safety system design involved in the occurrence shall be based on the comparison of these limits with the calculation results.

The calculations can be provided using 'conservative' or 'best estimate' approaches. Now the trend in accident analysis has continued to move to best estimate approach. If this approach is used, the code and model uncertainty should be evaluated. Code predictions are uncertain due to a number of uncertainty sources, e.g. code models, initial and boundary conditions, plant state, scaling and numerical solutions algorithm. As it is shown in Fig. 37, [12], usually the best estimate approach gives the lower calculated values in comparison to conservative approach. The conservative approach does not give any indication of the actual margins between the actual plant response and the conservatively estimated response.

By contrast, the uncertainty estimate provided in the best estimate approach is a direct measure of such margins. As a result, the best estimate approach may allow for the elimination of unnecessary conservatism in the analysis and may allow the regulatory body and plant operating organization to establish a more consistent balance for a wide range of acceptance criteria.

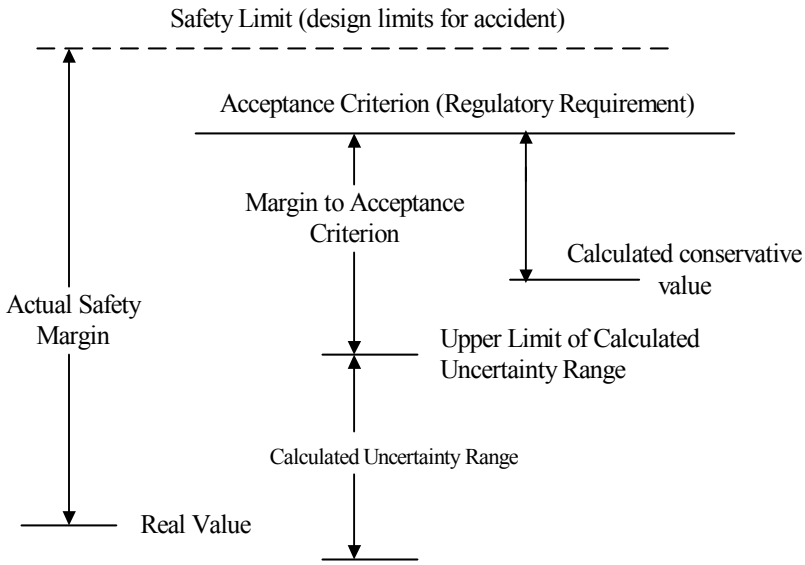

Fig. 37 – Best estimate and conservative safety analysis: definitions of acceptance criteria and safety margins, [12].

However for some cases, conservative modeling approaches could be used (to a large extent in analysis of DBA, for example) simply to avoid the cost of developing a more realistic model, even though conservative models are not specified by regulation. In this case, the conservative models are selected and evaluated on a case by case basis.

For both cases, 'best estimate' or 'conservative', it is necessary to distinguish two groups of limits: the safety limit and the acceptance criteria. The safety limit is a critical value of an assigned parameter associated with the failure of a system or a component. The acceptance criterion is the quantitative limitation of selected parameter or qualitative requirement set-up for the results of accident analysis. The specific safety limits and acceptance criteria for RBMK plants are presented below, together with selected (not-systematic) recommendation for evaluating safety margins corresponding to those criteria.

3.2.1. The RBMK acceptance criteria

The IAEA guidance at [13] deals with the RBMK acceptance criteria and was issued when the present report was completed. The content of this section reflects and summarizes the content of the mentioned IAEA guidance.

3.2.1.1. Fuel clad integrity

For the integrity of fuel claddings to be confirmed it is essential to ensure that the following maximum values of fuel rod parameters are not exceeded:

- Pellet volume – average fuel enthalpy of 710 kJ/Kg.
- Cladding temperature of 700 °C.

If the above mentioned acceptance criteria are exceeded, the safety limit on fuel melting temperature should be checked:

- Fuel temperature of 2800 °C.

Additional analysis for design basis accidents has to demonstrate that the cladding temperature, does not exceed the 1200 °C safety limit and the local depth of fuel cladding oxidation should not exceed 18% of the original thickness.

The additional analysis should also confirm the compliance with the requirement that the mass of zirconium cladding that reacted with steam should not exceed 1% of the total mass of fuel claddings in the core. This sets a limit to the release of hydrogen into the ALS.

3.2.1.2. Fuel channel integrity

It was agreed that for normal operation and with the re-tubing approach adopted in Russia (complete reactor re-tubing at a certain power production level, due to uncertainties in material properties and fabrication tolerances when local gas gap closure occurs), no fuel channel degradation mechanisms have been identified that could influence the fuel channel integrity.

The computational assessment of the pressure tube integrity in thermal-hydraulic and thermal-mechanical codes uses various experimental high temperature failure criteria: rupture temperature versus channel pressure (temperature criterion), rupture strain versus tube temperature (strain criterion), rupture stress versus tube temperature (stress criterion) and rupture strain power versus tube temperature (energy criterion).

The temperature failure criterion in the form of the tube rupture temperature T_{wr} dependence on the channel pressure is given in Fig. 38. The data are classified by the heating rates, the experiments with graphite blocks are marked with black symbols. The shaded region covers all combinations of T_w and p parameters in case of rupture. At higher heating rates the values of rupture temperature (dark-gray region) proved to be higher than the values obtained for low rates (light-gray region).

An energy criterion may be adopted for the thermal-mechanical code employed for calculating the deformation and for assessing the pressure tube integrity under accident conditions as shown in Fig. 39. This criterion is a specific rupture strain

power j_i (W/Kg) which is determined through the stress intensity σ_i, the material density ρ_w and the strain rate intensity ζi:

$$j_i = \frac{\sigma_i \zeta_i}{\rho_w}$$

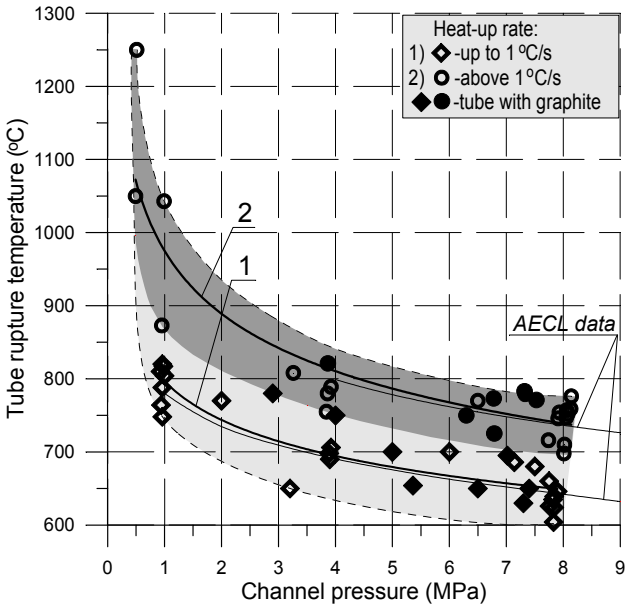

Fig. 38 – Pressure tube rupture temperature versus internal pressure

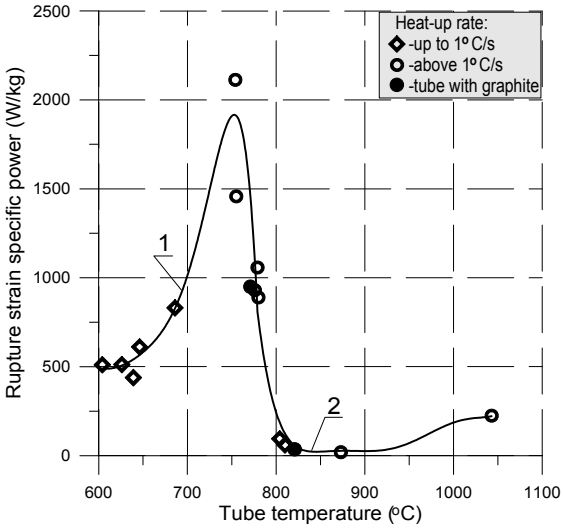

Fig. 39 – Specific rupture strain power as a function of tube temperature.

Simplified acceptance criteria can be used. If the following criteria are not exceeded the integrity of the pressure tubes will be maintained (see Fig. 38):

- Maximum fuel cladding temperature is less than 700°C.
- Maximum fuel channel pressure tube temperature less than 650 C.

Multiple pressure tube rupture sequence is a BDBA. In this case, the potential hazards are loss of the reactor cavity integrity and damage of metal structures of the reactor. To define the scope of MPTR beyond which the threat of reactor cavity destruction lies, it is necessary to perform analysis of the venting capacity of the system for reactor cavity protection against overpressure. The results of this analysis are useful in assessing the consequences of the beyond design basis accident leading to MPTR.

Events leading to multiple pressure tube rupture have received considerable attention in safety evaluation of RBMK, since they might develop into extended FP releases. Studies performed so far by Russian specialists indicate that the probability of such events is very low.

The partial break of a group distribution header was identified as a potential precursor for the MPTR. The present Project aims, among the other things, at establishing the realism of the MPTR as a consequence of identified precursor events, the reference one being the single channel blockage and the consequent (single) PT rupture.

3.2.1.3. MCC integrity

Various MCC sections are capable of withstanding different maximum (or design) pressures.

The MCC section between the gate valves of the MCP inlet pipes and the gate valves at the group distribution header (GDH) inlets, which can be shut off by isolating valves, can tolerate the greatest pressure. The permissible hydraulic test pressure at this section is 13.4 MPa.

Fuel channels are also tested under 13.4 MPa. The hydraulic test pressure adopted for the remaining MCC components, which is determined primarily by the strength of drum separators and steam lines, ranges from 10.1 to 10.4 MPa.

Since the MCC operates as a single system, the last of these values should be taken as an acceptance criterion.

3.2.1.4. RC integrity

The reactor cavity is formed by three metal structures: the top plate, the bottom plate and the barrel with a thermal expansion compensator. The barrel is hermetically welded to the top and bottom plates. The excessive pressure of 300 KPa in the reactor cavity may be regarded as a less conservative, ‘realistic’ criterion of reactor cavity failure. But more conservative value of 214 KPa is

adopted in analyses of the design basis accidents (in the case of Smolensk 3 NPP it was found that RC-SRV open at 277 KPa, [14]).

It was repeatedly shown in previous RBMK safety analyses that none of the design basis accidents would lead to MPTR, as already mentioned. Should analysis of any beyond design basis accident encounter a sequence of events with the ensuing rupture of more than one fuel channel, and if the MPTR extent can be determined, in such a case by analyzing the maximum capacity of the reactor cavity venting system (RCVS) it is possible to assess the reactor cavity integrity, i.e. the likely structural and mechanical consequences of such BDBA.

The methodology for assessing the venting capacity of the system involves modeling of the system thermal-hydraulics for an MPTR with various boundary conditions. The parameters conservative from the point of view of the maximum venting capacity should be selected based on phenomenological analysis. The ranges of possible variations of such parameters should be validated. Consideration should be given to the parameters affecting the flow rate of steam entering the stack and to the steam generation in case of pressure tube ruptures as well as to the parameters that influence the rate of steam venting from the reactor cavity under various boundary conditions.

Phenomenological analysis of the effect of various parameters on the maximum venting capacity allows classifying them into key parameters and those of secondary importance. Variation ranges are determined for the former, while the latter have the 'worst' values set for them, i.e. the values detracting from the maximum capacity of the RCVS.

The maximum venting capacity should be defined in terms of the number of broken pressure tubes with the resultant pressure in the reactor cavity, considering the venting capacity through the RC-SRV. The parametric results should demonstrate compliance with the acceptance criteria. Analysis of the maximum venting capacity should determine the dependence of the number of broken tubes on such a crucial parameter considering the RC-SRV.

3.2.1.5. ALS integrity

Accidental release upon a break in a circulation circuit pipe will be confined in a system of leaktight compartments equipped with devices for emergency steam condensation (pressure suppression system). However, the ALS does not cover all the circulation circuit pipes. Upper regions such as steam–water lines, the top part of the down-comers, equalizing pipes of the drum separators, and all the steam lines are found outside the ALS, in compartments designed to general building standards and rules. This means that these compartments afford no leak-tightness and are not nearly as strong as most of the ALS rooms. Analysis of the integrity of the ALS and other compartments of a power plant is an essential requirement of the safety analysis of NPP for all design basis accidents and beyond design basis accidents.

The maximum permissible pressures in compartments for MCC pipes and components and for ALS are reported in Tab. 10, [13]. Among the RBMK plants of the second generation, two different ALS configuration can be identified. Namely:

- At Leningrad 3 & 4 and Ignalina 1 &2, the system for condensation of accidental steam is housed in accident localization towers (ALT).
- At the other power plants, the system is found at lower elevations of the main building. In the case of a coolant leak, pressure relief in the ALS relies on passive condensing devices, i.e. pipes submerged under water on two decks of the PSP.

Leaktight compartments of Smolensk 1 and 2 and Kursk 3 and 4 have safety valves with an opening pressure difference of 270 KPa. Opening them allows the steam and gas mixture to be vented from the ALS to the atmosphere. The ALSs at Leningrad 3 and 4 and Ignalina 1 and 2 operate in this different manner: in the case of MCC pipe breaks inside leaktight compartments or in DGH-LWL compartments, the steam and gas mixture will be vented into the ALT via a steam discharge passage. With pipe breaks in the upper part of the circuit (DS compartment or the space above the reactor), excess steam will be vented directly to the atmosphere.

Tab. 10 – RBMK generations.

RBMK reactors	Generation
Leningrad 1 & 2	I
Chernobyl 1^{+} & 2^{+}	
Kursk 1 & 2	
Leningrad 3 & 4	II A
Ignalina 1^{+} & 2	
Chernobyl 3^{+} & 4^{+}	
Smolensk 1 & 2	II B
Kursk 3 & 4	
Smolensk 3	III
Kursk 5(*)	

($^{+}$) permanently shut-down; (*) under construction

Tab. 11 – ALS evolution in the various RBMK generations (see Tab. 10) and acceptance criteria

Compartment with MCC components	Permissible (excess) pressure (kPa)			
	Generation I	Generation II		Generation III
		A	B	
MCP pipes, suction and PH	40			
GDH, LWLs	40.0	80	80	80
SWL, SD, DC & SL	25			
DC	40			
Leaktight compartments		300	440 (270)	440 (270)
Steam distribution passage		80 (300)*	440	440
Air space of PSP			440	440
Air space of the enclosure			440	
Central Hall		2 (5)*	5	5.0
SD and space above reactor		25	25	25.0
Accident Localization Tower		80		

(*) Number in brackets refer to Ignalina 1 & 2

The ALSs of these units have two major distinctions from their counterparts at plants of the second generation: they have no enclosure to receive steam and gas from the reactor cavity and their PSP has only one elevation.

However, the ALS may loose its function of a safety barrier at a lower excess pressure due to opening of safety valves in the leaktight compartments, whereupon a radioactive release may occur at upper elevations of the reactor building.

The leaktight compartments and the air space of the PSP may suffer overpressure during LOCA with failure of the PSP cooling system (loss of ultimate heat sink), when steam condensation in the pool water is less effective at water temperatures exceeding about 85° C.

Therefore, either the maximum permissible water temperature (for example < 85° C) or the operating pressure difference of the safety valves may be adopted as an acceptance criterion for the PSP.

Hydrogen ignition is also a threat to the ALS integrity. The maximum permissible hydrogen concentration in any single ALS compartment is taken equal to 4% by volume in the analysis. Should this criterion value be reached, H_2 flammability must be comprehensively assessed, taking into consideration the time dependence and the characteristic boundary conditions of the accident scenario for the ALS.

3.2.1.6. The permissible radiation doses

According to the rules laid down by the national nuclear regulatory authority, the consequences of a DBA should never result in any population exposure that would

require any countermeasures to protect the people in the early period of the radiation accident.

The early phase (initial period) of an accident covers the time from its beginning to the time when the atmospheric release of radioactive substances is arrested. This period is assumed to be up to ten days. According to national regulatory requirements, the dose limits below which no urgent decisions have to be made during the early period of a radiation accident are:

- 0.5 cSv (rem) for the whole body.
- 5.0 cSv (rem) for the thyroid.

The design radius of the control area around an RBMK NPP is 3 km.

The main pathways of radiation effects on the population during this period are:
- External γ and β irradiation during the passage of the radioactive cloud.
- Internal irradiation through inhalation of radioactive substances.

The permissible radiation doses in DBA analysis should be confirmed with the following conservative assumptions:
a) The radioactive release to the environment is a single event of short duration, and the release height is equal to the source altitude above ground level.
b) The plume rise due to its buoyancy is disregarded.
c) The radiation doses are calculated for the worst weather conditions and for the specific elevation of the release source, with the wind speed and atmospheric conditions producing the greatest possible near ground concentrations of radionuclides.

According to national regulatory requirements, the probability of large radiological release for BDBA should be less than 10^{-7} per reactor-year.

3.2.2. Recent requirements by RosTechnadzor pertaining to BDBA analysis including SA

The concept of management of BDBA was finally generated in Russia after Chernobyl accident as an additional fourth level of in-depth safety barriers of the nuclear power plant. As a result, the concept of a 'beyond design basis accident' has appeared, i.e. an accident caused by initial events that have not been taken into account or accompanied by beyond additional single failures of safety systems in comparison with design basis accident, realization of erroneous decisions of the personnel which can lead to severe damages or melting of the reactor core. It is natural that consequences of such accident can be much severe, than at design basis accidents.

Management of BDBA according to [15] constitutes the envelope of the actions directed on prevention of development of DBA into BDBA and on mitigation of consequences of BDBA. For this purpose any technical means available in an

efficient condition intended for normal operation and providing safety at design basis accidents or for mitigation of consequences at beyond design basis accidents can be used. All these actions and special means form the mentioned above fourth level of in-depth safety barriers.

ОПБ-88/97 [15] — the Russian regulating document of the maximum conceptual level of hierarchy — defines the concept of safety accepted in Russia today. It was developed after the Chernobyl accident simultaneously with the IAEA document INSAG-3, [16], reflecting the modern concept of safety at the international level. As the comparative analysis of these documents performed by special consulting IAEA group in the report [17] has shown, the concept of safety reflected in ОПБ-88/97 basically corresponds to a modern international level.

The concept of beyond design basis accidents accepted in Russia is most completely reflected in ОПБ-88/97. In other normative documents of Russia it is supplemented only with some more specific requirements. The concept is based on the requirement of restriction of radiation influence at the BDBA level by employing of measures on their management and realization on a site of the nuclear power plant and surrounding it area of actions on protection of the personnel and the population. These measures are part of in-depth safety barriers and in item 1.2.3 ОПБ-88/97 are specified into detail.

For some BDBA, the level of restriction of radiation influence is caused by criterion of the radiation safety, established in the document [18] determining the requirements on layout of the nuclear power plant. This criterion limits so-called limiting emergency discharge at beyond design basis accidents so that irradiation doses of the concerned population (critical group) on the border of the zone of planning of protective actions and outside did not exceed 5 mSv for all body and 50 mSv for separate organs in the first year after the accident.

According to the requirement of item 1.2.17 ОПБ-88, the probability of limiting emergency discharge should be lower 10^{-7} on reactor in one year. It is necessary to avoid evacuation of the population located outside the specified zone of planning anti-emergency actions. If the given requirement is not achieved, additional technical measures on management of BDBA for mitigation its consequences should be accepted (first principle based on probability).

The second principle (item 1.2.14 ОПБ-88/97) establishes for any hypothetic (including BDBA) event that, on the basis of intrinsic features of the NPP or in case any AM procedure is not applicable, the development of measures on management of this event must be provided irrespective of its probability.

Additional means and strategies useful for the management of BDBA are discussed in ОПБ-88/97.

The Russian regulatory requirements regarding the mandatory execution of suitable probabilistic safety studies of nuclear power plants is defined by item 1.2.16 ОПБ-88 where PSA level 2 analyses are specifically mentioned. The IAEA recommendations of INSAG-6, [19], continue to remain valid.

In the mentioned regulatory documents it is recognized that lists of beyond design basis accidents cannot be developed only on the basis of probabilistic criteria. The application of deterministic principles and approaches is necessary, as outlined below.

Deterministic safety analysis is based upon the method of “postulated initial event” and the principle of “single failure” with the definition, for each accident, of meaningful sequence of events (i.e. DBA) and calculation transient scenarios and radiological consequences. This approach in essence is systematic and provides the necessary completeness and reliability for the safety analysis.

For beyond design basis accidents such an approach cannot be applied. BDBA arise at beyond design initial events or at occurrence of additional failures beyond the postulated “single failure”. As a result, the number of possible scenarios of beyond design basis accidents is practically unlimited. Therefore the possibility of application of the event-based approach for the management of BDBA shall be excluded. Rather BDBA management should be based on a symptom approach.

Levels of severity may characterize symptoms of BDBA conditions and are connected with the damage (or damage rate) of physical barriers and with the possibility of fission product release to the environment the on a way of release of radioactive products into an environment. For the nuclear power plants with RBMK reactors such barriers are fuel element, including a fuel matrix and cladding, fuel channel tube, bounds of reactor cavity, bounds of coolant circulation circuit and the leaktight protection of the reactor (reactor building). For the nuclear power plants with VVER reactors instead of fuel channel tube and bounds of reactor cavity, the reactor vessel is considered.

BDBA symptoms not related to any specified scenarios shall be adopted for the transition from DBA emergency (i.e. the domain of EOP) to the BDBA emergency (i.e. the domain of AM). The formation of a scale of emergency conditions and the possibility of their identification is rather essential. If any BDBA emergency condition cannot be identified, it should be excluded from the consideration for the planning of countermeasures.

The management of any emergency condition requires the identification and management of certain safety functions which performance could stop the further development of the accident (i.e. preventing transition of the given emergency condition to another with the higher level of severity), thus making possible to improve the starting emergency condition. Such safety functions can be named as critical.

Therefore, alongside with levels of severity of (BDBA) emergency conditions, the symptoms related to them and the critical safety functions should be determined.

In this way the entire set of considered BDBA emergency conditions is not defined in an objective way, but depends on our choice, so the selected BDBA emergency conditions can be considered as postulated. Making the analogy with the DBA conditions, where the method of "postulated initial event" is adopted, in the case of BDBA the method of "postulated emergency conditions" can be adopted.

For the development of manuals on management of BDBA it is necessary to define time and parametrical frameworks of occurrence of postulated emergency conditions (i.e. characterizing the concerned BDBA), in order to address the actions of operators, to establish diagnostic and functional priorities for each level of severity and to form a set of general functional instructions connected with the status of the relevant (and critical) safety functions. For this purpose it is necessary to execute detailed analyses of some characteristic BDBA scenarios. As a result from the above task, suitable lists of BDBA postulated emergency conditions shall be developed together with the corresponding symptoms and critical functions.

It shall be emphasized again that in this context, the development of the lists of BDBA (including the related predicted scenarios) play an important, but an auxiliary role. Definitely, the BDBA in the Russian normative documents is treated the same as the DBA i.e. a combination of deterministic and probabilistic approaches that meet the modern practice standard in the world is recommended.

3.3. Identification and characterization of selected RBMK accident scenarios and phenomena

The detailed analysis of phenomena relevant for the transient scenarios that constitute the objective of the PhD thesis are discussed hereafter. Then, in the following chapters of this document, details are given about results of codes and methods applications that have been achieved within the present framework and are connected with the quantities that control the concerned phenomena or transient scenarios.

Hereafter, introductive remarks are provided that also characterizes the state of the art in the knowledge of those RBMK accident scenarios and phenomena prior to the execution of the PhD activities. Most of the information is taken from documents issued within TACIS Project R2.03/97, [20]. References listed in this report are relevant for the characterization of RBMK scenarios.

3.3.1. Thermal-hydraulics of PS

The RBMK is a water cooled reactor. Therefore, transient phenomena studied for LWR are also supposed to be applicable in RBMK conditions. However, attention should be paid to the relevant range of parameters that can be largely different in LWR and RBMK situations. Typical examples are constituted by the length of the core active region, almost twice the value that characterize BWR, the presence of long (L/D >> 100) pipes at the inlet and the outlet of FC and of large volume (> 50 m^3) steam drum. All of this has large influence upon the nominal conditions pressure drop across the loop, upon the LOCA depressurization and upon stability

performance. An overview of key-subject and of phenomena taken from the validation of the Korsar code can be found in Tab. 12, [20]. The application of the table-of-phenomena approach is well established in nuclear reactor safety (e.g. including code validation), following the pioneering study performed by OECD/CSNI at the end of '80s, [21], [22], [23]. In the present case it also gives an idea of different relevance of thermal-hydraulic phenomena in the cases of VVER and RBMK. More detailed RBMK thermal-hydraulic phenomena can be found in Tab. 13, [20].

Tab. 12 – List of key-subjects and phenomena utilized for the assessment of Korsar code and comparison between VVER and RBMK.

Key-Subject	Phenomena	VVER	RBMK
Reactor kinetics (Point model)		R	R
Reactor kinetics (Spatial model)		R	R
Modeling of liquid absorber		R	N/A
Modeling of non-condensable gases	Non condensable gas	R	R
Critical discharge of the coolant	Break flow	R	R
Flow regimes in reactor core, core heat transfer (in the rod assemblies)	Core sub-critical heat transfer	R	R
	Core critical heat transfer	R	R
	Core supercritical heat transfer	R	R
	Quench front formation and propagation	R	R
	Radiation heat transfer	R	R
	Flooding of counter-current flows of water and steam in vertical channels	R	R
	Reflood	R	R
	Heat transfer in radial direction between different heat structures	N/A	R
Flow regimes and heat transfer in the steam generating channels	Sub-critical, critical and supercritical heat transfer	R	N/A
	Quench front formation and propagation	R	N/A
	Radiation heat transfer	R	N/A
	Counter-current flow	R	N/A
	Reflood	R	N/A
	Steam–water–gas mixture flow and heat transfer in reactor cavity	N/A	R

Tab. 12 (cont.) – List of key-subjects and phenomena utilized for the assessment of Korsar code and comparison between VVER and RBMK.

Key-Subject	Phenomena	VVER	RBMK
Flow regimes in reactor cooling circuit	Stratification of the two-fluid flow in the horizontal channels	R	R
	Natural circulation	R	R
	Separation of phases in tees	N/A	R
	Steam condensation during ECCS injection	R	R
	Counter-current water–air flow through perforated plates	R	R
	Flashing and condensation in DS	N/A	R
	Two-phase pump behavior	R	R
Severe accident propagation	Fuel melting and relocation	R	R
	Zirconium–steam reaction	R	R
	Steam–graphite interaction	N/A	R
	Fuel melt – pressure tube – graphite interaction	N/A	R

Tab. 13 – List of RBMK specific thermal-hydraulic phenomena for MCC.

Processes in drum separator

- Separation, water entrainment, steam carry under:
  - void fraction of 'water' volumes of DS.
- Dynamics of mass levels, their variation during power and/or pressure decrease:
  - Axial effects in DS:
    - Heat exchange steam–water–metal during variation of pressure.

Two-phase severely non-homogeneous phenomena and natural circulation in complex circuit during decrease of pressure, water inventory and velocity

- Separation in T-joints, headers, W-sections.
- Steam plugs and oscillations in steam water pipelines, group distribution headers, down-comers.
- CCF/ CCFL in parallel channels and inlet water pipelines.
- Self-sustaining flow oscillations in parallel channels.
- Degradation of natural circulation.

Tab. 13 (cont.) – List of RBMK specific thermal-hydraulic phenomena for MCC.

Fast thermal processes • Water blowdown from the circuit, water blow down from fuel channels during drop of flow rate or pressure, overflows between parallel channels. • Stagnation, oscillations, reverse and resumption of flow in different-heated channels. • Fronts of flooding and quenching in the channel with fuel assembly, distribution of ECCS water over differently heated fuel channels and GDH. • Dynamics of temperatures in fuel assemblies and pressure tubes; convection, radiation and heat conductivity from 'steamed' fuel channels to graphite column.
Slow processes in drained part of channels • Dynamics of formation of back flow during leak in the pressure part of the circuit. • Formation and movement of a physical level in fuel channels, water entrainment, heat removal above level. • Axial and longitudinal transport of heat to graphite and cooled channels. • Steam–zirconium reaction.
Quasi-stationary processes • Critical heat fluxes and critical powers of fuel channels. • Void distribution. • Post-dryout heat transfer under emergency conditions. • Oscillation in parallel channels. • Hydraulic resistance of fuel channel during sub-cooling at the inlet and overheating at the outlet. • Natural circulation. • Thermal-hydraulics (dryout, post-dryout heat transfer, formation of level) in downward two-phase flow.
Phenomena in reactor space, outside the channels • Two-phase flow after rupture, 3-D distribution of flow and pressure, separation in reactor space outside fuel channel during distortion of graphite columns. • Steam generation (quenching of graphite). • Condensation on CPS channels, role of non-condensable gases.
Processes in CPS channels • Hydraulic dynamics of low pressure downward flow in CPS channels. • Formation and stability of water film during decrease of flow rate, transfer and release of gases. • Dynamics of emergency drainage of CPS channels, processes of water drainage and dryout.

3.3.2. Three-dimensional neutron kinetics

The RBMK core consists of FC embedded into graphite stacks, subdivided into bricks (see Chapter 2). Looking at the neutron kinetics point of view, the core of a RBMK largely differs from the core of a LWR (namely a BWR) producing the same thermal power owing to the following:

a. Overall dimensions and, consequently, power per unit volume, that are respectively, much larger and much smaller (for a factor greater than 10, see Tab. 6).
b. Presence of the graphite as moderator.
c. Presence of a large variety of 'neutron kinetics cell types' (i.e. association of a graphite stack and of a different component):
    1. Active fuel.
    2. Additional absorber *(high pressure bypass*).
    3. Water column, i.e. w/o inside absorber (*high pressure bypass*).
    4. Reflector (*low pressure circuit*).
    5. CPS or 3 CR types (*low pressure circuit*):
        i. Manual CR,
        ii. Short CR,
        iii. Safety CR.
    6. Axial detector (*low pressure circuit*).
d. Lower enrichment and, consequently, need to control a lower excess reactivity owing to the 'continuous-fuel-reloading'.

Specific RBMK core features for 3D neutron kinetics are given in Tab. 14, [20]. All of this makes more stringent (related to BWR) the need to use 3D neutron kinetics for transient safety analyses.

The two-group cross-section libraries used to predict RBMK core physics are usually corrected for uncertainties in axial burn-up distribution, control rod positions and thermal-hydraulic feedback. Flux reconstruction methods or other correction procedures are applied. In the flux reconstruction method, the calculated 3-D flux distribution is compared to the readings of the in-core detectors and cross-sections are adjusted accordingly.

Tab. 14 – List of RBMK specific design features for the core neutron kinetics

Fuel cell: • Coolant density (0.0g/cm3 up to 1.0g/cm^3). • Graphite temperature (300 K up to 1100 K). • Fuel temperature (300 K up to 1500 K). • Xenon-concentration. • Coolant temperature. (300 K up to 557 K).
Non-fuel cells: • Control rod channels. • Additional absorber channels. • Reflector channels. • CPS-detector channels. **The cross-sections are typically derived as function of:** • Fuel burn-up. • Graphite temperature. • Water density (0÷0.78 g/cm^3 for cells in MCC loop) (0÷0.98 g/cm^3 for cells in CPS loop for hot power conditions) (0÷1.0 g/cm^3 for cold conditions in any cell).

4. THE TOOLS, THE METHODOLOGIES AND THE QUALIFICATION OF 3D NK COUPLED TH CODES ANALYSES

The execution of detailed and realistic NPP nuclear safety analyses requires the use of the state-of-the-art codes and methodologies. Information about these topics is given this chapter, together with some details about the procedure for codes and input decks qualification.

4.1. Neutron Transport codes

Performing reactor dynamic core calculations solving the neutron transport equation is something that is still impossible nowadays, because of the limits of current computational tools. For the RBMK, this is particularly true, considering its enormous geometrical dimensions (14 m of diameter per 7.5 m of height). Therefore, the use of these codes should be limited to the investigation of small parts of the reactor (e.g., the single fuel cell or small part of the reactor lattice). Nevertheless their use is precious in conducting in-depth calculations for assessing the effects of some local phenomena (e.g., for the RBMK, the assessment of the effects of a single channel voiding) and for performing the derivation of cell homogeneous cross sections to be used for the whole reactor core calculations by nodal diffusion codes.
During this PhD research activity, the situations for using neutron transport codes were identified and both deterministic and stochastic transport codes were applied.
Stochastic neutron transport simulation by the MCNP5 [24] Monte Carlo based method code was performed for obtaining detailed simulation of fuel cells during a flow blockage event. Instead, deterministic neutron transport codes DRAGON [56] and HELIOS [54] were applied in order to perform repetitive fuel lattice cells calculations for the production of several fuel cell homogenized cross-section database at several burnup steps. The description of the physical and numerical methods of all these codes and their structure is given hereafter.

4.1.1. The Monte Carlo code MCNP5

A comprehensive description of the MCNP code can be found in [24]. We reported here the main relevant features of the code for the use we did for the RBMK analysis.

4.1.1.1. General features

MCNP is a general-purpose, continuous-energy, generalized-geometry, time-dependent, coupled neutron/photon/electron Monte Carlo transport code. It can be used in several transport modes: neutron only, photon only, electron only, combined neutron/photon transport where the photons are produced by neutron interactions, neutron/photon/electron, photon/electron, or electron/photon.
The neutron energy regime is from 10^{-11} MeV to 20 MeV for all isotopes and up to 150 MeV for some isotopes, the photon energy regime is from 1 keV to 100 GeV, and the electron energy regime is from 1 KeV to 1 GeV. The capability to calculate

k_{eff} eigenvalues for fissile systems is also a standard feature and was heavily exploited for this PhD work.

The user creates an input file that is subsequently read by MCNP. This file contains information about the problem in areas such as: the geometry specification, the description of materials and selection of cross-section evaluations, the location and characteristics of the neutron, photon, or electron source, the type of answers or tallies desired, and any variance reduction techniques used to improve efficiency.

4.1.1.2. Monte Carlo Method vs. Deterministic Method

Monte Carlo methods are very different from deterministic transport methods. Deterministic methods, the most common of which is the discrete ordinates method, solve the transport equation for the average particle behavior. By contrast, Monte Carlo obtains answers by simulating individual particles and recording some aspects (tallies) of their average behavior. The average behavior of particles in the physical system is then inferred (using the central limit theorem) from the average behavior of the simulated particles. Not only are Monte Carlo and deterministic methods very different ways of solving a problem, even what constitutes a solution is different. Deterministic methods typically give fairly complete information (for example, flux) throughout the phase space of the problem. Monte Carlo supplies information only about specific tallies requested by the user.

4.1.1.3. The Monte Carlo Method

Monte Carlo can be used to duplicate theoretically a statistical process (such as the interaction of nuclear particles with materials) and is particularly useful for complex problems that cannot be modelled by computer codes that use deterministic methods. The individual probabilistic events that comprise a process are simulated sequentially. The probability distributions governing these events are statistically sampled to describe the total phenomenon. In general, the simulation is performed on a digital computer because the number of trials necessary to adequately describe the phenomenon is usually quite large. The statistical sampling process is based on the selection of random numbers—analogous to throwing dice in a gambling casino—hence the name “Monte Carlo.” In particle transport, the Monte Carlo technique is pre-eminently realistic (a numerical experiment). It consists of actually following each of many particles from a source throughout its life to its death in some terminal category (absorption, escape, etc.). Probability distributions are randomly sampled using transport data to determine the outcome at each step of its life.

Fig. 40 represents the random history of a neutron incident on a slab of material that can undergo fission. Numbers between 0 and 1 are selected randomly to determine what (if any) and where interaction takes place, based on the rules (physics) and probabilities (transport data) governing the processes and materials involved. In this particular example, a neutron collision occurs at event 1. The neutron is scattered in the direction shown, which is selected randomly from the physical scattering distribution.

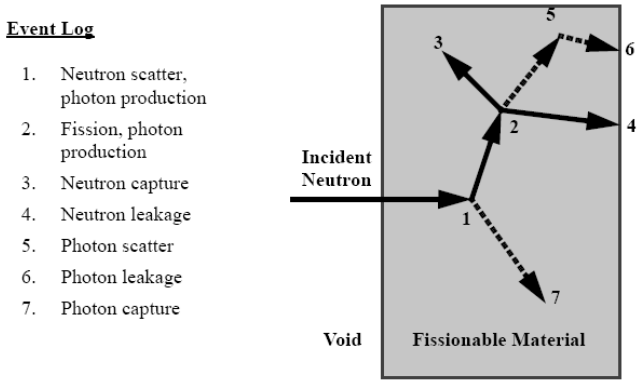

Fig. 40 – A typical neutron history simulation by MNCP5 (from [24])

A photon is also produced and is temporarily stored, or banked, for later analysis. At event 2, fission occurs, resulting in the termination of the incoming neutron and the birth of two outgoing neutrons and one photon. One neutron and the photon are banked for later analysis. The first fission neutron is captured at event 3 and terminated. The banked neutron is now retrieved and, by random sampling, leaks out of the slab at event 4. The fission-produced photon has a collision at event 5 and leaks out at event 6. The remaining photon generated at event 1 is now followed with a capture at event 7. Note that MCNP retrieves banked particles such that the last particle stored in the bank is the first particle taken out.

This neutron history is now complete.

As more and more such histories are followed, the neutron and photon distributions become better known. The quantities of interest (whatever the user requests) are tallied, along with estimates of the statistical precision (uncertainty) of the results.

4.1.1.4. Nuclear Data and Reactions

MCNP uses continuous-energy nuclear and atomic data libraries. The primary sources of nuclear data are evaluations from the Evaluated Nuclear Data File (ENDF) system [61], the Evaluated Nuclear Data Library (ENDL) [62], [55], Evaluated Photon Data Library (EPDL) [63], the Activation Library (ACTL) compilations from Livermore, and evaluations from the Nuclear Physics (T–16) Group at Los Alamos. Evaluated data are processed into a format appropriate for MCNP by codes such as NJOY [64], [65]. The processed nuclear data libraries retain as much detail from the original evaluations as is feasible to faithfully reproduce the evaluator's intent.
Nuclear data tables exist for neutron interactions, neutron-induced photons, photon interactions, neutron dosimetry or activation, and thermal particle scattering S(α,β).

Each data table available to MCNP is listed on a directory file, XSDIR. Users may select specific data tables through unique identifiers for each table, called ZAIDs. These identifiers generally contain the atomic number Z, mass number A, and

library specifier ID. Over 836 neutron interaction tables are available for approximately 100 different isotopes and elements. Multiple tables for a single isotope are provided primarily because data have been derived from different evaluations, but also because of different temperature regimes and different processing tolerances. More neutron interaction tables are constantly being added as new and revised evaluations become available.

4.1.1.5. Tallies and Output

The user can instruct MCNP to make various tallies related to particle current, particle flux, and energy deposition. MCNP tallies are normalized to be per starting particle except for a few special cases with criticality sources. Fluxes across any set of surfaces, surface segments, sum of surfaces, and in cells, cell segments, or sum of cells are also available. Tallies such as the number of fissions, the number of absorptions, the total helium production, or any product of the flux times the approximately 100 standard ENDF reactions plus several nonstandard ones may be calculated with any of the MCNP tallies. In fact, any quantity of the form (1)

$$C = \int \Phi(E) f(E) dE \qquad (1)$$

can be tallied, where $\Phi(E)$ is the energy-dependent fluence, and *f(E)* is any product or summation of the quantities in the cross-section libraries or a response function provided by the user.

4.1.1.6. Estimation of Monte Carlo Errors

MCNP tallies are normalized to be per starting particle and are printed in the output accompanied by a second number *R*, which is the estimated relative error defined to be one estimated standard deviation of the mean S_x divided by the estimated mean $\bar{x}$. In MCNP, the quantities required for this error estimate −the tally and its second moment− are computed after each complete Monte Carlo history, which accounts for the fact that the various contributions to a tally from the same history are correlated. For a well-behaved tally, *R* will be proportional to $1/N^{1/2}$ where *N* is the number of histories. Thus, to halve *R*, we must increase the total number of histories fourfold. For a poorly behaved tally, *R* may increase as the number of histories increases.

The estimated relative error can be used to form confidence intervals about the estimated mean, allowing one to make a statement about what the true result is. The Central Limit Theorem states that as *N* approaches infinity there is a 68% chance that the true result will be in the range $\bar{x}(1 \pm R)$ and a 95% chance in the range $\bar{x}(1 \pm 2R)$.

4.1.2. The deterministic transport codes

As stated before, HELIOS and DRAGON deterministic neutron transport codes were applied for the calculation of fuel cell homogenized cross sections database. Generation of a cross sections database for RBMK reactor, composed by several libraries, is considered a task requiring big efforts by the analysts. There are several reasons for this statement.

One of this is the intrinsic complexity of the RBMK system due, for example, to the very large number of different elementary cells, to the different types of CR or to the physical separation between moderator and coolant.

Difficulties are generally due also to some lack of accuracies in the acquisition of the basic input data (burn-up distribution, CR positions, coolant mass flow in each channel, graphite temperatures) in the NPP. Consequently, methods were introduced in the past for correcting the results obtained by the use of cross section libraries, in order to overcome the big uncertainties resulting in the transient core codes calculations. For example, in the flux reconstruction method, the calculated 3-D flux distribution is compared to the readings of the in-core detectors and cross-sections (e.g., the thermal fission cross sections, or $\nu\Sigma_f$) are adjusted accordingly "a posteriori" [25]. Calculations of the cross section libraries of this PhD research activity did not required application of "a posteriori" methods. In fact, to overcome in-core detectors inaccuracy, a first correction of the channels burnup distribution was performed before libraries calculation [60]. Nevertheless, local channels correction was executed always preserving the reactor macro-areas power distribution. Before the use of the aforementioned codes, a process for identifying the RBMK fuel cell peculiarities was performed. Codes selection was based on their capabilities in handling these peculiarities.

a) Geometric Capabilities

The code has to be able to model the elementary RBMK core cell made by a square hollow block of graphite measuring 0.25 x 0.25 m and made by other components of different shapes like fuel pins, pressure tube, additional absorber, control rods parts, neutron detectors and graphite radial reflector. Therefore, the capability to use Cartesian geometry is required. The code has to have the capability to handle also a "poly-cell" model, in order to calculate the feedback effects of the neighbor cells.

b) Physical Capabilities

An adequate range of the relevant physical parameters has to be considered by the code in order to calculate a good transport solution and in order to include the relevant feedback effects during the fuel cell homogenized cross sections libraries calculations. Different requirements can be listed for fuel and non-fuel cells (see Tab. 15) according to the family of transients that it should be analyzed.

Tab. 15 – Range of the physical parameters to be considered for Fuel and Non-fuel cells

Fuel cell	Non-fuel cells
• Fuel Burnup (0 – 20 MWd/KgU) • Coolant density (0.0 g/cm3 up to 1.0 g/cm^3) • Graphite temperature (300 K up to 1100 K) • Fuel temperature (300 K up to 1500 K) • Xe^{135} concentration (0, 2.0E+13, 4.5E+48 atoms/cm^3) • Coolant temperature (300 K up to 557 K)	• Graphite temperature (300 K up to 1100 K); • Water density (0÷0.78 g/cm^3 for cells in MCC loop) (0÷0.98 g/cm^3 for cells in CPS loop for hot power conditions) (0÷1.0 g/cm^3 for conditions in any neighbor cell) • CR position

4.1.2.1. The lattice physics code DRAGON

The computer code DRAGON [56] contains a collection of models that can simulate the neutron behavior of a unit cell or a fuel assembly in a nuclear reactor. It includes all of the functions that characterize a lattice cell code, namely: the interpolation of microscopic cross sections supplied by means of standard libraries; resonance self-shielding calculations in multidimensional geometries; multigroup and multidimensional neutron flux calculations that can take into account neutron leakage; transport-transport or transport-diffusion equivalence calculations as well as editing of condensed and homogenized nuclear properties for reactor calculations; and finally isotopic depletion calculations.

The code DRAGON contains a multigroup flux solver conceived that can use a various algorithms to solve the neutron transport equation for the spatial and angular distribution of the flux. Each of these algorithms is presented in the form of a one-group solution procedure where the contributions from other energy groups are considered as sources. The current release of DRAGON contains five such algorithms.

The JPM option that solves the integral transport equation using the *J±* method, (interface current method applied to homogeneous blocks); the SYBIL option that solves the integral transport equation using the collision probability method for simple 1D or 2D geometries and the interface current method for 2D Cartesian or hexagonal assemblies; the EXCELL/NXT option to solve the integral transport equation using the collision probability method for more general 2D geometries and for 3D assemblies; the MOCC option to solve the transport equation using the method of cyclic characteristics in 2D Cartesian, and finally the MCU option to solve the transport equation using the method of characteristics (non cyclic) for 3D Cartesian geometries.

The execution of DRAGON is managed via the GAN generalized driver. After the collision probability or response matrices associated with a given cell have been

generated, the multigroup solution module can be activated. This module uses the power iteration method and requires a number of iteration types. The thermal iterations are carried out by DRAGON so as to rebalance the flux distribution only in cases where neutron undergoes up-scattering.

The power iterations are performed by DRAGON to solve the fixed source or eigenvalue problem in the cases where a multiplicative medium is analyzed. The effective multiplication factor (k_{eff}) is obtained during the power iterations. A search for the critical buckling may be superimposed upon the power iterations so as to force the multiplication factor to take on a fixed value. DRAGON can access directly microscopic cross-section libraries defined according to the following standard formats: DRAGLIB, MATXS, WIMS–D4 [66],[67],[68],[69], and WIMS–AECL [70]. It has the capability of exchanging macroscopic cross-section libraries with a codes such as TRANSX–CTR or TRANSX–2 by the use of GOXS and ISOTXS format files. The macroscopic cross section can also be read in DRAGON via the input data stream. The code is modular and can be interfaced easily with other production codes.

4.1.2.2. The lattice physics code HELIOS

HELIOS [54] is a neutron and gamma transport code for lattice burnup, in general two-dimensional geometry. It was developed by Studsvik™ *ScandPower* since the 1993. The code version released in April 2000, HELIOS-1.6, was used for this PhD activity. As can be seen in Fig. 41, HELIOS is composed by several modules. In particular, there are:

- AURORA, the input processor code module
- ZENITH, the output processor code module

The data flow between these codes is via a data base that is accessed and maintained by the subroutine package HERMES.

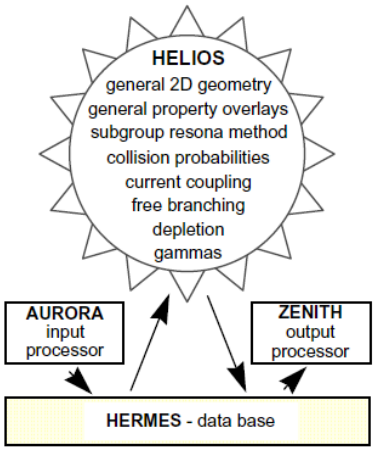

Fig. 41 – HELIOS package

AURORA reads, processes and saves the User's input. The result is a number of so-called 'User-arrays'. The User-arrays are written into the HERMES database for

retrieval by HELIOS and/or ZENITH. For each case HELIOS retrieves the input from the database and executes calculations specified. The input, except for the basic nuclear data in the library which are not user-specified consists of the following data types:

1. The nuclear data library with the basic nuclear data, which also defines the energy discretization (group structures) of the particle transport calculations.
2. Data that define the (initial) number densities of materials, and the elements of the albedo matrix.
3. Data that define the geometry of the system, including the spatial and angular discretization to be used in the transport calculations.
4. Data that assign one or more property sets to the geometric system, thus defining one or more states of the system.
5. Data that define the execution sequence of the calculations
6. Data that define what output will be saved

HELIOS consists of a main module, which calls nineteen computational modules, The first eleven modules treat the input data and they are called once per every case. Six of the remaining modules perform physics calculations, while the last two modules process the data for output and restart dumps. Most of these eight modules are called at least once per reactivity calculation point. The depletion module in only called if there is burnup or decay, while the module for the restart dumps is called only when such dumps are requested.

Therefore HELIOS performs the lattice calculations in the following manner. The methods described cover three areas:

- The geometric buildup of the system and its properties
- The physical methods to obtain fluxes, currents and number densities. This consists of five parts:
    - Calculating resonance-shielded microscopic Cross Sections
    - Calculating fluxes and currents by the current-coupling collision probability (CCCP) method for particle transport
    - Evaluating first-flight probabilities
    - Evaluating, with the B_1 method, the criticality spectrum, which is used to rebalance the spectrum of the CCCP solution
    - Solving the burnup chains to obtain new number densities.
- Output processing to obtain the output data arrays.

Almost all data in the library are based on the ENDF/B-VI data. The exceptions are the cross-sections of erbium and thulium isotopes and the (n,γ) matrices of many fission products. In the thermal and resolved-resonance energy regions, below 2 keV the cross-sections of the erbium and thulium isotopes are constructed by the RABBLE code.

Fig. 42 shows the flow scheme of library generation. The ENDF/B-VI files are processed with a version of NJOY91.13 [65] – with upgrades through version 91.105 that includes code RABBLE as a module. The main task of NJOY is to generate infinite-dilution neutron and gamma Cross Sections in 190 neutron and 48 gamma groups. Another NJOY task is to generate PENDF's which are files with

Cross Sections in many thousands of energy points that are input to RABBLE. While all isotopes must be processed with NJOY, only those to be treated as resonance isotopes by HELIOS have to be processed by RABBLE.

The GENDF group Cross Sections and the resonance-shielded Cross Sections produced by RABBLE are collected in the HERMES file, the master database. The creation of the database is one of the activities of HEBE code. Another activity of the HEBE code is to construct a master library for HELIOS from selected data in the database. With the master library HELIOS runs are made to generate flux spectra in different regions, at different temperatures and at different burnups.

In the third activity HEBE adds these spectra to the master database. In the fourth activity they are used to group-collapse the database into a condensed database, from which the condensed library is made.

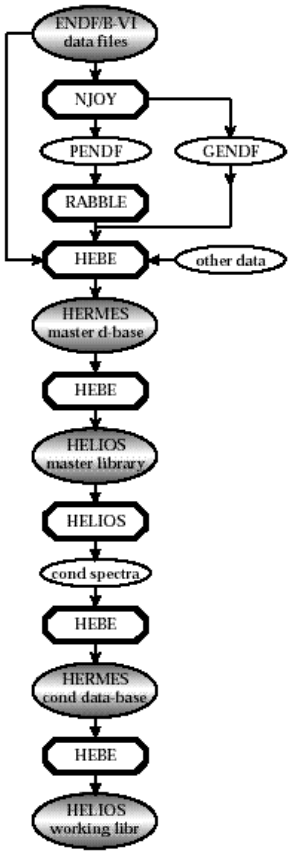

Fig. 42 – Flow scheme of library generation.

Presently, three libraries exist: the master library with 190/48 neutron/gamma groups: a fast reactor library with 112/18 neutron/gamma groups and a production library with 45/18 neutron/gamma groups. For the cross-section generation the

master library with 190/48 neutron/gamma groups were used. A comparison with the results from the 45/18 group library showed a good agreement to the master library.

286 isotopes, elements and mixtures are included in the HELIOS database, 28 heavy isotopes and 121 fission products. The code also contains resonance tables for 39 resonance isotopes (11 heavy isotopes, 28 fission products) and 23 burnable absorber and control isotopes. Isotopic compositions are automatically saved if they are to be used for branch-off calculations. Compositions (e.g. boron contents, water density, temperatures and material densities) can be changed in branch-offs.

One of the advantages of HELIOS is its geometry flexibility, which allows representing fully the RBMK cell geometry. The HELIOS modeling capabilities permit also to represent exactly non-homogeneous assembles (i.e. each rod in the assembly). The HELIOS method is the CCCP technique. HELIOS was qualified for RBMK applications based on cross code comparisons and using measured data of critical facilities [26].

First, in summary the important issues in the RBMK cross-section generation are:
- Input library – evaluated nuclear data files,
- Resonance treatment,
- Energy condensation,
- Main transport calculations,
- Homogenization,
- Depletion.

Interface to run the lattice physics code HELIOS in an automated manner to perform depletion and branch calculations, extract macroscopic cross-section and neutron kinetics data, and assemble them in the format of cross-section libraries was developed at the Reactor Dynamics and Fuel Management Group (RDFMG) of the Pennsylvania State University (PSU).

4.2. The RELAP5-3D system code

4.2.1. Introduction

The RELAP5 series of codes has been developed at the Idaho National Laboratory (INL) under sponsorship by the U.S. Nuclear Regulatory Commission (NRC), the U.S. Department of Energy (DOE), and a consortium of several countries and domestic organizations that were members of the International Code Assessment and Applications Programme (ICAP) and its successor, the Code Applications and Maintenance Programme. Specific applications of the code have included simulations of transients in LWR systems, such as loss of coolant, anticipated transients without scram (ATWS), and operational transients such as loss of feedwater, loss of offsite power, station blackout, and turbine trip.
RELAP5-3D, the latest code version in the series of RELAP5 codes, is a highly generic code that, in addition to calculating the behavior of a reactor coolant system during a transient, can be used for simulation of a wide variety of hydraulic

and thermal transients in both nuclear and nonnuclear systems involving mixtures of steam, water, non-condensable, and solute. Development of RELAP5-3D The RELAP5-3D code version is a successor to the RELAP5/MOD3 code that was developed at the INL for the NRC. Development of the RELAP5 code series began at the INL under NRC sponsorship in 1975 and continued through several released versions, ending in October 1997 with the soon to be released RELAP5/MOD3.3.

The U.S. DOE began sponsoring additional RELAP5 development in the early 1980s to meet its own reactor safety assessment needs. Following the accident at Chernobyl, DOE undertook a re-assessment of the safety of all of its test and production reactors throughout the United States. The RELAP5 code was chosen as the thermal-hydraulic analysis tool because of its widespread acceptance. Systematic safety analyses were carried out for the DOE that included the N reactor at Hanford, the K and L reactors at Savannah River, the Advanced Test Reactor (ATR) at INL, the High Flux Isotope Reactor (HFIR) and Advanced Neutron Source (ANS) at Oak Ridge, and the High Flux Beam Reactor (HFBR) at Brookhaven. DOE also chose RELAP5 for the independent safety analysis of the New Production Reactor (NPR) proposed for Savannah River before that programme was cancelled in the wake of the end of the cold war.

The application of RELAP5 to these various reactor designs created the need for new modelling capabilities. For example, the analysis of the Savannah River reactors necessitated the adding three-dimensional flow model and heavy water properties to the code. ATR required a new critical heat flux correlation applicable to its unique fuel design. All together, DOE sponsored improvements and enhancements have amounted to a multimillion-dollar investment in the code.

Toward the end of 1995, it became clear that the efficiencies realized by the maintenance of a single source code for use by both NRC and DOE were being overcome by the extra effort required to accommodate sometimes conflicting requirements. The code was therefore “split” into two versions, one for NRC and the other for DOE. The DOE version maintained all of had been sponsored by the DOE before and after the split.

4.2.2. Relationship of RELAP5-3D to prior versions

At the outset of the decision to split the code into NRC and DOE versions, the INL recognized the importance of retaining the pedigree stemming from the extensive validation history of RELAP5/MOD3. Consequently, the developmental activities with respect to RELAP5-3D since the split have been carefully integrated so as not to compromise this legacy validation. In fact, virtually all of the enhancements in RELAP5-3D are *optional* and *supplemental* to the proven performance of RELAP5/MOD3.2. Consequently, users of RELAP5-3D can confidently apply the code using existing, one-dimensional RELAP5/MOD3.2 input decks and expect their results to be the same or improved.

4.2.3. The Thermal-hydraulic part: the RELAP5-3D code

RELAP5-3D is a highly generic code that, in addition to calculating the behavior of a reactor coolant system during a transient, can be used for simulation of a wide variety of hydraulic and thermal transients in both nuclear and nonnuclear systems involving mixtures of vapor, liquid, non-condensable gases, and non-volatile solute.

The mission of the RELAP5-3D development program was to develop a code version suitable for the analysis of all transients and postulated accidents in LWR systems, including both large- and small-break loss-of-coolant accidents (LOCAs) as well as the full range of operational and fusion reactor transient applications.

Additional capabilities include space reactor simulations, gas cooled reactor applications, fast breeder reactor modeling, and cardiovascular blood flow simulations.

The RELAP5-3D code is based on a non-homogeneous and non-equilibrium model for the two-phase system that is solved by a fast, partially implicit numerical scheme to permit economical calculation of system transients. The objective of the RELAP5-3D development effort from the outset was to produce a code that included important first-order effects necessary for accurate prediction of system transients but that was sufficiently simple and cost effective so that parametric or sensitivity studies were possible.

The code includes many generic component models from which general systems can be simulated. The component models include pumps, valves, pipes, heat releasing or absorbing structures, reactor kinetics, electric heaters, jet pumps, turbines, separators, annuli, pressurizers, feedwater heaters, ECC mixers, accumulators, and control system components. In addition, special process models are included for effects such as form loss, flow at an abrupt area change, branching, choked flow, boron tracking, and non-condensable gas transport.

The system mathematical models are coupled into an efficient code structure. The code includes extensive input checking capability to help the user discover input errors and inconsistencies. Also included are free-format input, restart, renodalization, and variable output edit features. These user conveniences were developed in recognition that generally the major cost associated with the use of a system transient code is in the engineering labor and time involved in accumulating system data and developing system models, while the computer cost associated with generation of the final result is usually small.

The development of the models and code versions that constitute RELAP5-3D has spanned more than two decades from the early stages of RELAP5 numerical scheme development (circa 1976) to the present. RELAP5-3D represents the aggregate accumulation of experience in modeling reactor core behavior during accidents, two-phase flow processes, and LWR systems. The code development has benefited from extensive application and comparison to experimental data in the LOFT, PBF, Semiscale, ACRR, NRU, and other experimental programs.

The RELAP5-3D version contains several important enhancements over previous versions of the code. The most prominent attribute that distinguishes the RELAP5-3D code from the previous versions is the fully integrated, multi-dimensional thermal- hydraulic and kinetic modeling capability. This removes any restrictions on the applicability of the code to the full range of postulated reactor accidents.

Enhancements include a new matrix solver for 3D problems, new thermodynamic properties for water, and improved time advancement for greater robustness. The multi-dimensional component in RELAP5-3D was developed to allow the user to more accurately model the multi-dimensional flow behavior that can be exhibited in any component or region of a LWR system. Typically, this will be the lower plenum, core, upper plenum and downcomer regions of an LWR. However, the model is general, and is not restricted to use in the reactor vessel. The component defines a one, two, or three- dimensional array of volumes and the internal junctions connecting them. The geometry can be either Cartesian (x, y, z) or cylindrical (r, θ, z). An orthogonal, three-dimensional grid is defined by mesh interval input data in each of the three coordinate directions.

The new Border-Profile Lower Upper (BPLU) matrix solver is used to efficiently solve sparse linear systems of the form AX = B. BPLU is designed to take advantage of pipelines, vector hardware, and shared-memory parallel architecture to run fast. BPLU is most efficient for solving systems that correspond to networks, such as pipes, but is efficient for any system that it can permute into border-banded form. Speed-ups over the previously used sparse matrix solver are achieved in RELAP5-3D running with BPLU on multi-dimensional problems, for which it was intended. For one-dimensional problems, the BPLU solver runs as fast or faster than the previously used sparse matrix solver.

4.2.4. The three dimensional neutron kinetics routine: the NESTLE code

4.2.4.1. The Steady-State and the Transient Problem

The RELAP5-3D code allows to calculate a 3D core power distribution thanks to multi-dimensional neutron kinetics models based on NESTLE code, developed by Paul Turinsky and his co-workers at the North Carolina State University. This feature allows to compute the reactor fission power in either Cartesian or hexagonal geometry [24].

The subroutines taken from the NESTLE source code used to solve these problems were modified to be compatible with the coding standards and data storage methodology used in RELAP5-3D, and were inserted into RELAP5-3D. RELAP5-3D was modified to call the appropriate NESTLE subroutines depending upon the options chosen by the user.

The Nodal Expansion Method (NEM) is used to solve the neutron diffusion equations for the neutron flux in either two or four neutron energy groups. Quartic or quadratic polynomial expansions for the transverse integrated fluxes are employed for Cartesian or hexagonal geometries, respectively. E.g., the one

dimensional flux obtained by the transverse integration can be written (in the case of Cartesian geometry) as:

$$\bar{\phi}^{1}_{gx}(x) = \bar{\phi}^{1}_{g} + \sum_{n=1}^{N} a^{1}_{gxn} \; f_n(x)$$

(2)

where ϕ^1_g is the node average flux, implying for Equation (2) to be true that $f_n(x)$ must be chosen such that the basis functions satisfy

$$\int_{-\frac{\Delta x^1}{2}}^{\frac{\Delta x^1}{2}} f_n(x)dx = 0 \text{ for } n = 1, 2, ..., N.$$

, N=1 to 4

(3)

Transverse leakage terms are represented by a quadratic polynomial or constant for Cartesian or hexagonal geometry, respectively. E.g., the x-direction spatial dependence of the y-direction transverse leakage is approximated by:

$$\bar{L}^{1}_{gy}(x) \cong \bar{L}^{1}_{gy} + \rho^{1}_{gy1} f_1(x) + \rho^{1}_{gy2} f_2(x)$$

(4)

where L^1_{gy} is the average y-directed leakage in node **I**, and the coefficients ρ^1_{gy1} and ρ^1_{gy2} can be expressed in terms of average y-directed leakages of the two nearest-neighbor nodes along the x-direction (i.e. nodes **I-1** and **I+1**) so as to preserve the node average leakages of these three nodes. Discontinuity factors (DFs) are utilized to correct for homogenization errors.

Transient problems utilize a user specified number of delayed neutron precursor groups. Time discretization is done in a fully implicit manner utilizing a first-order difference operator for the diffusion equation, or:

$$\left.\frac{\partial \phi_g}{\partial t}\right|_{t_{n+1}} = \frac{\phi_g(t_{n+1}) - \phi_g(t_n)}{\Delta t_n}.$$

(5)

The precursor equations are analytically solved assuming the fission rate behaves linearly over a time-step.

Independent of problem type, an outer-inner iterative strategy is employed to solve the resulting matrix system. Outer iterations can employ Chebychev acceleration and the Fixed Source Scaling Technique to accelerate convergence [27], [28], [29], [30]. Inner iterations employ either a Red-Black Point or Line SOR iteration schemes, dependent upon problem geometry. Values of the energy group dependent optimum relaxation parameter and the number of inner iterations per outer iteration to achieve a specified L_2 relative error reduction are determined a

priori. The non-linear iterative strategy associated with NEM is utilized. This technique was developed by Smith [31], [32], [33], and successfully implemented into the Studsvik QPANDA and SIMULATE code packages.

The basic idea is applicable to the standard FDM solution algorithm of the multi-group diffusion equation. Solving the FDM based equation utilizing an outer-inner iterative strategy, every ΔN_0 outer iterations (where ΔN_0 is somewhat arbitrary but can be optimized) the so-called "two-node problem" calculation (a spatially-decoupled NEM calculation spanning two adjoining nodes) is performed for every interface (for all nodes and in all directions) to provide an improved estimate of the net surface current at that particular interface. Subsequently, the NEM estimated net surface currents are used to update (i.e. change) the original FDM diffusion coupling coefficients. Outer iterations of the FDM based equation are then continued utilizing the updated FDM coupling coefficients for ΔN_0 outer iterations.

The entire process is then repeated. This procedure of updating the FDM couplings is a convergent technique which progressively forces the FDM equation to yield the higher-order NEM predicted values of the net surface currents while satisfying the nodal balance equation, thus yielding the NEM results for the node-average flux and fundamental mode eigenvalue. The advantages of this technique come in many forms;

- the storage requirements are minimal because the two-node problem arrays are re-usable (disposable) at each interface,
- the rate of convergence is nearly comparable to that of the base FDM algorithm being used,
- the number of iteratively determined unknowns is reduced by a factor of 6 (node flux vs. partial surface current),
- and the simplicity of the algorithm and ease of implementation, compared to any other nodal technique, is far superior.

In addition, by selecting to not update the coupling coefficients in the non-linear iterative strategy, the finite difference method (FDM) representation, utilizing the box scheme, of the few-group neutron diffusion equation results. The implication is that the model can be utilized to solve either the nodal or FDM representation of the few-group neutron diffusion equation. In Fig. 43 the overall nested iterative solution strategy used within RELAP5-3D code for each attempted advancement is showed.

Two or four energy groups can be utilized, with all groups being thermal groups (i.e. upscatter exits) if desired. Three, two and one dimensional models can be utilized. Various core symmetry options are available, including quarter, half and full core for Cartesian geometry and one-sixth, one-third and full core for hexagonal geometry. Zero flux, non-reentrant current, reflective and cyclic boundary conditions are treated.

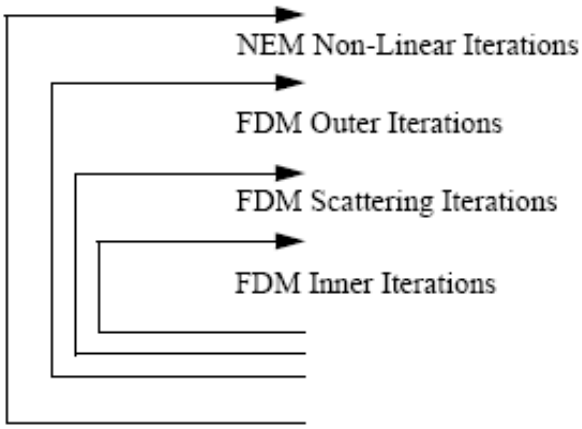

Fig. 43 – Overview of the nested iterative solution strategy

The neutron kinetics subroutines require as input the neutron cross-sections in the computational nodes of the kinetics mesh. A neutron cross-section model has been implemented that allows the neutron cross-sections to be parameterized as functions of RELAP5-3D heat structure temperatures, fluid void fraction or fluid density, poison concentration, and fluid temperatures. Thus this feature allows RELAP5-3D to be suitable for RBMK studies, allowing to calculate the graphite moderator temperature, the coolant density and of course the fuel temperature feed-back effects.

A flexible coupling scheme between the neutron kinetics mesh and the thermal-hydraulics spatial mesh has been developed to minimize the input data needed to specify the neutron cross-sections in terms of RELAP5-3D thermal-hydraulic variables.

A control rod model has been implemented so that the effect of the initial position and subsequent movement of the control rods during transients may be taken into account in the computation of the neutron cross-sections. The control system has been modified to allow the movement of control rods by control variables.

4.2.4.2. The Cross Section and the feedbacks

The inputs to the kinetics modules in RELAP5-3D consist of neutron cross sections, boundary conditions, control flags, control data, etc. Neutron cross sections are needed for each neutron energy group and kinetics node and consist of the diffusion coefficient (D), absorption cross section (Σ_a), fission cross section (Σ_f), the product of the mean number of secondary neutrons per fission and the fission cross section ($\nu\Sigma_f$), and the scattering cross section for scattering into the neutron energy group from the other neutron energy groups ($\Sigma s_{g'g}$). Discontinuity factors (DFs) for each face of the kinetics nodes are also needed for each energy group. The user supplies the control information and the boundary conditions as part of the required input data. The neutron cross sections are computed from a function selected from a set of built-in functions or a user supplied function whose

independent variables are weighted averages of RELAP5-3D hydraulic or heat structure variables.

There are four built-in neutron cross section functions from which the user can select or the user may supply his own function in the form of an external subroutine. The same user specified function is used for the computation of the neutron cross sections for all kinetics nodes. The coefficients in the first three built-in cross section functions for each of the cross sections are supplied through user input and a set of coefficients for the neutron cross sections is called a composition.

The user defines a number of compositions and specifies which composition is to be used for the computation of the neutron cross sections in each kinetics node in the reactor core model. The mapping of compositions to nodes is accomplished through the use of composition figures. A composition figure specifies the composition for all of the kinetics nodes in a single axial plane in the reactor model and composition figures are required for each axial plane in the reactor model. The user may specify as many composition figures as needed to describe the reactor and a composition figure may be assigned to more than one axial plane in the reactor model.

The user specifies the volumes and heat structures to be used in computing the weighted averages of thermal-hydraulic variables as well as the values of the weighting factors. A set of volume averaged properties consists of an average fluid density (or fluid vapor fraction depending on which neutron cross section function is selected by the user), an average fluid temperature, and an average poison density, while the average heat structure property is simply the average heat structure temperature.

The group of volumes and heat structures used to define sets of average thermal-hydraulic properties is called a zone. One of the built-in cross section functions uses a single set of average properties in a zone while the other two built-in neutron cross section functions use multiple sets of average volume and average heat structure properties in a zone. The user defines a number of zones and specifies which set of zone average thermal-hydraulic properties is to be used for the computation of the neutron cross sections in each node of the reactor core through the use of zone figures. A zone figure specifies which zone is to be used for the computation of the neutron cross sections for each node in an axial plane of the reactor. Zone figures are required for each axial plane in the reactor model and the same zone figure may be specified for more than one axial level. In addition to the weighted averages of hydraulic and heat structure variables, the neutron cross section function uses the position of the control rods as another independent variable.

A control rod model is used to determine the positions of the control rods and to compute the control rod variable needed by the neutron cross section function on each axial level in the reactor core. The three neutron cross section functions that the user may select to compute the neutron cross sections and the control rod model are described in the following section.

4.2.4.3. The GEN neutron cross section model

The last built-in cross section model is the most general built-in cross section model and was developed [34] as part of the RELAP5-3D code development project. The GEN cross section function uses a form similar to the HWR formulation except that the variable portion of the cross section is defined for three control states, active controlled, driver controlled and uncontrolled states. The GEN cross section function is given by

$$\Sigma_l^x = C_{fl}^a \Sigma_{xc}^a \left(1 + \frac{\delta\Sigma_{xc}^a}{\Sigma_{xc}^a}\right) + (1 - C_{fl}^a - C_{fl}^d)\Sigma_{xc}^u \left(1 + \frac{\delta\Sigma_{xc}^u}{\Sigma_{xc}^u}\right) + C_{fl}^d \Sigma_{xc}^d \left(1 + \frac{\delta\Sigma_{xc}^d}{\Sigma_{xc}^d}\right) \quad (6)$$

where:

$C_{fl}^{a,\,d}$ = control fraction for active and driver portions of the control rods in node **l**

$\Sigma_{xc}^{a,d,u}$ = base cross section of reaction type **x** for composition **c** for active controlled, driver controlled, or uncontrolled state

$\delta\Sigma_{xc}^{a,d,u}$ = variation of cross section for reaction type **x** for composition **c** due the changes in the thermal-hydraulic variables from the base thermal-hydraulic state for active controlled, driver controlled, and uncontrolled state

and composition **c** has been specified for node **l**.

The variations for the active controlled, driver controlled, and uncontrolled states are given by:

$$\frac{\delta\Sigma_{xl}}{\Sigma_{xl}^{base}} = \sum_{i \in N_v} a_{xin}\Delta\bar{T}_{mik} + \sum_{i \in N_v} b_{xin}\Delta\bar{\rho}_{mik} + \sum_{i \in N_v} c_{xin}(\Delta\bar{\rho}_{mik})^2 + \sum_{i \in N_v} d_{xin}\Delta\bar{B}_{ik} + \sum_{i \in N_s} e_{xin}\Delta\bar{T}_{sik} \quad (7)$$

where the coefficients **a**, **b**, **c**, **d**, and **e** are input separately for the active controlled, driver controlled, and uncontrolled states.

Therefore, each neutron cross section is the sum of the base cross section and the change in the cross section:

$$\Sigma_{xl} = \Sigma_{xl}^{base} + \delta\Sigma_{xl}$$

(8)

Where:

Σ_{xl}^{base} = base cross section of type **x** in node **l**

$\delta\Sigma_{xl}$ = change in cross section **x** in node **l** due to changes in the thermal-hydraulic state of the zone to which node **l** corresponds

Cf_l = control fraction in node **l**

a_{xin} = coefficient for change in cross section **x** of composition **n** due to changes in average moderator temperature of volume region **i**

ΔT_{mik} = change in average moderator temperature in volume region **i** of zone **k**, $(T_{mik} - T_{min}^{base})$

T_{mik} = average moderator temperature in volume region **i** of zone **k**

T_{min}^{base} = average moderator temperature in volume region **i** for composition **n** at base thermal-hydraulic conditions, e.g. full power steady state

N_V = number of volume regions in each zone

b_{xin} = linear coefficient in change of cross section **x** of composition **n** due to changes in average moderator density in volume region **i**

$\Delta\rho_{mik}$ = change in average moderator density in volume region **i** of zone **k,** $(\rho_{mik} - \rho_{min}^{base})$

ρ_{min}^{base} = average moderator density in volume region **i** for composition **n** at base thermal-hydraulic state

c_{xin} = quadratic coefficient in change of cross section **x** of composition **n** due to changes in average moderator density in volume region **i**

d_{xin} = coefficient for change in cross section **x** of composition **n** due to changes in average poison density in volume region **i**

ΔB_{ik} = change in average poison concentration in volume region **i** of zone **k**, $(B_{ik} - B_{in}^{base)}$

B_{in}^{base} = average poison concentration in volume region **i** for composition **n** at base thermal-hydraulic condition

e_{xin} = coefficient for change in cross section **x** of composition **n** due to changes

in average structure temperature of structure region **i**

ΔT_{sik} = change in the average structure temperature in structure region **i** of zone **k** (T_{sik} - T_{sin}^{base})

ΔT_{sin}^{base}= average structure temperature in structure region i of composition **n** for base thermal-hydraulic state

N_S = number of structure regions in each zone.

The nodal discontinuity factors are also computed from Equation (*6*) except that the thermal-hydraulic variations are identically zero and are therefore not included.

The GEN model subdivides each zone into a number of regions and define averages of volume and heat structure quantities for each region of a zone. The number of regions in a zone for the computation of volume average properties may be different from the number of regions in a zone for the computation of the heat structure average properties, but the number of volume regions and the number of heat structure regions is the same for each zone. The region average moderator temperature, the region average moderator density, the region average poison density, and the region structure temperature are computed using equations like, e.g., equation (9):

$$\overline{T}_{mik} = \frac{\sum_{j \in M_{ik}} W^{m}_{jik} T_{mj}}{\sum_{j \in M_{ik}} W^{m}_{jik}} \qquad (9)$$

where:

T_{mik} = average moderator temperature in volume region **l** of zone **k**

W^{m}_{ijk} = moderator temperature weighting factor for volume **j** in volume region **i** of zone **k**.

Other average quantities are calculated in a similar manner. The GEN cross section model can also use either the moderator density or the moderator void fraction depending upon which option the user specifies.

4.3. The Cross Section Processing methodology

4.3.1. Introduction

The execution of the 3D NK calculations requires the development and the use of a methodology for the cross section data processing. Each 3D NK code has its own input formalism for the use of these data and different approaches are possible. The GRNSPG was since, its institution, performing calculations with the most advanced of these methodologies and was actively participating in International Research Programs dealing with researches in such field, e.g. [43]. Thus, the PhD activities for the cross section processing were performed in such a framework.

4.3.2. The State of the Art methodologies

The need for a more accurate method of modelling cross-section variations for off-nominal core conditions is becoming an important issue with the increased use of coupled three-dimensional (3-D) neutronics/thermal-hydraulic simulations. In traditional reactor core analysis for both steady-state and transient calculations of LWR conventional nuclear power plants, condensed few-group two-dimensional (2-D) cross-section sets are used as input data.

These cross-section sets are generated by separate database calculations using characteristic weighting spectra and are parameterized in terms of burn-up and thermal-hydraulic feedback parameters. Under the real reactor conditions, especially in transient situations, these spectra change and the 2-D cross-section modeling based on a parameterization model only approximately describes the effects of neutron flux distributions, which change in space, time and energy. This so-called 2-D off-line cross-section generation and modeling constitutes a basic input data uncertainty affecting the results of coupled 3-D neutronics/thermal-hydraulic calculations.

Historically, a two-step process is applied in traditional reactor core analysis for both steady-state and transient applications. The first step in the process is to calculate few-group cross-sections with different dependencies (*i.e*. as a function of burn-up and local feedback parameters) for various regions of a reactor core in 2-D geometry, employing lattice physics codes such as CASMO [35], [36] and HELIOS [54]. The second step is to use this cross-section data in a 3-D nodal diffusion code for determination of different parameters throughout the reactor core. There are several shortcomings in this approach associated with both cross-section generation and cross-section modeling. In regard to the cross-section generation two shortcomings are addressed:

- The use of 2-D lattice physics codes for cross-section generation, based on the fact that the majority of current lattice physics codes use the collision probability method (CPM), becomes cumbersome and impractical in 3-D geometries.
- Current methodology homogenizes representative assemblies assuming symmetry (reflective) boundary conditions. This approach introduces significant errors in the determination of neutron flow among assemblies in

a real reactor core configuration. The errors are somewhat mitigated by the use of *ad hoc* assembly discontinuity factors for conventional reactor core analysis.

The amount of few-group cross-section data necessary for steady-state, depletion and transient analysis, is significant. Standard cross-section modeling for coupled 3-D steady state and transient simulations are based on the data generated in the so-called base and branch calculations using a lattice physics code. The cross-section history and instantaneous dependence models developed in this way are based on burn-up and local feedback parameters (*i.e.* fuel temperature, pressure, moderator temperature, void, boron concentration). The thermal-hydraulics model coupled with the neutronics simulator calculates these feedback parameters. Changing each of the parameters one at a time develops the instantaneous cross-section dependencies.
A typical dependence of a cross-section on a particular parameter is displayed in Fig. 44. This shows that over a large range of values the cross-section does not behave linearly.

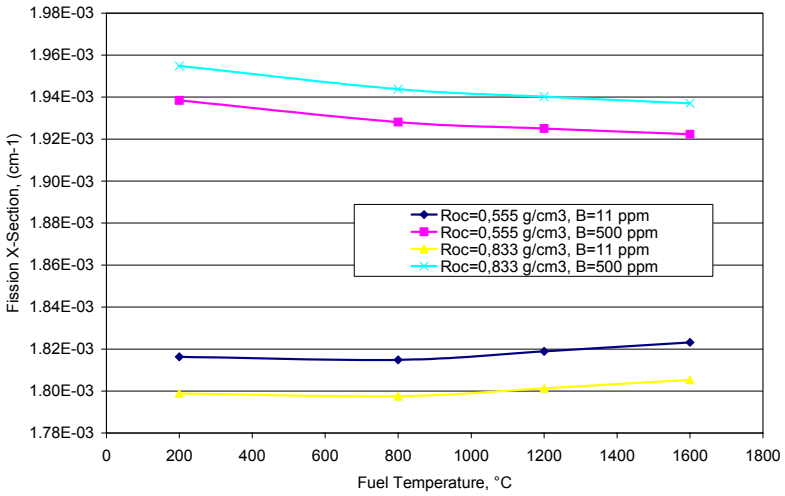

Fig. 44 – Cross Section dependence

More interesting cross-section behavior is shown in Fig. 45. The figure shows the interdependence of cross-sections when two parameters are varied at once. The cross-sections generated in this way are called cross-terms, since they are not dependent on just one parameter, but on all parameters. Such cross-term cross-sections have to be taken into account in transient analysis since they are actual points on the curved surface.

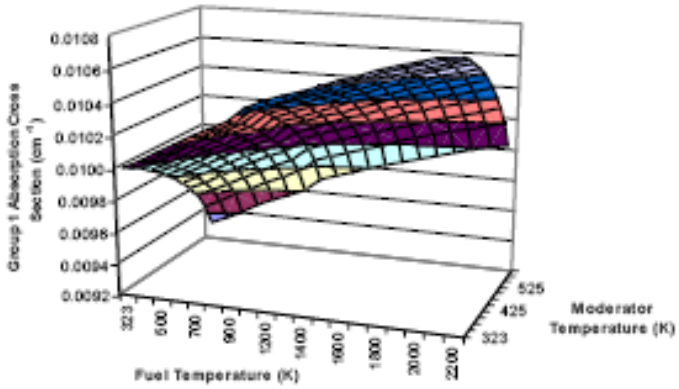

Fig. 45 – Cross-section interdependence between fuel temperature and moderator temperature

However, standard methods (currently used in core steady-state, depletion and transient analysis) such as the polynomial fitting procedure (usually based on Taylor expansions) do not take these cross-terms into account. Since these methods utilize no cross-term dependencies on local feedback parameters they are especially inaccurate for transients in which large departures from nominal conditions exist.

The typical calculation points necessary to develop the cross-section derivatives used in the polynomial fitting procedure can be seen from the schematic given in Fig. 46. For simplicity only two parameters are shown, fuel temperature (T_F) and moderator temperature (T_M).

This method uses a cross-section calculation at average conditions, shown as the black dot, as a reference value. From the reference value parameter perturbations are performed to develop cross-sections at different conditions, shown by the red dots. In this method only one parameter is varied at a time, all other parameters remain at average conditions.

Once the new cross-section is established along with the magnitude of the individual parameter variation, a derivative can be constructed which is used directly in the polynomial equation. Using these derivatives along with the average cross-sections, a cross-section can be calculated at any reactor condition.

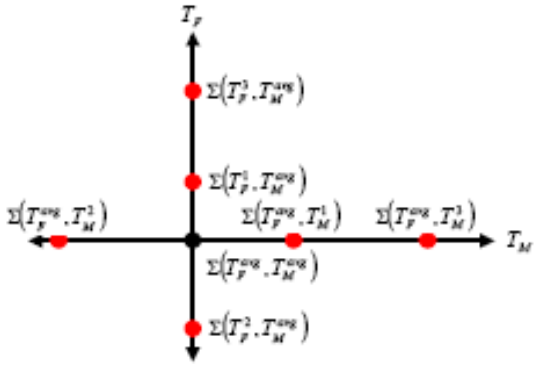

Fig. 46 – Cross-section calculation points for the polynomial fitting procedure

The most significant problem with this procedure is that it becomes more inaccurate as the parameter variations get farther away from average conditions. The areas where the polynomial fitting procedure becomes inaccurate are shown as the blue hashes in Fig. 47. The increased inaccuracy of the cross-sections calculated in these regions is more important in transient analysis where parameter variations extend into this region during a typical transient calculation.

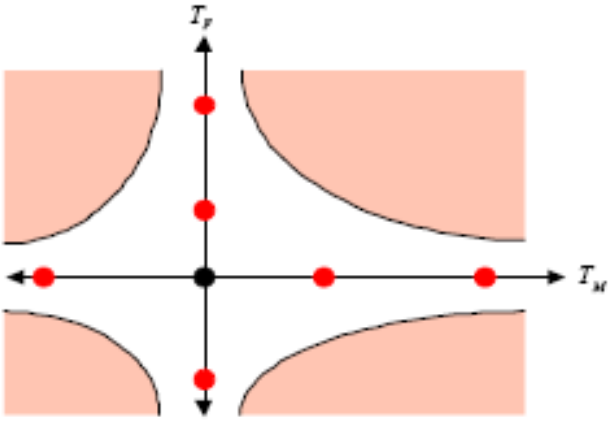

Fig. 47 – Areas of inaccurate cross-section calculation using the polynomial fitting procedure

The widely used CASMO/SIMULATE cross-section parameterization model attempts to model the cross-section cross-term dependence involving an approximate type of cross-section representation [35].

Each cross-section can be evaluated as a summation of base and partial values. The base cross-sections represent the burn-up dependence (exposure, spectral

history and control history) while the partial cross-sections represent the instantaneous dependence on local feedback parameters. Performing branch calculations generates the partial cross-sections, where again as with the polynomial fitting procedure only one feedback parameter is changed for a given perturbation. The model tries to account for the cross-term dependence by using separate partial cross-sections for different feedback effects. While the model is an improvement over the polynomial fitting procedure it is limited to small perturbations.

To remedy the inaccuracies of the procedures described above, PSU has developed a sophisticated, unique cross-section representation methodology for 3-D coupled transient calculations [37]. The method developed at PSU employs not only the cross-section at average conditions, but also the cross-term cross-sections, as can be seen in Fig. 48. Cross-term cross-sections are cross-sections calculated by varying two or more parameters at the same time. The cross-sections are then tabulated in N-dimensional tables. The N-dimensional tables are then interpolated for the appropriate cross-section value. The tabulated cross-sections completely encompass the full range of conditions that may be present during the initial steady state and the transient. This method is called the Adaptive High-order Table Look-up Method (AHTLM) [38]. In the AHTLM the user develops an operating condition box-envelope. This box bounds the expected range of change of the feedback parameters during both steady-state and transient operation. The cross-sections are then calculated for the bounding box edges and within the box. These reference cross-section values are placed in multi-dimensional tables that are used in a sophisticated table interpolation method that is employed to calculate the cross-sections.

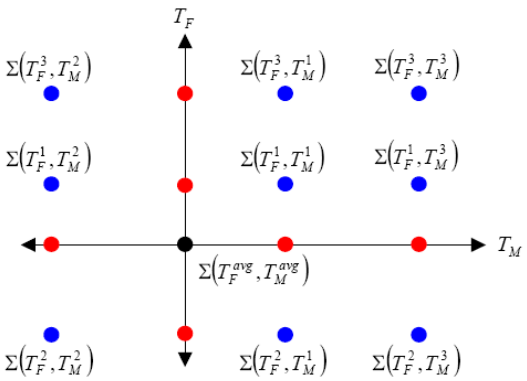

Fig. 48 – The PSU transient cross-section representation

The advantage of this method is that there is no chance that the calculation of the cross-section can be outside the bounds set by the user and to involve extrapolation procedure. In addition, this approach helps to improve the accuracy of modeling the cross-section variations by avoiding user-calculated coefficients that could contain errors. This method takes into account the non-linear thermal-

hydraulic feedback parameter phenomena that are critical for the accurate prediction of cross-section behavior.

4.3.3. The Methodology for the RBMK calculations

The RBMK cross section libraries were developed according to the AHTLM procedures. As reported in section 4.5.2, data were parameterized considering a relevant set of variables (fuel temperature, moderator temperature, coolant density), and a their suitable range. Nevertheless, due to the fact that the RELAP5-3D (NESTLE) did not allowed on-line cross section interpolation (see section 4.2.4.2), several relevant modifications were performed.

A 4D linear interpolation routine was used for calculating at the beginning of the transient the reference cross section. Cross section variation coefficients were instead calculated using a Least Square Methods interpolation routine. Thus, the resulting cross section representation was a standard “polynomial fitting” procedure (see section 4.5.2.2 for more details). A check of trend of the main cross sections as function of the main physical parameters confirmed their linear behavior, allowing the NESTLE GEN Cross Section representation without major approximations. An example of the main cross sections trends is given in Fig. 49, Fig. 50.

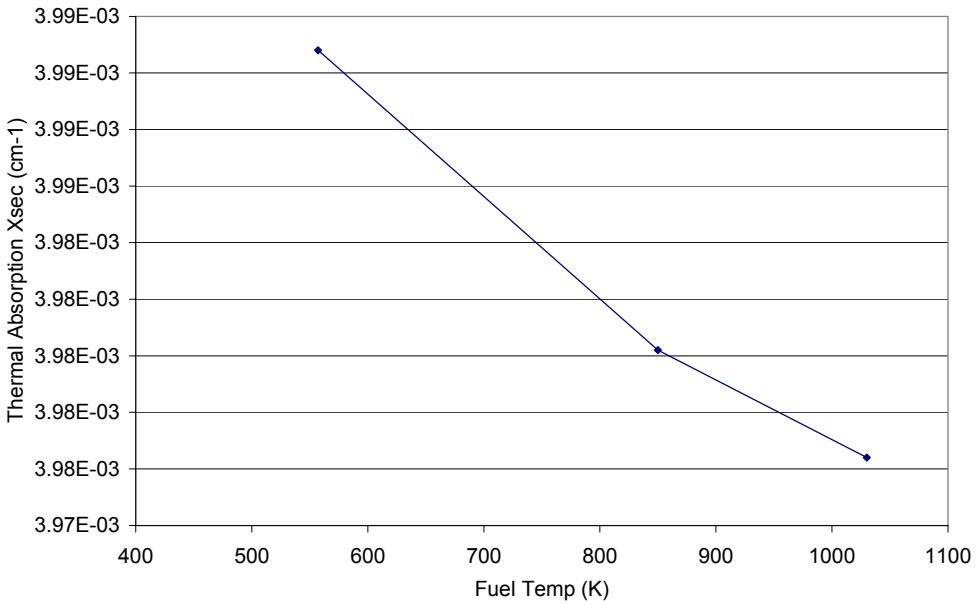

Fig. 49 – RBMK Libraries Cross Section – Thermal absorption trend for composition 29 (see section 4.5.2)

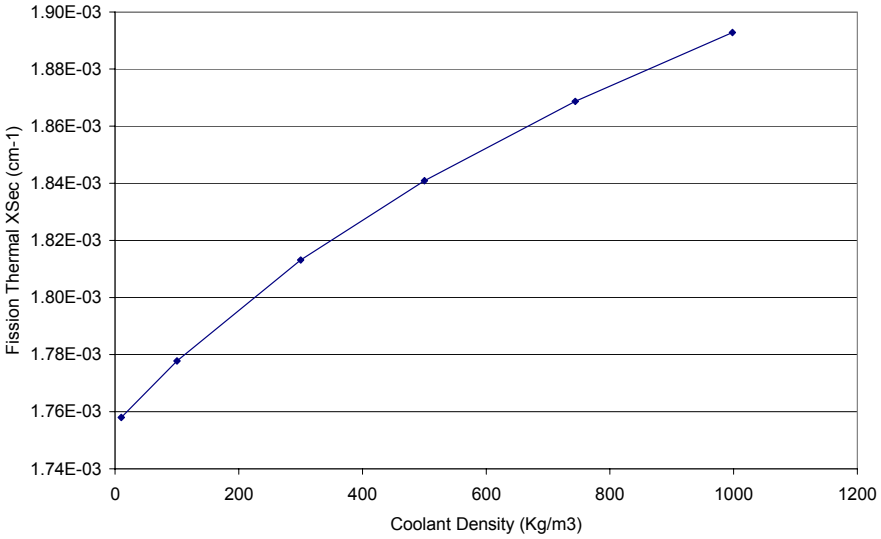

Fig. 50 – RBMK Libraries Cross Section – Thermal fission trend for composition 29 (see section 4.5.2)

Nevertheless, the calculated cross section libraries structure, allows a future use of an on-line interpolation as soon as RELAP5-3D will include this option.

4.4. The coupling methodology

Certain requirements with regard to the coupling of thermal-hydraulic system codes and neutron kinetics codes should be considered, e.g., [39], [40], [41], [42]. The objective of these requirements is to provide accurate solutions in a reasonable amount of CPU time in coupled simulations of detailed operational transient and accident scenarios.

These requirements are met by the development and implementation of six basic components of the coupling methodologies:
1) Coupling approach – integration algorithm or parallel processing.
2) Ways of coupling – internal or external coupling.
3) Spatial mesh overlays.
4) Coupled time-step algorithms.
5) Coupling numerics – explicit, semi-implicit and implicit schemes.
6) Coupled convergence schemes

Detailed explanation of the previous points can be found in [43]. It should be noted that for the execution of the plant SS and transient calculation, RELAP5-3D code exploits an integration algorithm (i.e., NESTLE code is fully integrated into the system code) performing an internal coupling. Mesh overlays between NESTLE and RELAP5-3D TH module are managed through the use of dedicated input deck cards. The time steps are instead governed by the TH module.

4.5. The procedure for code application including the nodalization

4.5.1. Introduction

The calculation of 3D NK TH transients by a system code like RELAP5-3D code requires several “auxiliary” steps, or development of cross section libraries and validation calculations. In Fig. 51 is given the main steps followed for the calculations performed during this PhD thesis.

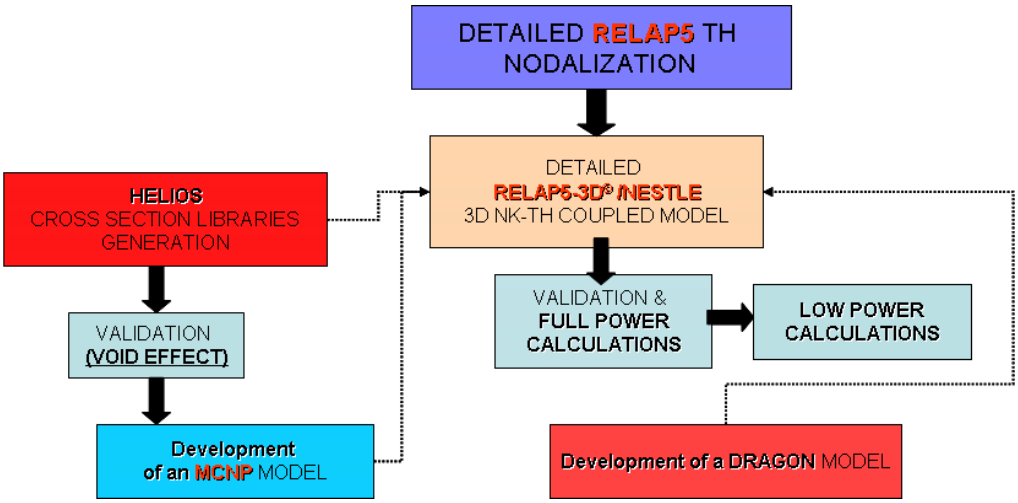

Fig. 51 – Codes and Models developed for 3D NK TH RBMK analyses

The firs step concerned the developed of a Smolensk-3 TH nodalization for the RELAP5 TH code. A very detailed model of the plant was developed, comprehensive of both the MCC, the SD, part of the SL and with a core TH description based on 50 FC. Active and passive heat structures were also taken into account. This model is described in section 4.5.3.
The second step concerned the development of a 3D NK model. This was then coupled with the full TH hydraulic model of the previous step and with a simplified one. The 3D NK model and its coupling scheme are described in section 4.5.4 and 4.5.4.1 respectively.
A third (parallel to the second one) step was the development, in collaboration with the RDFMG of PSU, of suitable RBMK cross section libraries by the HELIOS code. This model is described in section 4.5.2.
Coupled codes calculations of a specific transient, the FC blockage, prompted the necessity to perform detailed Monte Carlo simulation of the involved Fuel Cells. This constituted the fourth step and it was performed developing a MCNP5 model, described in section 4.5.5.
The fifth and last step was the development by the lattice physics code DRAGON of fuel cell spectrum-weighted microscopic cross sections libraries for Xenon, in

order to simulate by the 3D NK TH RELAP5-3D code the low power transient, i.e., a Chernobyl like accident. The DRAGON model is described in section 4.5.6

4.5.2. The HELIOS code model

4.5.2.1. Core geometry

The developed HELIOS RBMK fuel assembly (cell) model was a single cell with reflective boundary conditions, with which depletion and branch calculations were performed. In addition a HELIOS RBMK non-fuel assembly (cell) model was developed. In this case the cell was surrounded by eight fuel cells (color set calculations).

All of the fuel cells were assumed to have the same burnup. The graphite temperature was assumed to be uniform in the whole color set (macro cell). Only branch calculations were performed with this model by varying coolant density in the non-fuel cell, coolant density in surrounding fuel cells, and graphite temperature in the non-fuel cell

The HELIOS sophisticated methods address properly all of these issues and HELIOS can be used for the RBMK cross-section generation and modeling. There was no need for additional ad-hoc corrections of the macroscopic cross-sections or burnup as it is generally done for RBMK with the cross-sections generated by other codes (e.g., WIMS, see section 4.1.2).

Radially, the core was divided into square cells with a pitch 25.0 cm, each corresponding to one channel, plus a four rows of radial reflector blocks of the same size (shaded area in Fig. 35, Fig. 55 and Fig. 56).

As reported in Chapter 2, there are a total of 2488 channels, 1570 fuel channels, 314 non-fuel channels, and 604 reflector channels. Axially, the reactor core was divided into 10 layers with a height (starting from the bottom) of 70.0 cm, adding up to a total active core height of 700 cm. Both upper and lower axial reflectors have a thickness of 30 cm.

The axial nodalization scheme accounts for material changes in the fuel design and for the exposure variations. Zero flux boundary conditions were specified on outer reflector surface for both radial and axial reflectors. The geometric model for the developed elementary cells is respectively shown in and in Fig. 52 for the Fuel-Cell and Fig. 53 for the Non-Fuel Cell.

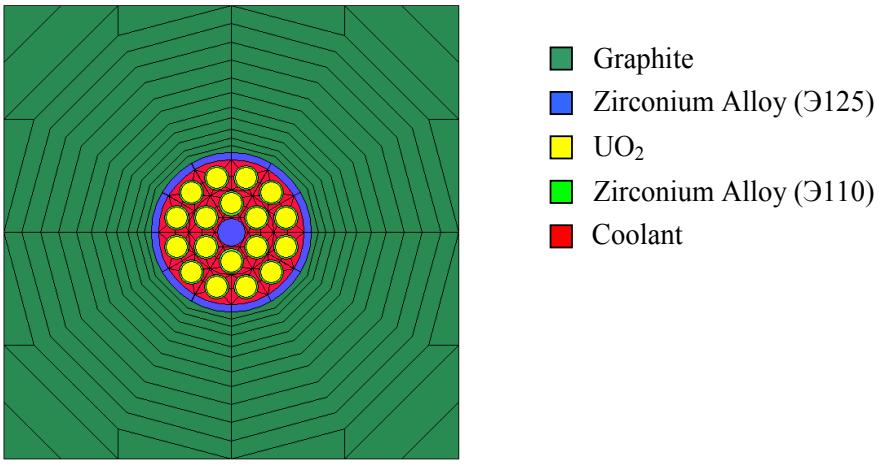

Fig. 52 – HELIOS modeling of RBMK FC cell

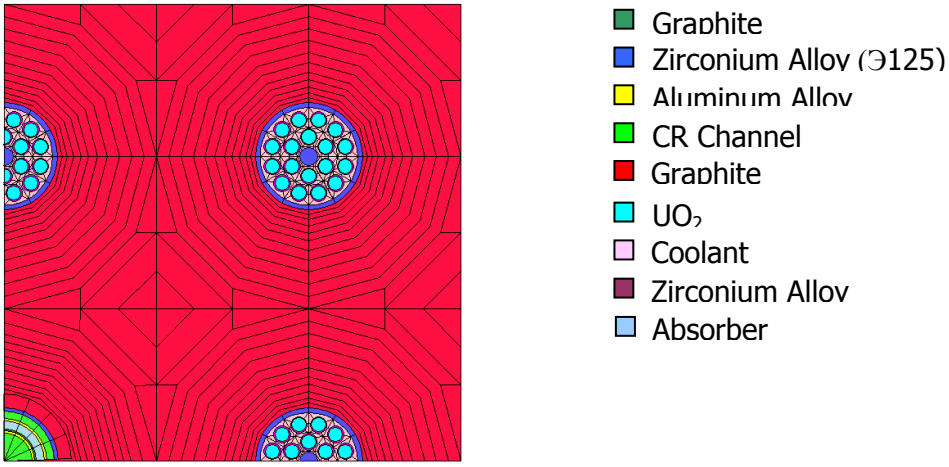

Fig. 53 – HELIOS modeling of RBMK MCR cell

The number of axial mesh used in the HELIOS core modeling is given in Fig. 54. A detailed description of the TH coupled part can be found further below in this document.

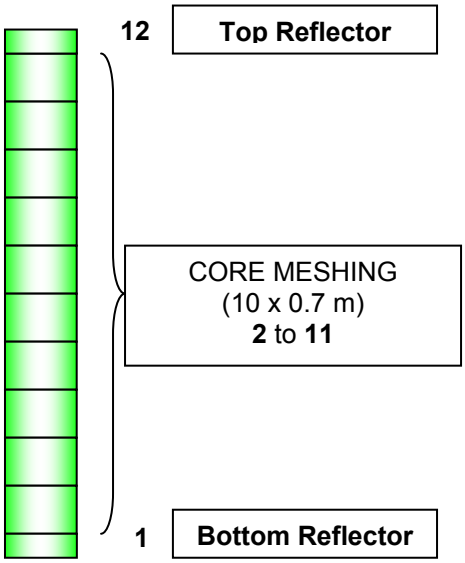

Fig. 54 – Core neutron kinetic mesh

Fuel channels with different ^{235}U enrichments are present in the core. 48 fuel channels have 2.0% enriched fuel and 1522 fuel channels have 2.4% enriched fuel. HELIOS model took into account these differences and the reactor fuel burnup map. The three different types of control rods were also modeled, or the 155 manual control rods with its three parts – absorber, connecting rod, and displacer (made of graphite) –, the shortened control rods (32 in the core) with its two parts – absorber and displacer – and the safety control rod type (24 in the core) with their absorber. The rest of the non-fuel channels modeled were axial detector channels (12 in the core), additional absorber (90 in the core), and water column (1 in the core). Each of these different fuel channels, were identified by a number. Their physical characteristics (i.e., enrichment, burnup, fuel/non fuel channel) are reported in Tab. 16, Tab. 17. Their location in the reactor core lattice are instead given in Fig. 55, Fig. 56.

Tab. 16 – Definition of fuel channel types

Channel type	Enrichment, % w/o	Exposure, MWd/kgU
1	2.0	6.75
2	2.0	14.25
3	2.0	14.75
4	2.0	15.25
5	2.0	15.75
6	2.0	16.25

Tab. 16 (cont.) – Definition of fuel channel types

Channel type	Enrichment, % w/o	Exposure, MWd/kgU
7	2.0	16.75
8	2.0	17.25
9	2.0	17.75
10	2.0	18.25
11	2.0	19.75
12	2.0	20.25
13	2.4	0.25
14	2.4	0.75
15	2.4	1.25
16	2.4	1.75
17	2.4	2.25
18	2.4	2.75
19	2.4	3.25
20	2.4	3.75
21	2.4	4.25
22	2.4	4.75
23	2.4	5.25
24	2.4	5.75
25	2.4	6.25
26	2.4	6.75
27	2.4	7.25
28	2.4	7.75
29	2.4	8.25
30	2.4	8.75
31	2.4	9.25
32	2.4	9.75
33	2.4	10.25
34	2.4	10.75
35	2.4	11.25
36	2.4	11.75
37	2.4	12.25
38	2.4	12.75
39	2.4	13.25
40	2.4	13.75
41	2.4	14.25
42	2.4	14.75
43	2.4	15.25
44	2.4	15.75
45	2.4	16.25
46	2.4	16.75
47	2.4	17.25
48	2.4	17.75

Tab. 16 (cont.) – Definition of fuel channel types

Channel type	Enrichment, % w/o	Exposure, MWd/kgU
49	2.4	18.25
50	2.4	18.75
51	2.4	19.25
52	2.4	19.75
53	2.4	20.25
54	2.4	20.75
55	2.4	21.25
56	2.4	21.75
57	2.4	22.25
58	2.4	22.75
59	2.4	23.25
60	2.4	23.75
61	2.4	24.25

Tab. 17 – Definition of non-fuel channel types

Channel type	Description	Enrichment of surrounding Fuel Channels, % w/o	Exposure of surrounding Fuel Channels, MWd/kgU
62	Axial Detector Channel	2.4	10.00
63	Manual Control Rods	2.4	10.00
64	Shortened Control Rods	2.4	10.00
65	Safety Control Rods	2.4	10.00
66	Additional Absorber	2.4	10.00
67	Water Column	2.4	10.00
68	Radial Reflector	2.4	10.00
69	Radial Reflector	2.4	10.00
70	Radial Reflector	2.4	10.00

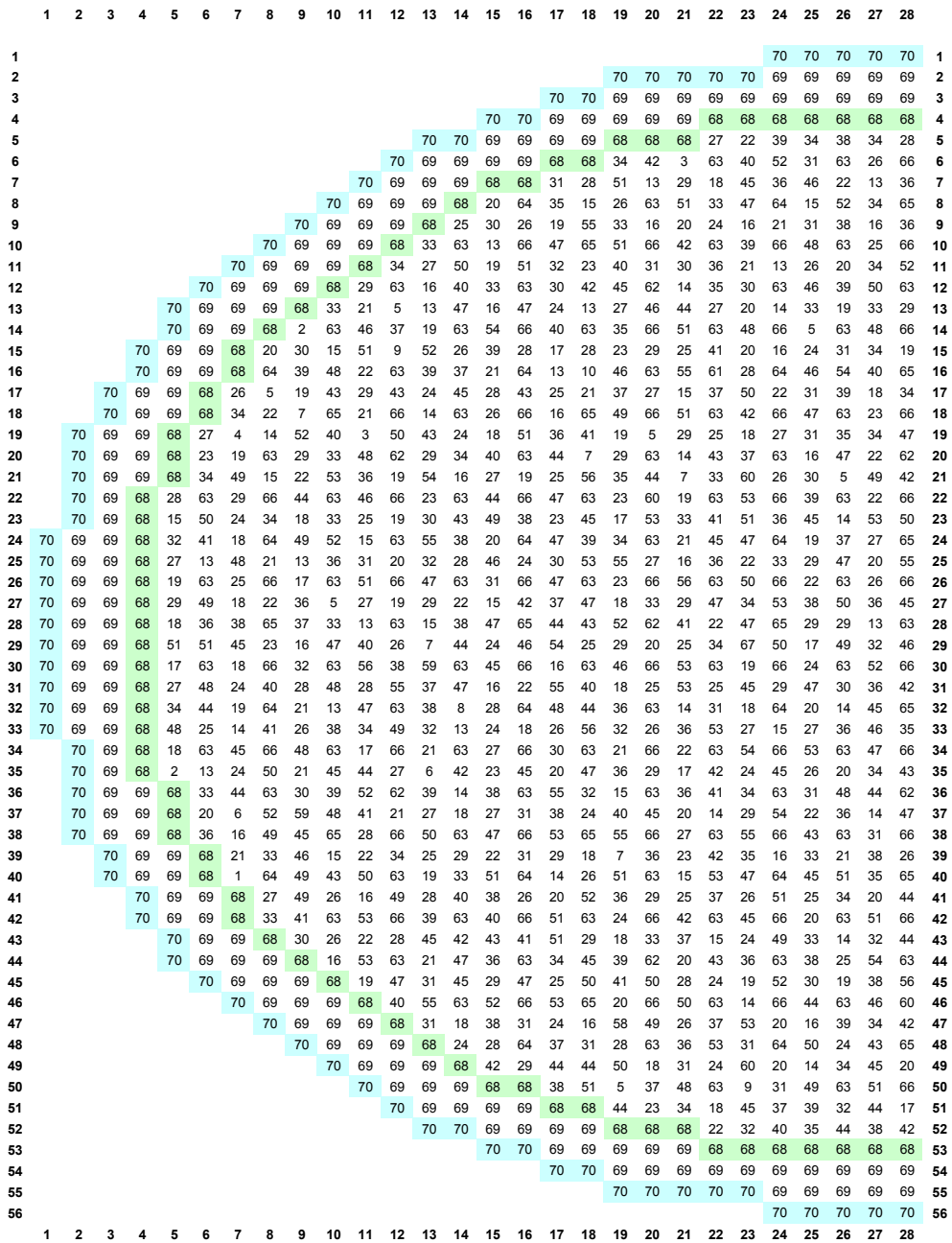

Fig. 55 – Two-dimensional channel type map (core left part)

	29	30	31	32	33	34	35	36	37	38	39	40	41	42	43	44	45	46	47	48	49	50	51	52	53	54	55	56	
1	70	70	70	70	70																								**1**
2	69	69	69	69	69	70	70	70	70	70																			**2**
3	69	69	69	69	69	69	69	69	69	69	70	70																	**3**
4	68	68	68	68	68	68	68	69	69	69	69	69	70	70															**4**
5	35	13	29	45	29	22	26	68	68	68	69	69	69	69	70	70													**5**
6	49	63	18	36	39	63	44	37	32	36	68	68	69	69	69	69	70												**6**
7	51	39	47	37	48	15	19	54	30	40	34	25	68	68	69	69	69	70											**7**
8	40	44	22	64	26	37	51	63	18	46	13	64	30	26	68	69	69	69	70										**8**
9	17	54	31	46	52	34	24	13	36	34	25	37	39	47	16	68	69	69	69	70									**9**
10	21	63	44	66	14	63	45	66	39	65	21	66	18	63	46	26	68	69	69	69	70								**10**
11	31	26	34	23	53	22	30	34	47	47	44	47	52	24	13	40	30	68	69	69	69	70							**11**
12	36	44	48	63	7	39	50	62	47	51	17	63	32	37	49	63	18	38	68	69	69	69	70						**12**
13	53	50	30	17	25	15	42	39	5	54	25	45	52	16	45	53	24	44	36	68	69	69	69	70					**13**
14	22	63	47	66	42	63	26	44	40	63	20	66	19	63	50	37	50	63	51	20	68	69	69	70					**14**
15	44	36	44	4	26	21	35	56	22	40	15	41	27	35	31	43	18	36	31	34	28	68	69	69	70				**15**
16	40	29	19	64	17	40	9	63	52	48	53	64	50	16	54	63	25	50	52	64	23	68	69	69	70				**16**
17	14	46	51	22	32	28	32	54	39	35	33	27	24	32	23	29	13	42	43	31	17	30	68	69	69	70			**17**
18	25	63	47	66	55	63	18	66	33	65	24	66	46	63	40	66	22	65	52	66	3	2	68	69	69	70			**18**
19	44	23	53	24	42	30	25	36	23	40	36	42	19	36	46	49	41	48	25	20	32	15	21	68	69	69	70		**19**
20	15	35	32	63	56	40	54	63	49	46	54	63	33	34	13	62	28	40	44	63	27	40	47	68	69	69	70		**20**
21	49	38	15	21	31	21	25	21	28	38	27	40	23	50	18	43	16	47	30	45	20	49	42	68	69	69	70		**21**
22	26	63	32	66	45	63	49	66	54	63	48	66	44	63	26	66	24	63	50	66	24	63	21	33	68	69	70		**22**
23	18	13	21	38	14	43	17	37	32	45	18	23	14	33	53	20	13	30	44	14	20	15	51	15	68	69	70		**23**
24	43	44	46	64	46	36	29	63	49	38	50	64	48	37	30	63	52	47	24	64	48	27	37	6	68	69	69	70	**24**
25	33	18	25	50	30	56	25	50	32	23	28	16	27	47	24	52	16	31	35	19	3	55	22	34	68	69	69	70	**25**
26	50	63	46	66	24	63	15	66	43	63	54	66	32	63	32	66	43	63	26	66	45	63	42	2	68	69	69	70	**26**
27	31	26	20	46	17	50	20	49	25	41	28	40	17	49	18	45	34	42	4	17	27	34	20	37	68	69	69	70	**27**
28	22	40	35	65	43	25	31	62	42	44	43	65	40	44	35	63	23	41	13	65	43	13	51	8	68	69	69	70	**28**
29	37	7	17	22	36	60	32	43	16	53	37	41	45	19	31	50	28	38	25	41	37	27	34	17	68	69	69	70	**29**
30	25	63	48	66	53	63	47	60	37	63	22	66	48	63	25	66	22	63	48	66	48	63	52	37	68	69	69	70	**30**
31	32	14	44	37	23	38	22	58	49	28	17	38	27	44	20	13	34	6	23	3	25	48	21	36	68	69	69	70	**31**
32	22	39	42	64	30	36	56	63	16	53	47	64	21	33	38	63	50	18	13	64	18	31	5	40	68	69	69	70	**32**
33	16	55	44	21	45	20	26	45	33	55	23	15	29	54	15	53	36	40	29	23	28	53	37	4	68	69	69	70	**33**
34	47	63	45	66	52	63	51	66	26	63	41	66	44	63	20	66	22	63	16	66	17	63	19	37	68	69	70		**34**
35	23	5	17	21	28	50	35	23	19	42	28	20	25	51	41	34	17	28	34	47	30	51	6	30	68	69	70		**35**
36	14	38	31	63	35	40	18	63	33	51	56	63	40	40	45	62	51	12	24	63	25	40	36	68	69	69	70		**36**
37	19	52	45	15	27	55	30	43	39	38	19	45	26	54	41	38	7	15	46	47	13	30	23	68	69	69	70		**37**
38	27	63	39	66	46	63	21	66	20	65	47	66	16	63	49	44	39	65	21	66	37	63	31	68	69	69	70		**38**
39	35	22	46	18	25	42	33	37	49	44	48	33	50	26	36	53	18	43	46	24	33	28	68	69	69	70			**39**
40	54	40	26	64	15	52	57	63	45	54	30	64	22	44	20	63	52	44	32	64	18	23	68	69	69	70			**40**
41	25	17	45	35	22	27	34	18	14	24	48	39	29	13	30	49	32	13	52	26	29	68	69	69	70				**41**
42	49	63	24	66	44	63	52	66	46	63	44	66	32	63	20	66	21	63	46	14	38	68	69	69	70				**42**
43	14	40	19	57	33	41	37	34	29	34	26	52	29	45	27	43	15	52	40	40	68	69	69	70					**43**
44	25	35	36	63	54	7	17	62	50	14	19	63	39	33	52	63	22	30	34	68	69	69	69	70					**44**
45	31	55	26	32	25	32	35	22	38	33	23	52	17	45	47	14	50	39	68	69	69	69	70						**45**
46	19	63	43	66	47	63	51	66	6	65	27	66	23	63	53	32	30	68	69	69	69	70							**46**
47	38	42	21	16	22	18	27	31	19	40	49	38	51	35	40	35	68	69	69	69	70								**47**
48	42	7	52	64	50	38	51	63	47	15	54	64	24	37	17	68	69	69	69	70									**48**
49	49	33	23	31	23	26	11	24	52	27	45	32	28	31	68	69	69	69	70										**49**
50	49	63	47	50	46	63	46	48	41	63	40	19	68	68	69	69	69	70											**50**
51	43	23	41	15	40	35	49	36	16	32	68	68	69	69	69	69	70												**51**
52	32	42	45	48	44	44	43	68	68	68	69	69	69	69	70	70													**52**
53	68	68	68	68	68	68	68	69	69	69	69	69	70	70															**53**
54	69	69	69	69	69	69	69	69	69	69	70	70																	**54**
55	69	69	69	69	69	70	70	70	70	70																			**55**
56	70	70	70	70	70																								**56**
	29	**30**	**31**	**32**	**33**	**34**	**35**	**36**	**37**	**38**	**39**	**40**	**41**	**42**	**43**	**44**	**45**	**46**	**47**	**48**	**49**	**50**	**51**	**52**	**53**	**54**	**55**	**56**	

Fig. 56 – Two-dimensional channel type map (core right part)

Thus, seventy channel types were identified within the core geometry. Each channel type is then defined by several “compositions”, according to its material properties (due to changes in the fuel design) and burn-up. The axial locations of compositions for each fuel type is shown in Tab. 18. The normalized axial exposure distribution for the different fuel types is given in Tab. 19.

4.5.2.2. The Cross-section library

The required set of 2-group macroscopic cross sections for fuel channels consists of the following seven types of cross-sections:

- diffusion coefficient, fast group (D_1),
- diffusion coefficient, thermal group (D_2),
- removal cross-section, fast group ($\Sigma_{a1}+\Sigma_{s12}$),
- absorption cross-section, thermal group (Σ_{a2}),
- neutron generation cross-section, fast group ($\nu\Sigma_{f1}$),
- neutron generation cross-section, thermal group ($\nu\Sigma_{f2}$),
- neutron transfer cross-section from fast to thermal group (Σ_{s12}).

Separate cross-sections were calculated for upper and lower parts of fuel assemblies. For the non-fuel channels the following types of 2-group cross-sections were obtained:

- diffusion coefficient, fast group (D_1),
- diffusion coefficient, thermal group (D_2),
- removal cross-section, fast group ($\Sigma_{a1}+\Sigma_{s12}$),
- absorption cross-section, thermal group (Σ_{a2}),
- neutron transfer cross-section from fast to thermal group (Σ_{s12}).

Also, a complete set of assembly discontinuity factors (ADF) were calculated. All these cell parameters were expressed as a function of the fuel temperature, moderator temperature, and coolant density for each composition. The group inverse neutron velocities were also provided for each composition.

The expected range of the transients was covered by the selection of an adequate range for the independent variables shown in Tab. 20.

Dependence of the cross-sections on the above variables was specified through a three-dimensional look-up table. Each composition was assigned to a cross-section set containing separate tables for the diffusion coefficient, cross-sections, and ADF, with each point in the table representing a possible core state. A linear interpolation scheme could be used to obtain the appropriate total cross-sections from the tabulated ones based on the reactor conditions being modeled (see Fig. 57).

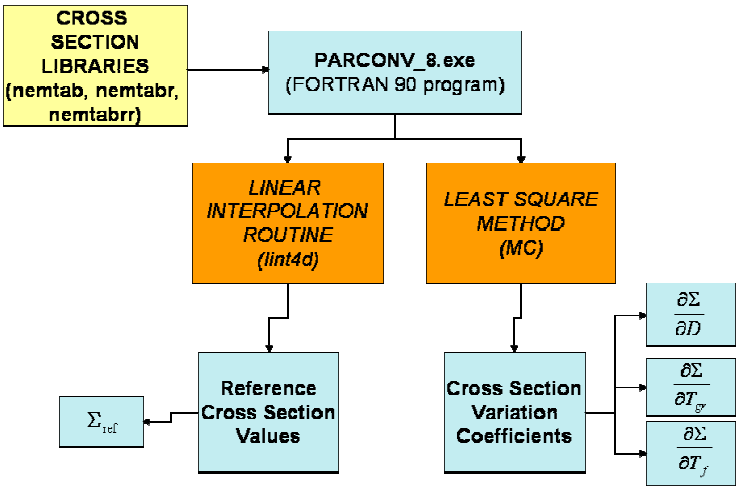

Fig. 57 – Interpolation Scheme for Cross Sections parameters

For this purpose, a 4D Linear Interpolation Routine (lint4D) implemented in a FORTRAN 90 program was used. Finally, after the calculation of the Cross Section Variation Coefficients (i.e. with the Least Square Method) too, it was possible to implement in the 3D NK code all the Cross Section related information, e.g. using a Cross Section representation like that one reported in Equation (*10)*:

$$\Sigma(Tf, Tgr, D) = \Sigma_{ref} + \frac{\partial \Sigma}{\partial Tf}\Delta Tf + \frac{\partial \Sigma}{\partial Tgr}\Delta Tgr + \frac{\partial \Sigma}{\partial D}\Delta D \qquad (10)$$

where:
Σ_{ref} = Reference Cross Section
T_f = Fuel Temperature
T_{gr} = Graphite Temperature
D = coolant density

Tab. 21 and Fig. 58 shows in details the definition of a cross-section table associated with a composition. All cross-section sets are assembled into a cross-section library. The cross-sections were provided in separate libraries for rodded **(nemtabr)** (absorber part of the control rods), unrodded compositions **(nemtab)** (fuel channels, displacer parts of the control rods, water column, additional absorber, and axial detector channels) and **nemtab** (connecting rod of the manual control rods). The format of each library was as follows:

- The first line of data was used to show the number of data points used for the independent thermal-hydraulic (T-H) parameters. These parameters included fuel temperature, moderator temperature, coolant density
- Each cross-section set is in the order shown in Tab. 21. Each table is in the format described in Fig. 58. First, the values of the independent thermal-hydraulic parameters used to specify that particular set of cross-

sections are listed, followed by the values of the cross-sections. Finally, the group inverse neutron velocities complete the data for a given cross-section set.

- The dependence of the reflector and of CPS cross-section on thermal-hydraulic parameters is also modeled. This is because the reflector and CPS cross-sections are generated by performing lattice physics transport calculations, including the next fuel region. Therefore, the feedback parameters should be taken from the neighboring fuel region.

Tab. 18 – Composition numbers in axial layers for each channel type

Bottom

	1	2	3	4	5	6	7	8	9	10	11	12	13	14	15	16	17	18	19	20	21	22	23
1	671	671	671	671	671	671	671	671	671	671	671	671	671	671	671	671	671	671	671	671	671	671	671
2	1	11	21	31	41	51	61	71	81	91	101	111	121	131	141	151	161	171	181	191	201	211	221
3	2	12	22	32	42	52	62	72	82	92	102	112	122	132	142	152	162	172	182	192	202	212	222
4	3	13	23	33	43	53	63	73	83	93	103	113	123	133	143	153	163	173	183	193	203	213	223
5	4	14	24	34	44	54	64	74	84	94	104	114	124	134	144	154	164	174	184	194	204	214	224
6	5	15	25	35	45	55	65	75	85	95	105	115	125	135	145	155	165	175	185	195	205	215	225
7	6	16	26	36	46	56	66	76	86	96	106	116	126	136	146	156	166	176	186	196	206	216	226
8	7	17	27	37	47	57	67	77	87	97	107	117	127	137	147	157	167	177	187	197	207	217	227
9	8	18	28	38	48	58	68	78	88	98	108	118	128	138	148	158	168	178	188	198	208	218	228
10	9	19	29	39	49	59	69	79	89	99	109	119	129	139	149	159	169	179	189	199	209	219	229
11	10	20	30	40	50	60	70	80	90	100	110	120	130	140	150	160	170	180	190	200	210	220	230
12	675	675	675	675	675	675	675	675	675	675	675	675	675	675	675	675	675	675	675	675	675	675	675

Top

Bottom

24	25	26	27	28	29	30	31	32	33	34	35	36	37	38	39	40	41	42	43	44	45	46
671	671	671	671	671	671	671	671	671	671	671	671	671	671	671	671	671	671	671	671	671	671	671
231	241	251	261	271	281	291	301	311	321	331	341	351	361	371	381	391	401	411	421	431	441	451
232	242	252	262	272	282	292	302	312	322	332	342	352	362	372	382	392	402	412	422	432	442	452
233	243	253	263	273	283	293	303	313	323	333	343	353	363	373	383	393	403	413	423	433	443	453
234	244	254	264	274	284	294	304	314	324	334	344	354	364	374	384	394	404	414	424	434	444	454
235	245	255	265	275	285	295	305	315	325	335	345	355	365	375	385	395	405	415	425	435	445	455
236	246	256	266	276	286	296	306	316	326	336	346	356	366	376	386	396	406	416	426	436	446	456
237	247	257	267	277	287	297	307	317	327	337	347	357	367	377	387	397	407	417	427	437	447	457
238	248	258	268	278	288	298	308	318	328	338	348	358	368	378	388	398	408	418	428	438	448	458
239	249	259	269	279	289	299	309	319	329	339	349	359	369	379	389	399	409	419	429	439	449	459
240	250	260	270	280	290	300	310	320	330	340	350	360	370	380	390	400	410	420	430	440	450	460
675	675	675	675	675	675	675	675	675	675	675	675	675	675	675	675	675	675	675	675	675	675	675

Top

Bottom

47	48	49	50	51	52	53	54	55	56	57	58	59	60	61	62	63	64	65	66	67	68	69	70
671	671	671	671	671	671	671	671	671	671	671	671	671	671	671	671	671	671	671	671	671	671	671	671
461	471	481	491	501	511	521	531	541	551	561	571	581	591	601	611	621	631	641	651	661	672	673	674
462	472	482	492	502	512	522	532	542	552	562	572	582	592	602	612	622	632	642	652	662	672	673	674
463	473	483	493	503	513	523	533	543	553	563	573	583	593	603	613	623	633	643	653	663	672	673	674
464	474	484	494	504	514	524	534	544	554	564	574	584	594	604	614	624	634	644	654	664	672	673	674
465	475	485	495	505	515	525	535	545	555	565	575	585	595	605	615	625	635	645	655	665	672	673	674
466	476	486	496	506	516	526	536	546	556	566	576	586	596	606	616	626	636	646	656	666	672	673	674
467	477	487	497	507	517	527	537	547	557	567	577	587	597	607	617	627	637	647	657	667	672	673	674
468	478	488	498	508	518	528	538	548	558	568	578	588	598	608	618	628	638	648	658	668	672	673	674
469	479	489	499	509	519	529	539	549	559	569	579	589	599	609	619	629	639	649	659	669	672	673	674
470	480	490	500	510	520	530	540	550	560	570	580	590	600	610	620	630	640	650	660	670	672	673	674
675	675	675	675	675	675	675	675	675	675	675	675	675	675	675	675	675	675	675	675	675	675	675	675

Top

Tab. 19 – Normalized axial exposure

Axial layer #	2	3	4	5	6	7	8	9	10	11
Fuel 2.0%	0.758	1.036	1.087	1.118	1.154	1.160	1.113	1.029	0.915	0.629
Fuel 2.4%	0.756	1.076	1.126	1.143	1.170	1.164	1.103	1.006	0.878	0.577

Tab. 20 – Range of independent variables

T fuel (K)	T moderator (K)	Rho coolant (kg/m^3)	T fuel (K)	T moderator (K)	Rho coolant (kg/m^3)
557.00	557.00	10.00	557.00	557.00	500.00
850.00	557.00	10.00	850.00	557.00	500.00
1030.00	557.00	10.00	1030.00	557.00	500.00
557.00	700.00	10.00	557.00	700.00	500.00
850.00	700.00	10.00	850.00	700.00	500.00
1030.00	700.00	10.00	1030.00	700.00	500.00
557.00	856.00	10.00	557.00	856.00	500.00
850.00	856.00	10.00	850.00	856.00	500.00
1030.00	856.00	10.00	1030.00	856.00	500.00
557.00	1060.00	10.00	557.00	1060.00	500.00
850.00	1060.00	10.00	850.00	1060.00	500.00
1030.00	1060.00	10.00	1030.00	1060.00	500.00
557.00	557.00	100.00	557.00	557.00	744.00
850.00	557.00	100.00	850.00	557.00	744.00
1030.00	557.00	100.00	1030.00	557.00	744.00
557.00	700.00	100.00	557.00	700.00	744.00
850.00	700.00	100.00	850.00	700.00	744.00
1030.00	700.00	100.00	1030.00	700.00	744.00
557.00	856.00	100.00	557.00	856.00	744.00
850.00	856.00	100.00	850.00	856.00	744.00
1030.00	856.00	100.00	1030.00	856.00	744.00
557.00	1060.00	100.00	557.00	1060.00	744.00
850.00	1060.00	100.00	850.00	1060.00	744.00
1030.00	1060.00	100.00	1030.00	1060.00	744.00
557.00	557.00	300.00	557.00	557.00	998.00
850.00	557.00	300.00	850.00	557.00	998.00
1030.00	557.00	300.00	1030.00	557.00	998.00
557.00	700.00	300.00	557.00	700.00	998.00
850.00	700.00	300.00	850.00	700.00	998.00
1030.00	700.00	300.00	1030.00	700.00	998.00
557.00	856.00	300.00	557.00	856.00	998.00
850.00	856.00	300.00	850.00	856.00	998.00
1030.00	856.00	300.00	1030.00	856.00	998.00
557.00	1060.00	300.00	557.00	1060.00	998.00
850.00	1060.00	300.00	850.00	1060.00	998.00
1030.00	1060.00	300.00	1030.00	1060.00	998.00

Tab. 21 – Key to macroscopic cross-section tables

T_{F1}	T_{F2}	T_{F3}	T_{M1}	T_{M2}	Where: T_F – fuel temp. [K] T_M – moderator temp. [K] ρ_C – coolant density [kg/m^3] f – same as T_F m – same as T_M c – same as ρ_C
T_{M3}	T_{M4}	ρ_{C1}	ρ_{C2}	ρ_{C3}	
ρ_{C4}	ρ_{C5}	ρ_{C6}	Σ_1(f1,m1,c1)	Σ_2(f2,m1,c1)	
Σ_3(f3,m1,c1)	Σ_4(f1,m2,c1)	Σ_5(f2,m2,c1)	Σ_6(f3,m2,c1)	Σ_7(f1,m3,c1)	
Σ_8(f2,m3,c1)	Σ_9(f3,m3,c1)	Σ_{10}(f1,m4,c1)	Σ_{11}(f2,m4,c1)	Σ_{12}(f3,m4,c1)	
Σ_{13}(f1,m1,c2)	Σ_{14}(f2,m1,c2)	Σ_{15}(f3,m1,c2)	Σ_{16}(f1,m2,c2)	Σ_{17}(f2,m2,c2)	
Σ_{18}(f3,m2,c2)	Σ_{19}(f1,m3,c2)	……			
		……	Σ_{71}(f2,m4,c6)	Σ_{72}(f3,m4,c6)	

```
**************************************************************************
        NEM – Cross-Section Table Input
*
*       T Fuel          T Mod.          Rho Cool.       CXe
          3               4               6               0
*
**********    X-Section Set #
  #
**************************************************************************
        Group No. 1
*
*************   Diffusion Coefficient Table
*
*************   Absorption X-Section Table
*
*************   Fission X-Section Table
*
*************   Nu-Fission X-Section Table
*
*************   Scattering From Group 1 to 2 X-Section Table
*
*************   Assembly Discontinuity Factors Table
*
**************************************************************************
        Group No. 2
*
*************   Diffusion Coefficient Table
*
*************   Absorption X-Section Table
*
*************   Fission X-Section Table
*
*************   Nu-Fission X-Section Table
*
*************   Assembly Discontinuity Factors Table
*
**************************************************************************
*************   Inv. Neutron Velocities
*
```

Fig. 58 – Macroscopic cross-section table's structure

4.5.3. The RELAP5-3D TH nodalization

The detailed description of the RELAP5 nodalization developed for Smolensk-3 NPP is presented in [44]. An idea of the nodalization can be derived from Fig. 59 to Fig. 63. Two models of the NPP were developed, one representing the NPP up to the turbine, the other one (simplified), representing only the MCC from the MCPs exit up to the SD inlet. The latter one was used for 3D NK TH analyses were it was not necessary to model the whole primary circuit (e.g., CR / CR group withdrawal). All the nodalizations are divided into two parts identified as right and left side. Both sides are modeled in the same way, i.e., the main components (pumps, pipes, steam drums) are identical. An higher resolution of the core is achieved for the right side (47 channels modeled versus 8 for the left side), thus the right side is considered as the damaged one during the safety analyses.
As it can be seen in Fig. 59, all the main hydraulics components of the plant are modeled. Starting from the Steam Drums (SD), both two are represented by a set of branches and pipes, Fig. 61 in order to reproduce the stratification that ensures the gravity driven steam separation. The water (in the lower part) and the steam (in the upper part) zones of the SD are linked each other by a water and steam bridge. Two pipes joined to the top of each SD drive the steam to the steam ring where the steam lines are connected. All the safety valves (e.g. BRU-K, MSV and ICV) are considered in the input deck. The nozzle of the feed-water system is represented by the jet mixer component to simulate the suction effect of these devices.

The two feed-water systems (one per each SD) are simulated by a time dependent volume and a time dependent junction with a nominal imposed mass flow rate. The jet mixer components are joined to two pipes that simulate the downcomer. These two pipes are connected to four branches that simulate the suction header, Fig. 62. Four pipes supply the water from the suction header to four pumps connected via other pipe components to a pressure header schematized by eight branches. 22 GDH are simulated by 22 pipes (8 pipes for the left side) and, at the end of each of them, one branch is placed. 47 pipes (8 pipes for the left side) divided into 59 volumes represent the water lines and the fuel channels, up to the connection with the steam water line, with different scaling factor ranging from 1 up to 34 (from 62 to 134, for the left side). Additional 47 pipes (8 pipes for the left side) simulate the steam water lines connected to the lower part of the SD, Fig. 63.
The additional absorbers are simulated with a unique pipe (the same subdivision of the core channel has been used) together with its water line and steam water line. One separate circuit is reproduced to simulate the control rod and radial reflector cooling channels (one hydraulic channel for the CR cooling and one for the reflector).

All the passive components have the relative mono-dimensional heat structure divided into five radial mesh points and they are considered insulated on one side. The active heat structures that simulate the fuel are divided into 12 radial mesh points and into 20 axial parts. They are, on the left side, thermally coupled with the corresponding hydraulic volume of the core channel, on the right side insulated.

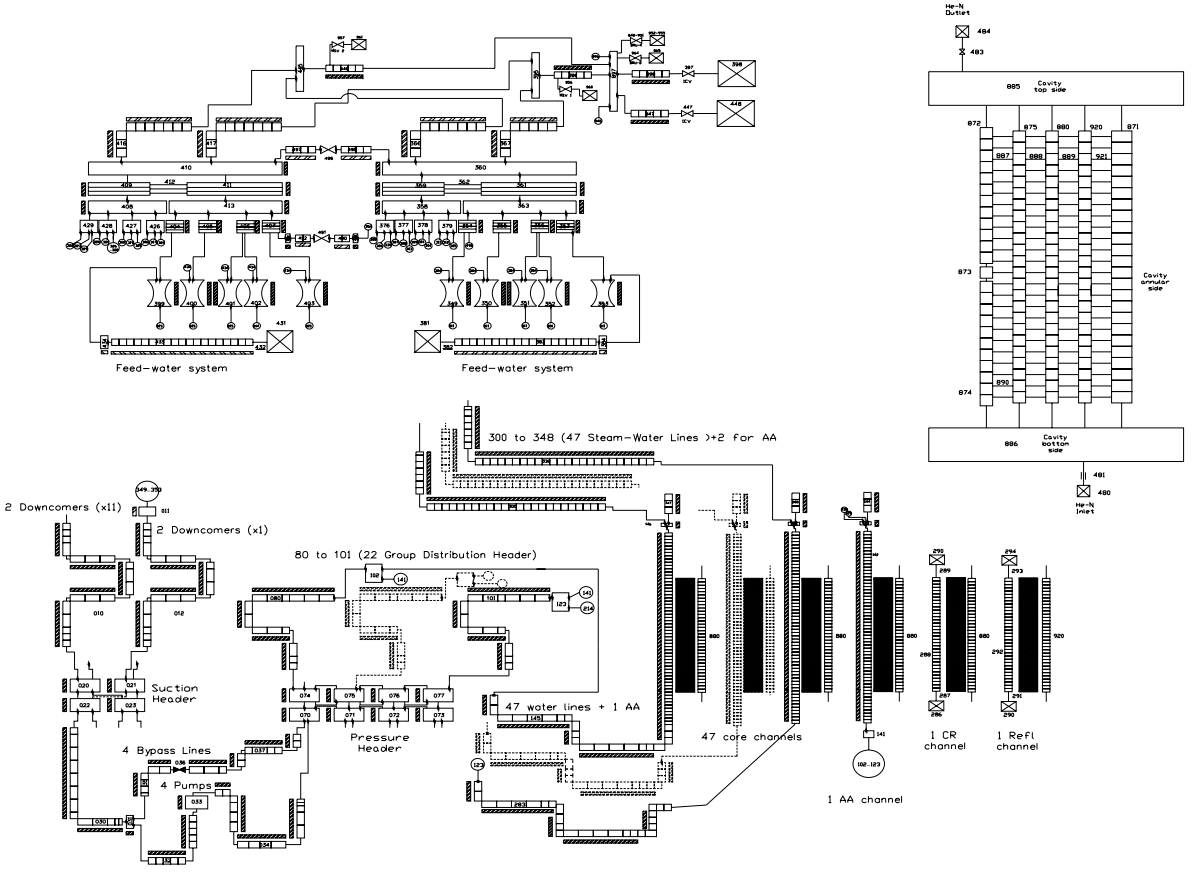

Fig. 59 – Sketch of the reference RELAP5-3D TH nodalization of Smolensk-3 (only left MCC showed)

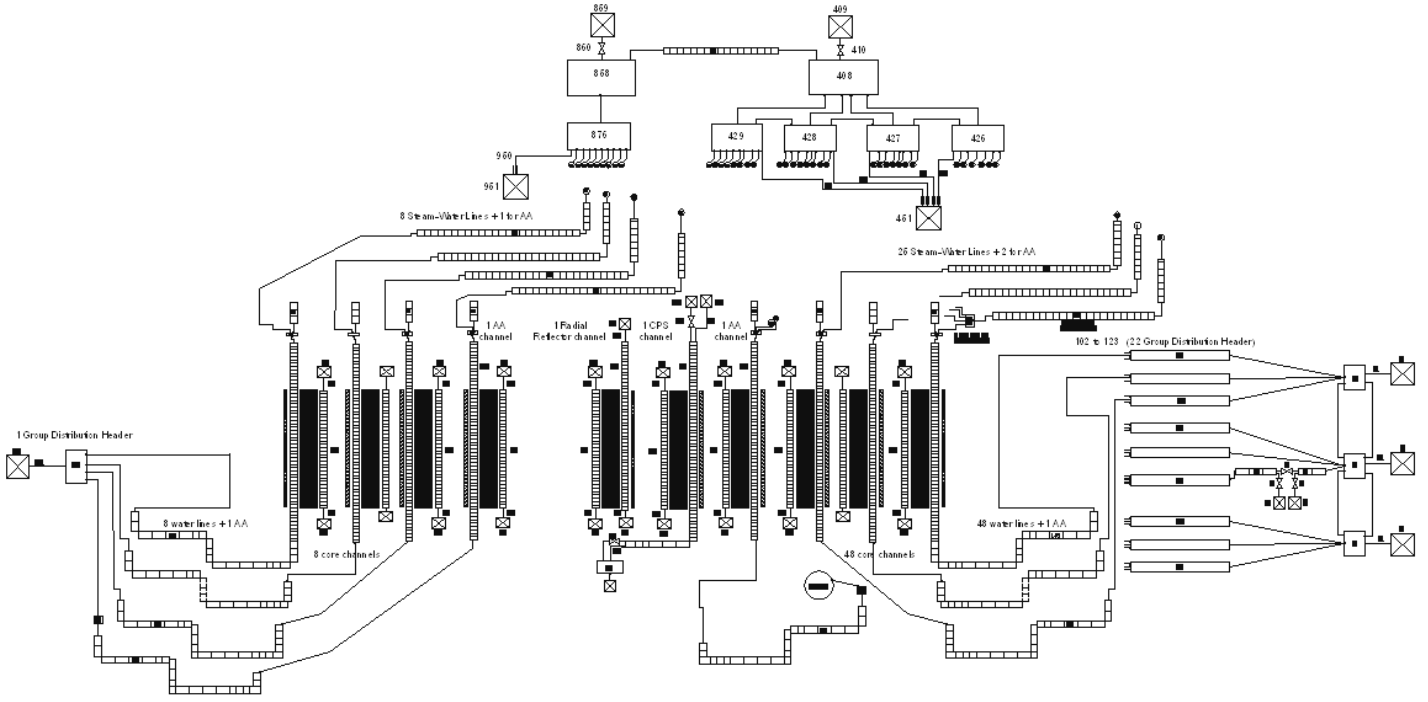

Fig. 60 – Sketch of the simplified RELAP5-3D TH nodalization (Left and Right MCC)

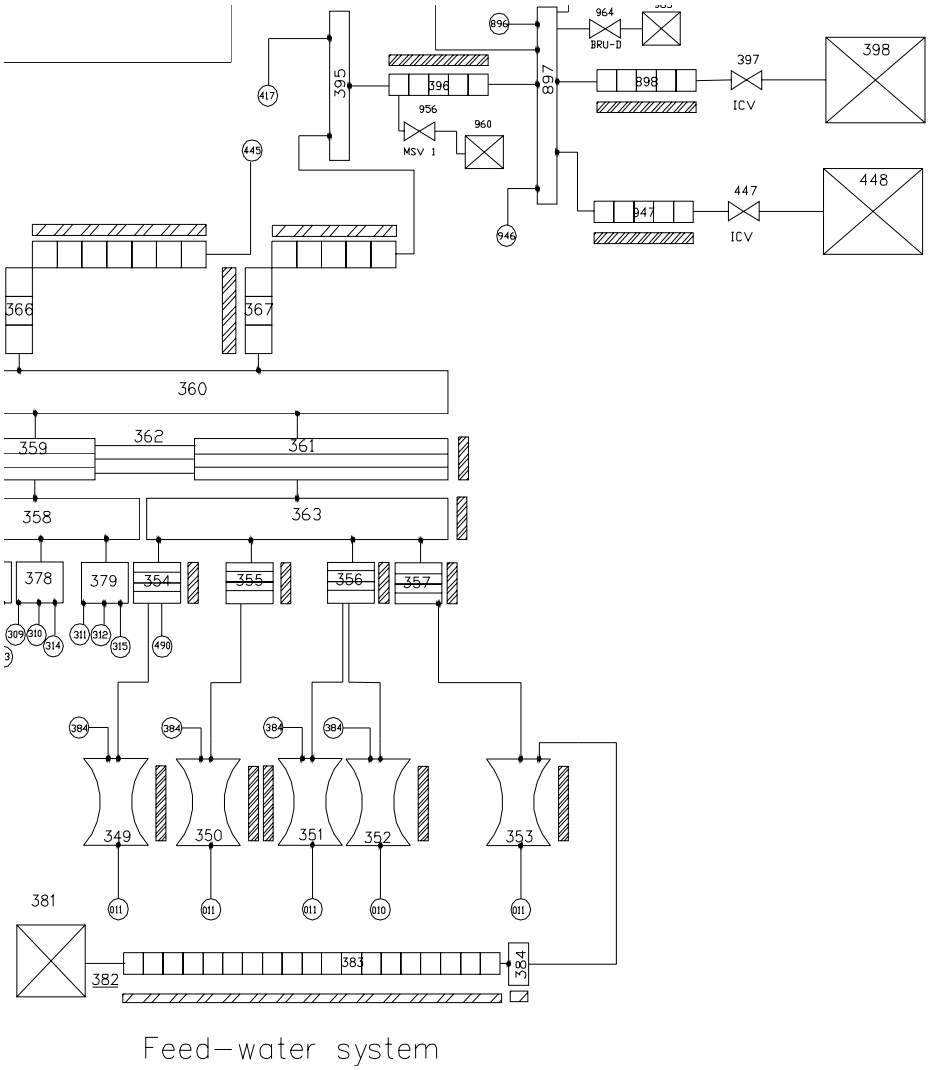

Fig. 61 – RELAP5-3D model of Smolensk 3 NPP: nodalization sketch of FW and SL systems.

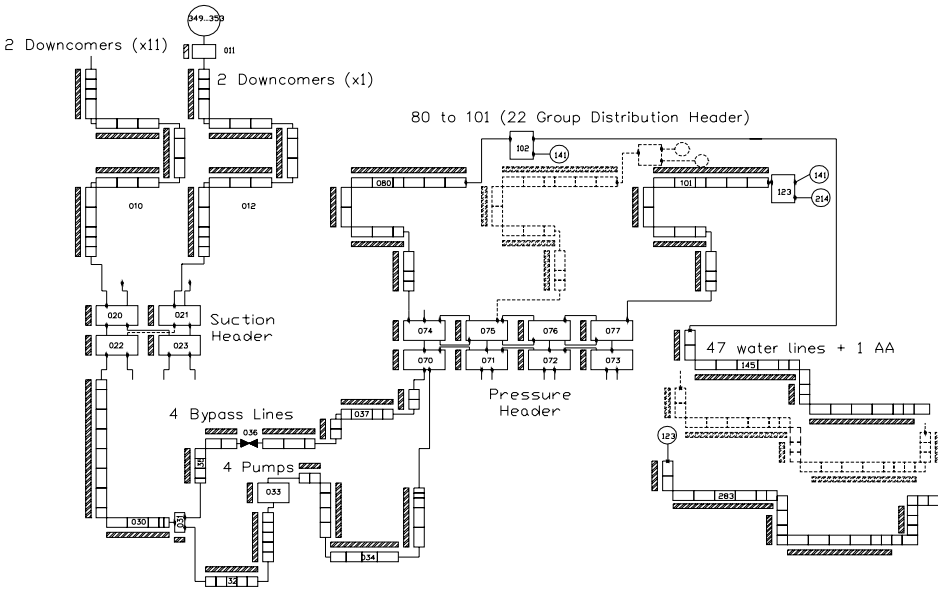

Fig. 62 – RELAP5-3D model of Smolensk 3 NPP: nodalization sketch of downcomers up to the water lines.

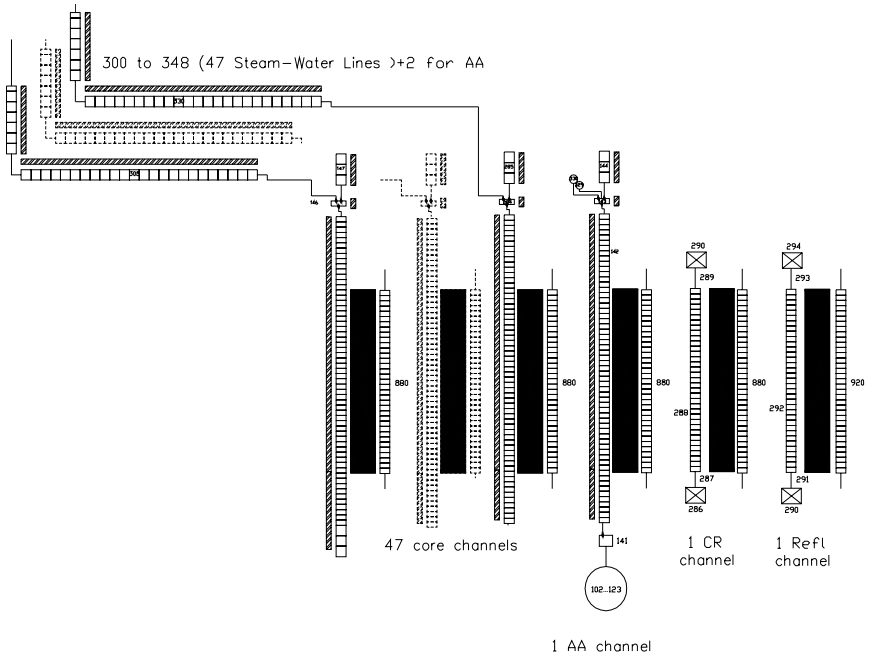

Fig. 63 – RELAP5-3D model of Smolensk 3 NPP: nodalization sketch of core, FC exit lines and CPS cooling system.

The thermal structures used to simulate the pressure tube, the graphite rings and the graphite bricks are divided into 12 radial meshes and in 24 axial parts in order to consider the axial reflector. They are thermally coupled with the core channel at the inner side and with the corresponding pipe of the reactor cavity at the outer side.

The ECCS included in the model of the Smolensk 3 NPP are, Fig. 64:

- Main-subsystem 1 and 2 including two trains of accumulators. Each train is composed by 6 accumulators. The two trains are connected to the headers to inject water in the damaged side of the core.
- Main-subsystem 3: this system injects water in the damaged side of the core by connecting to the main feed water pumps. The feed water pumps take water from the deareators.
- Long term sub-system damaged core side 1, 2 and 3: the system is constituted by three trains. Each train includes two pumps injecting in the damaged side of the core the water from the PSP in the ASL.
- Long term sub-system undamaged core side 1, 2 and 3: the system is constituted by three trains. Each train includes one pump. The pumps inject in the undamaged side of the core the water from the clean condensate tank.

The twelve accumulators of the Main sub-system 1 and 2 are schematized. In the model the accumulators injection is stopped when the level is low to avoid nitrogen injection in the MCC. The model makes possible to manage separately injection capability of any accumulators, if needed, simply changing the intervention logic that is separately implemented for each accumulator.

The Main sub-system 3 is schematized with a “tmdpjun” component simulating the main feed water pumps and a “tmdpvol” component simulating the thermal hydraulic condition of the water in the deaerators. The “tmdpjun” component makes possible a specific simulation of the mass flow-rate of the main feed water pumps for this system separated by the simulation of the feed water pumps of the MCC; this schematization has been preferred to avoid any “complicated interaction” with the model of the pumps used in the MCC. In addition this model makes available to change easily the mass flow-rate trend of the pumps to take into account the effects of LOOP and to control the integral mass flow-rate through the pumps: this value is used to check if the deaerators contain water to be injected.

The three trains of the Long term sub-system for the damaged core side are separately modeled. Each model includes a “tmdpjun” component connected whit the PSP simulating the two pumps of each train. Each train can be isolated if needed to investigate transient involving ECCS failure. The three train of the Long term sub-system for the undamaged core side are separately modeled. Each model includes a “tmdpjun” component simulating the pump of each train. Each train can be isolated if needed to investigate transient involving ECCS failure. The clean condensate tanks are schematized by a suitable “tmdpvol” component reproducing the thermal hydraulic condition of the water into the tank. The integral mass flow-rate exiting from the “tmdpvol” component is computed by the model to check the amount of water available to be injected by the system.

The Main sub-system 1, 2 and 3 and the Long term sub-system for the damaged core side 1, 2 and 3 are connected to three main distribution headers; each header is connected to all the 22 GDH schematized for the right side of the core; this side is supposed to be the damaged side of the core. The three trains of the long term sub-system for the undamaged core side 1, 2 and 3 are connected together in a single common distribution header because only one GDH is schematized for the right side of the core (suppose to be the undamaged side).

The logic of actuation of the systems is implemented especially in relation to accident involving break occurrence in component in the ALS (e.g. rupture in the piping downstream the MCP up to core inlet). The ECCS intervention logic for other kind of accident (i.e. feed water pipe break) can be implemented adding some specific conditions because the model does not include some special rooms where ECCS actuation signals are generated in some transients (e.g. no feed water compartment is modeled and the pressure increase in the this compartment as a consequence of a feed water piping break is not reproduced).

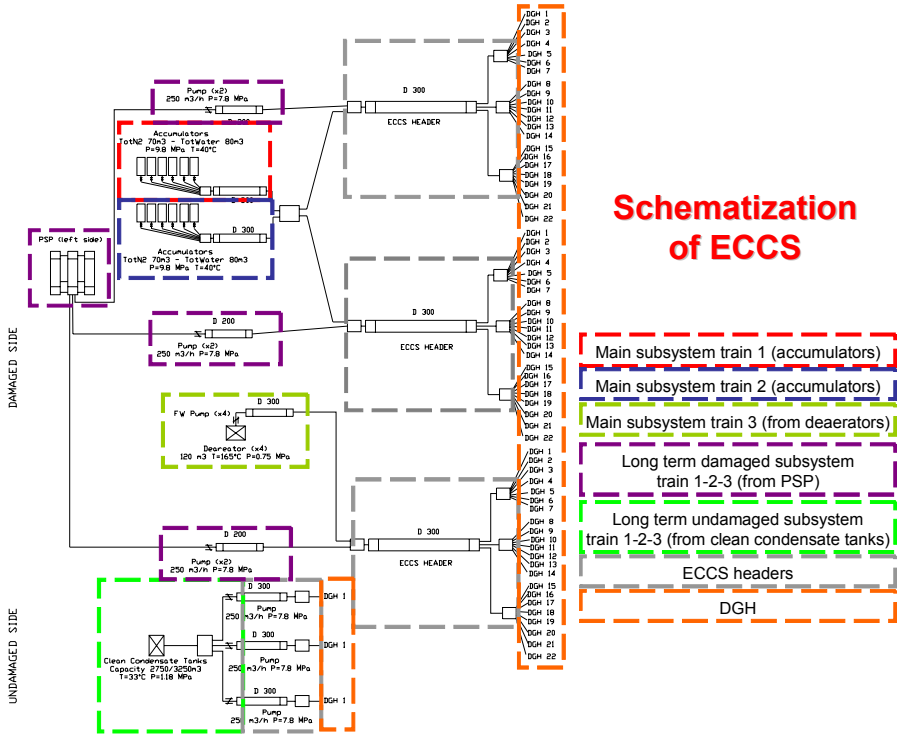

Fig. 64 – Relap5 UNIPI model of Smolensk 3 NPP: nodalization sketch of ECCS.

In Tab. 22 and Tab. 23 is reported, as already mentioned at the beginning of the present section, the list of all the components modeled identified by the RELAP5-3D card numbers and components.

Tab. 22 – Relap5 UNIPI model of Smolensk 3 NPP: correspondence between nodes and NPP components (left side).

LEFT SIDE		
Component	**ID of node**	**Node type**
Downcomer	010, 012, 014, 016	Pipe
	011, 015	Branch
Suction headers	020, 021, 022, 023	Branch
Suction piping	030, 040, 050, 060	Pipe
	031	Branch
	032, 042, 044	Pipe
Bypass line	035, 045, 055, 065	Pipe
	036, 046, 056, 066	Valve
	037, 047, 057, 067	Pipe
MCP	033, 043, 053, 063	Pump component
Pressure pipes after the pumps	034, 044, 054, 064	Pipe component
Pressure headers	070, 071, 072, 073	Branch
	074, 075, 076, 077	Branch
Group distribution header	80÷86, 87÷91, 92÷96, 97÷101	Pipe
	102÷123	Pipe
Additional absorber channel	141	Branch
	142	Pipe
	143	Branch
	144	Pipe
Core channels	145, 148, …, 285	Pipe

Tab. 22 (cont.) – Relap5 UNIPI model of Smolensk 3 NPP: correspondence between nodes and NPP components (left side).

LEFT SIDE		
Component	**ID of node**	**Node type**
Core channels	146, 149, …, 286	Branch
	147, 150, …, 287	Pipe
Steam water pipes	300÷348 for the core channels	Pipe
	329, 330 for the additional absorber	Pipe
Steam Drum 1	354÷357	Pipe
	376÷379	Branch
	358, 363	Branch
	359, 361	Pipe
	360	Branch
Jet spray system for SD 1	349÷353	Jet mixer
Water bridge	489	Branch
	490	Pipe
	491	Valve
	492	Pipe
	488	Branch
Steam bridge	495	Pipe
	496	Valve
	497	Pipe
Steam Line after SD 1	366÷367	Pipe
Steam drum 2	404÷407	Pipe
	426÷429	Branch
	408, 413	Branch
	409, 411	Pipe
	410	Branch
Jet spray system for SD2	399÷403	Jet mixer
Steam Line after SD2	416÷417	Branch

Tab. 22 (cont.) – Relap5 UNIPI model of Smolensk 3 NPP: correspondence between nodes and NPP components (left side).

LEFT SIDE		
Component	**ID of node**	**Node type**
Steam rings steam lines and turbines	395, 445	Branch
	396, 446	Pipe
	897	Branch
	898, 947	Pipe
	397, 447	Trip valve
	398, 448	Time dependent volume
Feed-water system 1	381	Time dependent volume
	382	Time dependent junctions
	383	Pipe
	384	Branch
Feed-water system 2	431	Time dependent volume
	432	Time dependent junctions
	433	Pipe
	434	Branch

Tab. 23 – Relap5 UNIPI model of Smolensk 3 NPP: correspondence between nodes and NPP components (right side).

RIGHT SIDE		
Component	**ID of node**	**Node type**
Downcomer	510, 512, 514, 516	Pipe
	511, 515	Branch
Suction headers	520, 521, 522, 523	Branch
Suction piping	530, 540, 550, 560	Pipe

Tab. 23 (cont.) – Relap5 UNIPI model of Smolensk 3 NPP: correspondence between nodes and NPP components (right side).

RIGHT SIDE		
Component	**ID of node**	**Node type**
	531, 541, 551, 561	Branch
	532, 542, 544	Pipe
Bypass line	535, 545, 555, 565, 537, 547, 557, 567	Pipe
	536, 546, 556, 566	Valve
MCP	533, 543, 553, 563	Pump component
Pressure pipes after the pumps	534, 544, 554, 564	Pipe component
Pressure headers	570, 571, 572, 573, 574, 575, 576, 577	Branch
Group distribution header	580	Pipe
	602	Branch
Additional absorber channel	641	Branch
	642	Pipe
	643	Branch
	644	Pipe
Core channels	645, 648, …, 666	Pipe

Tab. 23 (cont.) – Relap5 UNIPI model of Smolensk 3 NPP: correspondence between nodes and NPP components (right side).

RIGHT SIDE		
Component	**ID of node**	**Node type**
	646, 649, …, 667	Branch
	647, 650, …, 668	Pipe
Steam water pipes	805÷812 for the core channels	Pipe
	829, 830 for the AA	Pipe
Steam Drum 1	854÷857	Pipe
	876÷879	Branch
	858, 863	Branch
	859, 861	Pipe
	860	Branch
Jet spray system for SD 1	849÷853	Jet mixer
Water bridge	989	Branch
	990	Pipe
	991	Valve
	992	Pipe
	988	Branch
Steam bridge	995	Pipe
	996	Valve
	997	Pipe
Steam Line after SD 1	866, 867	Pipe
Steam drum 2	904÷907	Pipe
	926÷929	Branch
	908, 913	Branch
	909, 911	Pipe
	910	Branch
Jet spray system for SD2	899÷903	Jet mixer

Tab. 23 (cont.) – Relap5 UNIPI model of Smolensk 3 NPP: correspondence between nodes and NPP components (right side).

RIGHT SIDE		
Component	**ID of node**	**Node type**
Steam Line after SD2	916, 917	Branch
Steam rings and turbines	895, 945	Branch
	896, 946	Pipe
Feed-water system 1	881	Time dependent volume
	882	Time dependent junctions
	883	Pipe
	884	Branch
Feed-water system 2	931	Time dependent volume
	932	Time dependent junctions
	933	Pipe
	934	Branch

4.5.4. The NESTLE 3D NK nodalization and the coupling

RELAP5-3D NK model was developed according to data reported in Chapter 2 of this document, so the main parameters (power, burnup, CR position, channels flow-rate) were referring to the Smolensk-3 NPP core status of 16 October 1996. RELAP5-3D reactor core model is composed by 2488 channels. 1570 Fuel Channel, 314 Non-Fuel Channels (CRs, Axial Detectors, Additional Absorber, Water Column), 604 Radial Reflector Channels are modeled.

Radially the core was divided into square cells with a pitch of 0.25 m, each one corresponding to a core channel. Thus, the model resulted in a 56 per 56 squared arrays (see Fig. 68).

Axially the core was divided by 12 planes. First and twelfth plane have an axial dimension of 0.3 m (i.e. corresponding to the graphite bottom and top reflectors), planes from 2 to 11 have a dimension of 0.7 m. A sketch of the Fuel Channel Neutronic Mesh is reported in Fig. 65. It has to be noted that the axial mesh utilized is equal to the axial mesh used for the HELIOS code Cross Sections calculations.

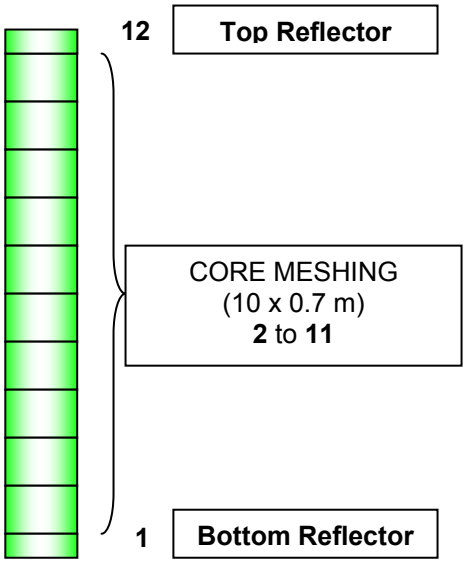

Fig. 65 – RELAP5-3D Core neutron kinetic mesh

All different CR types are implemented in the RELAP5-3D code, with the correct insertion direction and the appropriate physical structure (absorber + connecting rod+ graphite displacer for MCR, only absorber for FASS, absorber + graphite displacer for SHR). Their numeration with their arrangement is shown in Fig. 69; their insertion depth is reported in Tab. 9 as indicated by the plant data in the chapter 2 of this document. This CR configuration has to be intended for all calculations here reported, where it is not specified a different one.

4.5.4.1. 3D NK-TH Coupling Scheme

Because of the different mesh dimension between the core TH nodalization (0.35 m) and the 3D NK axial mesh (0.7 m), the coupling procedures connected two thermal-hydraulic mesh points to one neutron kinetic mesh point. Instead the dimension of the TH node for the bottom and top reflector was the same one of the neutron kinetic node (i.e. 0.3 m). The heat structures of the fuel and of the graphite have the same axial dimension of the corresponding TH node and are, for this reason, coupled in the same way with the NK nodes. In Fig. 66 it can be viewed the coupling scheme between the HELIOS, NESTLE and RELAP5 nodalization.

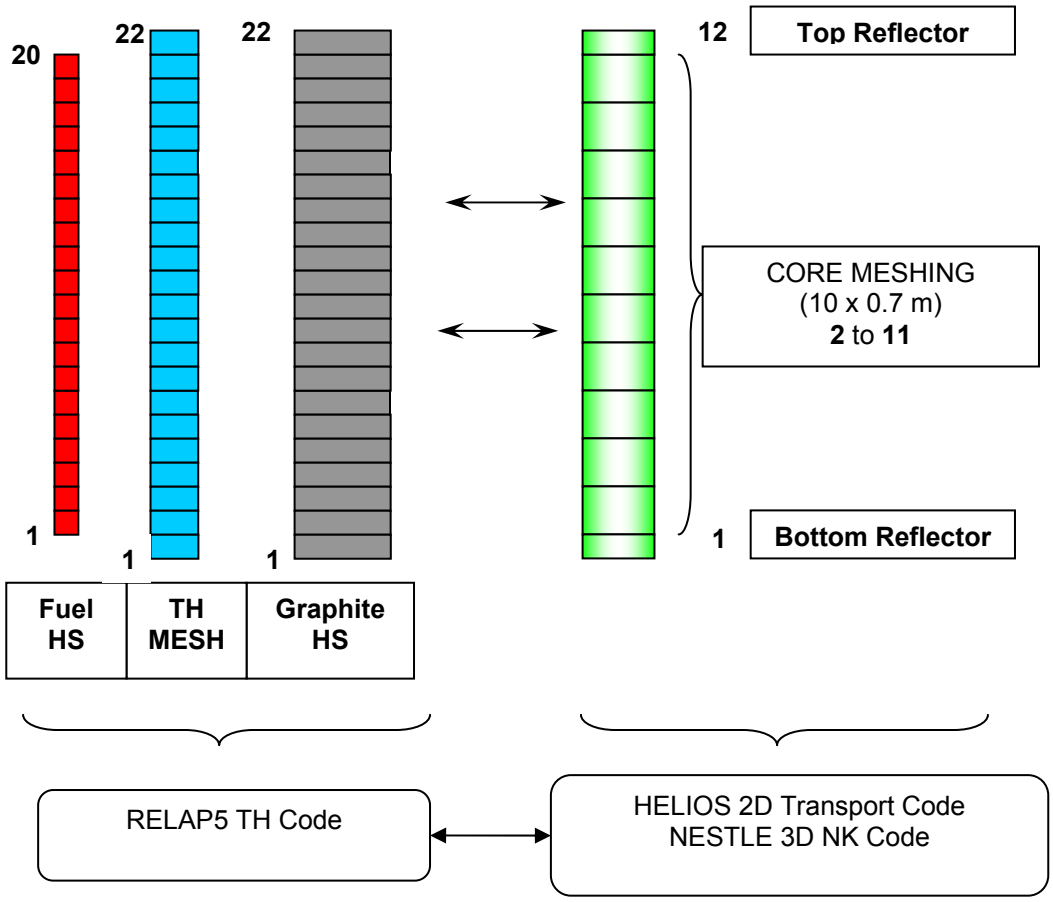

Fig. 66 – TH / 3D NK & Lattice Codes meshes coupling

Neutronic nodes were coupled to a total of 56 thermal-hydraulic channels according to the maps showed in Fig. 68. Left part of the core was modeled with:

- 8 TH channels (grouped in NK Zone # 46 to # 53)
- 1 GDH

Right part was instead modeled with:

- 48 TH channels (grouped in NK Zone # 2 to 45, 56, 57, 58,60)
- 22 GDH

All the three types of Control Rods (Manual, Shortened, Safety) and the Axial Detectors were modeled with an equivalent TH channel (equivalent TH channel #288, Zone 54). Instead the Additional Absorber and the Water Column were coupled to two TH channel, one for both halves (equivalent TH channel #142, #642, NK Zone #55 and #59). Radial Reflector neutron kinetics nodes were coupled with an equivalent TH channel too (equivalent TH channel #292, Zone #1) simulating the cooling circuit.

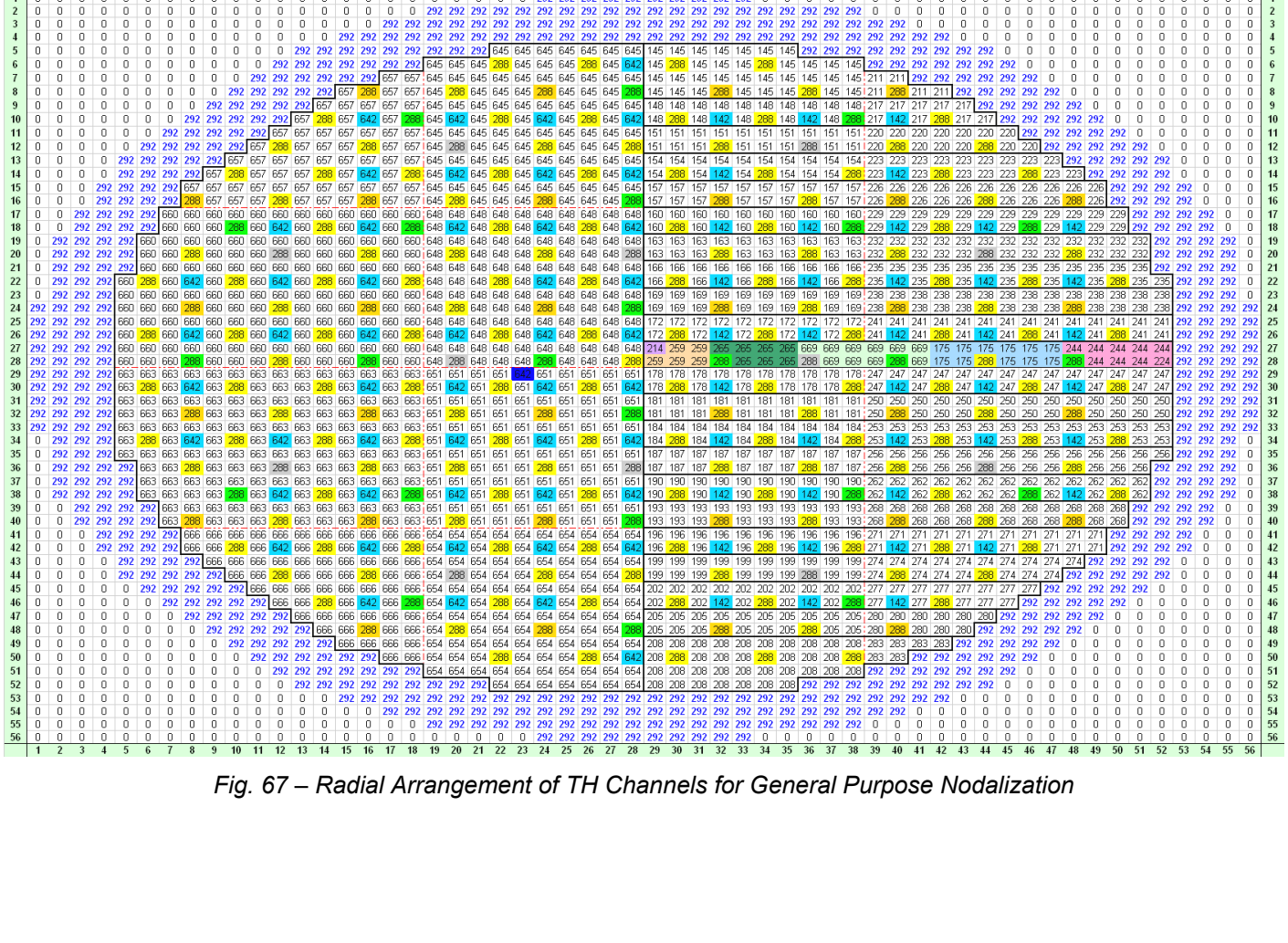

Fig. 67 – Radial Arrangement of TH Channels for General Purpose Nodalization

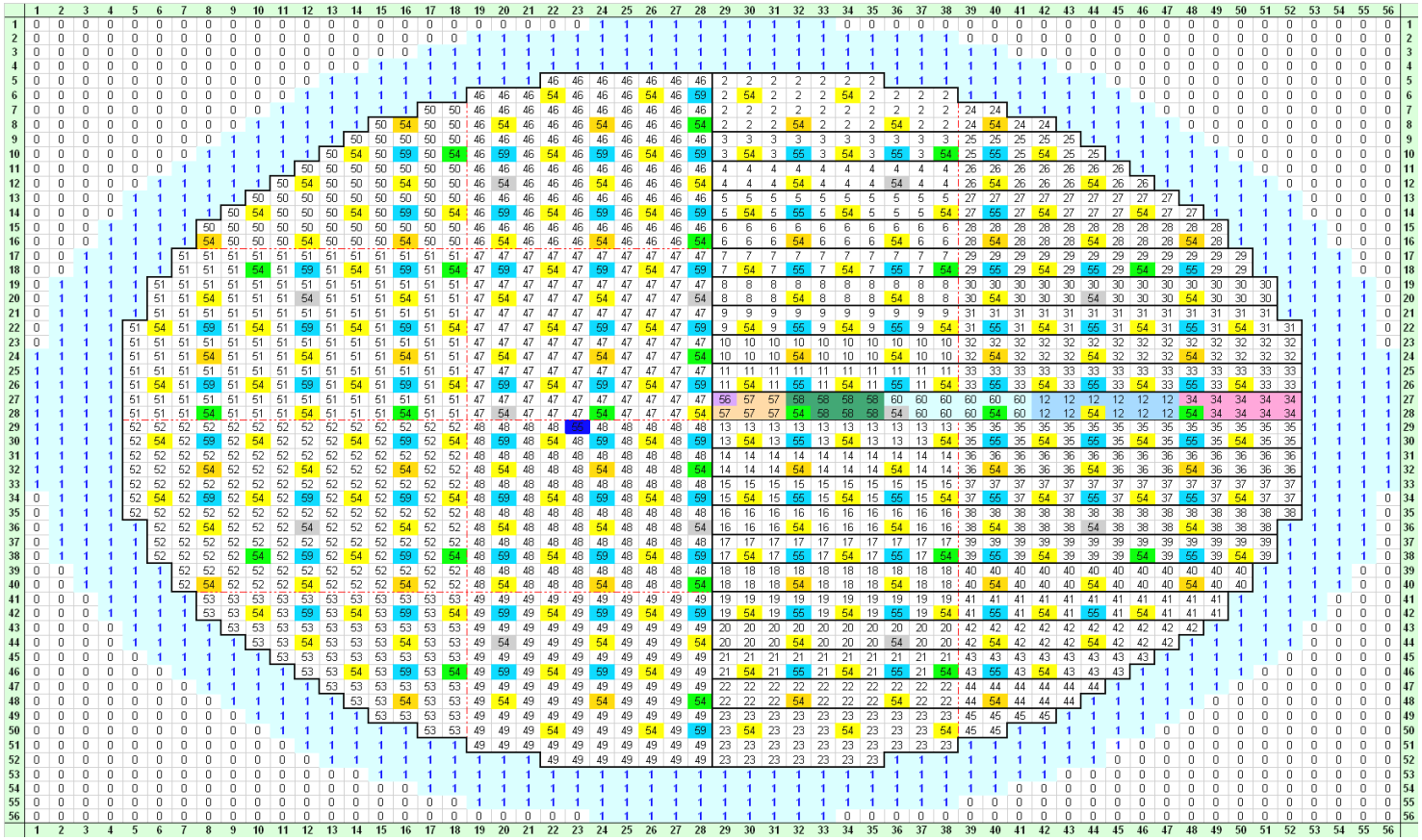

Fig. 68 – Correlation map between TH channels, TH Zones and NK Nodes for General Purpose Nodalization

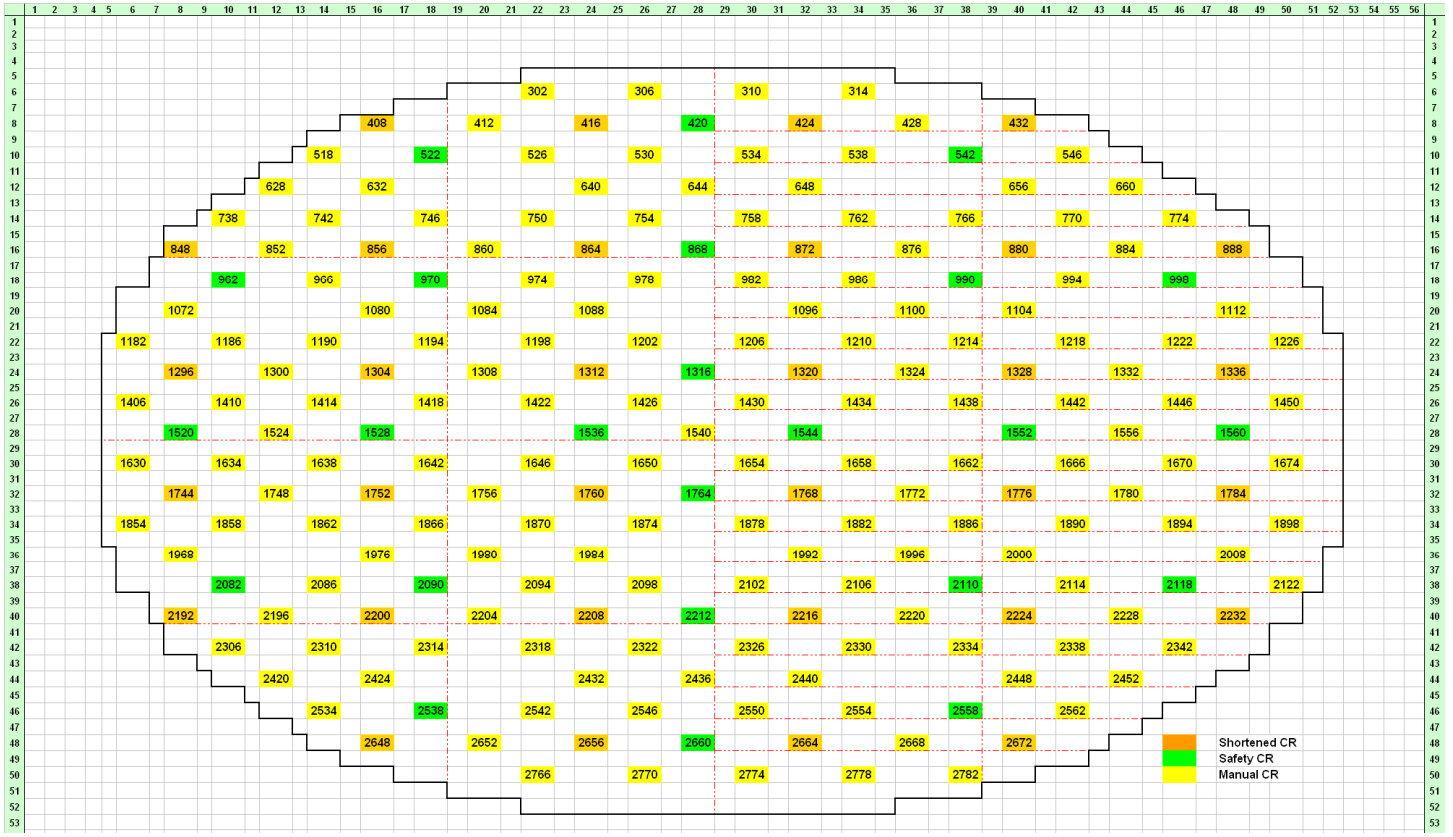

Fig. 69 – CR Numbers & Types – RELAP5-3D Numeration

Finally, all the neutron kinetics nodes, grouped in 60 Macro – Zones, were coupled to a total of 60 TH channels according to the map showed in Fig. 67.

4.5.4.2. Some considerations on the axial meshing scheme

Some considerations on numerics and FD methods can help to derive the maximum size of the node to be used by the NESTLE code. As reported in section 4.2.4, NESTLE calculations are by default employing NEM, providing sufficient robustness and accuracy in the neutron flux distribution calculations. Nevertheless, the implemented non-linear strategy allows to result in a FD calculation by choosing to not update each *n* outer iterations the coupling coefficients between two nodes (see section 4.2.4.1). It is well known that, using a FD method the error on the flux calculation is proportional to the size of the node and to the migration length. For example, for a 1D mono-energetic FD discretization it results that [71]:

$$\varepsilon_R \cong \frac{3}{4}\left(\frac{\Delta_l}{L}\right)^2 + \ldots \qquad (11)$$

where:
Δ_l = dimension of node **l**
ε_R = error on the flux calculation
L = cell diffusion length

The RBMK neutronic characteristics, with a greater diffusion (and migration) length allows the use of a relatively large (compared, e.g. to a BWR) node dimension. From Tab. 4 of this report it results that $1/L^2$ for RBMK is $5.03*10^{-3}$ while for BWR $2.07*10^{-1}$. Therefore, a reasonable accuracy can be get with a RBMK node size also of the order of 100 cm size [89]. Several tests were performed for a SS configuration, halving the axial discretization length and changing the numerical solution scheme. Some results of these sensitivities are showed in Fig. 70 and Fig. 71.

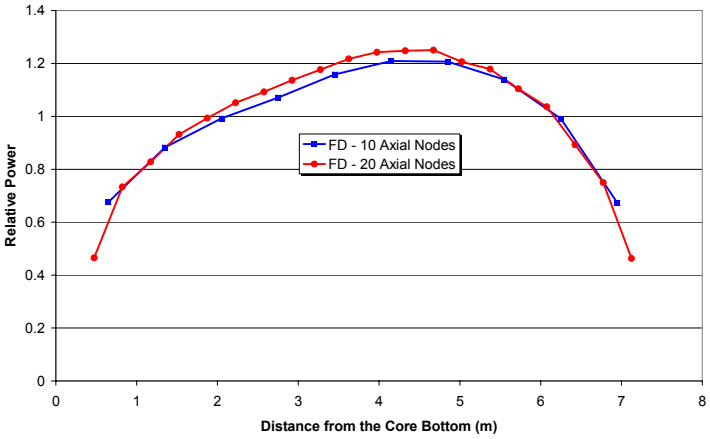

Fig. 70 – Relative Axial Power: SS sensitivity, FD method calculations

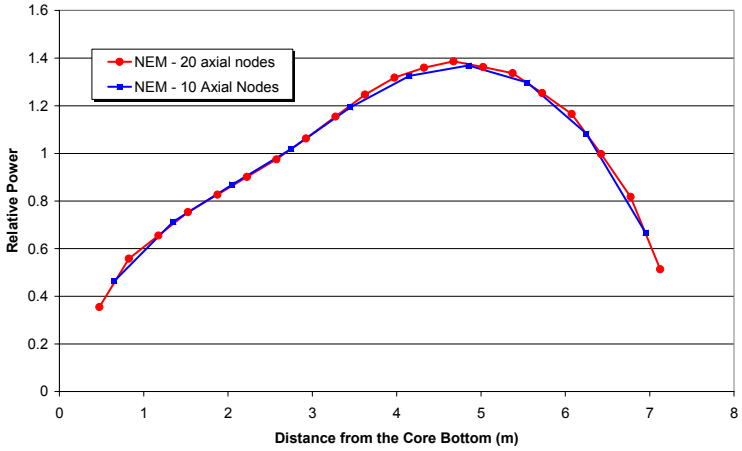

Fig. 71 – Relative Axial Power: SS sensitivity, NEM calculations

It was found that the use of a 22 axial nodes (20 for the active zone plus 2 for the top and bottom reflectors) scheme (node length for the active zone = 35 cm) did not improve the calculation accuracy in a significant manner. On the other hand, the computational time increased dramatically (more than doubling in the cases of both FD and NEM). Thus, the use of NEM with a 12 axial nodes (10 nodes of 70 cm length for the active zone plus 2 for the top and bottom reflectors) was chosen for all the SS and transient calculations.

4.5.5. The MCNP5 code model

4.5.5.1. Reference Geometry Material

Cell modeling by MCNP5 code was done according to the following geometrical data (see Fig. 72 and Tab. 25). These data were supplied by Russian Research Center Kurchatov Institute (RRC KI) [73].

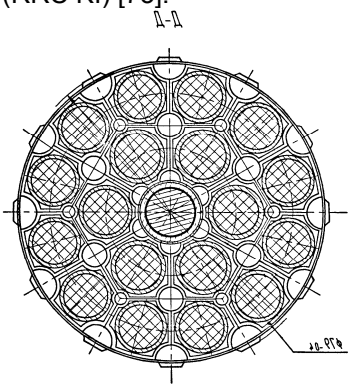

Fig. 72 – Fuel Channel Cross-View

- Distance inner row fuel rod axis - center of fuel assembly axis: 1.6 cm
- Distance outer row fuel rod axis - center of fuel assembly axis: 3.1 cm

4.5.5.2. Reference Material data

Material compositions for MCNP5 input decks were also supplied by RRC KI and are reported in Tab. 24 and Tab. 25.

Tab. 24 – Nuclear densities in fresh fuel, 10^{24} atoms/cm^3

Fuel type	**2,0 %**	**2,4 %**
^{235}U	4.3386E-4	5.2063E-4
^{238}U	2.0991E-2	2.0905E-2
^{16}O	4.4283E-2	4.4283E-2

Tab. 25 – Geometry and material composition of fuel cell

Element	**Size, cm**	**Nuclear density, 10^{24}/см^3**
Central rod	R_{outer}=0,75	Zr = 4,287*10^{-2} Hf= 7,06*10^{-6} Nb= 1,069*10^{-3}
Fuel	R_{outer}=0,5850	See Tab. 24
Clad	R_{inner}=0,5850 R_{outer}=0,6815	Zr= 4,338*10^{-2} Hf= 1,35*10^{-5} Nb= 8,135*10^{-4}
Water with mixed holding greed (Water density 0.998 g/cm^3)	Inside tube	H= 6.6177*10^{-2} O= 3.3088*10^{-2} Fe= 4,774*10^{-4} Cr= 1,3395*10^{-4} Ni= 6,593*10^{-5}
Tube	R_{inner}=4,0 R_{outer}=4,4	Zr= 4,287*10^{-2} Hf= 7,06*10^{-6} Nb=1,069*10^{-3}
Graphite	25x25	C= 0,084233 B^{10}= 1.8*10^{-8}

For voiding calculation, concentrations of hydrogen and oxygen were taken as zero, the other one were unchanged. Temperature of all cell components was fixed at 300 K. These geometric and composition data were used for the all reference criticality calculations given in this document.

4.5.5.3. MCNP5 Reference Model Geometry

Geometric dimensions and materials data used for developing the following model are reported in the previous paragraph. An infinite – along z-axis – geometry was considered. Model pictures are given in Fig. 73 and Fig. 74.

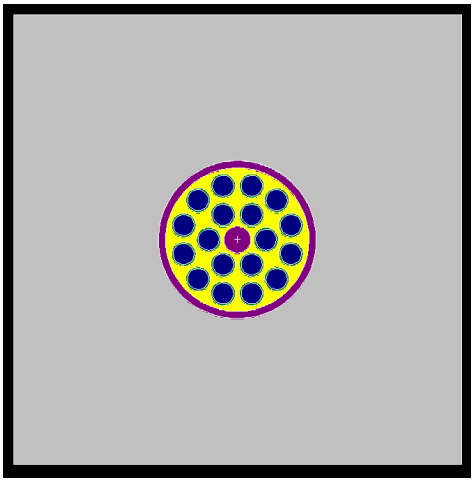

Fig. 73 – Fuel Cell in XY plane (at Z=10)

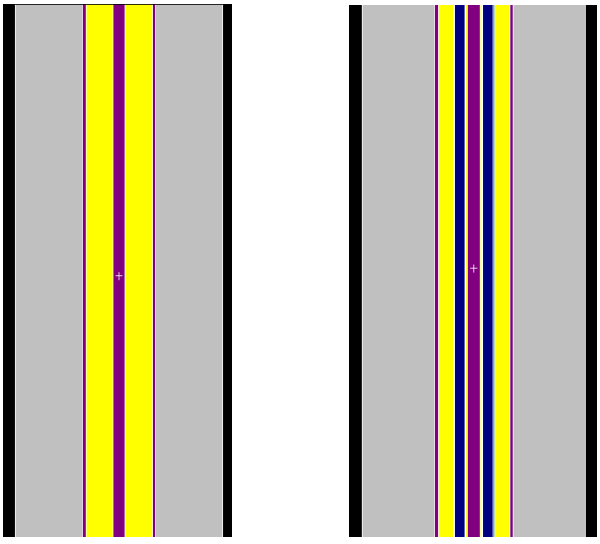

Fig. 74 – Fuel Cell in YZ and XZ plane (at X=0 and Y=0)

4.5.5.4. MCNP5 Cross Section Libraries

ENDL92 [62] and ENDF-B/VI.6 [61] continuous cross section data library was used for reference calculations. Temperature was set up at 300 K. Thermal S(α,β) tables were used to correctly represent the role of molecular forces acting on the hydrogen and carbon atoms in the water and in the moderator, respectively.

4.5.5.5. Boundary Conditions

Specular reflective boundary conditions (J(μ) = J(-μ)) were implemented on the XZ and YZ planes delimiting the graphite block.

4.5.6. The DRAGON code model

DRAGON is a 2D-3D deterministic transport code, so the implemented model was similar to the MCNP and HELIOS ones and it consisted of a 2D simulation of a single fuel channel with the relative graphite block. A picture of the model is given in Fig. 75.

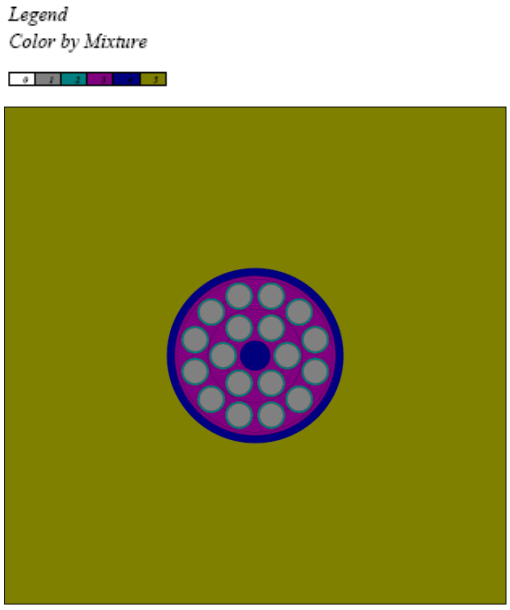

Fig. 75 – DRAGON RBMK FC model

The source data for the model set up were taken from [73] and are consistent with the data reported in Tab. 24 and Tab. 25.

4.5.6.1. Cross Section Libraries

The DRAGON code can use different format of multi-group cross sections libraries. The WIMS-D libraries, developed by the IAEA in the framework of the WIMS-D Library Update Project were used. They have are composed by 69 and 172 energy groups and an extensive description of them can be found in [58].

4.5.6.2. Boundary Conditions

Reflective boundary conditions on the model periphery were imposed for all the DRAGON calculations.

4.5.6.3. Calculation modules

DRAGON code is a modular code and can perform the same type of calculation using different solution algorithms. Several options were tested, resulting in the selection of the modules reported in Fig. 76 [59].

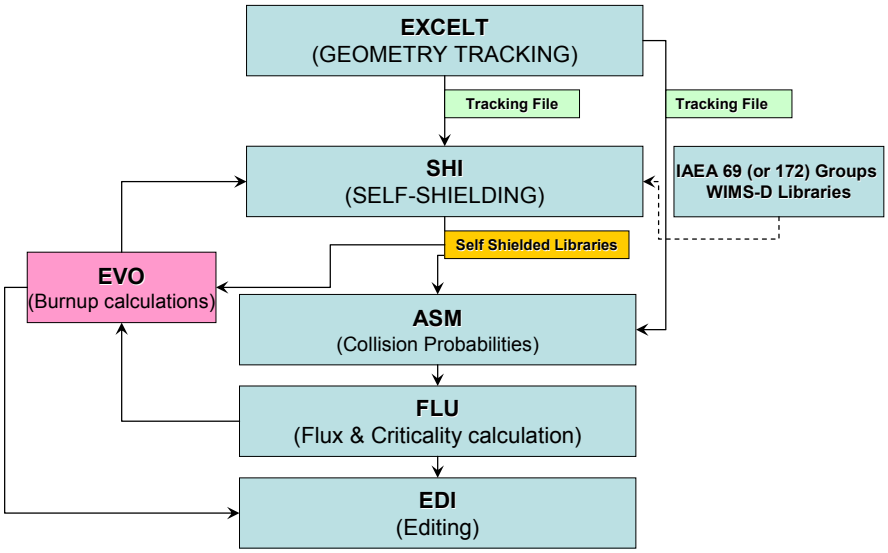

Fig. 76 – DRAGON code: calculation scheme used for RBMK calculations

After the geometry and the material definition, DRAGON code effectuated the geometry tracking using the EXCELL (Isotropic) tracking module. This information was then used for the self shielding calculation and for the collision probabilities matrix calculations. The use of the previous data (self-shielded libraries plus collision probabilities matrix) allow DRAGON to calculate the multigroup transport solution for the considered model. EDI module is then used for printing results and for performing eventual homogenizations. EVO module was also used iteratively for the burnup calculations.

4.6. The Qualification

The execution of nuclear reactor calculations should be performed according to the best international practice guidelines (e.g., [45], [46]), and with a level of quality comparable to the one used in other fields of the nuclear technology. Therefore the most rigorous methodologies for calculations should be developed and submitted to the review of the scientific and technical community (e.g., through participation to international benchmarks and/or thorough review of a Safety Authority). The calculation methodologies developed at the GRNSPG/UNIPI and applied here for these RBMK analyses were discussed and tested in an international framework during several Projects and publications (e.g., see [43], [47], etc.)
The GRNSPG/UNIPI calculation methodologies are mainly based on the respect of the followings criteria:

- Use of the most advanced codes. Codes versions used for calculations are "frozen" (no beta or testing versions of codes are used). Code should not modified by the user.
- Code user should be "qualified" (see [48] for the meaning of "qualified user")
- Nodalizations and input decks developed should pass a "steady-state" and "on transient" qualification process [49].

In the following paragraphs, information about the codes and the models qualification process is reported.

4.6.1. Codes qualification

4.6.1.1. The RELAP5-3D validation for RBMK analyses

RELAP5-3D code was validated for pressure tube graphite moderated reactors in the framework of several Projects managed by the US-DOE for the study of the American production reactors and for the study of the RBMK reactors in the aftermath of the Chernobyl accident (see the code description paragraph).

Example of code modifications for considering RBMK peculiarities of RBMK are, e.g., the implementation of Osmachkin TH correlation, the implementation of a special RBMK option for handle Kurchatov Institute' generated Cross Section Libraries.

The multidimensional neutron kinetic model in RELAP5-3D based on NESTLE code, was extensively validated [75],[76]. Since the 1990 it was adapted and used for the RBMK analyses too. In the literature it can be found recently published papers [77], [78], [79], focused to develop RELAP5-3D models for RBMK system (more precisely for Ignalina and Kursk NPPs). All these analyses use the RELAP5-3D code developed by INL.
E.g., a validation of the nodal kinetics part of the RELAP5-3D was made using steady-state data and using reactor power reduction and feedwater flow rate perturbation transients data from the Ignalina NPP in [78], [79].

4.6.1.2. The HELIOS code validation for RBMK analyses

HELIOS is an industrial world-wide recognized lattice physics code, with capabilities to model the most complex geometries. This characteristic and a several RBMK related activities like [26] and [50], suggested its application to RBMK calculations.

4.6.1.3. The DRAGON code validation for RBMK analyses

DRAGON code is a lattice physics code developed by the Politecnique of Montreal with the support of the Canadian nuclear industry and utilities. Its main applications are for heavy water reactor studies. Nevertheless the geometry modeling capabilities as well as the IAEA multi-group libraries developed during an International Research Project [69] allows its applications to RBMK reactors too. DRAGON validation works for this reactor technology was not found in the literature before the execution of the present activities.

4.6.1.4. The MCNP validation for RBMK analyses

MCNP5 is an extensively validated code, used world-wide as a code for reference calculations. ENDFB-VI continuous energy cross section libraries were validated for RBMK analyses [74]. Comparison of MCNP5 results with Russian Monte Carlo codes like MCU code showed comparable agreements with experimental data [51].

4.6.2. Model and Nodalization qualification

4.6.2.1. RELAP5-3D TH nodalization qualification

The nodalization qualification procedure proposed at GRNSPG has been applied. This consisted of two main steps: steady state level qualification and on-transient level qualification. The first part of the procedure is considered. A comprehensive documentation of the activity can be found in [44].

A nodalization is qualified at the steady state level if it has a geometrical fidelity of the simulated plant and if it shows a stable time trend of the main thermal-hydraulic parameters.

Relevant geometrical data are compared with the design data and a set of acceptable errors in Tab. 26. A demonstration of the geometrical fidelity of the nodalization can be derived from Fig. 77. Key thermal-hydraulic parameters are considered in Tab. 27 and in Fig. 78 to Fig. 82. Emphasis is given, when reporting selected curves, to the void fraction in the core and to the initial temperature distribution inside graphite stacks, including radial and axial distributions.

The completed nodalization qualification process shows that the Smolensk 3 nodalization is qualified at the steady state level.

Tab. 26 – RELAP5-3D Smolensk 3 NPP: nodalization: qualification at steady state level, key MCC geometric parameters.

QUANTITY	Unit	Design	RELAP5-3D Right side / Left side	Acceptable Error +	Error	Notes
Circuit volume	m^3	667.67 667.67	667.78 667.78	1%	0.01%	
Active structures heat transfer area (overall)	m^2	12134.42 (fuel & PT) 19904 (Graphite-Gap)	12135.66 17476.36	0.1%	-0.01% -12.2%	External radius calculated to preserve the mass
Active structures heat transfer volume (overall)	m^3	14.4 1088.2	14.4 1088.8	0.2%	0.02% -0.05%	
Graphite blocks total mass	Ton	1850	1851		0.05%	

+ The % error is defined as the ration (reference or measured value – calculated value)/(reference or measured value); “The dimensional error” is the numerator of the above expression

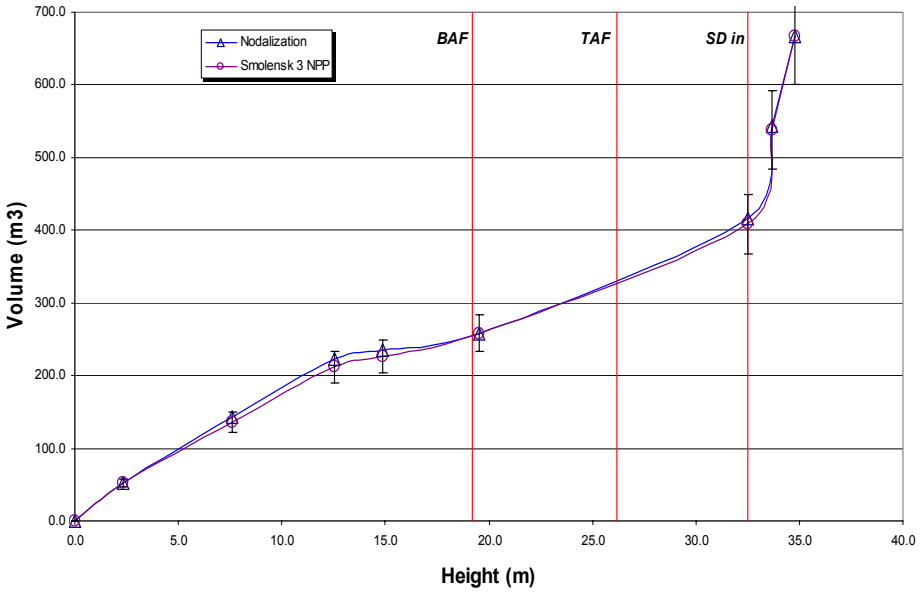

Fig. 77 – RELAP5-3D Smolensk 3 NPP: nodalization qualification at steady state level, comparison between adopted and reference (design) volume vs. height curve of MCC.

Tab. 27 – RELAP5-3D Smolensk 3 NPP: nodalization qualification at steady state level, key MCC thermal-hydraulic parameters.

Quantity	Unit	Design	RELAP5-3D		Acceptable Error (%)+	Error° (%)		Notes
			Right side					
			left side					
Thermal power	MW	1606	1594		2	-0.75		
		1565	1567			0.13		
DS pressure	MPa	6.86	6.865	6.863	0.1	0.07	0.04	On all SD dome
			6.862	6.863		0.03	0.04	
Core inlet temperature	°C	270	269.5		0.5	-0.19		
			269.1			-0.33		
DS inlet temperature	°C	284	284.66		0.5	0.23		
			284.65			0.23		
Void Fraction at DS Inlet	%	80	82.5		10.0	3.13		
			82.4			3.00		
DS feed water temperature	°C	165	165		0.5	0.0		Imposed Value
MCP speed	Rad/s	104.6	104.71		1	0.11		
			104.71			0.11		

Tab. 27(cont.) – RELAP5-3D Smolensk 3 NPP: nodalization qualification at steady state level, key MCC thermal-hydraulic parameters.

Quantity	Unit	Design	RELAP5-3D Right side / left side		Acceptable Error (%)+	Error° (%)		Notes
Pressure drop on the water line	MPa	0.5*	0.8		10	N/A		Ref. for 2.9 MW channel
						N/A		
Pressure drop on the core		0.657*	0.475			N/A		
						N/A		
Steam-water line pressure drop		0.392*	0.249			N/A		
						N/A		
Total pressure drop on the FC	MPa	1.549	1.524		10	1.6		
MCP head	MPa	1.51	1.507		10	-0.20		
		1.51	1.518			0.53		
DS mass inventory	m^3	85	85.27	84.89	2	-0.3	0.1	Liquid Fraction Vol
			84.47	85.49		0.6	-0.5	
Total loop coolant flow rate	Kg/s	5157.9	5196.6		2	0.75		
		5103.9	5112.5			0.17		
Technological channel flow rate	Kg/s	5064.9	5099.2		2	0.68		
		4987.9	5001.0			0.26		
Additional absorber flow rate	Kg/s	93	97.4		10	4.74		
		116	111.5			-3.89		

* Reference conditions refer to the maximum power channel (3.2 MW).
+ The % error is defined as the ration (reference or measured value – calculated value)/(reference or measured value); "The dimensional error" is the numerator of the above expression

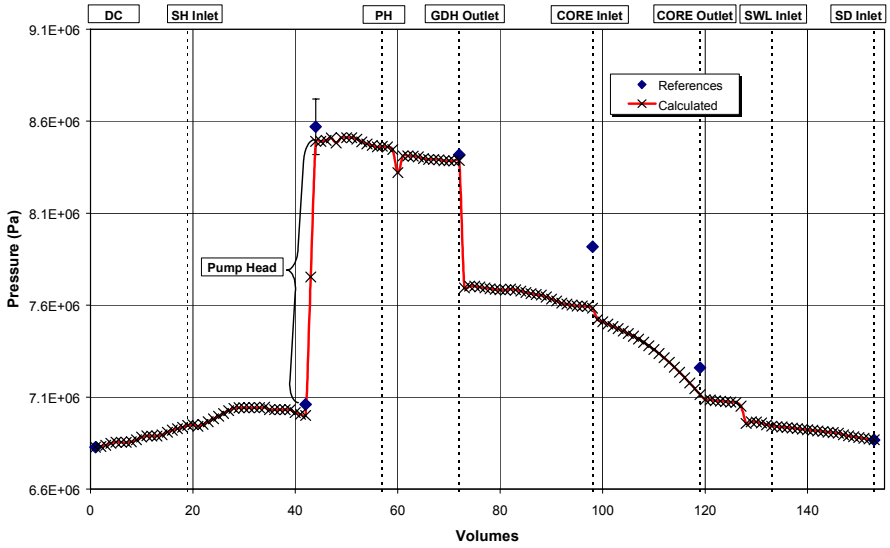

Fig. 78 – RELAP5-3D Smolensk 3 NPP: nodalization qualification at steady state level, comparison between steady state and reference (nominal conditions) pressure distribution along the MCC.

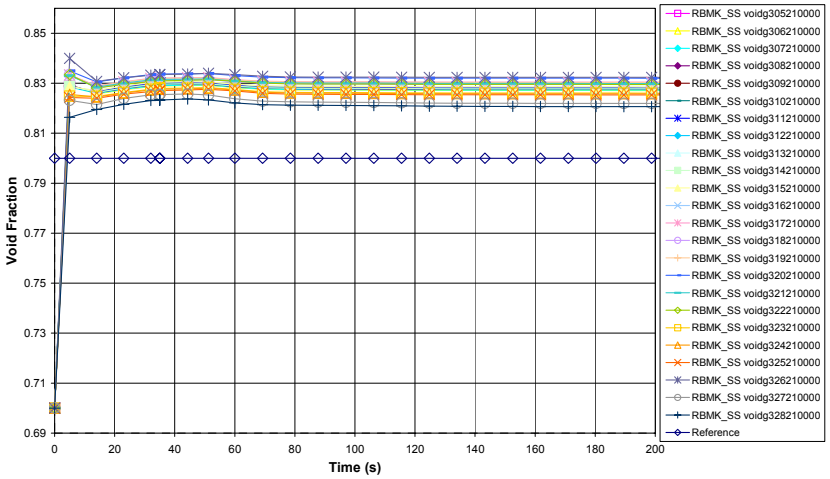

Fig. 79 – RELAP5-3D Smolensk 3 NPP: nodalization qualification at steady state level, comparison between steady state and reference (nominal conditions) void fraction at SD inlet, right part, channels 1-24.

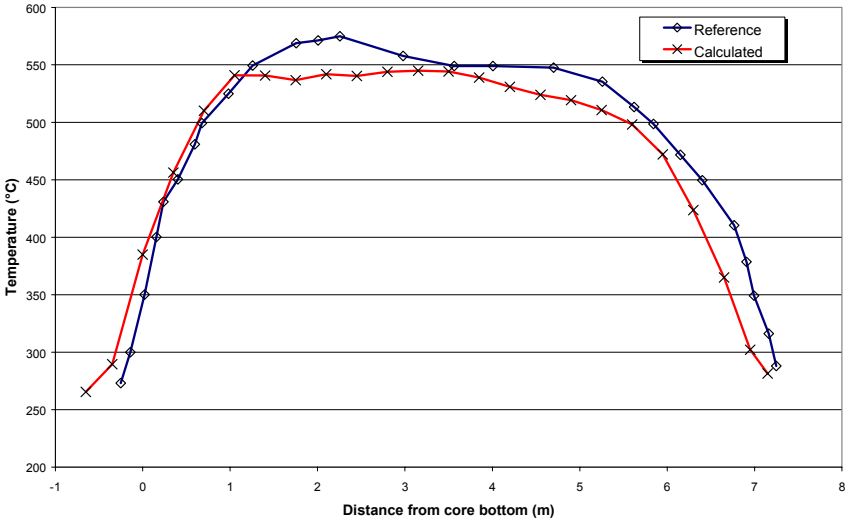

Fig. 80 – RELAP5-3D Smolensk 3 NPP: nodalization qualification at steady state level, comparison between steady state and reference (nominal conditions) graphite axial temperature at outer surface.

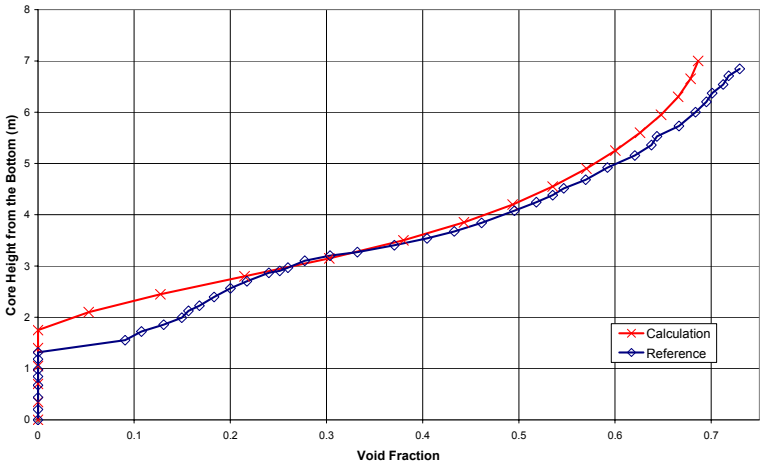

Fig. 81 – RELAP5-3D Smolensk 3 NPP: nodalization qualification at steady state level, comparison between steady state and reference (nominal conditions) FC void fraction (2.01 MW)

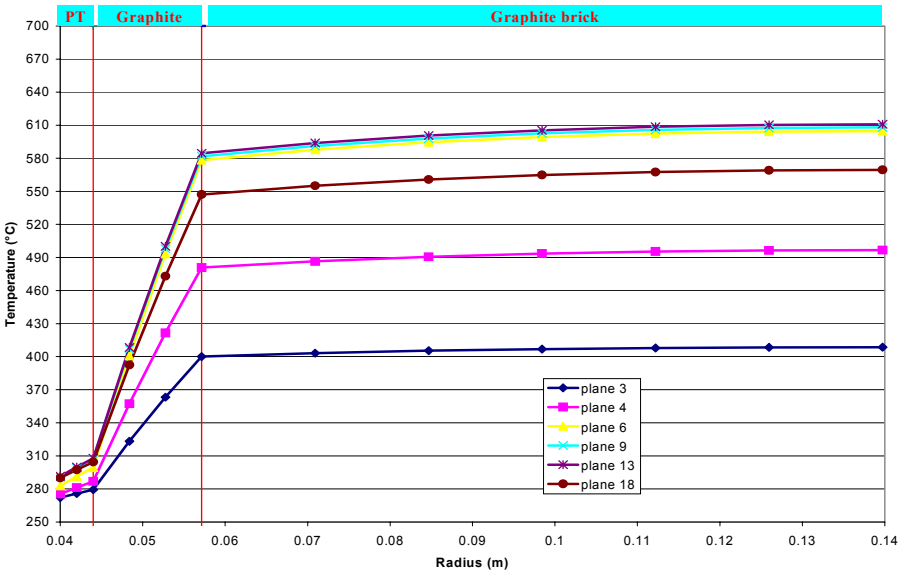

Fig. 82 – RELAP5-3D Smolensk 3 NPP: nodalization qualification at steady state level, radial temperature distribution of graphite at various elevations along the FC stack.

4.6.2.2. RELAP5-3D 3D NK nodalization qualification

Steady state calculations for the RELAP5-3D code neutron kinetics model validation were performed. When available, the results were compared with the NPP data, otherwise only calculated results were reported. As can be seen in Fig. 83 and Fig. 84, the calculated trends of the axial power are similar to those measured in the NPP.

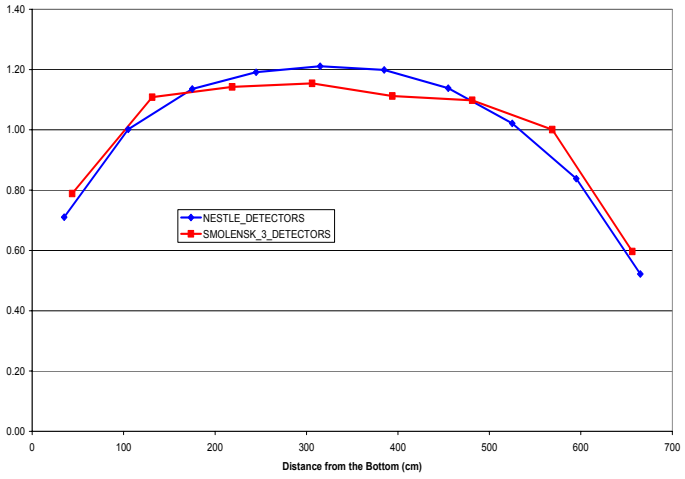

Fig. 83 –RELAP5-3D Smolensk 3 Axial Power

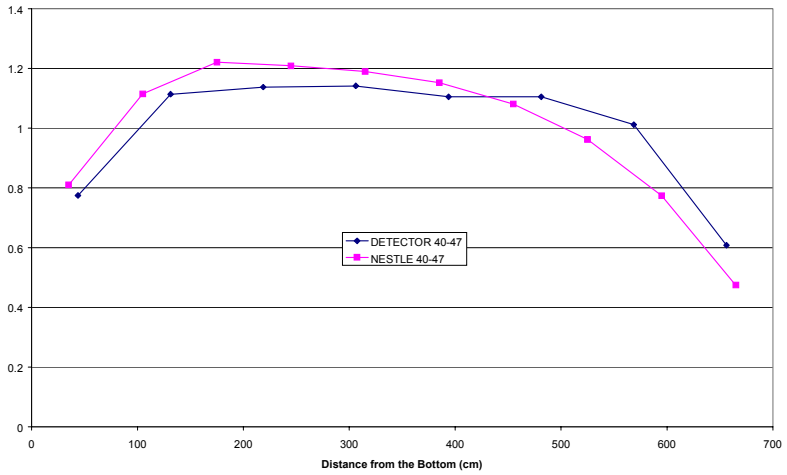

Fig. 84 – Smolensk 3 nodalization qualification for 3D NK-TH Relap5/Nestle code: axial power distribution in selected FC (coordinate 40-47)

Tab. 28 – RELAP5-3D Axial Peaking Factor

Axial Peaking Factor (F_z) (from Bottom of the Core)	
Maximum	1.21 at (at 3.15 m)
Minimum	0.522 (at 6.478 m)

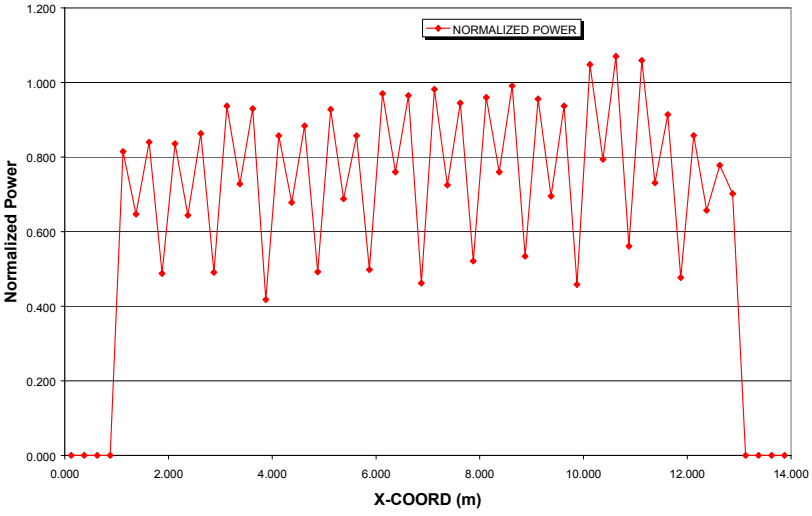

Fig. 85 – RELAP5-3D Radially Averaged Power

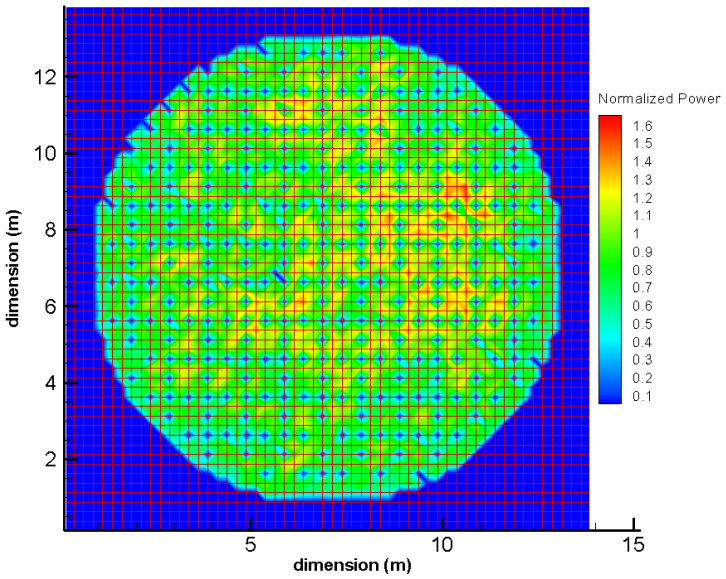

Fig. 86 – RELAP5-3D Relative Radial Power

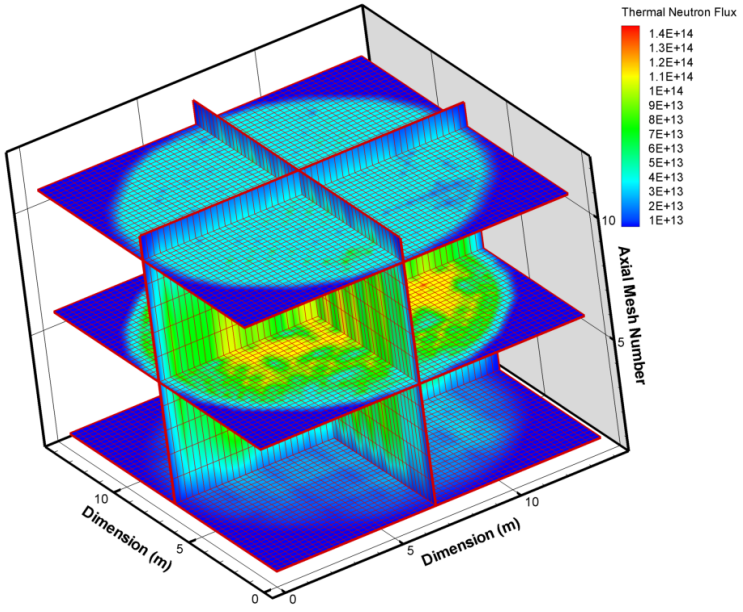

*Fig. 87 – 3D Thermal Neutron Flux Distribution (n/(cm^2*sec))*

Tab. 29 – RELAP5-3D Channels Radial Averaged Power

	Normalized Power	Thermal Power (MW)	Channel Position (xx-yy)
Maximum	1.6942	3.4091	43-20
Minimum	0.53410	1.0813	15-49

Tab. 30 – RELAP5-3D Reactor core Neutron Kinetics Parameters

Parameter		Value
K-eff		1.01359 (at HFP)
Void Reactivity Feedback		
	CPS	+ 0.125 β/s (*)
	FC + AA	- 0.16 β
CR Worth		
	MCR	- 12 β
	MCR & FASS	- 14 β
	FASS	- 1.7 β

(*) Imposed Value, [8].

Tab. 31 – RELAP5-3D adopted delayed neutron fraction data

Group	Decay Constants (s^{-1})	Delayed Neutron Fraction, %
1	0.0125	0.0167
2	0.0305	0.0987
3	0.111	0.0912
4	0.305	0.2094
5	1.13	0.1013
6	3.0	0.0399
TOTAL β: 0.5572		

In Fig. 85, the radially averaged Power profile of the core is reported; the peaking trend is due to the presence in the averaging columns of a different number of active channels. From this picture is resulting that in the right side of the core there is a higher power production.

In Fig. 87 the 3D thermal neutron flux distribution calculated by RELAP5-3D is reported. From Fig. 86 and Tab. 29 it can be seen that the radial peak factor is ranging from a minimum of 0.53410, localized in a channel in the bottom left quadrant of the core, to a maximum of 1.6942, localized in the upper right quadrant. These values can be connected to the fuel burnup distribution in that zone and to the adopted CRs position (see Tab. 9).
In Tab. 30 are reported the reactivity coefficients calculated for the insertion of the all type of CR (MCR, FASS and MCR and FASS together). It should be noted that during these calculations, the Shortened CR where always supposed to be in the same position (see Tab. 9). In the same table are also reported the values of the reactivity inserted in case of total and partial MCC voiding and in case of CPS

cooling system voiding. It should be noted, also for its implications for the safety of the RBMK system that only in the last case there was a positive reactivity feedback during a LOCA.

In Tab. 31 are reported the delayed neutron fraction data used for the neutron kinetics calculation. They refer to a fuel with an average burnup of 20 MWd/KgU.

4.6.2.3. HELIOS model qualification

Calculations comparison performed with MCNP and HELIOS about the k_{eff} for an RBMK-1000 infinite lattice was executed. The results showed that the greater deviations between the two codes are in the FC with lower enrichment FC (see Tab. 32).

Tab. 32 – Comparison between HELIOS and MCNP codes of the k_{inf} for a RBMK lattice (Temp. 300 K, fresh fuel)

Presence of coolant in the channel	Enrichment, %	k_{inf}		Relative Difference,%
		MCNP (NIKIET)	HELIOS	
YES	2.0	1.27332	1.27838	0.40
YES	2.4	1.33144	1.33594	0.34
NO	2.0	1.32256	1.31549	-0.53
NO	2.4	1.36991	1.36475	-0.38

A comparison of the difference value between the two k_{inf} showed that HELIOS model underestimates the effect of a FC voiding more than MCNP model. HELIOS error in this case is around 25% in absolute value for both different FC (see Tab. 33).

Tab. 33 – Void Effects by HELIOS and MCNP Codes, absolute units

Fuel enrichment, %	MCNP (NIKIET)	HELIOS	ε, (HELIOS/MCNP) %
2.0	0.04924	0.03711	- 24.6
2.4	0.03847	0.02881	- 25.1

4.6.2.4. The MCNP5 model qualification

MCNP5 criticality calculation were run for estimating the k_{inf} of the system. 10050 neutron cycles were calculated, using 10^4 neutron per cycle, thus totaling 100.5 Million of Histories (MH). The first 50 neutron cycles calculation (i.e., 0.5 MH) were skipped for statistical purposes. Both ENDL and ENDF/B-VI [61] were used for reference calculations. An example of the convergence of the kinf and of the fission source distribution through the Shannon Entropy measurement is given in Fig. 88, Fig. 89.

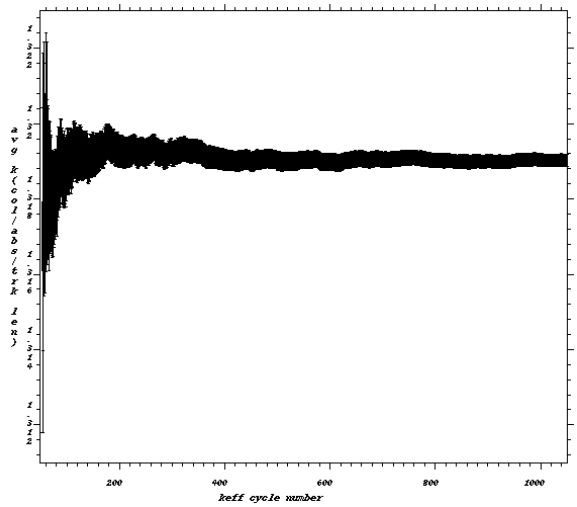

Fig. 88 – k_{inf} trend versus cycle number

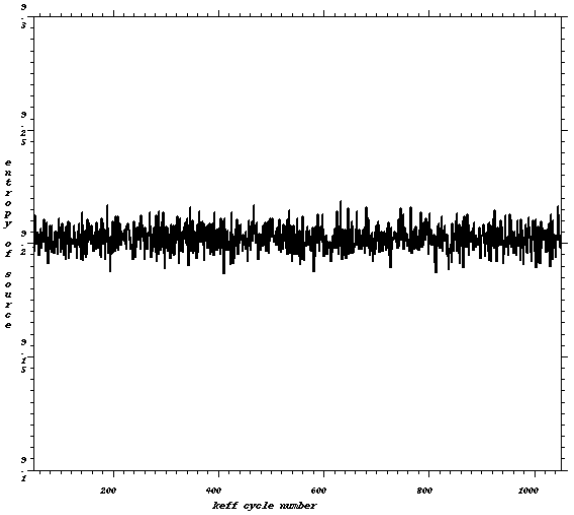

Fig. 89 – Shannon Entropy trend versus cycle number

Tab. 34 – Results for the reference calculations

Run ID	UO_2 Enrichment, %	Presence of coolant in the channel	k_{inf}	Standard Deviation (pcm)
RBMK20 (ENDL)	2.0	YES	1.22864	5
RBMK20A (ENDL)	2.0	NO	1.25134	5
RBMK40 (ENDL)	2.4	YES	1.28352	5
RBMK40A (ENDL)	2.4	NO	1.29895	5
RBMK20 (ENDF-B-VI)	2.0	YES	1.27449	5
RBMK20A (ENDF-B-VI)	2.0	NO	1.31911	5
RBMK40 (ENDF-B-VI)	2.4	YES	1.33159	5
RBMK40A (ENDF-B-VI)	2.4	NO	1.36892	5

4.6.2.4.1. Sensitivity analyses

A series of sensitivity analyses were performed in order to:

- assess the model developed;
- evaluate the effects of the main input parameters on the calculations results.

For the sake of simplicity, sensitivities were performed using results from the ENDL 2.0% fuel calculations only. In the followings paragraphs, the description of how the main parameters were changed is reported.

4.6.2.4.2. Geometry Variation

Two calculations were performed with a finite-along-the-z-axis model, using 35 and 70 cm tall models respectively. Reflection condition were applied to the bottom and the top XY surfaces. Finite 3x3 and 5x5 lattices of identical RBMK FC cell were considered too (see Fig. 90, Fig. 91).

4.6.2.4.3. Cross Section Libraries Variation

Different cross section libraries were used in order to assess their effects on the calculation results. The following two cases were investigated:

- Multi-group Cross Section Libraries MGXSNP (at 300 K) [80].

4.6.2.4.4. Boundary Conditions

A “white” reflective boundary condition was used instead of the normal reflection one.

4.6.2.4.5. Calculation Parameters Variation

Two different calculation parameters were changed in order to assess their effects on the results:

- Number of neutron cycles: 250;
- Total number of neutron histories: 1.5 MH.

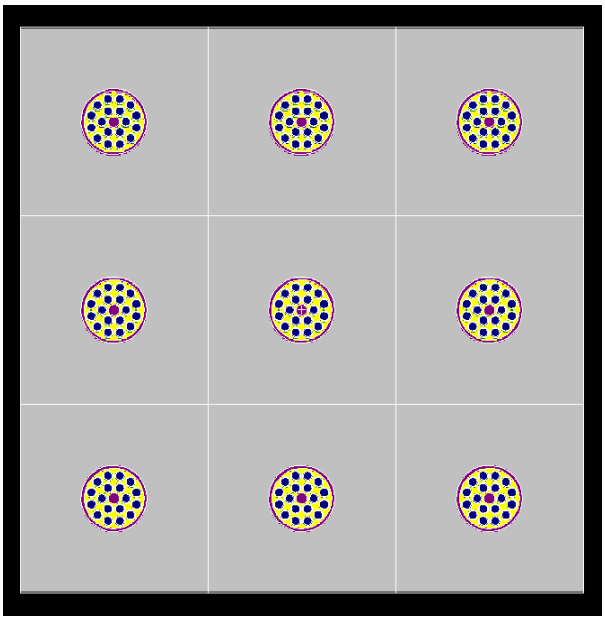

Fig. 90 – 3 x 3 Lattice

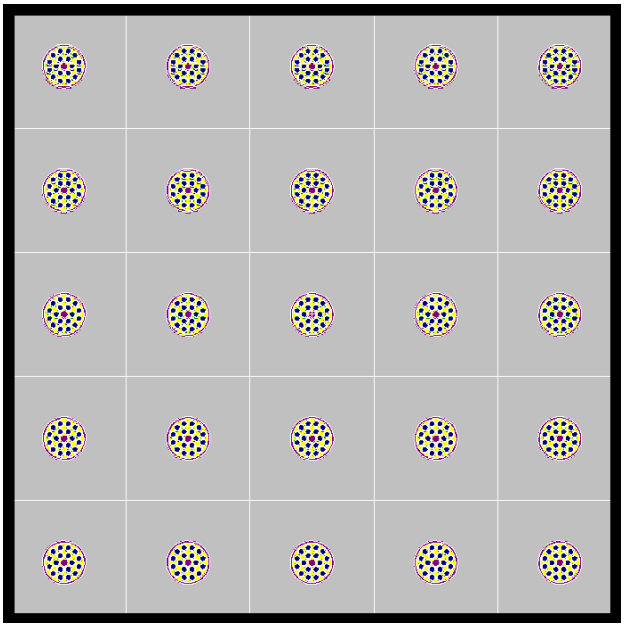

Fig. 91 – 5 x 5 Lattice

4.6.2.4.6. Results of Sensitivity Analyses

Results from sensitivity analyses reported in Tab. 35 showed that:

- geometry limitation along z-axis does not influence significantly the results;
- use of lattice models (3x3 or 5x5) does not influence significantly the results;
- Multi-group cross section libraries MGXNSP as well as activation of thermal model S(α,β) have the strongest influence on the k_{inf} (some percent);
- decreasing of number of cycles/total number of neutron histories cause the increase of the results variance.

Tab. 35 – Results from sensitivity calculation

Run ID #	Sensitivity Parameter	k_{inf}	Standard Deviation (pcm)	Variation with reference case, %
RBMK16L	Geometry: H=70 cm	1.22863	5	-0.8e-3
RBMK16K	Geometry: H=35 cm	1.22882	5	+0.015
RBMK26	Geometry: 5 x 5 lattice	1.22870	5	-0.004
RBMK28	Geometry: 3 x 3 lattice	1.22860	5	-0.003
RBMK24	XSec: No S(α, β) model	1.24122	5	+1.0
RBMK22	XSec: Multigroup MGXSNP	1.27339	5	+3.6
RBMK19	Boundary: White reflection	1.22850	5	-0.011
RBMK20I	Calculation: 1.5 MH	1.22855	39	N/A
RBMK21	Calculation: 250 cycles	1.22842	34	N/A

NIKIET MCNP results for criticality calculations of an RBMK cell were supplied to GRNSPG/UNIPI during the framework of the TACIS Project R2.03/97 by RRC KI. They are reported in Tab. 36; in the fifth column, a comparison with the UNIPI results presented in this document is given.

Tab. 36 – Comparison between NIKIET and GRNSPG criticality calculations

Water in channel	Fuel enrich., %	NIKIET MCNP (k_{inf})	GRNSPG MCNP (ENDL) (k_{inf})	Deviation NIKIET/ GRNSPG (ENDL), %	GRNSPG MCNP (ENDF/B-VI) (k_{inf})	Deviation NIKIET/GRNSPG (ENDF/B-VI) %
YES	2.0	1.27332	1.22864	+3.6	1.27449	+0.09
YES	2.4	1.33144	1.28352	+3.7	1.33159	+0.01
NO	2.0	1.32256	1.25134	+5.7	1.31911	-0.26
NO	2.4	1.36991	1.29895	+5.4	1.36892	-0.07

Tab. 37 – Comparison between RRC-KI and GRNSPG results for voiding effect

Fuel enrichment (%)	Voiding NIKIET (Δk_{inf})	Voiding GRNSPG/ENDL (Δk_{inf})	Deviation, (NIKIET/GRNSPG-ENDL), %	Voiding GRNSPG/ENDF/B-VI (Δk_{inf})	Deviation, (NIKIET/GRNSPG-ENDF/B-VI), %
2.0	0.04924	0.02270	+117	0.04462	-9.3
2.4	0.03847	0.01543	+150	0.03733	-2.9

From the comparison, a large deviation was observed when using for calculation the ENDL libraries. This could be explained by the presence of relevant uncertainties in some of the cross sections used for calculation. Therefore all the successive MCNP calculations were executed using the ENDF-B/VI libraries.

4.6.2.5. The DRAGON model qualification

Comparison of the reference calculations performed by different codes and input decks are given in Tab. 38. A good agreement resulted in the prediction of the k_{inf} between the independent NIKIET MCNP4C calculations and DRAGON calculations. This agreement increased when considering the DRAGON calculations performed with a 172 groups cross section libraries.

Tab. 38 - Comparison of the reference criticality calculations Monte Carlo versus DRAGON code

Water in channel	Fuel Enr., %	NIKIET MCNP4C – ENDF/B data (k_{inf})	DRAGON /EXCELL IAEA 69 Groups libr. (k_{inf})	Deviation NIKIET/GRNSPG, %	GRNSPG DRAGON/ EXCELL IAEA 172 Groups libr. (k_{inf})	Deviation NIKIET/GRNSPG, %
YES	2.0	1.27332	1.278768	-0.4	1.277029	-0.3
YES	2.4	1.33144	1.335680	-0.3	1.334003	-0.2
NO	2.0	1.32256	1.312085	+0.8	1.315861	+0.5
NO	2.4	1.36991	1.359907	+0.7	1.363961	+0.4

The comparison of the calculated FC voiding effect (Tab. 39) showed an underestimation by DRAGON code. This underestimation is greater when using few energy groups (69) and when considering higher enrichment of the fuel. It is interesting to note that also the other deterministic lattice physics code, HELIOS, showed the same problem when considering the voiding effect (underestimation of roughly -25% was found).

The roots of this underestimation should lie both in the data libraries as well as in the neutron transport solution methods.

Tab. 39 – Comparison between RRC-KI and DRAGON results for voiding effect

Fuel enrichment (%)	Voiding NIKIET (Δk_{inf})	Voiding DRAGON 69 groups(Δk_{inf})	ε, (DRAGON 69/NIKIET), %	Voiding DRAGON 172 groups(Δk_{inf})	Deviation, (NIKIET/DRAGON 172), %
2.0	0.04924	0.03332	-32.3%	0.03883	-21.1%
2.4	0.03847	0.02423	-37.0%	0.02996	-22.1%

5. THE APPLICATION TO REALISTIC TRANSIENTS ANALYSES

5.1. Hot Full Power Analyses

In this chapter, the results from a series of transient calculations are reported. All transients were calculated considering the plant at Hot Full Power (HFP), or 3159 MW. This allowed to maximize the power and temperature excursions of the fuel element calculated in a realistic safety analyses by the best estimate (BE) code RELAP5-3D.
The selection of these transients was performed in order to investigate the main relevant physical phenomena for the RBMK technology (see chapter 3 of this document), to test the developed coupled codes model capabilities, to asses the safety level of the RBMK system.

Six transients are here presented. They are considered the most significant to be analyzed by coupled codes technology [52]. They are:

- CR withdrawal: Reactivity Initiated Event (RIA), transient involving asymmetric power and flux perturbation;
- CR group withdrawal: as the previous one, but with a more significant reactivity insertion;
- GDH blockage: decrease of coolant flow event, transient involving possible coupled flow and power oscillations;
- Single FC blockage: decrease of coolant flow event, local transient, influences from and on neighbor channels to be assessed;
- GDH rupture: loss of coolant event (LOCA), Design Basis Accident (DBA);
- CPS cooling circuit LOCA: Beyond Design Basis Accident (BDBA) LOCA, accident involving strong reactivity insertion

All these transients, except the GDH rupture, were calculated using the simplified RELAP5-3D model (see Fig. 60 in the previous chapter), simulating only the reactor core with imposed boundary conditions. The GDH rupture, since it involved the feedback from more NPP components (e.g., MCPs and SD), was instead calculated using the full scale nodalization (see Fig. 59).

5.1.1. Reactivity Initiated Accidents

In these two transients, the CR/CRs were selected among the ones having the highest worth. Their positions in the core is given in the Fig. 92.
Since in the RBMK, the CR are designed to operate in a low pressure circuit (the CPS cooling circuit, operating at atmospheric pressure), they cannot be ejected (e.g., like could happen in a PWR). Therefore, it has to be assumed that the cause of this events is a malfunction of the CPS or a wrong action by the reactor operator.

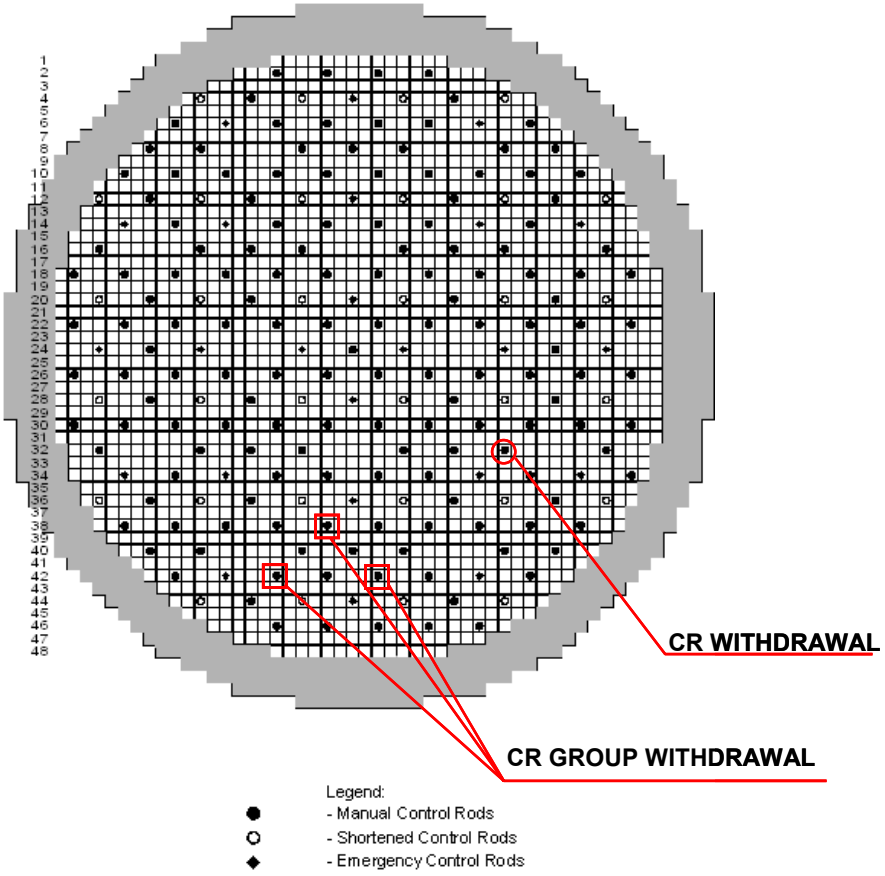

Fig. 92 – CR Cartogram for RELAP5-3D RIA calculations

5.1.1.1. CR Withdrawal

The main purpose of the analysis of the CR withdrawal event is the evaluation of the overall core power (even in relation to the achievement of the scram set-point) and the demonstration of the capabilities of the developed code model to deal with this event. After a preliminary calculation of the worth of the all MCR, the CR with higher worth (resulted to be the #151 according to map of Fig. 35) was selected to be withdrawn during this transient. An 'ad-hoc' TH and 3D NK nodalization was developed in order to investigate the effects on the neighbor channels too (Fig. 93 and Fig. 94).

Selected results of the event originated by a spurious single CR withdrawal are given from Fig. 95 to Fig. 101. The CR withdrawal event resulted to be:

- 0.0 s: onset of control rod #151 withdrawal with the speed 40 cm/s (1 rod with initial insertion depth of 6.70 m from bottom of top reflector);

- 17 sec.: reactor peak power (3350 MW – 106% of Nominal Power, see Fig. 95)

The scram signal is generated if the reactor power reaches the level of 110% of nominal power (3475 MW). The scram delay time is 0.25 s and the speed of CR insertion is 3.5 and 0.5 m/s for safety and manual CR, respectively.

It can be noted that the power surge in not large enough to generate the AZ scram signal, which set point is 110% of nominal power. The extraction of this MCR control rod from the core results in a mild increase of power in all channels, Fig. 96. In Fig. 96, Fig. 97 and Fig. 98 are reported the neighbor channels power trends and their equivalent mass flow and void fraction. All these parameters were slightly affected by the transient. In Fig. 99, Fig. 100 and Fig. 101 there are also reported the temperatures trends of clad, of fuel centerline and of Graphite hot spot.

All the investigated parameters did not exceed the safety thresholds.

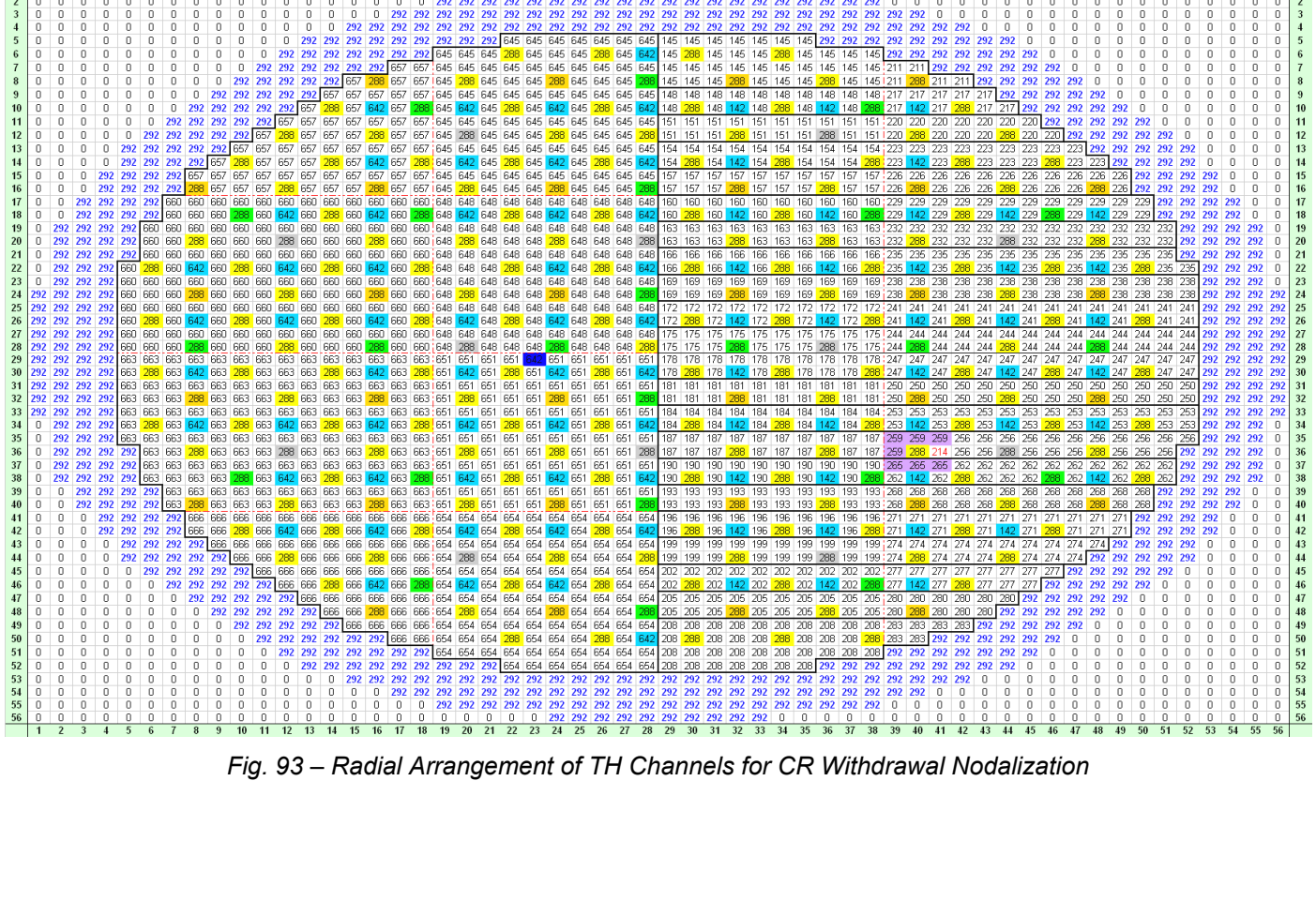

Fig. 93 – Radial Arrangement of TH Channels for CR Withdrawal Nodalization

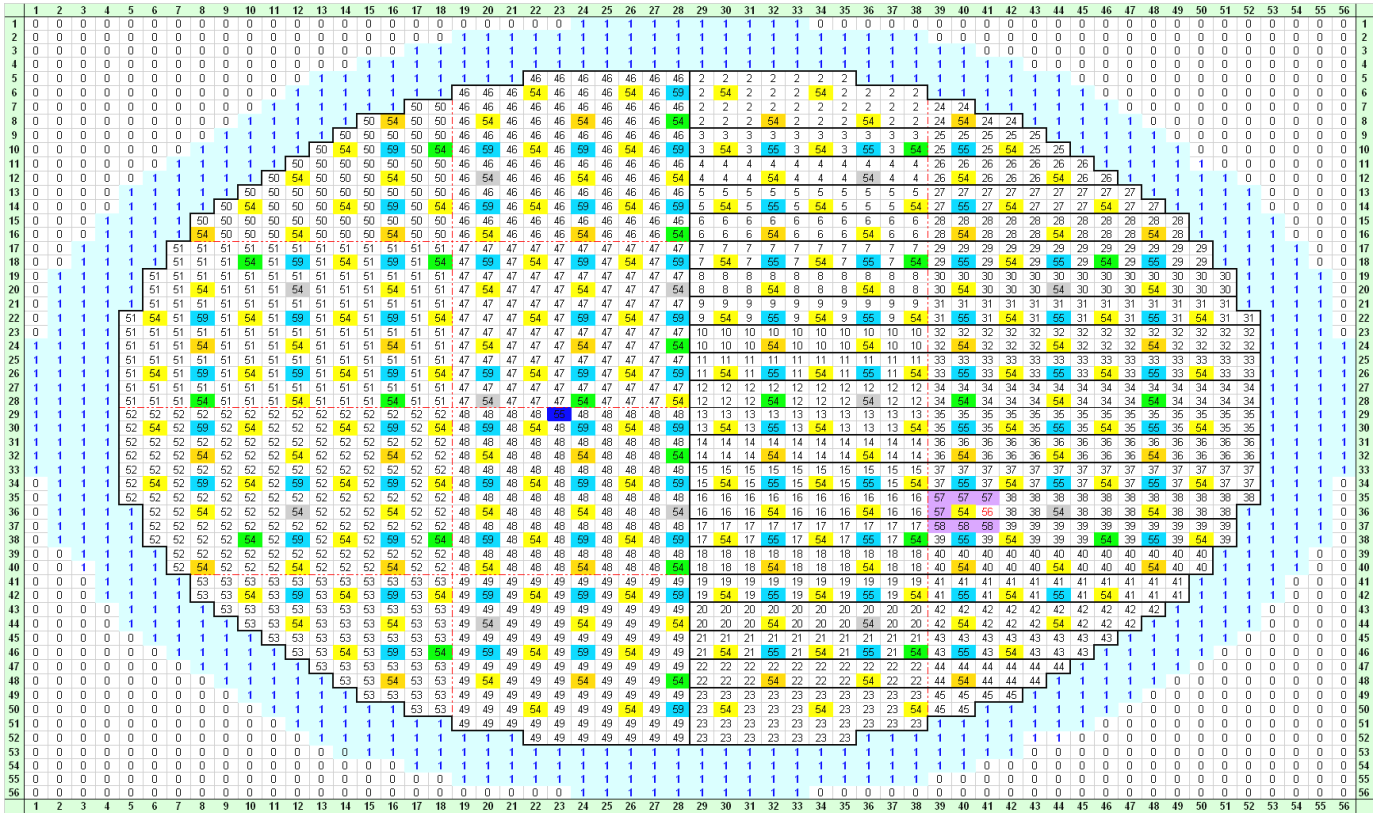

Fig. 94 – Correlation map between TH channels, TH Zones and NK Nodes for CR Withdrawal Nodalization

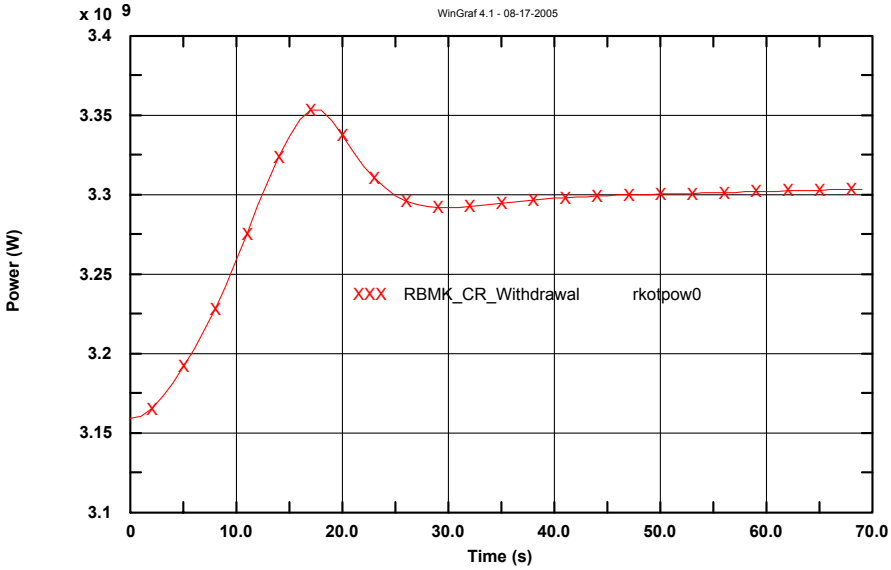

Fig. 95 – Total Reactor Power

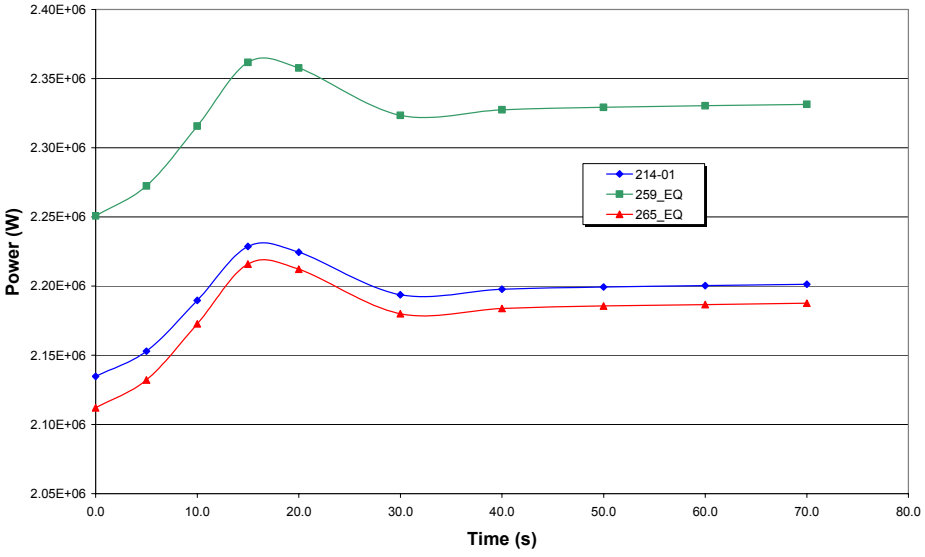

Fig. 96 – 1 FC equivalent Power

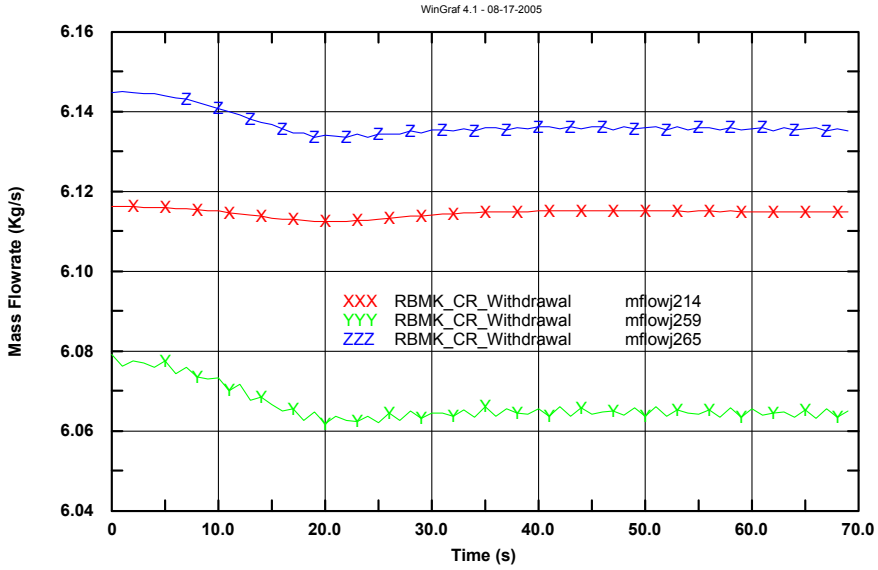

Fig. 97 – 1FC Equivalent Coolant Mass Flow – 214, 259, 265 channel

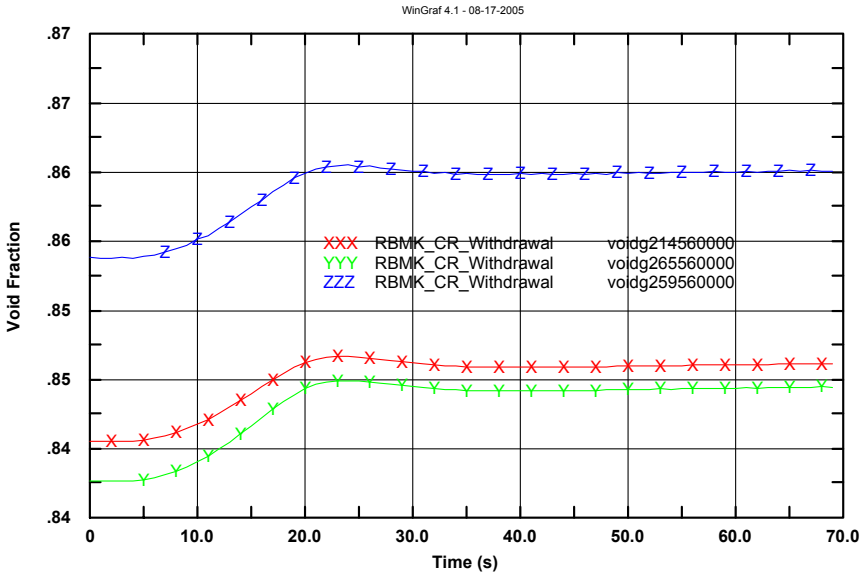

Fig. 98 – Void Fraction at the exit of FC 214, 259, 265

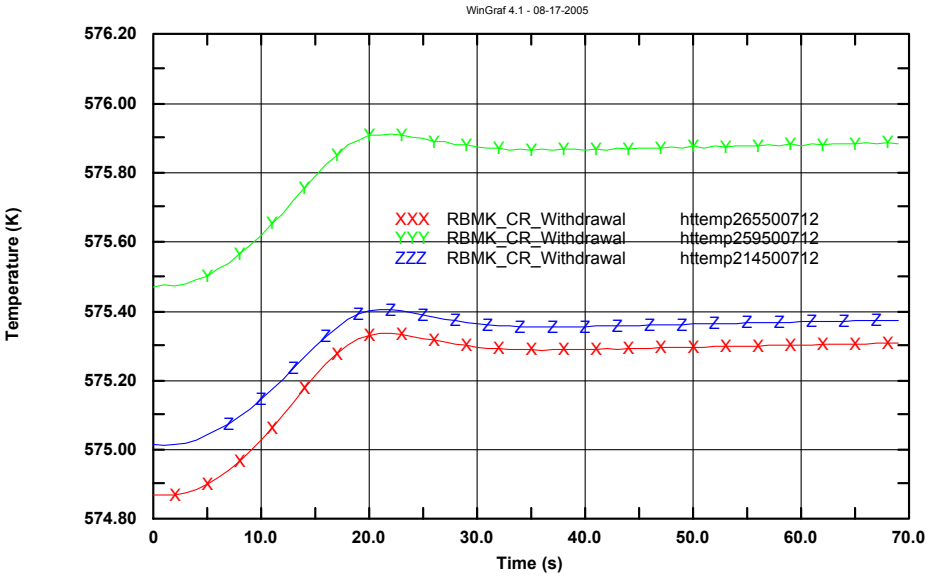

Fig. 99 – Clad Temperature at Hot Spot

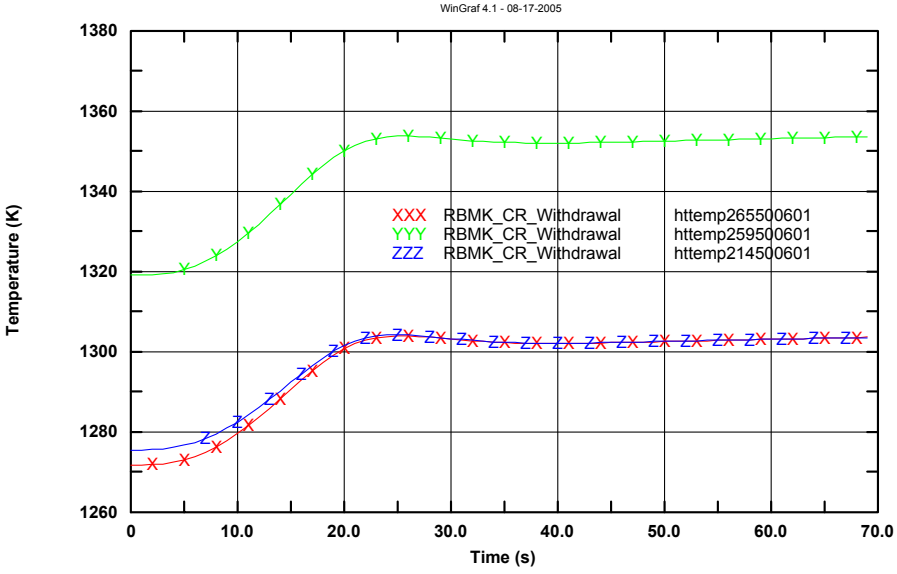

Fig. 100 – Fuel CL temperature

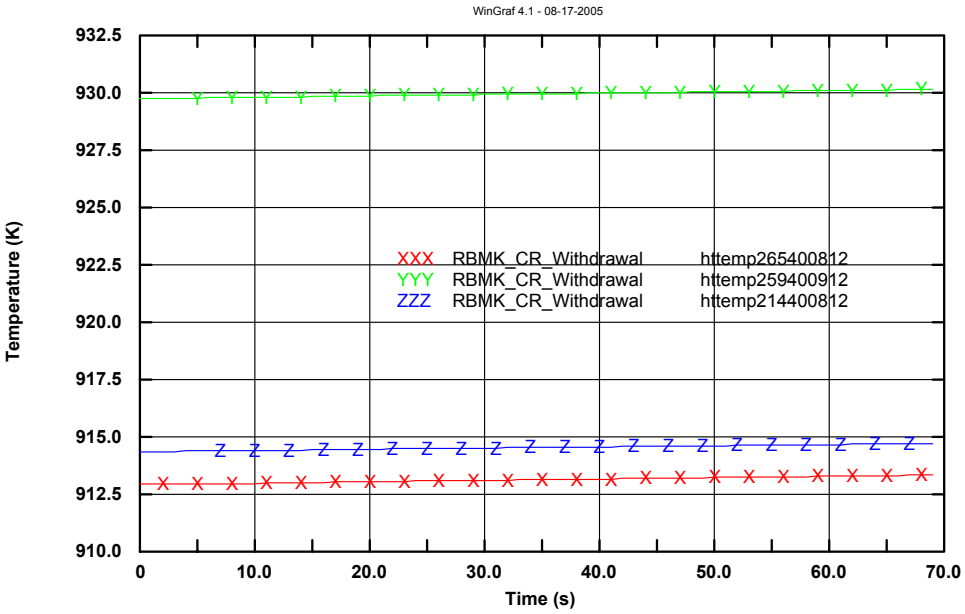

Fig. 101 – Graphite Temperatures

5.1.1.2. CR Group Withdrawal

The main purpose of the analysis of the CR-Group-Withdrawal event is the evaluation of the overall core power and the demonstration of the capabilities of the adopted code system to deal with this event. The event is originated by a spurious signal for CR bank (or group) withdrawal. The uncontrolled withdrawal of a peripheral control rod bank occurs (3 CR, the #179, #194 and the #196 with initial insertion depth of 5.80 m from bottom of top reflector, see Fig. 92).

An 'ad-hoc' TH and 3D NK nodalization was developed in order to investigate the effects on the neighbor channels too (Fig. 102 and Fig. 103).

The temporal development of the transient resulted to be:

1) 0 sec. – onset of CR Group withdrawal with the speed of 40 cm/s;
2) 7 sec – generation of AZ signal (Reactor power: 110% of Nominal Power, see Fig. 104)
    a. Insertion of all MCR with a speed of 50 cm/s
    b. Insertion of all SR with a speed of 350 cm/s

The withdrawal speed is 0.40 m/s. The scram signal is generated when the reactor power reaches the level of 110% of nominal power (3475 MW). The scram delay time is 0.25 s.

Key results are given in Fig. 104 to Fig. 111. The set-point for scram signal is achieved in a few seconds and total core power decreases as reported in Fig. 104. Fission power in equivalent FC (per individual channel) is given in Fig. 105 and

axial power distribution can be found in Fig. 111. Dangerous fuel rod temperature excursions are not predicted (Fig. 108), therefore reactor safety limits are preserved.

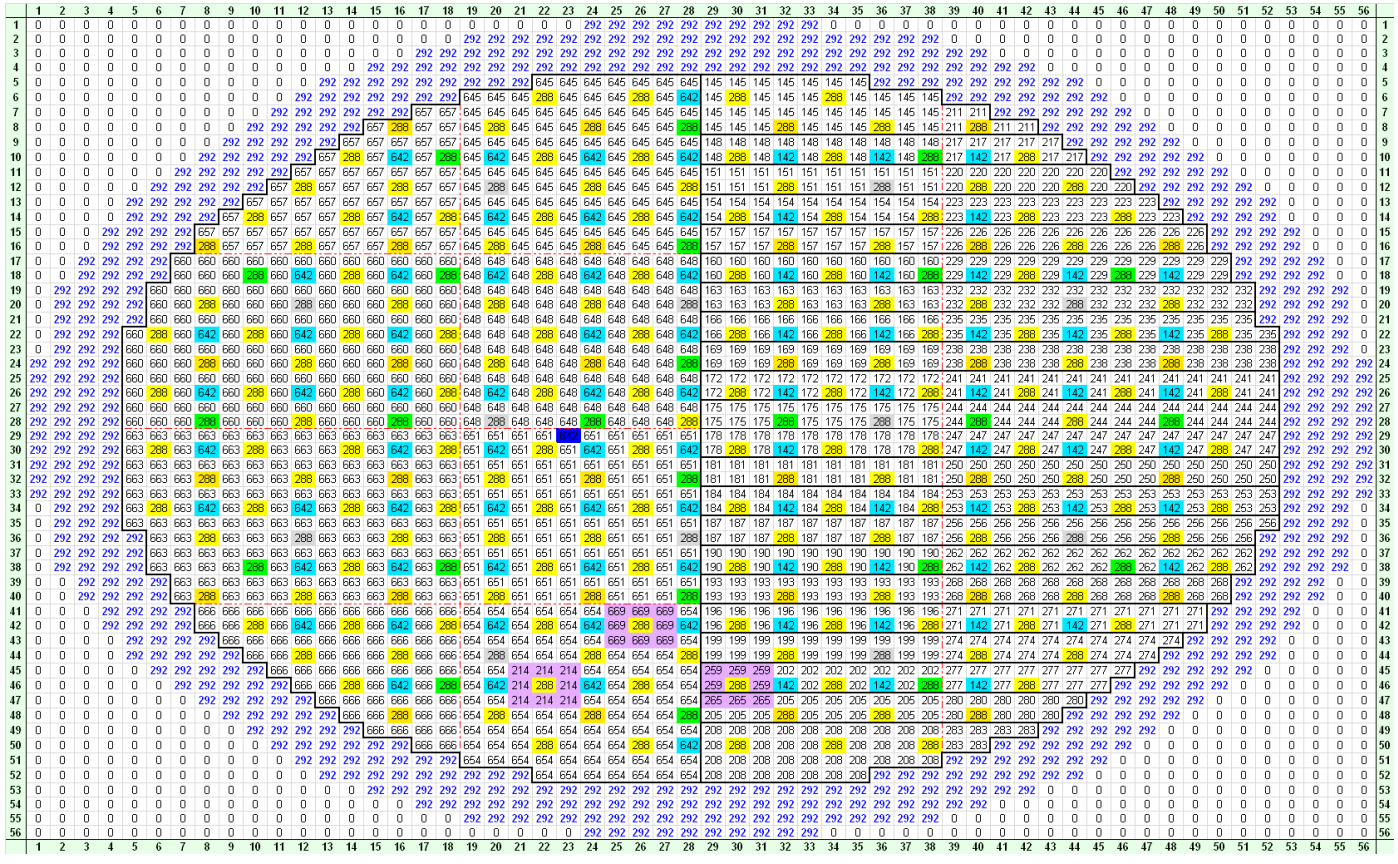

Fig. 102 – Radial Arrangement of TH Channels for CR Bank Withdrawal Nodalization

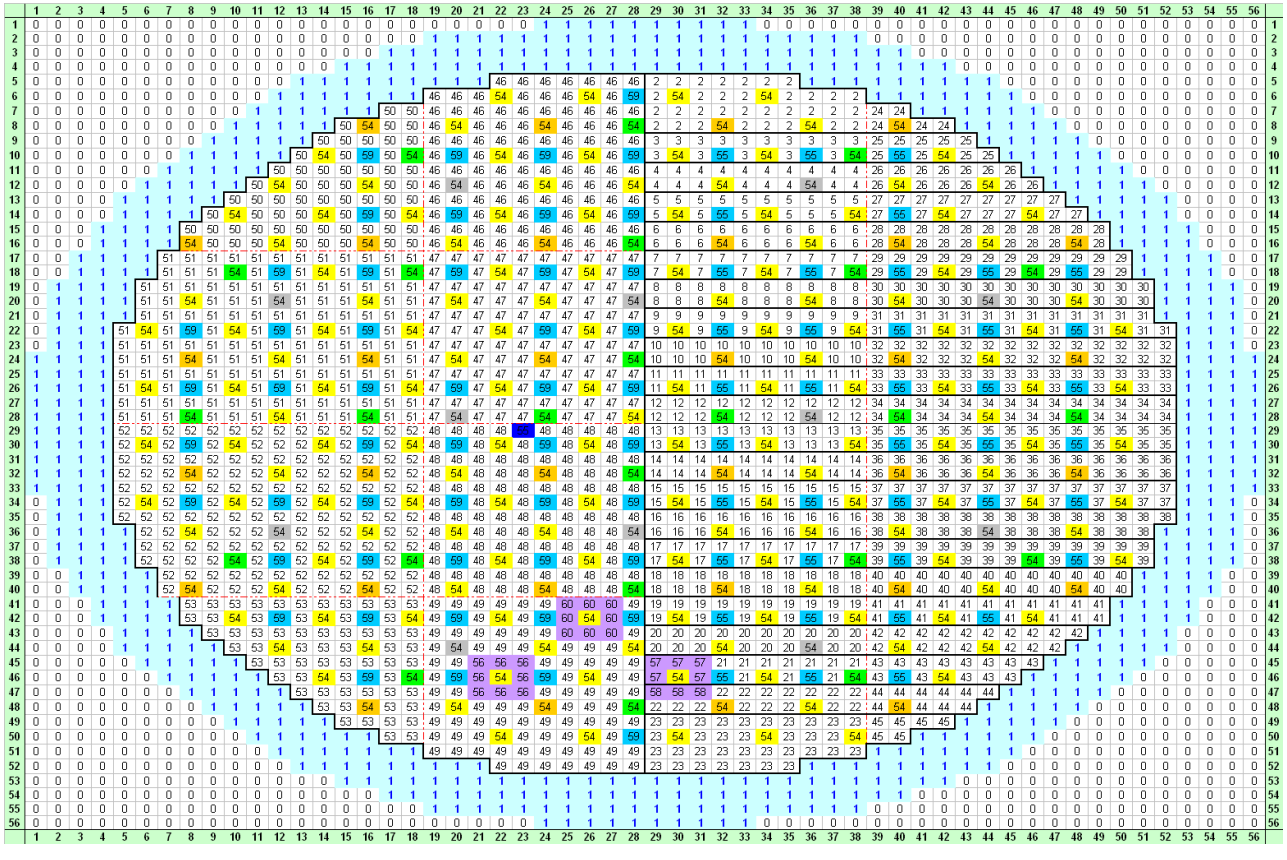

Fig. 103 – Correlation map between TH channels, TH Zones and NK Nodes for CR Bank Withdrawal Nodalization

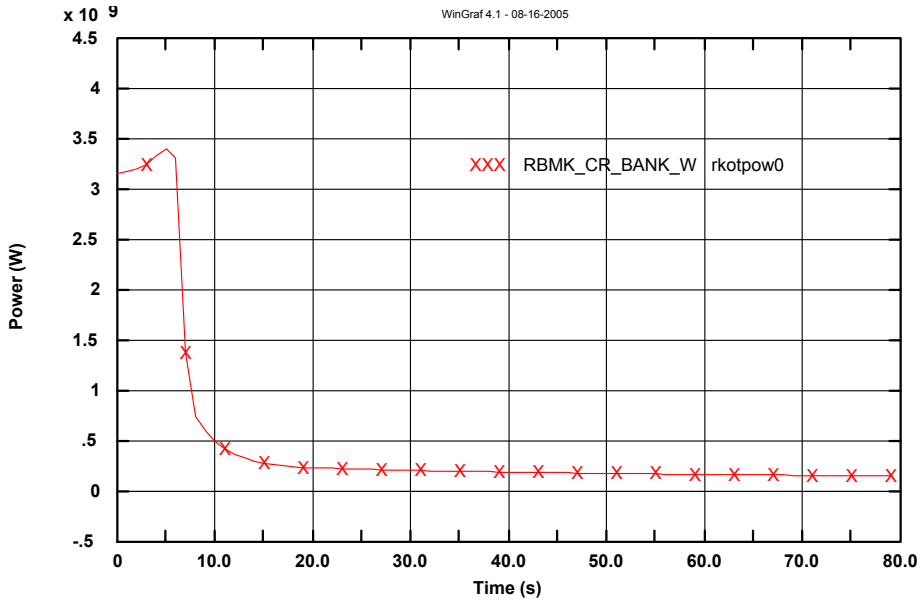

Fig. 104 – Reactor Power

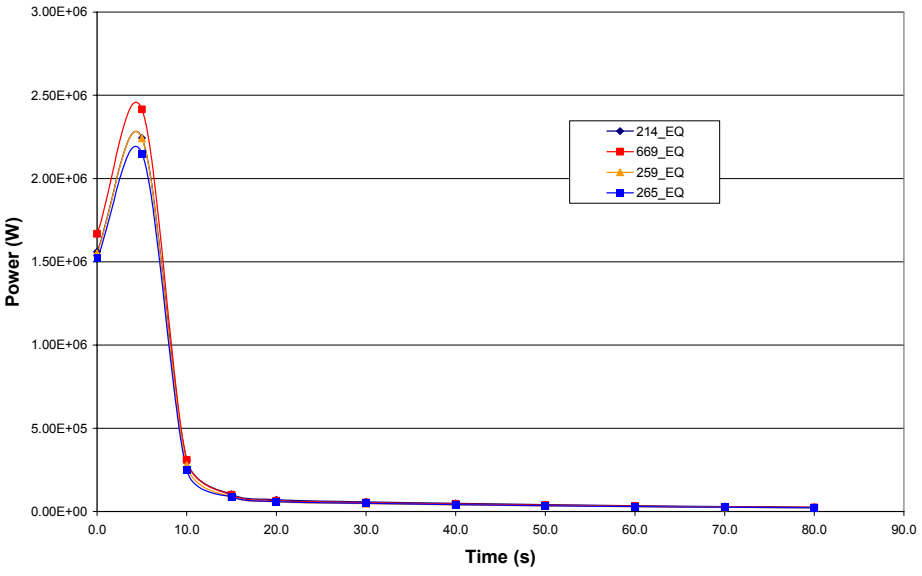

Fig. 105 – 1 FC Equivalent Power

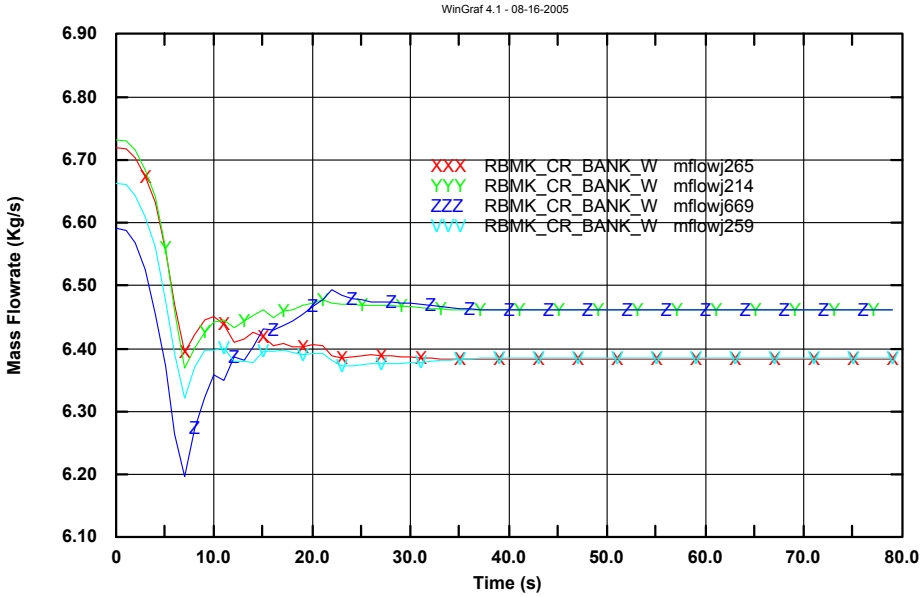

Fig. 106 – Equivalent 1FC mass flow rate

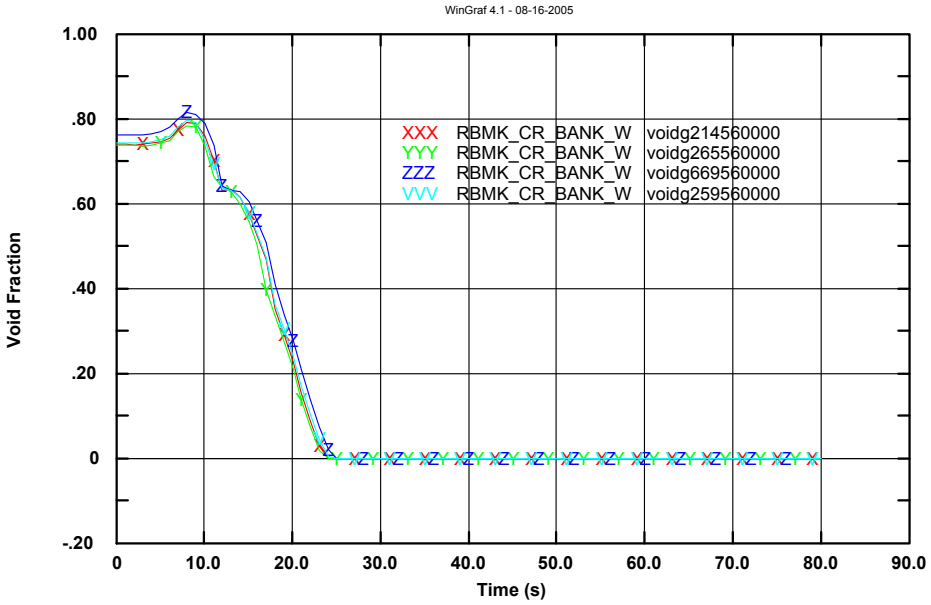

Fig. 107 – Top FC void fraction

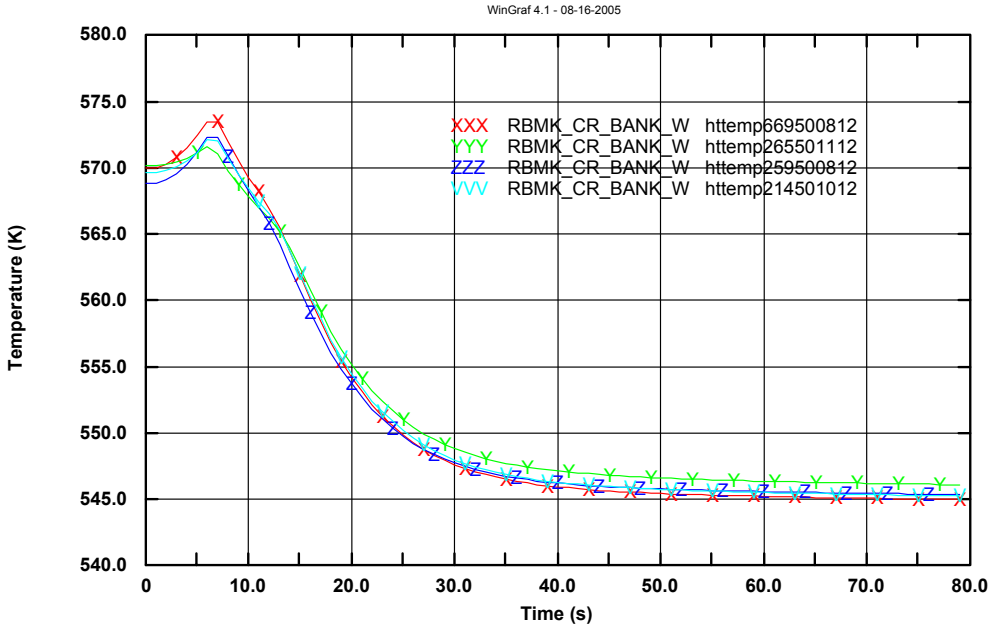

Fig. 108 – Hot Spot Clad Temperatures

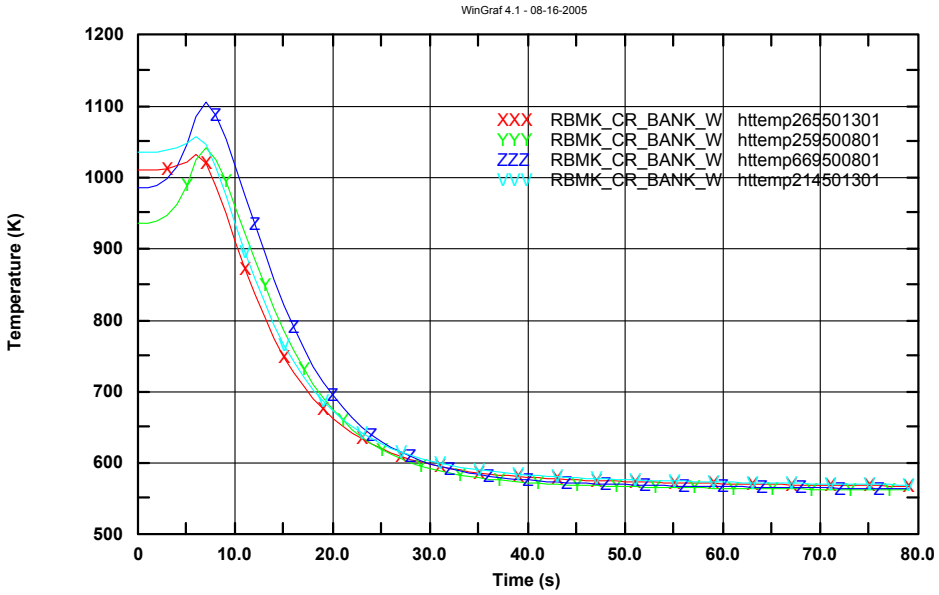

Fig. 109 – Hot Spot Fuel CL temperature

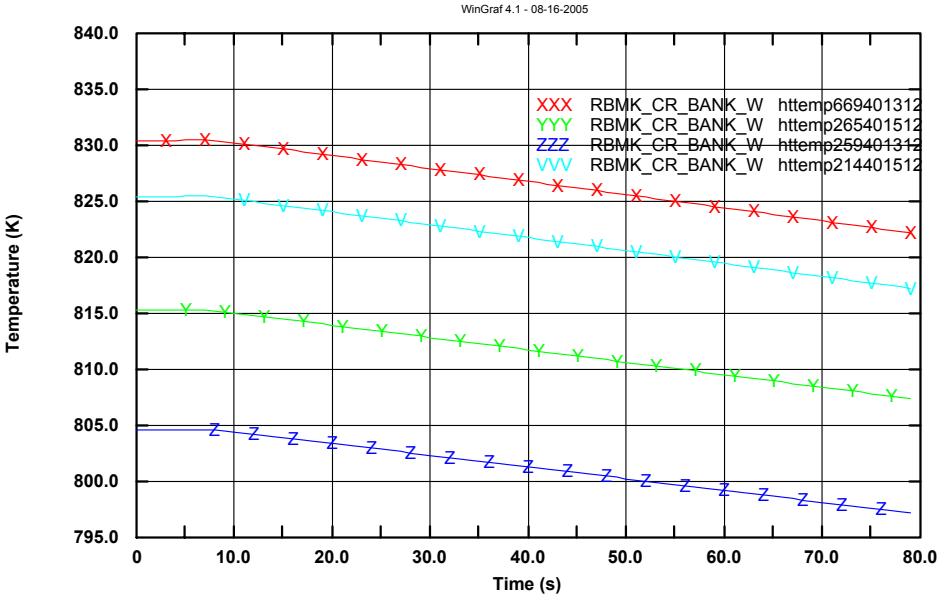

Fig. 110 – Hot Spot Graphite Outer Temperature

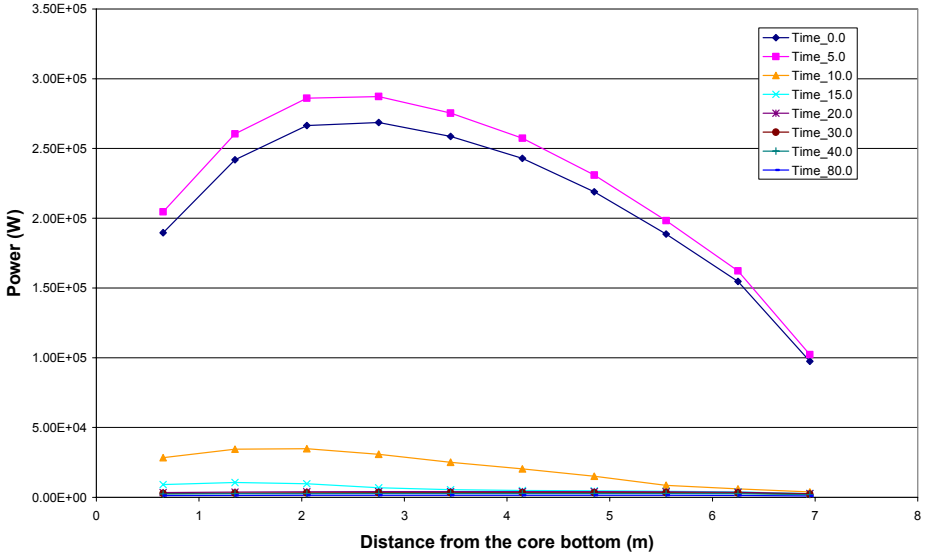

Fig. 111 – 1 FC - Equivalent axial Power

5.1.2. Decrease of coolant flow event

5.1.2.1. GDH blockage

The main purpose of the analysis of the GDH-blockage event is the evaluation of the power inside the affected FCs and the demonstration of the capabilities of the adopted code system to deal with this event. The event is supposed to be originated by the blockage of the 11th GDH on the right half of the MCC, Fig. 67. The available bypass mass flow rate is 60 Kg/s for the affected GDH. The emergency protection signal is generated when the reactor power reaches the level of 110% of nominal power (i.e. 3475 MW) or if one PT rupture occurs. The scram delay time is 0.25 s and the speed of CR insertion is 3.5 and 0.5 m/s for safety and manual CR, respectively.

Key results are given in Fig. 112 to Fig. 121. The total core power decreases soon after the accident start, Fig. 112. Flow oscillations are predicted in the FC of the affected GDH (see Fig. 113 and Fig. 114) that cause rod surface temperature excursions in some of the channels early into the transient, Fig. 118. This is one reason for global core power decrease (e.g. Fig. 112). The PT temperature is reported in Fig. 120. During the calculated transient duration, the PT temperature does overpass the safety limit.

In connection with FC thermo-hydraulic instabilities (e.g. flow-rates, Fig. 113, Fig. 114) it must be noted that a physical response of the system can be obtained when each FC of the affected GDH is modeled. This implies modeling accurately the length and the geometrical discontinuities of each of the 43 individual pipes connected with the affected GDH (i.e. from the GDH to the FC inlet in the core region) and from the individual FC outlet and the SD. This is well beyond the scope of the present activity.

Conditions for PT rupture are reached for Smolensk at different times (these could not be reached in Ignalina NPP because of the special-additional scram signal considered that causes an early core power reduction following scram). The present results, i.e. PT rupture in 300 s of calculation, show the importance of the 3D NK coupled TH model.

The close connection between thermal-hydraulic instabilities and occurrence of CHF in the rod bundle and consequent rod surface temperature rise can be noted from Fig. 118. The further consequence is the PT wall temperature above the acceptable threshold, as already emphasized.

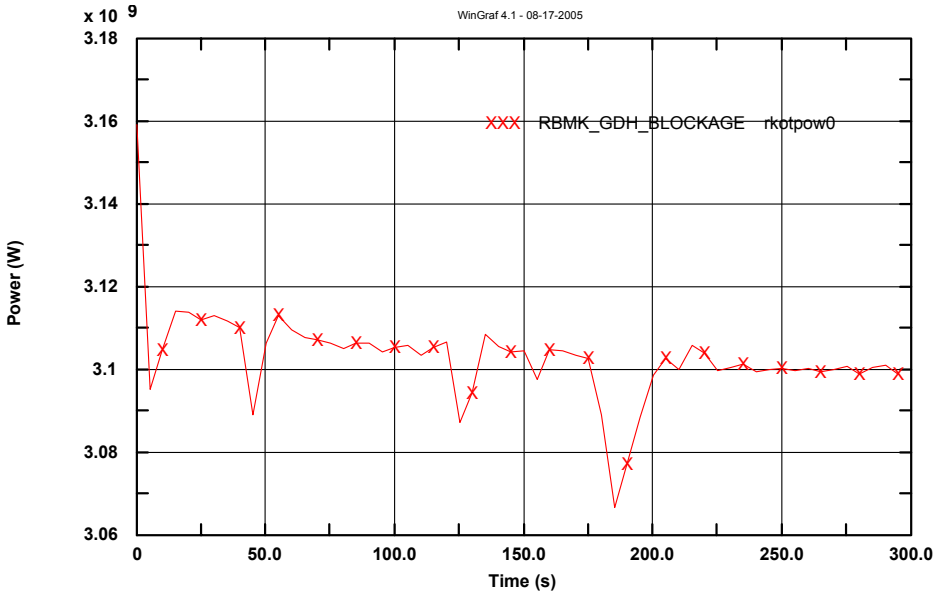

Fig. 112 – Reactor Power

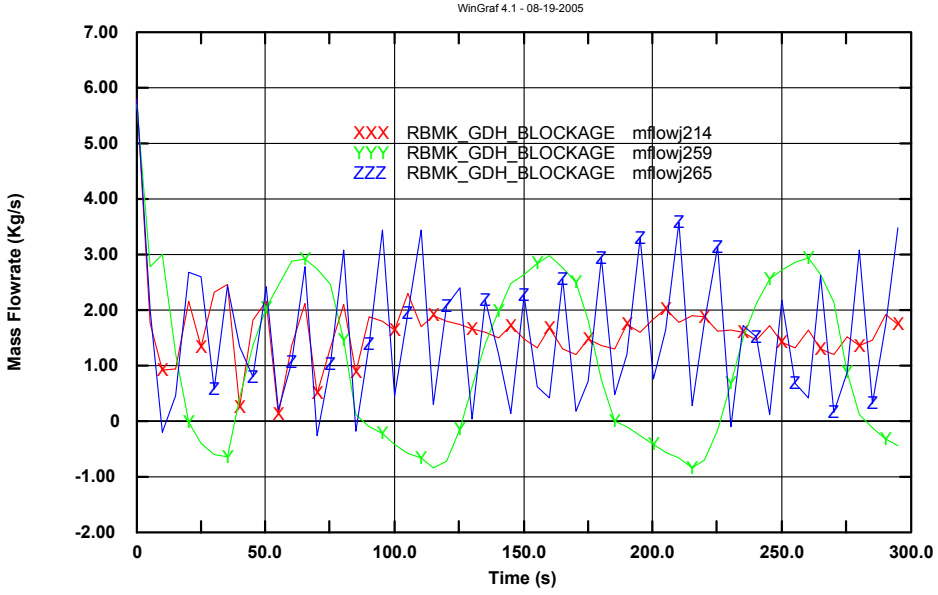

Fig. 113 – 1FC Equivalent Mass Flow Rate (channels 265, 259, 214)

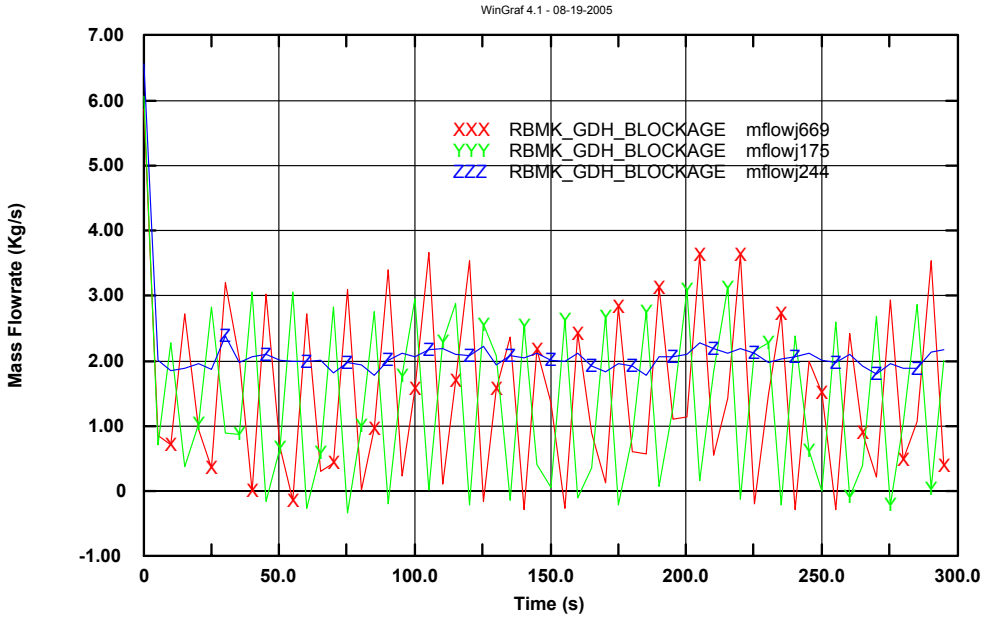

Fig. 114 – 1FC Equivalent Mass Flow Rate (channels 244, 175, 669)

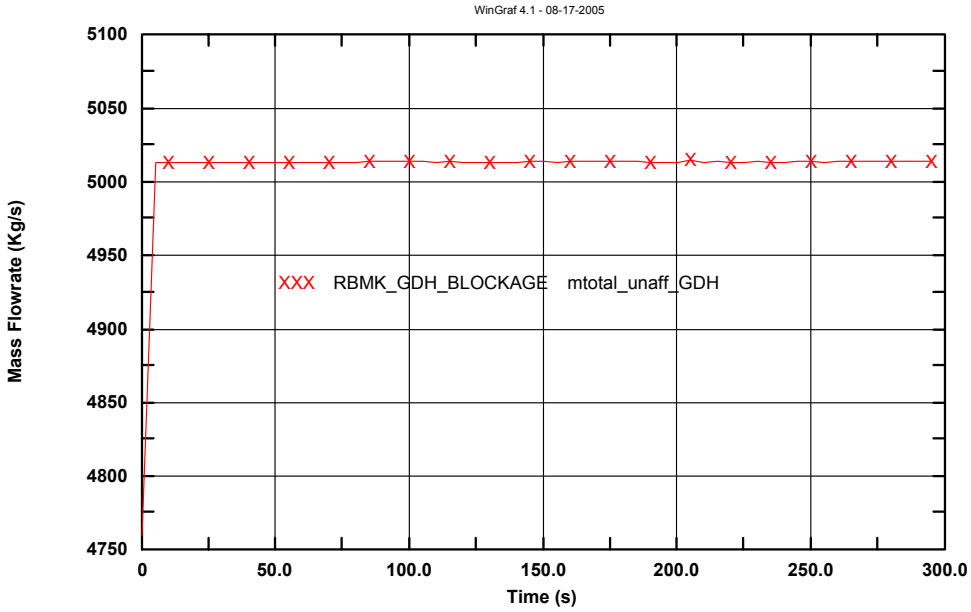

Fig. 115 – Total Mass Flow in not-affected GDHs (Right Half)

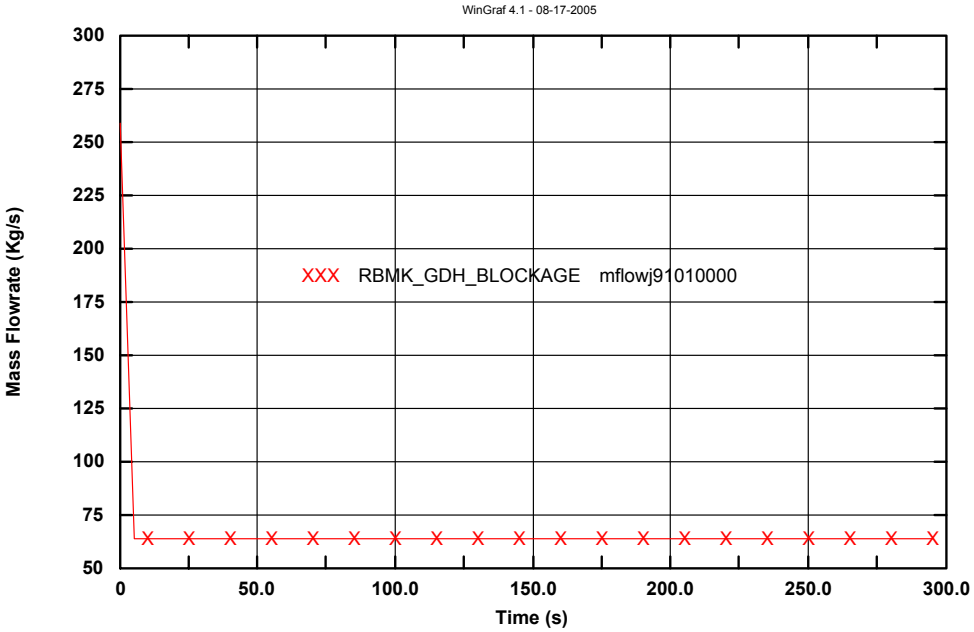

Fig. 116 – Mass Flowrate in the affected GDH

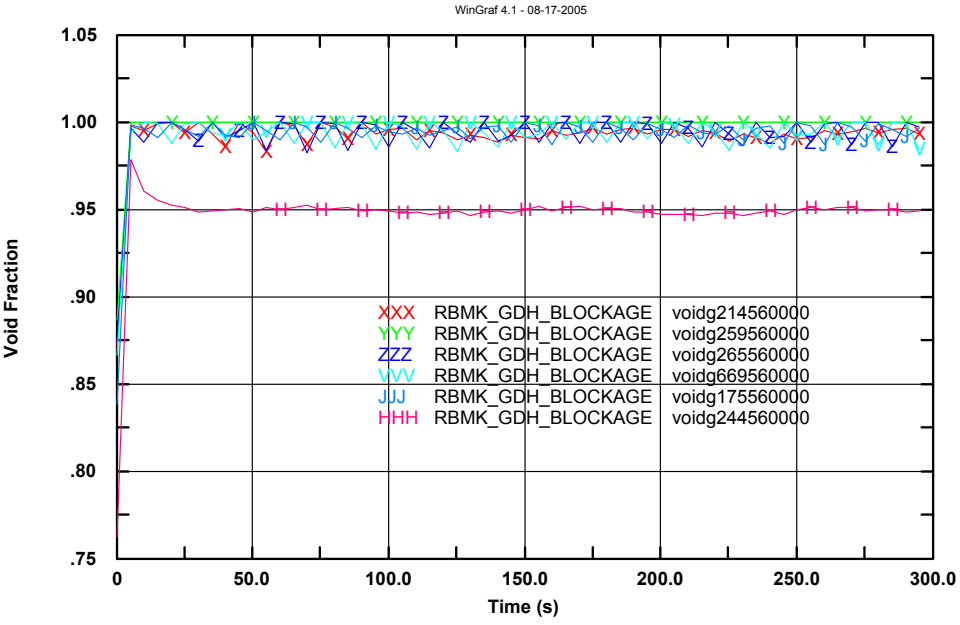

Fig. 117 – Void Fraction at top of affected GDH FCs

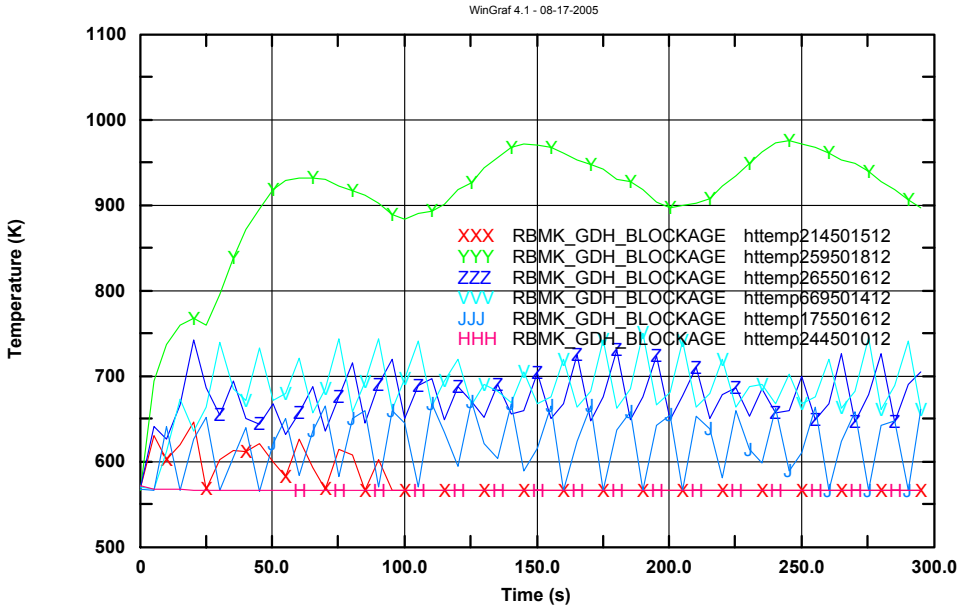

Fig. 118 – Hot Spot Clad Temperatures - FC 214, 259, 265, 175, 244

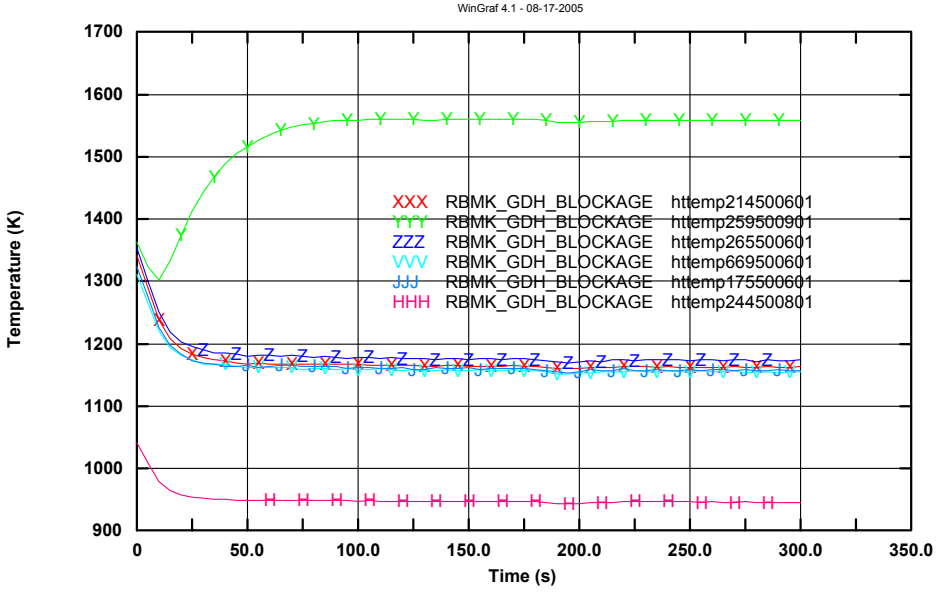

Fig. 119 – Hot Spot Fuel CL Temperatures - FC 214, 259, 265, 175, 244

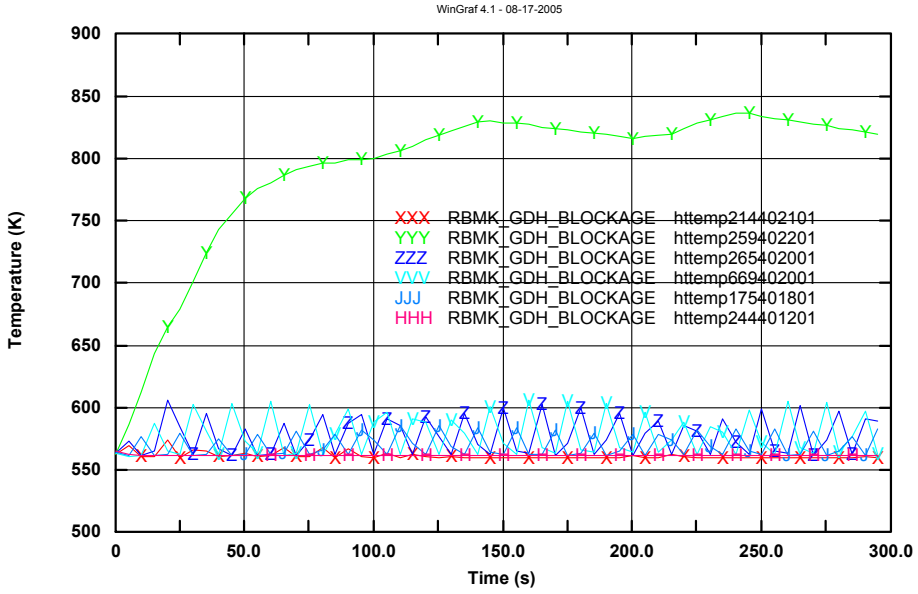

Fig. 120 – Pressure Tubes temperatures at Hot Spot – FC 214, 259, 265, 175

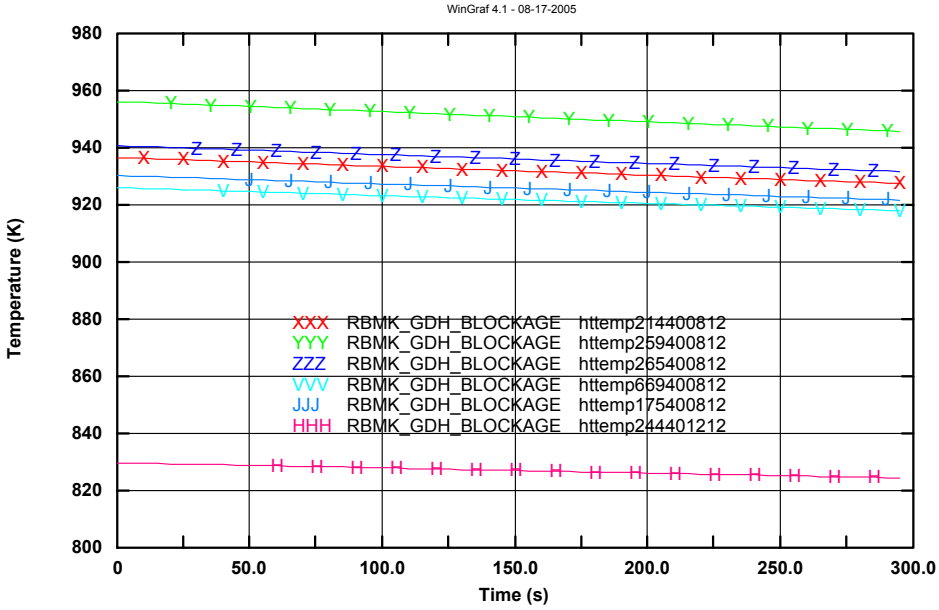

Fig. 121 – Graphite Temperatures

5.1.2.2. Fuel Channel Blockage: the System Code Analysis

The main purpose of the analysis of the Fuel Channel (FC) Blockage event is the evaluation of the affected FC power. This is relevant to calculate the time of the PT failure and, therefore, the time available for any corrective action. Following FC blockage, two counteracting main phenomena contribute to the variation of the local (i.e. of the affected FC) fission power: a) the voiding that causes an easier way for graphite moderated neutron to reach the fuel bundle; b) the fuel temperature increase consequence of lack of cooling, that through the Doppler effect tends to cause a greater parasitic neutron capture, thus introducing the potential for power decrease. Both phenomena depend upon burn-up and, to a lower extent, upon the position of the FC in the core region.

The analysis has been conducted, assuming no scram, with reference to the FC indicated in the bottom left part of Fig. 67 (channel ID is 214 and surrounding group of channel ID is 259). Key results are given in Fig. 122 to Fig. 128. It can be seen that the affected FC power substantially decreases soon after the event, Fig. 126, with overall core power slightly influenced by the event, Fig. 123. Conditions for fuel rod damage and PT failure are reached in a few tens of seconds after the transient start, Fig. 127 and Fig. 128, respectively.

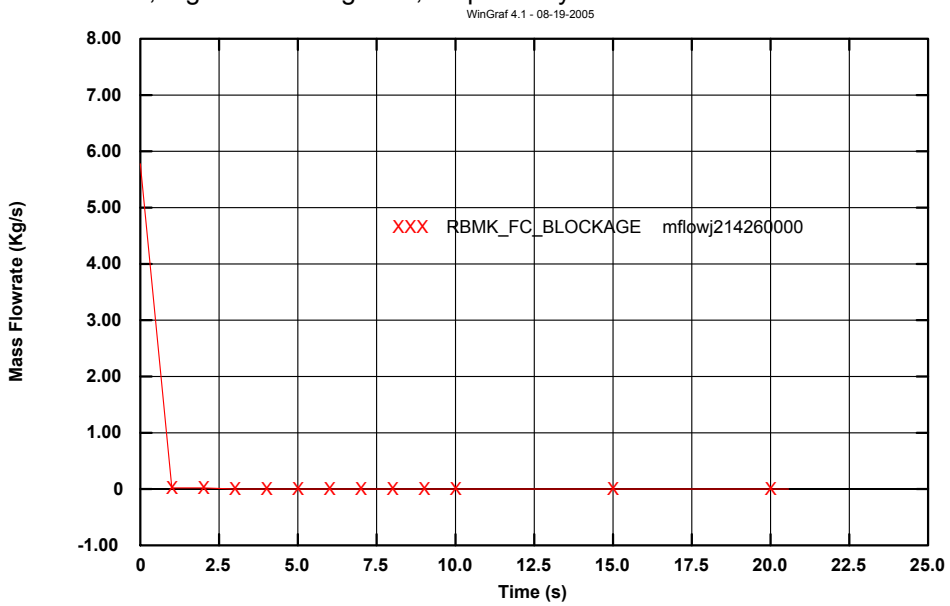

Fig. 122 – Relap5-3D/Nestle coupled 3D NK TH FC blckage analysis of Smolensk 3 RBMK NPP: flow-rate in the affected FC

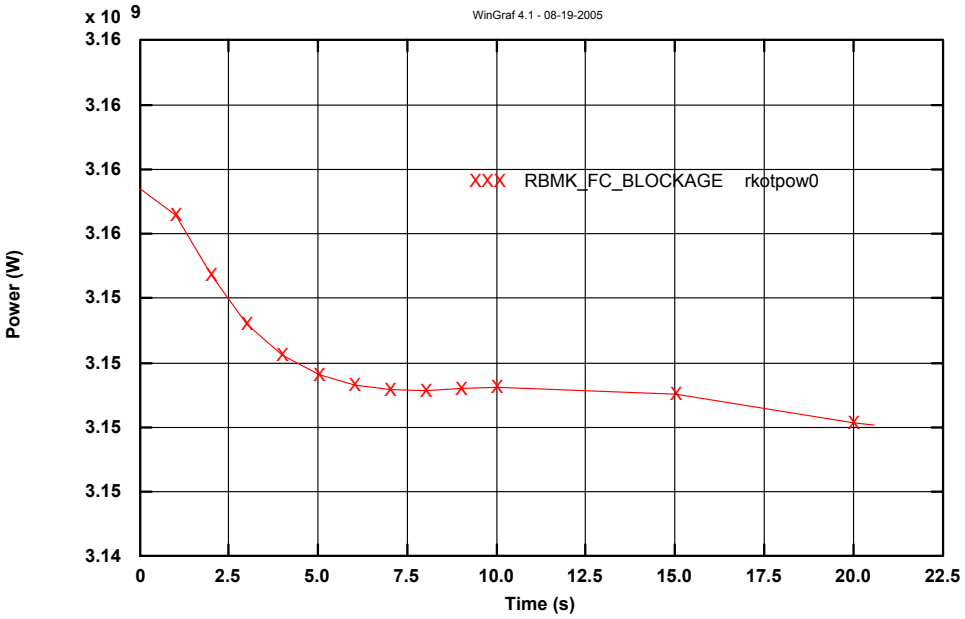

Fig. 123 – Relap5-3D/Nestle coupled 3D NK TH FC blckage analysis of Smolensk 3 RBMK NPP: core power

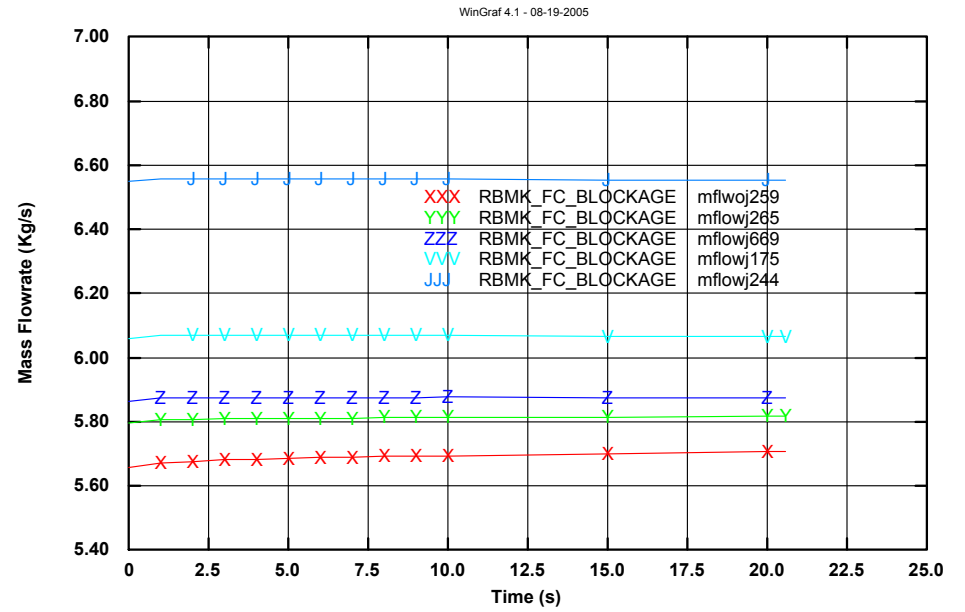

Fig. 124 – Mass Flowrate in the other channels of the affected GDH

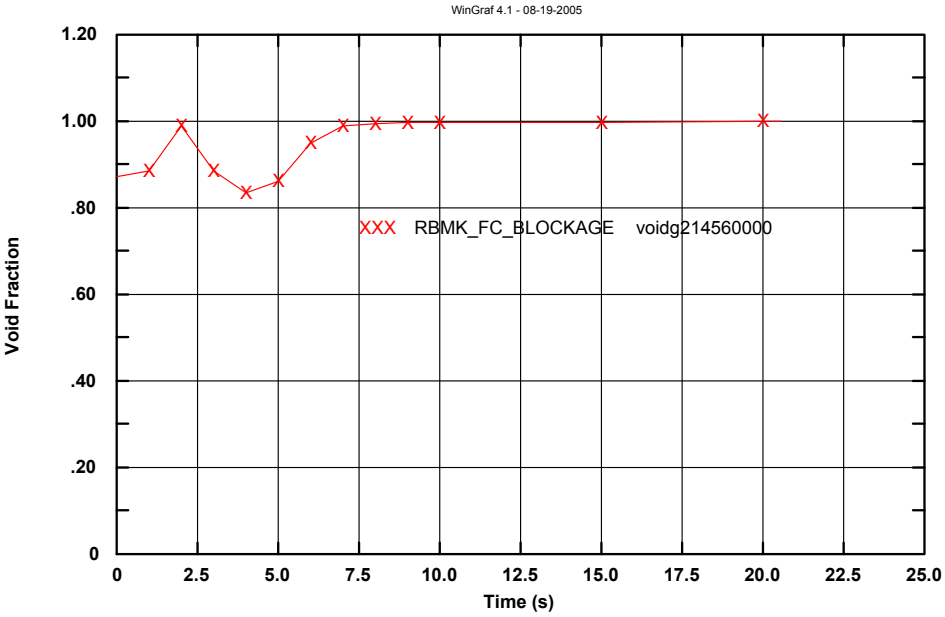

Fig. 125 – Void Fraction at the Blocked Channel Exit

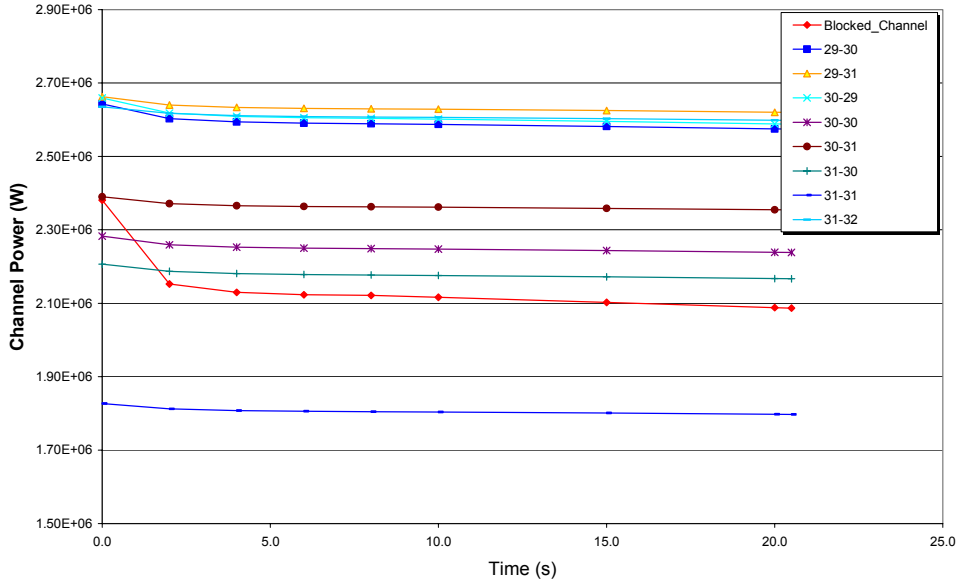

Fig. 126 – Affected FC power and power (per unit FC) in neighbouring FC.

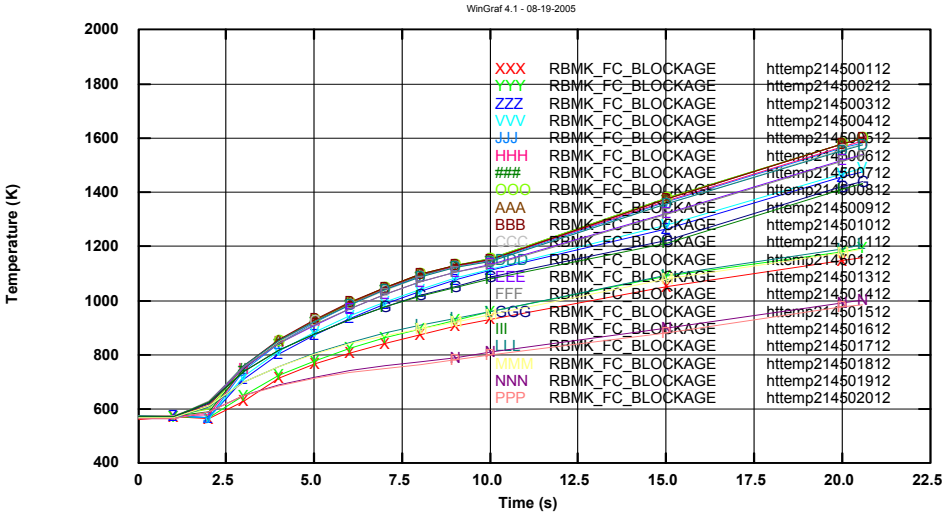

Fig. 127 – Rod surface temperature at different elevations in the affected FC.

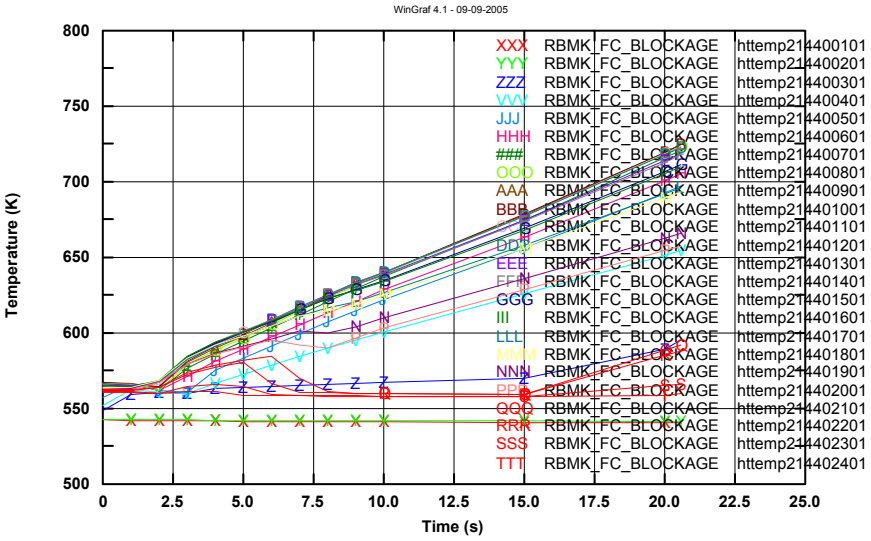

Fig. 128 – PT temperature at different elevations in the affected FC.

5.1.2.3. The Fuel Channel Blockage: the FC criticality calculations

In order to perform precise criticality analyses for a FC flow blockage accident, Monte-Carlo code MCNP5 calculations were performed considering as calculation domain a single FC and a 3x3 lattice of RBMK cells. Boundary conditions for MCNP5 input were derived by a previous transient calculation by state-of-the-art codes HELIOS/RELAP5-3D.

The changes of the main physical parameters (e.g. fuel and water/steam temperature, water density, graphite temperature) at different time intervals of the FC blockage transient were evaluated by a RELAP5-3D calculation. This information was used to set up further MCNP5 inputs. Criticality analyses were performed for different systems (single channel and lattice) at those transient' states, obtaining global criticality versus transient time. Finally the weight of each parameter's change (fuel overheating and channel voiding) on global criticality was assessed.

5.1.2.3.1. Introduction

Cell k_{inf} was calculated for several physical states occurring during a Fuel Channel Blockage (FCB) event. Fuel and moderator temperatures as well as coolant density values at different time-steps were obtained by a previously executed 3D NK – TH calculation by RELAP5-3D code. These values are given in Tab. 40.

Tab. 40 – Cell parameter variation during a FCB event by RELAP5-3D code

Transient Time (s)	Avg. Fuel Temperature (K)	Coolant Density (Kg/m^3)	Coolant Temperature (K)	Avg. Moderator Temperature (K)
0.0	800	543	563	850
8.0	1100	18.63	836	850
15.0	1300	15.2	1000	850
20.0	1500	12.6	1194	850

In order to assess the effects played by the different models, several calculations were run for both single FC models (with fuel 2.0% and 2.4%) and for lattice fuel channels models, considering FC blockage occurring in the central FC of the lattice. Results are reported hereafter.

5.1.2.3.2. Single Fuel Channel - 2.0% Fuel

Criticality Calculations

Excluding the reference state at 0.0 second (run ID *Xi*), 9 runs were executed (see Tab. 40) changing, in each run:

- all parameters, thus obtaining system criticality (runs *X1, X4, X7*);
- only coolant parameters, thus assessing voiding effect (runs *X2, X5, X8*);
- or only fuel temperature, thus assessing Doppler effect (runs *X3, X6, X9*).

All parameter changes were done according to values reported in Tab. 40. Results of cell k_{inf} with standard deviation are reported in Tab. 41 and Fig. 129. Low variance was obtained running 10^3 active cycles, simulating 10^4 neutrons histories per cycle.

Tab. 41 – 2.0% fuel cell criticality during a FCB event considering occurrence of all phenomena, of channel voiding, of Doppler effect

Transient Time (s)	System criticality			Channel voiding			Doppler Effect		
	RUN ID	k_{inf}	σ (pcm)	RUN ID	k_{inf}	σ (pcm)	RUN ID	k_{inf}	σ (pcm)
0.0	*Xi*	1.28033	15	N/A	N/A	N/A	N/A	N/A	N/A
8.0	*X1*	1.27654	17	*X2*	1.28343	15	*X3*	1.27395	15
15.0	*X4*	1.27590	16	*X5*	1.28319	16	*X6*	1.27382	16
20.0	*X7*	1.27581	16	*X8*	1.28290	16	*X9*	1.27323	15

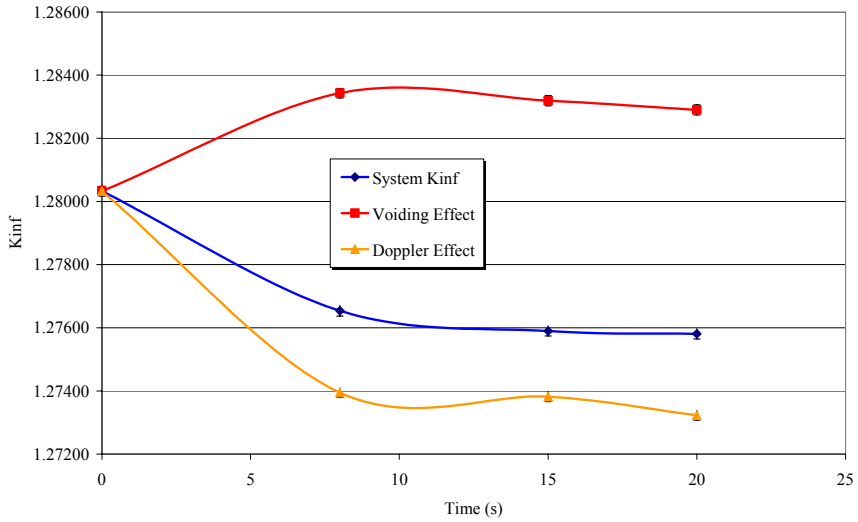

Fig. 129 – 2.0% fuel cell criticality during a FCB event considering occurrence of all phenomena, of channel voiding, of Doppler effect

Some considerations were obtained by a qualitative analysis of the previous results. FC total reactivity during this kind of transient seemed reduced thanks to overwhelming negative reactivity insertion by Doppler effect; this phenomenon looked opposed to the positive reactivity insertion generated by void effect.

Reaction Rates and neutron flux tallying

In order to have a rigorous justification for the previous results, reaction rates tallies for *Xi* to *X3* runs were executed, assessing the effects of the main phenomena (fuel overheating and channel voiding) on the neutron fluxes and reaction rates. Results

for runs *Xi* to *X3* are given in Tab. 42. The effects of parameters changes on the different tallies for runs *X1, X2, X3* compared with run *Xi* is showed in Tab. 43. Low variance for the tallies was obtained running a large number (10^8) of neutron histories. Tallies were executed dividing the energy domain into two energy groups: the fast group (from 14 MeV to 0.625 eV) and the thermal group (from 0.625 eV to 0 eV).

Tab. 42 – 2.0% fuel cell reaction rates and fluxes for runs Xi to X3

TALLYING Fuel 2.0%	*Xi*		*X1*		*X2*		*X3*	
	Thermal	Total	Thermal	Total	Thermal	Total	Thermal	Total
	Fast		Fast		Fast		Fast	
$\Sigma_{fission} * \phi$	3.52E-04	3.87E-04	3.42E-04	3.86E-04	3.44E-04	3.88E-04	3.50E-04	3.85E-04
	3.49E-05		4.34E-05		4.34E-05		3.48E-05	
$\Sigma_{absorption}$ *(fuel)* $* \phi$ *(excluding fission)*	1.49E-04	2.54E-04	1.47E-04	2.74E-04	1.47E-04	2.72E-04	1.48E-04	2.56E-04
	1.05E-04		1.28E-04		1.25E-04		1.08E-04	
$\Sigma_{absorption} * \phi$ *(in the water)*	2.27E-05	2.40E-05	3.56E-06	3.87E-06	3.58E-06	3.89E-06	2.26E-05	2.39E-05
	1.33E-06		3.10E-07		3.11E-07		1.33E-06	
ϕ *(in fuel)*	2.90E-03	8.39E-03	3.21E-03	1.03E-02	3.21E-03	1.03E-02	2.90E-03	8.38E-03
	5.49E-03		7.09E-03		7.11E-03		5.48E-03	
$\Sigma_{scattering} * \phi$ *(in the graphite)*	2.12E-03	3.67E-03	2.28E-03	4.32E-03	2.28E-03	4.33E-03	2.12E-03	3.67E-03
	1.55E-03		2.04E-03		2.05E-03		1.55E-03	

Tab. 43 – 2.0% fuel cell – Ratio of Tallies, %

Ratios of Tallies - Fuel 2.0%	*X1/Xi, %*		*X2/Xi, %*		*X3/Xi, %*	
	Thermal	Total	Thermal	Total	Thermal	Total
	Fast		Fast		Fast	
$\Sigma_{fission} * \phi$	-2.8	-0.3	-2.2	0.2	-0.5	-0.5
	24.3		24.5		-0.2	
$\Sigma_{absorption}$ *(fuel)* $* \phi$ *(excluding fission)*	-1.2	8.0	-0.8	7.1	-0.4	0.9
	21.1		18.3		2.7	
$\Sigma_{absorption} * \phi$ *(water)*	-84.3	-83.9	-84.2	-83.8	-0.4	-0.4
	-76.7		-76.7		-0.4	
ϕ *(in fuel)*	10.7	22.8	10.7	23.0	-0.1	-0.2
	29.1		29.5		-0.2	
$\Sigma_{scattering} * \phi$ *(graphite)*	7.3	17.6	7.4	17.8	-0.1	-0.1
	31.9		32.1		-0.1	

Considering Tab. 43, the followings can be stated.

- Channel voiding and steam overheating (run *X2*) is causing a large drop in the neutron absorption by the water (-83%) and a shift of the energy spectrum of the neutrons towards higher energies (flux hardening, +29%); consequently, an increase of the neutron flux ($\phi = n*v$) results (+23%). Faster flux is increasing the scattering reaction rates in the graphite block (+32% in epithermal-fast zones); hardened flux is increasing neutron absorption and neutron fissions in epithermal-fast zones (+18% and +24.5% respectively). Neutron multiplication per generation (i.e., k_{inf}) is increased as result from the sum of all these effects.
- Fuel overheating (run *X3*) as a sensible impact on the neutron population, interesting neutron absorption epithermal-fast zones; consequently a decrease on neutron population and fissions result.
- The results from the physical simulation of both effects and its comparison with the reference case (fuel and coolant overheating, run *X1*) is reproduced in the first column of Tab. 42 and Tab. 43 respectively. The coolant overheating is causing a flux hardening that results in an increase of the scattering reaction rates in the graphite block, in an increase of the neutron flux, and in an increase of the fast fissions (ε term in the k_{inf} factor). Fuel overheating is instead causing an increase of the neutron absorption (p term in the k_{inf} factor) in the and contributing to the decrease of thermal fissions. The overall number of fissions (tallying on fast and thermal energies groups) is therefore decreased. Thus, the system criticality decrease (see Fig. 129).

5.1.2.3.3. Single FC – 2.4% Fuel

Criticality Calculations

The same considerations exposed in the previous paragraph can be applied for the single FC with the 2.4% enriched fuel. The identification of the different cases is done using the same nomenclature specified above. From Tab. 44 and Fig. 130 respectively, it results that the system k_{inf} is always decreasing, also when considering channel voiding effect only. The explanation of these phenomena is given in the next paragraph.

Tab. 44 – 2.4% fuel cell criticality during a FCB event considering occurrence of all phenomena, of channel voiding, of Doppler effect

Transient Time (s)	System criticality			Channel voiding			Doppler Effect		
	RUN ID	k_{inf}	σ (pcm)	RUN ID	k_{inf}	σ (pcm)	RUN ID	k_{inf}	σ (pcm)
0.0	*Xi*	1.33503	15	N/A	N/A	N/A	N/A	N/A	N/A
8.0	*X1*	1.32694	17	*X2*	1.33383	16	*X3*	1.32873	16
15.0	*X4*	1.32680	16	*X5*	1.33369	16	*X6*	1.32850	16
20.0	*X7*	1.32637	16	*X8*	1.33375	16	*X9*	1.32788	15

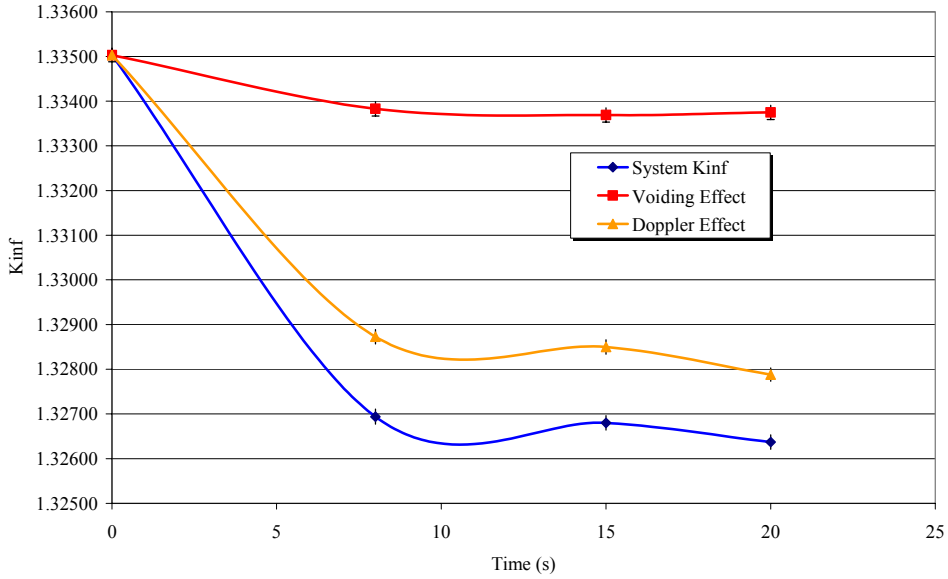

Fig. 130 – 2.4% fuel cell criticality during a FCB event considering occurrence of all phenomena, of channel voiding, of Doppler effect

Reaction Rates and neutron flux tallying

As for the 2.0 % single FC case (see previous paragraphs for calculation parameter specifications), several tallies were executed, measuring the effects of the main phenomena (fuel overheating and channel voiding) on the neutron fluxes and reaction rates. Results for runs *Xi* to *X3* are given in Tab. 45. The effects of parameters changes on the different tallies for runs X1, X2, X3 compared with run Xi is showed in Tab. 46.

Tab. 45 – 2.4% fuel cell reaction rates and fluxes for runs Xi to X3

TALLYING Fuel 2.4%	*Xi*		*X1*		*X2*		*X3*	
	Thermal	Total	Thermal	Total	Thermal	Total	Thermal	Total
	Fast		Fast		Fast		Fast	
$\Sigma_{fission} * \phi$	3.65E-04	4.04E-04	3.52E-04	4.01E-04	3.55E-04	4.03E-04	3.63E-04	4.02E-04
	3.91E-05		4.87E-05		4.88E-05		3.91E-05	
$\Sigma_{absorption}$ *(fuel)* $* \phi$ *(excluding fission)*	1.39E-04	2.45E-04	1.36E-04	2.64E-04	1.37E-04	2.62E-04	1.38E-04	2.47E-04
	1.06E-04		1.28E-04		1.25E-04		1.09E-04	
$\Sigma_{absorption} * \phi$ *(in the water)*	2.00E-05	2.13E-05	3.10E-06	3.41E-06	3.12E-06	3.43E-06	1.99E-05	2.12E-05
	1.32E-06		3.06E-07		3.06E-07		1.31E-06	
ϕ *(in fuel)*	2.54E-03	8.01E-03	2.79E-03	9.84E-03	2.79E-03	9.86E-03	2.54E-03	7.99E-03
	5.47E-03		7.05E-03		7.07E-03		5.46E-03	
$\Sigma_{scattering} * \phi$ *(in the graphite)*	1.97E-03	3.52E-03	2.09E-03	4.13E-03	2.10E-03	4.14E-03	1.97E-03	3.51E-03
	1.55E-03		2.04E-03		2.04E-03		1.54E-03	

Tab. 46 – 2.4% fuel cell criticality during a FCB event considering occurrence of all phenomena, of channel voiding, of Doppler effect, %

TALLYING Fuel 2.4%	*X1/Xi, %*		*X2/Xi, %*		*X3/Xi, %*	
	Thermal	Total	Thermal	Total	Thermal	Total
	Fast		Fast		Fast	
$\Sigma_{fission} * \phi$	-3.3	-0.6	-2.8	-0.1	-0.5	-0.5
	24.4		24.6		-0.2	
$\Sigma_{absorption}$ *(fuel)* $* \phi$ *(excluding fission)*	-1.8	8.0	-1.3	7.0	-0.4	0.9
	20.7		18.0		2.6	
$\Sigma_{absorption} * \phi$ *(water)*	-84.5	-84.0	-84.4	-83.9	-0.4	-0.4
	-76.8		-76.8		-0.4	
ϕ *(in fuel)*	9.8	22.9	9.9	23.1	-0.1	-0.2
	29.0		29.3		-0.2	
$\Sigma_{scattering} * \phi$ *(graphite)*	6.2	17.4	6.3	17.6	-0.1	-0.1
	31.7		31.9		-0.1	

From Tab. 45 and Tab. 46, the following considerations result:

- channel voiding and steam overheating (run *X2*) is causing a large drop in neutron absorption by water (-84%) and a shift of the neutron energy spectrum towards higher energies (+29%). Consequently, an increase of

the neutron population (+23%) results. The faster neutron flux is increasing the scattering reactions in the graphite block (+32% in epithermal-fast zones) as well as epithermal neutron absorption and fast fissions reaction rates in the epithermal-fast zones (+18% and +24.6% respectively). The voiding effect on k_{inf} is negative (k_{inf} is slightly decreasing) because the fissions reaction rates are decreasing in thermal zone more than for the 2.0% fuel case. Therefore, a sensible reduction of the number of neutrons from fissions results, causing a reduction of the k_{inf}.

- Fuel overheating (run *X3*) has a sensible impact on the neutron population, interesting neutron absorption epithermal-fast zones; consequently a slight decrease of the neutron population and of fissions reaction rates result. The magnitude of the reductions is the same as for the 2.0% fuel case.
- The results from the physical simulation of both effects and its comparison with the reference case (fuel and coolant overheating, run *X1*) is reproduced in the first column of Tab. 45 and Tab. 46 respectively. The coolant overheating is causing a flux hardening that results in an increase of the scattering reaction rates in the graphite block, in an increase of the neutron flux, and in an increase of the fast fissions. Fuel overheating is instead causing an increase of the neutron absorption and contributing to the decrease of thermal fissions. The overall number of fissions (tallying on fast and thermal energies groups) is therefore decreased, in this case more than in the 2.0% fuel case. Thus, the system criticality decreases (see Fig. 130).

5.1.2.3.4. *Lattice Cell Analysis*

Similar analyses were performed for studying the effects of channel voiding and fuel overheating phenomena when they take place in a FC of a lattice, i.e. simulating an event more similar to what is occurring in a real RBMK core. For this purpose, the 3x3 lattice model was used, considering blockage of the central FC. Analyses were performed for the following configurations:

1. 2.0 % fuel lattice
2. 2.4 % fuel lattice
3. 2.4 % fuel lattice with 2.0 % fuel for blocked channel

Results of these analyses are reported in the following paragraphs.

2.0 % Fuel : Criticality Calculations

Results of criticality calculations are given in Tab. 47 and in Fig. 131. Very low variance was obtained running 10^4 neutron histories for 10^4 active neutron cycles (10^8 MH). Doppler and voiding effect in the central FC produced the same qualitative effects on the lattice reactivity as in the case of a single FC with 2.0% enriched fuel (i.e., positive and negative insertion, for voiding and Doppler respectively). System criticality is instead, in this case, increased.

It should also be noted that in all these simulations with lattice of FCs, the magnitude of k_{inf} change is smaller than in the case of single FCs simulations (tens of pcm compared to hundreds of pcm, respectively).

For the identification of the different cases, the same nomenclature specified in the previous paragraphs was used.

Tab. 47 – 2.0% fuel lattice criticality during a FCB event on central channel considering occurrence of all phenomena, of channel voiding, of Doppler effect

Transient Time (s)	System criticality			Channel voiding			Doppler Effect		
	RUN ID	k_{inf}	σ (pcm)	RUN ID	k_{inf}	σ (pcm)	RUN ID	k_{inf}	σ (pcm)
0.0	*Xi*	1.28030	5	N/A	N/A	N/A	N/A	N/A	N/A
8.0	*X1*	1.28068	5	*X2*	1.28139	5	*X3*	1.27957	5
15.0	*X4*	1.28066	5	*X5*	1.28128	5	*X6*	1.27966	5
20.0	*X7*	1.28058	5	*X8*	1.28132	5	*X9*	1.27957	5

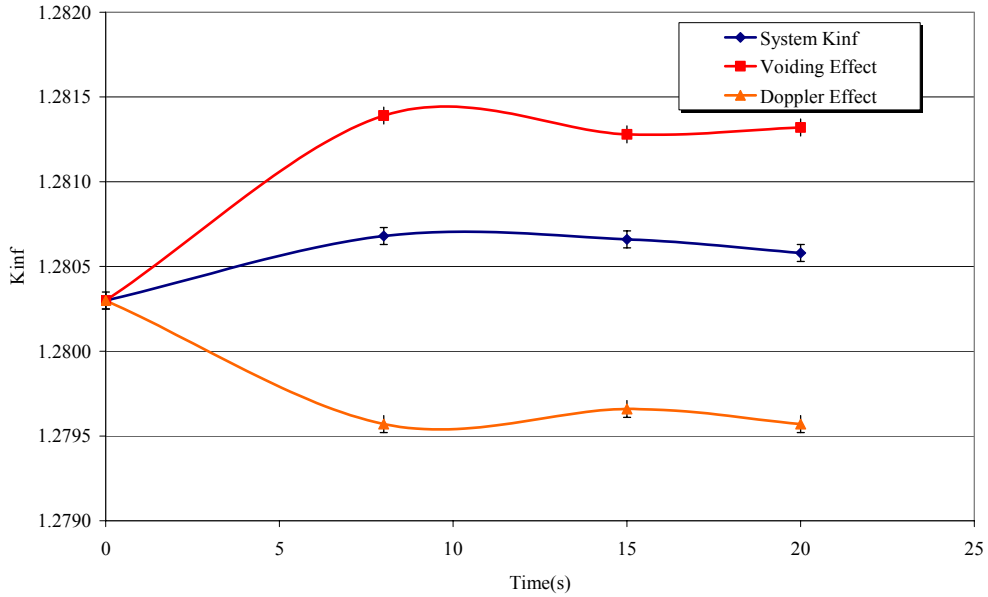

Fig. 131 – 2.0% fuel lattice criticality during a FCB event on central channel considering occurrence of all phenomena, of channel voiding, of Doppler effect

2.0 % Fuel : Reaction Rates and neutron flux tallying

As for the single FC calculations, several reaction rates and flux tallies were executed assessing the effects of the main phenomena. Results for runs *Xi* to *X3* are given in Tab. 48 and Tab. 49, reporting values for the central channel (blocked channel) and for the border channels of the lattice. The effects of parameters changes on the different tallies for runs *X1, X2, X3* in comparison with run *Xi* is

showed in Tab. 50. Low variance for the tallies was obtained running a large number of neutron histories (10^8 MH).

Tab. 48 – 2.0% lattice fuel cells reaction rates and fluxes for runs Xi and X1

TALLYING Lattice Fuel 2.0%	Xi				X1			
	Central		Border		Central		Border	
	Thermal / Fast	Total	Thermal / Fast	Total	Thermal / Fast	Total	Thermal / Fast	Total
$\Sigma_{fission} * \phi$	3.91E-05 / 3.88E-06	4.30E-05	3.91E-05 / 3.88E-06	4.30E-05	3.42E-05 / 3.96E-06	3.81E-05	3.97E-05 / 3.96E-06	4.36E-05
$\Sigma_{absorption}$ (fuel) * ϕ (excluding fission)	1.65E-05 / 1.17E-05	2.82E-05	1.65E-05 / 1.17E-05	2.82E-05	1.46E-05 / 1.13E-05	2.60E-05	1.67E-05 / 1.20E-05	2.87E-05
$\Sigma_{absorption} * \phi$. (in the water)	2.52E-06 / 1.48E-07	2.67E-06	2.52E-06 / 1.48E-07	2.67E-06	3.55E-07 / 2.76E-08	3.83E-07	2.55E-06 / 1.52E-07	2.70E-06
ϕ (in fuel)	3.22E-04 / 6.10E-04	9.32E-04	3.23E-04 / 6.11E-04	9.33E-04	3.18E-04 / 6.64E-04	9.82E-04	3.27E-04 / 6.22E-04	9.49E-04
$\Sigma_{scattering} * \phi$ (in the graphite)	2.36E-04 / 1.72E-04	4.08E-04	2.36E-04 / 1.72E-04	4.08E-04	2.28E-04 / 1.84E-04	4.12E-04	2.39E-04 / 1.76E-04	4.15E-04

Tab. 49 – 2.0% lattice fuel cells reaction rates and fluxes for runs X2 and X3

TALLYING Lattice Fuel 2.0%	X2				X3			
	Central		Border		Central		Border	
	Thermal / Fast	Total	Thermal / Fast	Total	Thermal / Fast	Total	Thermal / Fast	Total
$\Sigma_{fission} * \phi$	3.43E-05 / 3.97E-06	3.83E-05	3.97E-05 / 3.96E-06	4.36E-05	3.89E-05 / 3.86E-06	4.28E-05	3.91E-05 / 3.88E-06	4.30E-05
$\Sigma_{absorption}$ (fuel) * ϕ (excluding fission)	1.47E-05 / 1.11E-05	2.58E-05	1.67E-05 / 1.20E-05	2.87E-05	1.65E-05 / 1.20E-05	2.85E-05	1.65E-05 / 1.17E-05	2.82E-05
$\Sigma_{absorption} * \phi$. (in the water)	3.56E-07 / 2.76E-08	3.84E-07	2.55E-06 / 1.52E-07	2.70E-06	2.51E-06 / 1.47E-07	2.66E-06	2.52E-06 / 1.48E-07	2.66E-06

Tab. 49(cont.) – 2.0% lattice fuel cells reaction rates and fluxes for runs X2 and X3

TALLYING Lattice Fuel 2.0%	X2				X3			
	Central		Border		Central		Border	
	Thermal / Fast	Total	Thermal / Fast	Total	Thermal / Fast	Total	Thermal / Fast	Total
$\dot{\phi}$ (in fuel)	3.17E-04	9.84E-04	3.27E-04	9.49E-04	3.22E-04	9.29E-04	3.23E-04	9.33E-04
	6.67E-04		6.22E-04		6.07E-04		6.11E-04	
$\Sigma_{scattering}^{*}\ \dot{\phi}$ (in the graphite)	2.28E-04	4.12E-04	2.39E-04	4.15E-04	2.36E-04	4.08E-04	2.36E-04	4.08E-04
	1.84E-04		1.76E-04		1.72E-04		1.72E-04	

Tab. 50 – 2.0% lattice fuel cell – Ratio of Tallies, %

Ratios of Tallies - Lattice Fuel 2.0%	X1/Xi , %				X2/Xi , %				X3/Xi , %			
	Central		Border		Central		Border		Central		Border	
	Th. / Fast	Tot.	Th. / Fast	Tot.	Th. / Fast	Tot.	Th. / Fast	Tot.	Th. / Fast	Tot.	Th. / Fast	Tot.
$\Sigma_{fission}^{*}\ \dot{\phi}$	-12.7	-11.3	1.4	1.4	-12.3	-11.0	1.4	1.4	-0.4	-0.4	0.0	0.0
	2.1		2.1		2.4		2.1		-0.3		0.0	
$\Sigma_{absorption}^{*}$ ϕ (fuel)	-11.4	-8.0	1.4	1.8	-11.1	-8.7	1.4	1.8	-0.3	0.8	0.0	0.0
	-3.3		2.4		-5.4		2.4		2.4		0.0	
$\Sigma_{absorption}^{*}\ \dot{\phi}$ (water)	-85.9	-85.6	1.4	1.4	-85.8	-85.6	1.4	1.4	0.0	-0.4	0.0	0.0
	-81.4		2.4		-81.3		2.4		-0.5		0.0	
ϕ(fuel)	-1.5	5.3	1.4	1.7	-1.6	5.6	1.4	1.7	0.0	-0.4	0.0	0.0
	8.9		1.9		9.4		1.8		-0.5		0.0	
$\Sigma_{scattering}^{*}\ \dot{\phi}$ (graphite)	-3.3	1.0	1.1	1.7	-3.3	1.1	1.1	1.7	0.0	-0.1	0.0	0.0
	7.0		2.5		7.2		2.5		-0.2		0.0	

From Tab. 48 to Tab. 50, the followings can be stated.

- Central FC coolant overheating (run *X2*) is causing a large drop in the neutron absorption by the water (-86%) and a shift of the energy spectrum of the neutrons towards fast energies (flux hardening, +9.4%, sensibly less than +29% occurring in the single FC model because of neutron leakages). This is causing a neutron leakage towards border FC of the lattice; accordingly, there is an increase of the fast scattering (+7.2%) in the central graphite block and a decrease of total fission (-11%) and absorption (-8.7%) reaction rates in the fuel of the central FC. The reaction rates of the border FCs are instead all increased of some percent.

- Fuel overheating is affecting only the reaction rates of the central FC. Neutron absorption is increased in the fuel.
- The results from the physical simulation of both effects (fuel and coolant overheating, run X1) are reported in the first column of Tab. 48 and Tab. 50 respectively. The coolant overheating in the central FC is causing a flux hardening that results in an increase of the scattering reaction rates in the graphite block, in an increase of the neutron flux and fast fissions and in an increase of neutron leakages toward peripheral FCs. Reaction rates in the peripheral FCs increase of some percents, while the overall fission and absorption reaction rates of the central FC are sensibly reduced (-11% and -8% respectively). The system neutron multiplication capability (i.e., k_{inf}) is slightly increased (see Fig. 131).

2.4 % Fuel: Criticality Calculations

Results of criticality calculations for the 2.4% enriched fuel are given in Tab. 51 and in Fig. 132. Also in this case, very low variance was obtained running 10^4 neutron histories for 10^4 active neutron cycles (i.e., 10^8 MH). Doppler and voiding effect in the central FC produced negative and positive reactivity insertion respectively; system criticality did not change. For the indication of the different cases, the same nomenclature specified in the previous paragraphs was used.

Tab. 51 – 2.4% fuel lattice criticality during a FCB event on central channel considering occurrence of all phenomena, of channel voiding, of Doppler effect

Transient Time (s)	System criticality			Channel voiding			Doppler Effect		
	RUN ID	k_{inf}	σ (pcm)	RUN ID	k_{inf}	σ (pcm)	RUN ID	k_{inf}	σ (pcm)
0.0	*Xi*	1.33513	5	N/A	N/A	N/A	N/A	N/A	N/A
8.0	*X1*	1.33511	5	*X2*	1.33573	5	*X3*	1.33435	5
15.0	*X4*	1.33512	5	*X5*	1.33575	5	*X6*	1.33442	5
20.0	*X7*	1.33503	5	*X8*	1.33574	5	*X9*	1.33439	5

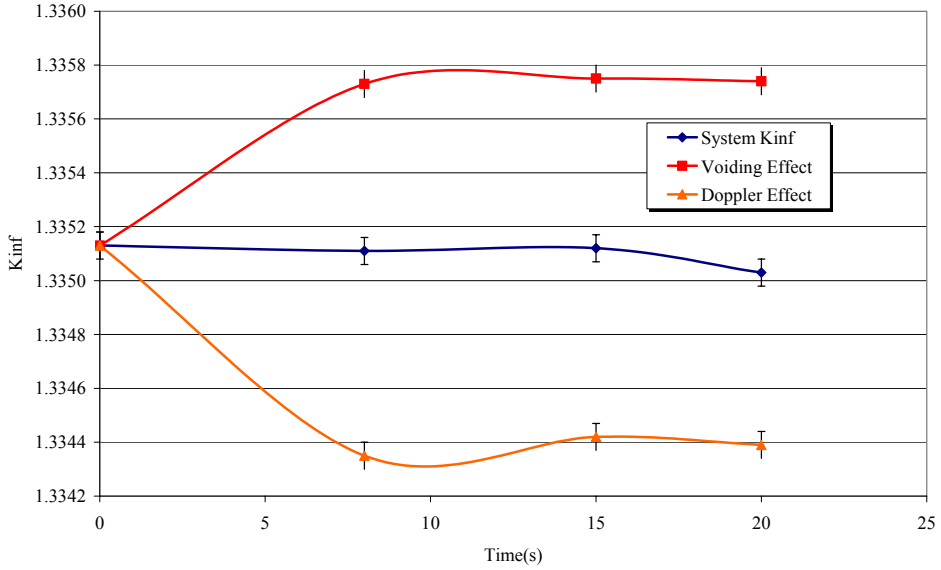

Fig. 132 – 2.4% fuel lattice criticality during a FCB event on central channel considering occurrence of all phenomena, of channel voiding, of Doppler effect

2.4 % Fuel: Reaction Rates and neutron flux tallying

Reaction rates tallies were executed assessing the effects of the main phenomena. Results for runs *Xi* to *X3* are given in Tab. 52 and Tab. 53 (see the previous paragraphs for the nomenclature and for details about calculation procedure), reporting tallies values for the central channel (blocked channel) and for the border channels of the lattice. The effects of parameters changes on the different tallies for runs X1, X2, X3 in comparison with run Xi is showed in Tab. 54.

Tab. 52 – 2.4% lattice fuel cells reaction rates and fluxes for runs Xi and X1

TALLYING Lattice Fuel 2.4%	Xi				X1			
	Central		Border		Central		Border	
	Thermal / Fast	Total	Thermal / Fast	Total	Thermal / Fast	Total	Thermal / Fast	Total
$\Sigma_{fission} * \phi$	4.05E-05 4.35E-06	4.49E-05	4.05E-05 4.35E-06	4.49E-05	3.53E-05 4.44E-06	3.98E-05	4.10E-05 4.44E-06	4.55E-05
$\Sigma_{absorption}$ (fuel) * $\Sigma\phi$ (excluding fission)	1.54E-05 1.18E-05	2.72E-05	1.54E-05 1.18E-05	2.72E-05	1.36E-05 1.14E-05	2.50E-05	1.56E-05 1.21E-05	2.77E-05
$\Sigma_{absorption}$ (water) * ϕ	2.22E-06 1.46E-07	2.37E-06	2.22E-06 1.47E-07	2.37E-06	3.11E-07 2.72E-08	3.38E-07	2.25E-06 1.50E-07	2.40E-06
ϕ (in fuel)	2.82E-04 6.07E-04	8.90E-04	2.83E-04 6.08E-04	8.91E-04	2.77E-04 6.62E-04	9.39E-04	2.87E-04 6.20E-04	9.06E-04
$\Sigma_{scattering}$ (graphite) * ϕ	2.19E-04 1.72E-04	3.91E-04	2.19E-04 1.72E-04	3.91E-04	2.11E-04 1.84E-04	3.94E-04	2.21E-04 1.76E-04	3.97E-04

Tab. 53 – 2.4% lattice fuel cells reaction rates and fluxes for runs X2 and X3

TALLYING Lattice Fuel 2.4%	X2				X3			
	Central		Border		Central		Border	
	Thermal / Fast	Total	Thermal / Fast	Total	Thermal / Fast	Total	Thermal / Fast	Total
$\Sigma_{fission} * \phi$	3.55E-05 4.44E-06	3.99E-05	4.11E-05 4.44E-06	4.55E-05	4.03E-05 4.33E-06	4.47E-05	4.05E-05 4.35E-06	4.48E-05
$\Sigma_{absorption}$ (fuel) * ϕ (excluding fission)	1.37E-05 1.11E-05	2.48E-05	1.56E-05 1.21E-05	2.77E-05	1.54E-05 1.21E-05	2.74E-05	1.54E-05 1.18E-05	2.72E-05
$\Sigma_{absorption}$ (water) * ϕ	3.12E-07 2.72E-08	3.39E-07	2.25E-06 1.50E-07	2.26E-06	2.22E-06 1.46E-07	2.36E-06	2.22E-06 1.47E-07	2.37E-06
ϕ (in fuel)	2.77E-04 6.64E-04	9.41E-04	2.87E-04 6.19E-04	9.06E-04	2.82E-04 6.05E-04	8.87E-04	2.83E-04 6.08E-04	8.91E-04
$\Sigma_{scattering}$ (graphite) * ϕ	2.11E-04 1.84E-04	3.95E-04	2.21E-04 1.76E-04	3.97E-04	2.19E-04 1.72E-04	3.91E-04	2.19E-04 1.72E-04	3.91E-04

Tab. 54 – 2.4% lattice fuel cells – Ratio of Tallies, %

Ratios of Tallies - Lattice Fuel 2.4%	X1/Xi, %				X2/Xi, %				X3/Xi, %			
	Central		Border		Central		Border		Central		Border	
	Th. Fast	Tot.	Th. Fast	Tot.	Th. Fast	Tot.	Th. Fast	Tot.	Th. Fast	Tot.	Th. Fast	Tot.
$\Sigma_{fission} * \phi$	-12.7	-11.3	1.3	1.4	-12.5	-11.0	1.3	1.4	-0.4	-0.4	0.0	0.0
	2.1		2.1		2.2		2.1		-0.3		0.0	
$\Sigma_{absorption} * \phi$ (fuel)	-11.5	-7.9	1.3	1.8	-11.3	-8.7	1.3	1.8	-0.3	1.0	0.0	0.0
	-3.2		2.4		-5.4		2.4		2.7		0.0	
$\Sigma_{absorption} * \phi$ (water)	-86.0	-85.7	1.3	1.4	-86.0	-85.7	1.3	1.4	-0.3	-0.3	0.0	0.0
	-81.4		2.4		-81.4		2.4		-0.5		0.0	
ϕ . (in fuel)	-1.8	5.5	1.4	1.7	-2.0	5.7	1.4	1.7	0.0	-0.3	0.0	0.0
	8.9		1.9		9.3		1.8		-0.4		0.0	
$\Sigma_{scattering} * \phi$ (graphite)	-3.8	0.9	1.0	1.6	-3.8	1.0	1.1	1.7	0.0	-0.1	0.0	0.0
	6.9		2.4		7.1		2.4		-0.2		0.0	

From to Tab. 52 to Tab. 54, the followings can be stated:

- Central FC coolant overheating (run *X2*) is causing a large drop (-86%) in central FC of neutron absorption rates and a shift of the neutron energy spectrum toward higher energies (+7.1% for fast scattering reaction rates in central channel graphite and +9.3% increase of the fast flux). This causes an increase of neutron leakage from the central FC to the border FCs, a sensible reduction of the fissions and neutron absorption in the fuel of central FC (-11%). The reaction rates in the border FCs are instead increased of some percent by the neutron leakages from the central FC.
- Central FC fuel overheating (run *X3*) is causing an increase of 1.0% in the neutron absorption rate. Border FCs are not perturbed by this phenomenon.
- The results from the physical simulation of both effects (fuel and coolant overheating, run *X1)* are reported in the first column of Tab. 52 and Tab. 54. The involved phenomena are the same as those reported in the 2.0% case analysis. The k_{inf} resulted to be not affected by these phenomena, i.e., there is a very close balance between neutron absorption and neutron production .

2.4 % fuel lattice with 2.0 % fuel in the central channel : criticality calculations

The purpose of this simulation was to simulate one of the possible zone configuration of an RBMK core. Today, the RBMK core is mostly composed by 2.4% FCs and by few 2.0% FCs (e.g, a configuration for Smolensk-3 NPP core resulted in about 1522 channel with 2.4% fuel and just 48 channels with 2.0% fuel). The following model was considered:

- Central FC with 2.0% fuel
- Border elements of a 3x3 FC lattice with 2.4% fuel

The results of criticality calculations are reported hereafter (see Tab. 55 and Fig. 133).

Tab. 55 – 2.4% fuel lattice w/ central 2.0% FC: criticality during a FCB event on central channel considering occurrence of all phenomena, of channel voiding, of Doppler effect

Transient Time (s)	System criticality			Channel voiding			Doppler Effect		
	RUN ID	k_{inf}	σ (pcm)	RUN ID	k_{inf}	σ (pcm)	RUN ID	k_{inf}	σ (pcm)
0.0	*Xi*	1.32934	5	N/A	N/A	N/A	N/A	N/A	N/A
8.0	*X1*	1.33021	5	*X2*	1.33068	5	*X3*	1.32862	5
15.0	*X4*	1.33012	5	*X5*	1.33074	5	*X6*	1.32866	5
20.0	*X7*	1.33004	5	*X8*	1.33068	5	*X9*	1.32857	5

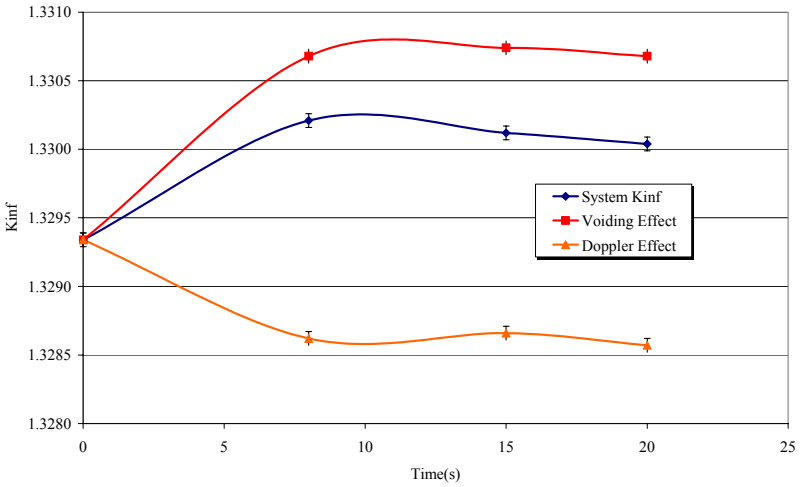

Fig. 133 – 2.4% fuel lattice w/ central 2.0% FC: criticality during a FCB event on central channel considering occurrence of all phenomena, of channel voiding, of Doppler effect

2.4 % fuel lattice with 2.0 % fuel in the central channel : Reaction Rates and neutron flux tallying

Reaction rates tallies were executed assessing the effects of the main phenomena. Results for runs *Xi* to *X3* are given in Tab. 56 and Tab. 57 (see the section 5.1.2.3.2 for the nomenclature and for details about calculation procedure), reporting tallies values for the central FC (blocked channel) and for the border FCs of the lattice. The effects of parameters changes on the different tallies for runs *X1, X2, X3* in comparison with run *Xi* is showed in Tab. 58.

Tab. 56 – 2.4% lattice fuel w/ 2.0% central FC: reaction rates and fluxes for runs Xi and X1

TALLYING Lattice FC 2.4% - Central FC 2.0%	Xi				X1			
	Central		Border		Central		Border	
	Thermal / Fast	Total	Thermal / Fast	Total	Thermal / Fast	Total	Thermal / Fast	Total
$\Sigma_{fission} * \phi$	3.73E-05 / 3.71E-06	4.10E-05	4.07E-05 / 4.37E-06	4.51E-05	3.23E-05 / 3.81E-06	3.62E-05	4.13E-05 / 4.46E-06	4.58E-05
$\Sigma_{absorption}$ (fuel) * ϕ (excluding fission)	1.57E-05 / 1.14E-05	2.71E-05	1.55E-05 / 1.18E-05	2.73E-05	1.39E-05 / 1.11E-05	2.50E-05	1.57E-05 / 1.21E-05	2.78E-05
$\Sigma_{absorption}$ (water) * ϕ	2.40E-06 / 1.44E-07	2.54E-06	2.24E-06 / 1.47E-07	2.38E-06	3.36E-07 / 2.70E-08	3.63E-07	2.27E-06 / 1.50E-07	2.42E-06
ϕ (in fuel)	3.08E-04 / 5.79E-04	8.87E-04	2.84E-04 / 6.12E-04	8.96E-04	3.02E-04 / 6.34E-04	9.35E-04	2.88E-04 / 6.23E-04	9.11E-04
$\Sigma_{scattering}$ (graphite) * ϕ	2.24E-04 / 1.68E-04	3.92E-04	2.20E-04 / 1.72E-04	3.93E-04	2.16E-04 / 1.80E-04	3.96E-04	2.23E-04 / 1.76E-04	3.99E-04

Tab. 57 – *2.4% lattice fuel w/ 2.0% central FC: reaction rates and fluxes for runs X2 and X3*

TALLYING Lattice FC 2.4% - Central FC 2.0%	X2				X3			
	Central		Border		Central		Border	
	Thermal / Fast	Total	Thermal / Fast	Total	Thermal / Fast	Total	Thermal / Fast	Total
$\Sigma_{fission} * \phi$	3.25E-05 / 3.82E-06	3.63E-05	4.13E-05 / 4.46E-06	4.58E-05	3.71E-05 / 3.70E-06	4.08E-05	4.07E-05 / 4.37E-06	4.51E-05
$\Sigma_{absorption}$ (fuel) * ϕ (excluding fission)	1.39E-05 / 1.09E-05	2.48E-05	1.57E-05 / 1.21E-05	2.78E-05	1.57E-05 / 1.17E-05	2.73E-05	1.55E-05 / 1.18E-05	2.73E-05
$\Sigma_{absorption}$ (water) * ϕ	3.38E-07 / 2.71E-08	3.65E-07	2.27E-06 / 1.50E-07	2.42E-06	2.39E-06 / 1.43E-07	2.53E-06	2.24E-06 / 1.47E-07	2.38E-06
ϕ (in fuel)	3.01E-04 / 6.36E-04	9.37E-04	2.88E-04 / 6.23E-04	9.11E-04	3.08E-04 / 5.76E-04	8.84E-04	2.84E-04 / 6.12E-04	8.96E-04
$\Sigma_{scattering}$ (graphite) * ϕ	2.16E-04 / 1.80E-04	3.96E-04	2.23E-04 / 1.76E-04	3.99E-04	2.23E-04 / 1.68E-04	3.92E-04	2.20E-04 / 1.72E-04	3.93E-04

Tab. 58 – 2.4% lattice fuel cell w/ 2.0% central FC: Ratio of Tallies, %

Ratios of Tallies - Lattice FC 2.4% - central FC 2.0%	X1/Xi, %				X2/Xi, %				X3/Xi, %			
	Central		Border		Central		Border		Central		Border	
	Th. / Fast	Tot.	Th. / Fast	Tot.	Th. / Fast	Tot.	Th. / Fast	Tot.	Th. / Fast	Tot.	Th. / Fast	Tot.
$\Sigma_{fission} * \phi$	-13.2 / 2.7	-11.8	1.3 / 2.1	1.4	-12.9 / 2.9	-11.4	1.3 / 2.1	1.4	-0.5 / -0.3	-0.4	0.0 / 0.0	0.0
$\Sigma_{absorption} * \phi$ (fuel)	-11.9 / -2.4	-7.9	1.3 / 2.3	1.7	-11.6 / -4.6	-8.7	1.3 / 2.3	1.8	-0.4 / 2.5	0.8	0.0 / 0.0	0.0
$\Sigma_{absorption} * \phi$ (water)	-86.0 / -81.2	-85.7	1.3 / 2.3	1.4	-85.9 / -81.2	-85.7	1.3 / 2.3	1.4	-0.3 / -0.5	-0.3	0.0 / 0.0	0.0
ϕ (in fuel)	-2.0 / 9.5	5.5	1.4 / 1.8	1.6	-2.1 / 9.9	5.7	1.4 / 1.8	1.6	0.0 / -0.5	-0.3	0.0 / 0.0	0.0
$\Sigma_{scattering} * \phi$ (graphite)	-3.4 / 6.9	1.0	1.1 / 2.3	1.6	-3.5 / 7.2	1.1	1.1 / 2.3	1.6	0.0 / -0.2	-0.1	0.0 / 0.0	0.0

From Tab. 56 to Tab. 58 the followings can be stated:

- the involved phenomena are the same as for the other cases analyzed (see 2.0% and 2.4% lattice case analyses); this configuration allows a stronger hardening of the flux (+9.5% compared to +8.9% for the 2.0% and 2.4% fuel) that is reflected in a greater decrease of the fissions in the central FC (-11.8% versus -11.3% for the other cases) and of the thermal absorption (-11.9% versus -11.4/-11.5% for the other cases); on the other hand, fast neutron fission are increased more than in the other cases (+2.7% versus +2.1%).
- the system k_{inf} increased more than for the 2.0% fuel lattice case (+87 pcm versus +38 pcm). This could be explained by the higher enrichment of the fuel lattice considered in this case.

5.1.2.3.5. Conclusions

Criticality and reaction rates analyses of a FC blockage accident were performed, deriving boundary conditions and main parameters changes by a previously executed RELAP5-3D calculation. It was found thatt during such type of accident the fission reaction rates were significantly reduced (average of -11%) in the FC where the blockage was occurring.
This was due to:

- the increased neutron leakage towards the other un-perturbed FCs; this phenomenon was caused by the shift of the neutron energy spectrum towards epithermal-fast regions (flux “hardening”) as a consequence of the coolant overheating and density reduction;
- the increased neutron absorption by Doppler effect in the overheated fuel of the blocked FC.

The other important outcome of these calculations was the estimation of the neighboring channels behavior; because of the increased neutron leakage from the blocked FC, all the reaction rates in these un-perturbed FCs are increased by 1-2%, thus not producing any relevant effects of safety concern.

Finally, it should be noted that these calculations reported here were performed assuming fresh fuel (i.e., no presence of Plutonium was considered). Therefore, further MCNP calculations should consider, through the use of appropriate depletion codes (e.g., ORIGEN code), the effects of actinides and fission products. Other improvements could be obtained by the modeling of the Additional Absorber also.

5.1.3. LOCA events

5.1.3.1. CPS LOCA

The CPS is cooled by a low pressure loop independent from the MCC. However leakages from the loop may occur. This justifies the analysis of the CPS-LOCA event. The main purpose for the analysis is the calculation of the overall core power response.
It was supposed that the initiating event was the rupture of the CPS cooling system collector and that the voiding of the CR channels occur in 40 seconds (see Fig. 138). This last assumption is considered conservative [81].
The time trend of the main events is:

1) 0.0sec - onset of the CPS LOCA
2) 24.5 sec – AZ scram signal for reactor power equal to 110% of Nominal Power (Fig. 134)
3) 50.0 sec – voiding of the CPS LOCA completed (Fig. 138)

The power surge in the FC is roughly the same (Fig. 135). Because the actuation of AZ scram signal, the fuel clad temperatures at the hot spots is not of safety concern (Fig. 137).

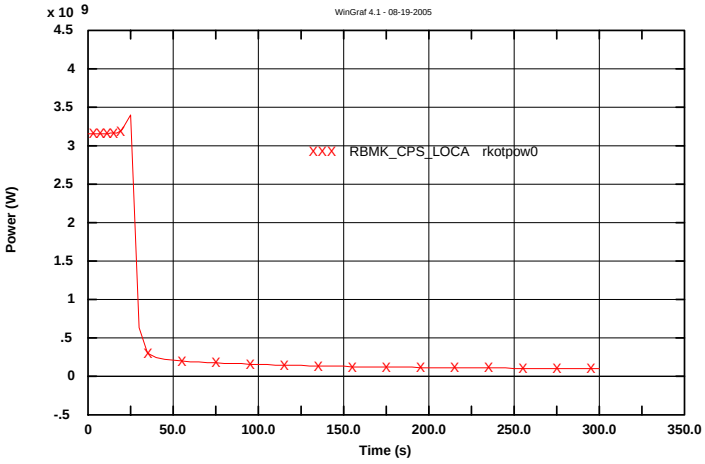

Fig. 134 – Reactor Power

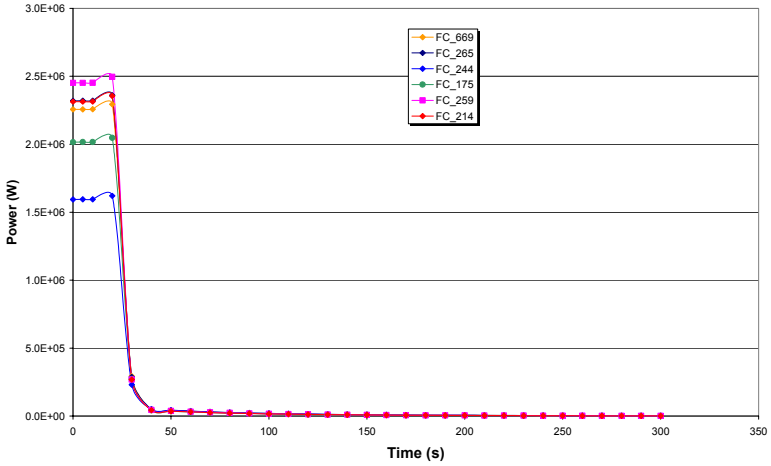

Fig. 135 – Power in FC of 11th GDH of right MCC part

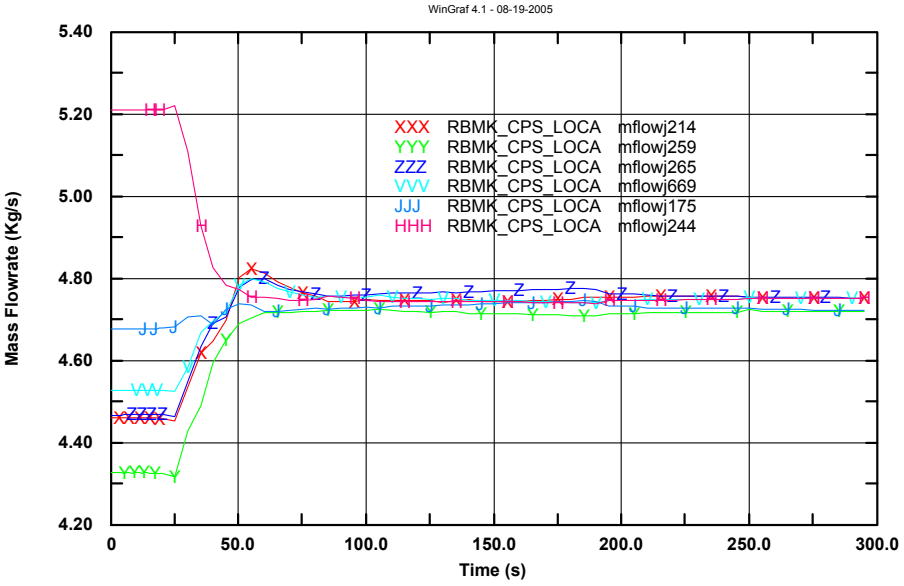

Fig. 136 – Equivalent Mass Flowrate in FC of 11th GDH of right MCC part

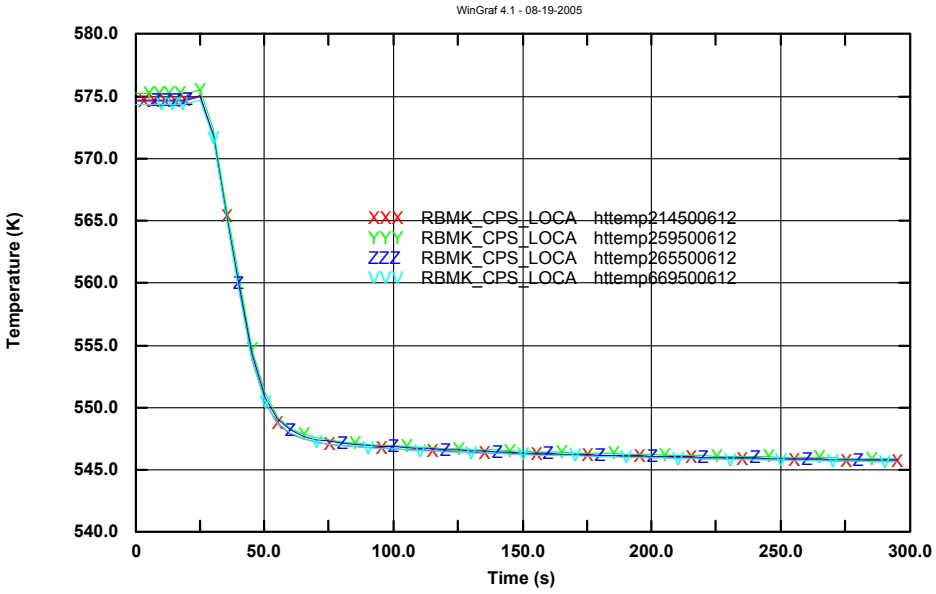

Fig. 137 – Hot Spot Clad Temperature in FC 214, 259, 265, 669

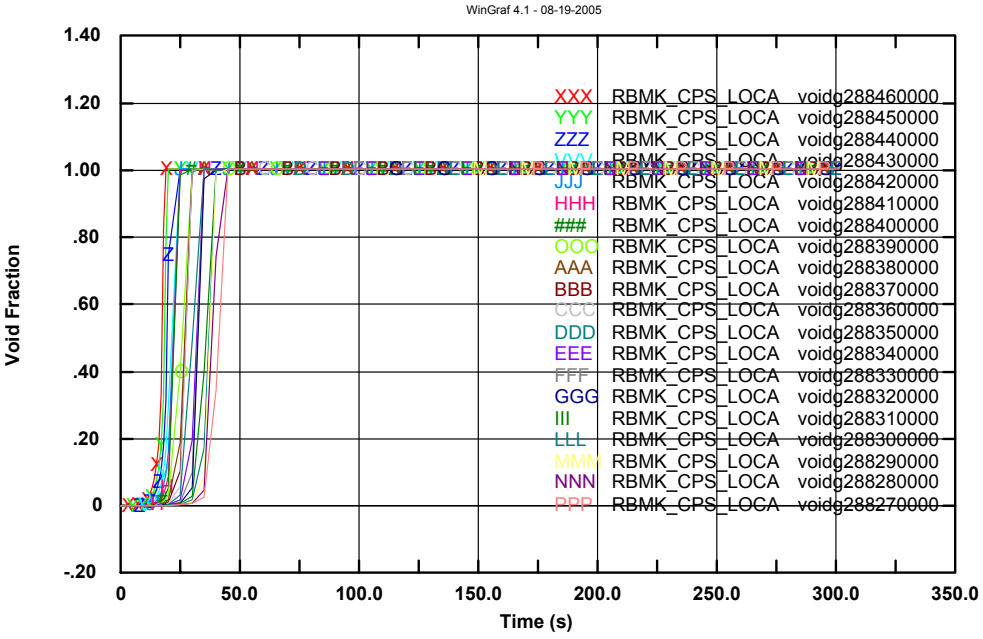

Fig. 138 – Void fraction in CPS Cooling Channel

5.1.3.2. GDH LOCA (rupture after the GDH check valve)

The main purpose of the analysis of the GDH LOCA simulation is the evaluation of the overall MCC response with main consideration to the core power and the demonstration of the capabilities of the adopted code system to deal with this event. However, this even is not the most severe LOCA. The event is originated by the break of one GDH, with breaking occurring after the GDH check valve. Conditions for scram occurrence are the same as in the previous sections.

The 'standard' TH and 3D NK nodalization was developed in order to investigate the effects on the all channels of the affected GDH (see Fig. 67 and Fig. 68).
The temporal development of the transient resulted to be:

1) 0 sec. – onset of the break;
2) 0.4 sec – onset of the SCV closure
3) 1.6 sec – AZ scram signal – insertion of MCR and FASS in the core
    a. Insertion of all MCR with a speed of 50 cm/s
    b. Insertion of all Safety Rods with a speed of 350 cm/s

Immediately after the GDH break, flow rates of FC connected to the affected GDH, revert their flow directions (see Fig. 140 and Fig. 141). Coolant flows into reactor compartment from the PH and from the DS connected to the FC of the affected GDH (Fig. 142). Due to power decrease following AZ activation and flow reverse, the void fraction at the exit of the accident FC's decrease firstly because of saturated water delivery from DS and then grows up to 1.0 after complete DS depletion (Fig. 145). At the same time pressure decrease in FC's, results in channels' voiding, in deterioration of heat removal from fuel rod surfaces (Fig. 146 to Fig. 150) and in void fraction growth at the entrance of the accident FC's (Fig. 144). The clad temperature is decreased thanks to the combined effects of the power decrease caused by the scram and thanks to the steam flow coming from DS. In Fig. 151 it is possible to observe that the PT temperature trends are not of safety concern

Decrease of full reactor power to 30% $N_{ном}$ occurs quickly after AZ signal, therefore closure of the MCP valve plates is actuated in the NPP. Nevertheless, as Russian calculation demonstrated, MCP flowrate increases for a while because the reduction of the total hydraulic MCC resistance for the leak opening. At the end of calculation the pressure in the intact GDH of the left half starts to decrease, causing left half MCP degradation due to cavitations.

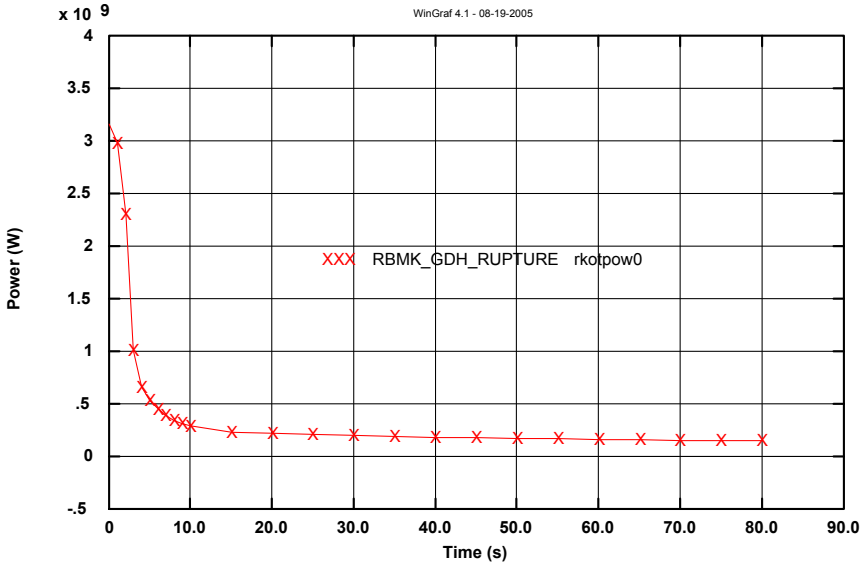

Fig. 139 – Reactor Power

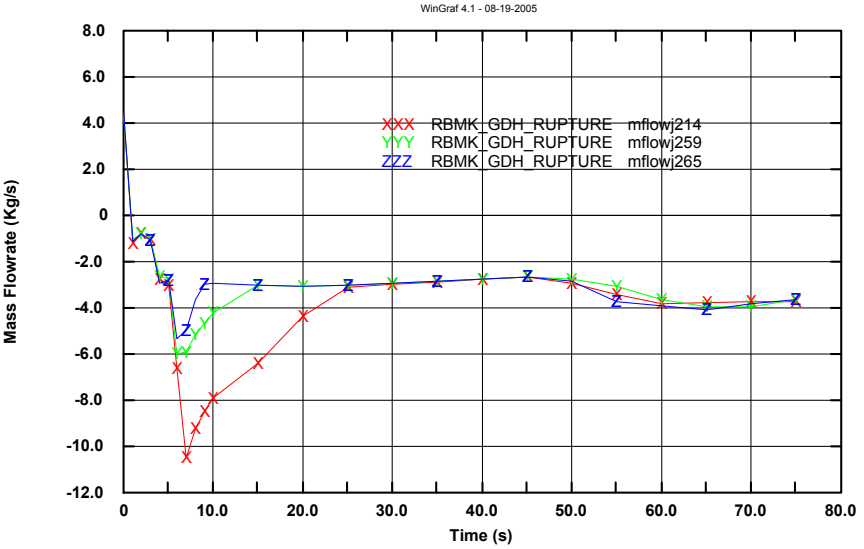

Fig. 140 – Mass Flow rate in affected Channels 214, 259, 265

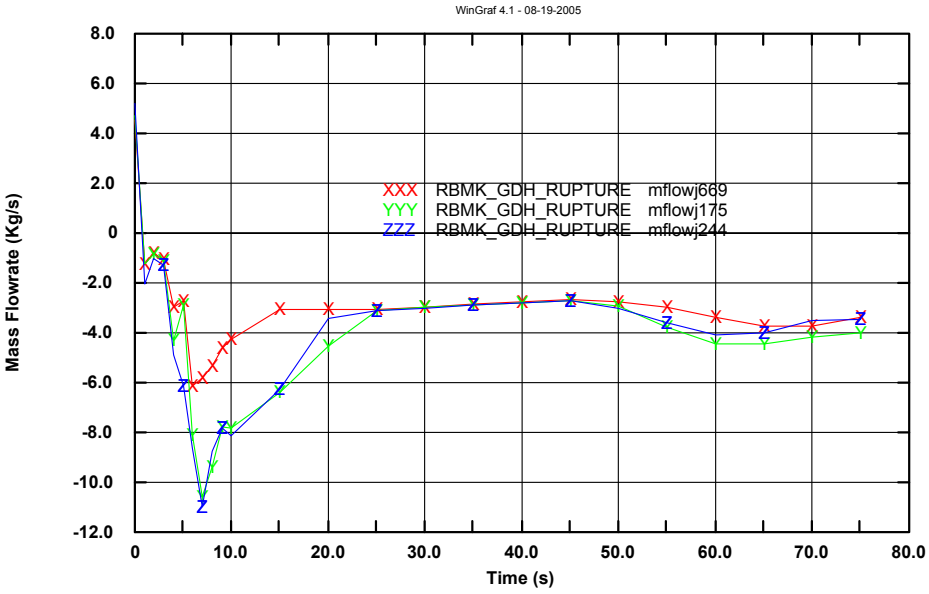

Fig. 141 – Mass Flow rate in affected Channels 669, 175, 244

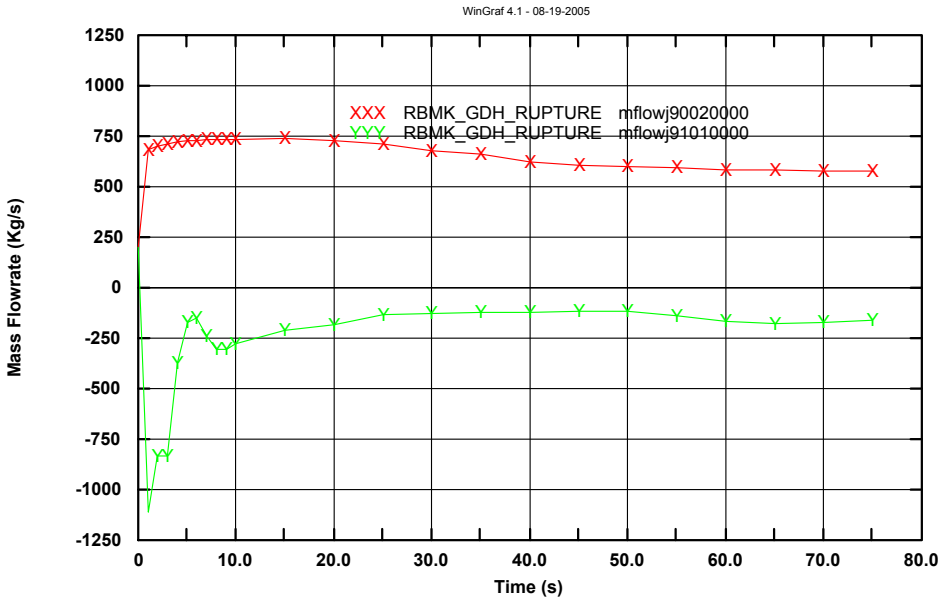

Fig. 142 – Mass Flowrate at GDH rupture

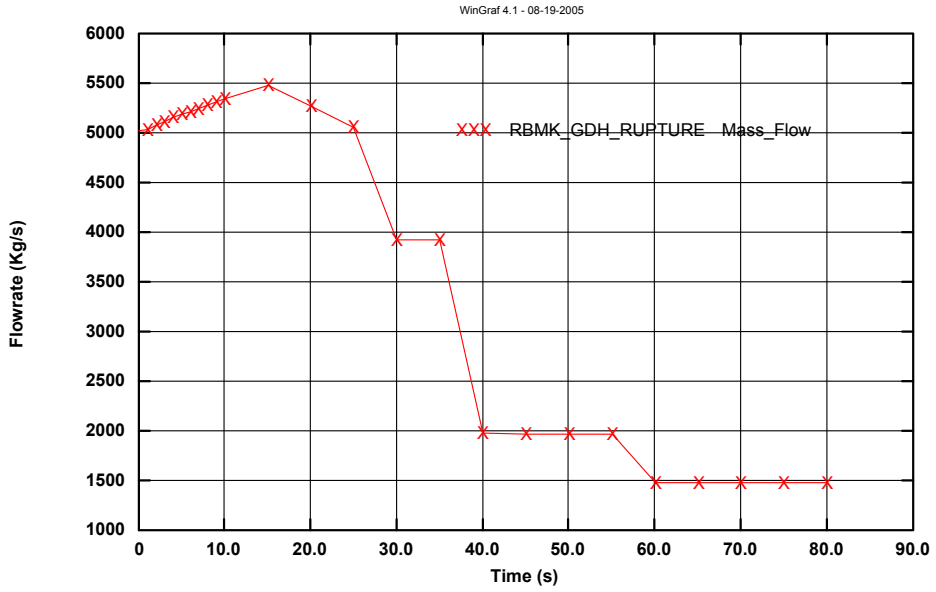

Fig. 143 – Imposed Mass flow rate in damaged MCC part

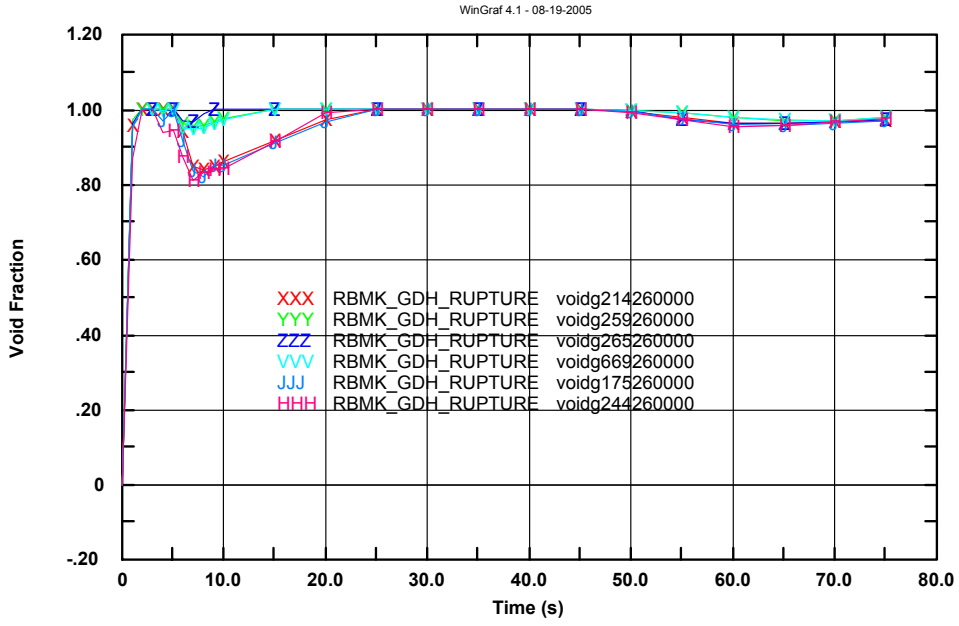

Fig. 144 – Void Fraction at Core Inlet

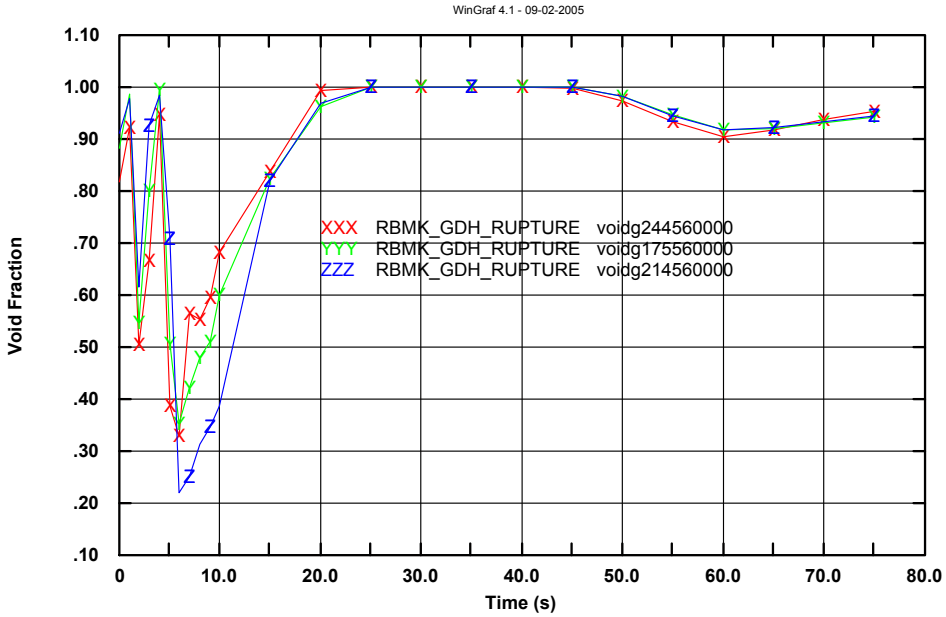

Fig. 145 – Void Fraction at core outlet

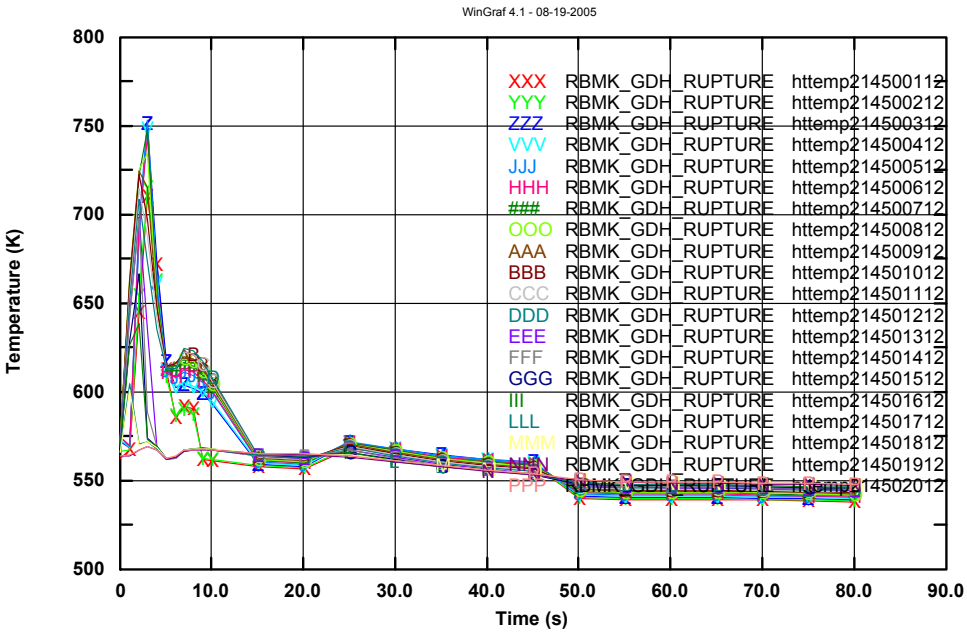

Fig. 146 – Clad Temperature in FC 214

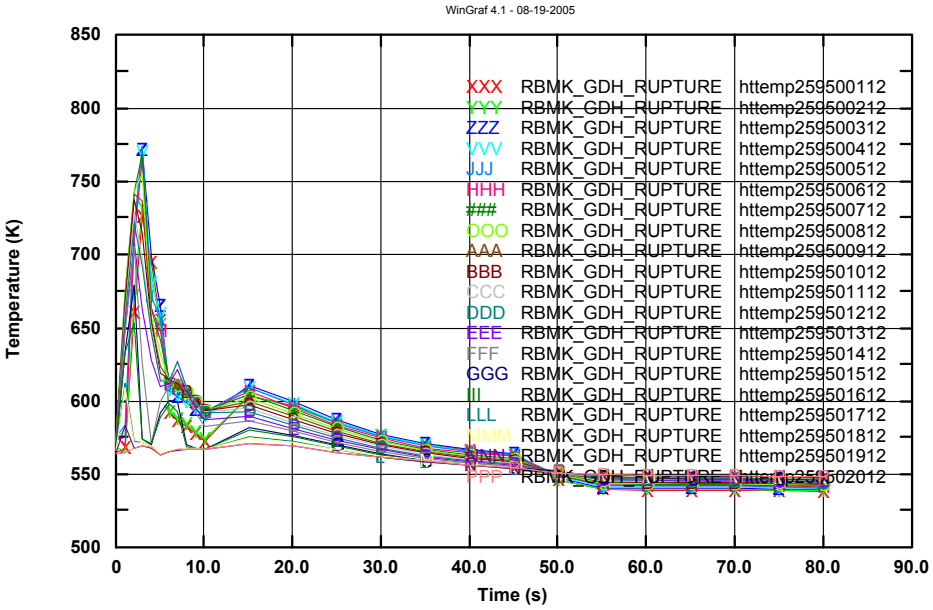

Fig. 147 – Clad Temperature in FC 259

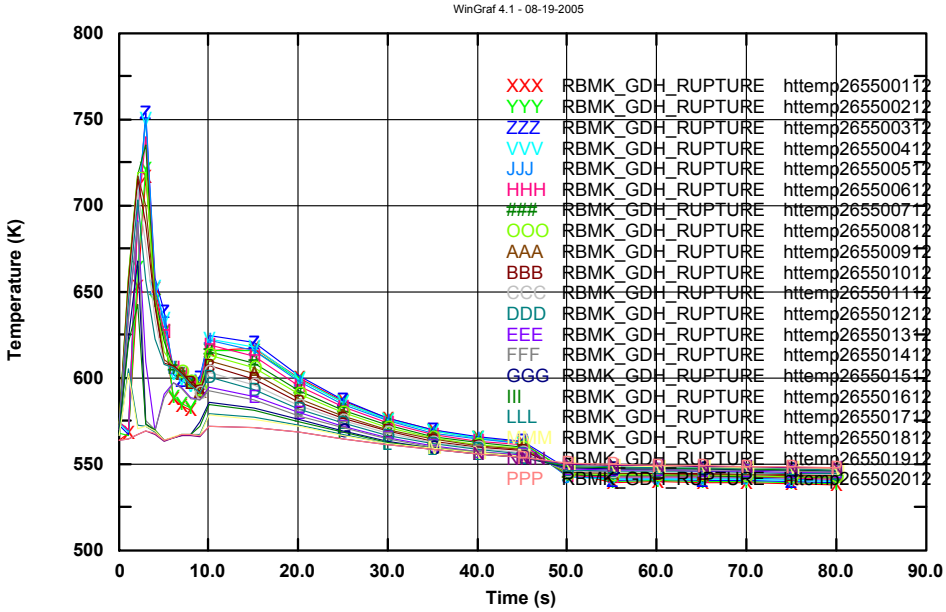

Fig. 148 – Clad Temperature in FC 265

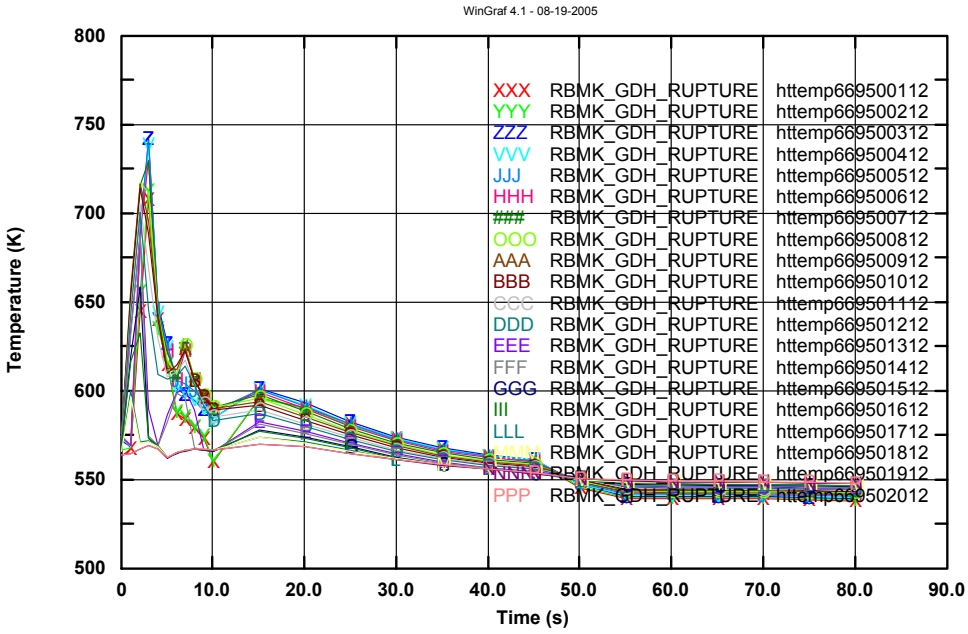

Fig. 149 – Clad Temperature in FC 669

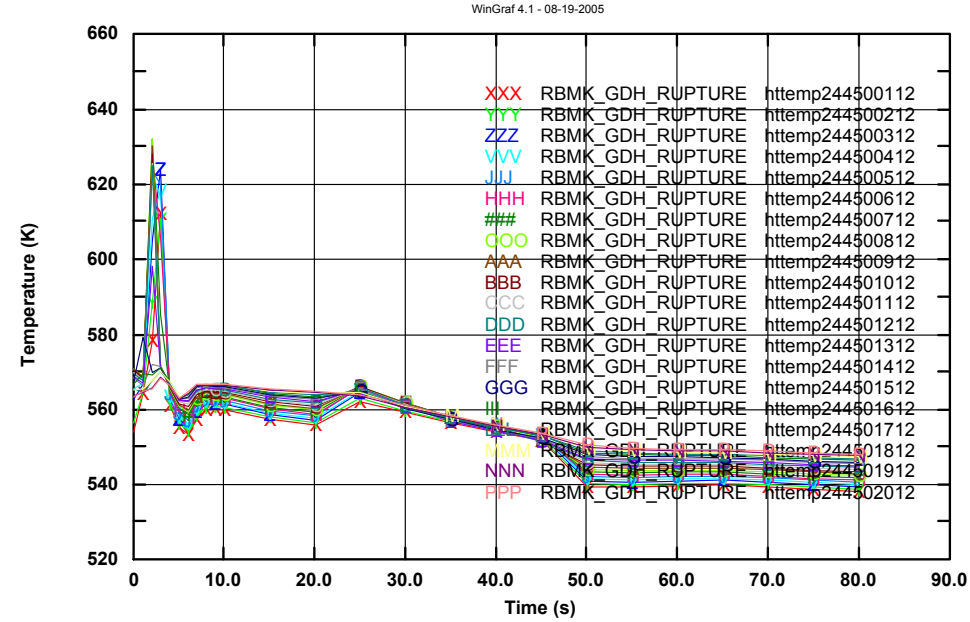

Fig. 150 – Clad Temperature in FC 244

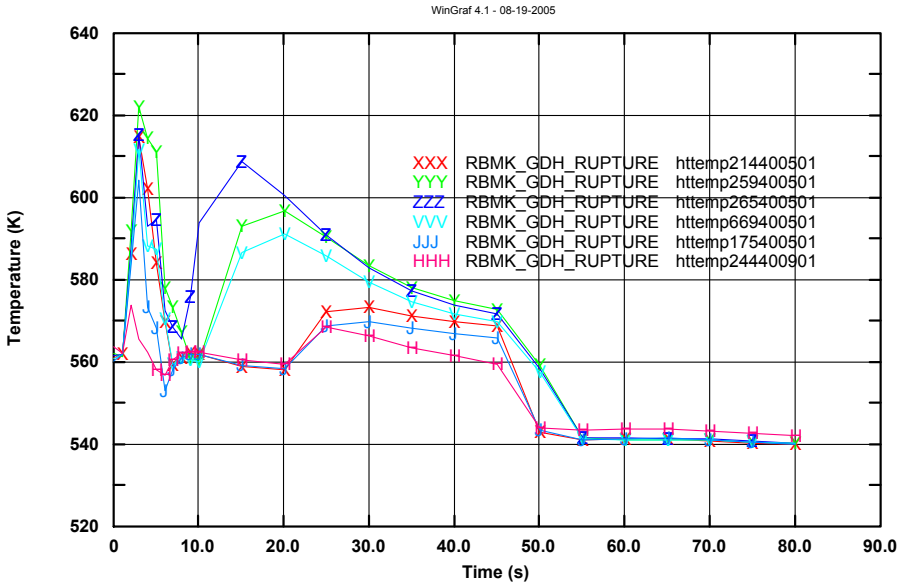

Fig. 151 – PT Hot Spots temperatures

5.2. Conclusion

A wide spectrum of combined 3D NK TH analyses by the RELAP5-3D code were executed. The classification of the accidents was the following:

- Reactivity Initiated Accident (RIA): CR withdrawal and CR group withdrawal
- Decrease of coolant event: Single FC blockage, GDH blockage
- LOCA: GDH LOCA, CPS cooling circuit LOCA

All of the considered accidents were DBA, with the exception of CPS cooling circuit LOCA. The results showed that in the case of CR withdrawal and CR group withdrawal any safety threshold was overcome as well as during the GDH LOCA. This because of some intrinsic good qualities of the RBMK design, e.g.:

- In the case of GDH LOCA, a large water inventory is available in the DS, allowing a cooling by a backflow of the fuel rods
- CR are located in a circuit that is physically separated from the Primary Side. Therefore, they are operating in a low pressure environment (i.e, namely atmospheric pressure) that excludes their rapid ejection, as in the case, e.g., of a PWR

On the other hand, two safety barriers are lost during the FC blockage event and during the GDH blockage. Fuel rods and PT are overheating during the FC blockage, leading to the release of radioactivity into the ALS. The Monte Carlo analyses allowed to analyze the physic of the neutronics phenomena involved during a FC voiding (increased leakages, Doppler effect). The

GDH blockage is an accident leading to a sharp coolant flow reduction in all the channels (generally 42 FC) of the affected GDH. Flow oscillations are induced and in some FC this could lead to PT and fuel rods overheating, with their consequent disruptions and release of radioactivity in the MCC and the ALS if any scram signal is actuated in time. The modeling of all the single FC connected to the affected GDH is mandatory in order to derive acceptable conclusions for a licensing safety analyses [82].

Last, the CPS cooling circuit LOCA is a BDBA accident leading to a rapid insertion of positive reactivity. The installation of dedicated scram rods (the safety rods) not affected by the LOCA is avoiding dangerous consequences for the reactor.

6. THE EXTREME CASE

6.1. Introduction

A comprehensive safety analysis of the RBMK system should not preclude the calculation of events occurring at low power. This because of the particular features of this reactor that can lead to significant changes of reactivity coefficients and in some particular situations to the neutronic decoupling of some zones of the core (see Chapter 2 of this document for a description of the neutronics characteristics of RBMK). The notorious event of Chernobyl sadly demonstrated the vulnerability and the instability of these systems when brought to low power.

However, it should be stressed that after that event, extensive hardware and procedure modifications were implemented in order to minimize or avoid some dangerous situations. The reference RBMK unit studied during this PhD thesis (Smolensk-3 NPP) already included some important changes that enhanced its stability at low power (e.g., U enrichment at 2.4%, higher number of AA, the new design of CR). Nowadays, in order to further improve the reactor safety levels (e.g., reducing the positive void effect), all RBMK in Russia operates with fuel having an enrichment of 2.8%, in conjunction with the use of Erbium as burnable poison. Thus, the analyses that are showed here applies to an intermediate step of the evolution of the RBMK configuration.

6.2. The Chernobyl event

We reported here a brief overview of the Chernobyl accident, in order to get the reader familiar with the quite complex chains of events that caused the reactor destruction. The main source document for the reconstruction of this event was the IAEA INSAG-7 report [83]. Other sources were also [84], [85].

The main aspects that differed the Chernobyl-4 from the Smolensk-3 here analyzed are the following:

- fuel enrichment at 2.0% instead of 2.4%;
- small number of Additional Absorber,
- As a consequence of the previous bullets, a greater void coefficient of reactivity (total vaporization of the coolant was estimated in +4-5 β)
- Different design of CPS. In particular:
    - MCR with a shorter graphite follower that allowed to some water to be present on the bottom of the CR channels when the CR itself was completely extracted (see Fig. 152)
    - Greater time for the insertion of CR (18 seconds)

The accident occurred during the execution of a turbine trip test at low power, in the first hours of the 26 April 1986. The test was conducted in order demonstrate the capability of the turbo-generator to produce enough power, during the run-down, for the unit's internal requirements. In particular, the test should have had demonstrate the capability to power the MCP and the FW pumps.

The run-down concept was accepted and included in the design of NPP equipped with RBMK reactors. For example, it was reported in the Technical Safety Report of Smolensk that ".[..] during a DBA involving the total loss of power for the unit's internal requirements, cooling water should be fed to the damaged part by FW pumps powered by the turbo-generator rundown" [86].

This kind of test was already performed at other RBMK units, considering it as a merely electrical test. Instead, what resulted was that these tests should have had to be considered as complex unit tests, and should have had involve the General Designer, the Chief Design Engineer, the Scientific Manager and the Regulatory Body.

The Chernobyl 4 test differed from the other tests and that contributed to the accident were the following conditions:

- Reduced power (200 MWth instead of the prescribed 700 MWth)
- Extreme Xenon poisoning of the core: the test was delayed by the electric grid manager and a wrong operator action caused a sudden reactor power reduction (to 30 MWth) for several minutes (see Tab. 59)
- Complete extraction of several MCR, with consequent reduction of ORM
- 4 MCP in operations per side, with a decreased level of subcooling at the inlet of the core

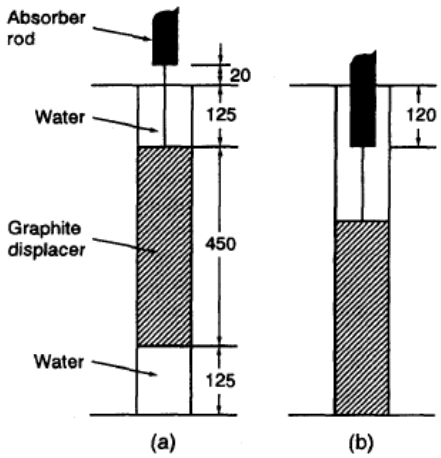

Fig. 152 – MCR configuration of Chernobyl-4 reactor

The sequence of the events for the Chernobyl-4 accident, as it was recorded by the plant instrumentation, is given in report Tab. 59. This was used as reference for the transient reconstruction (see the following paragraph).

Tab. 59 – Chernobyl-4 accident, sequence of the events

Time	Event
25 April 1986	
01:06	Start of reactor power reduction; ORM equals 31 MCRs
03:45	Start of replacement of the nitrogen—helium gas mixture with nitrogen in the gas cooling system for the reactor graphite stack
03:47	Reactor thermal power is 1600 MW
from 04:13 until 12:36	Sequential measurement of the control system parameters and vibration characteristics of turbo-generator No. 7 and turbo-generator No. 8 at constant thermal power of 1500 MW
07:10	ORM equals 13.2 manual control rods
13:05	Disconnection of turbo-generator No. 7 from the system
14:00	Disconnection of the ECCS from the multipass forced circulation circuit (MFCC)
14:00	Postponement of testing programme requested by Kiev power grid controller
15:20	ORM equals 16.8 manual control rods
18:50	Power supply to auxiliary equipment not involved in the tests switched to working transformer No. T6
23:10	Power reduction continued, ORM equals 26 manual control rods
26 April 1986	
00:05	Reactor thermal power was 720 MW
00:28	At reactor thermal power of about 500 MW transfer made from the local to global main range automatic power control (automatic power controllers Nos. 1 and 2). During the transfer there was a reduction in thermal power to 30 MW (neutron power to zero), which was not envisaged in the testing programme. Measures to increase the power were taken
00:34:03	Emergency fluctuations of water level in steam separator drums
00:36:24	The EPS trip point in response to a pressure drop in the steam separator drums was changed from 55 to 50 kg/cm2
from 00:39:32 until 00:43:55	Diagnostic Parameter Recording Program (DREG) did not work Personnel blocked the EPS signal which would have shut down the two turbo-generators
from 00:41 until 01:16	Disconnection of turbo-generator No. 8 from the system to determine the vibration characteristics during rundown
01:03	Reactor thermal power increased to 200 MW and stabilized
01:03	Seventh main circulating pump was put into operation (MCP No. 12)
01:07	Eighth MCP was put into operation (MCP No. 22)
from 01:12:10 until 01:18:49	DREG program did not work

Tab. 59(cont.) – Chernobyl-4 accident, sequence of the events

Time	Event
26 April 1986	
from 01:19:44 until 01:19:57	'One overcompensation upwards' signal on
01:22:30	The parameters were recorded on magnetic tape (calculations were performed at the Smolensk plant after the accident using the PRIZMA program; ORM proved to be equal to 8 manual control rods)
01:23:04	'Oscilloscope is on' signal was given; emergency stop valves of turbo-generator No. 8 were closed. The rundown was started of four MCPs: MCPs Nos. 13 and 23 (section 8RA) and MCPs Nos. 14 and 24 (section 8RB)
01:23:10	DBA button was pressed
01:23:30	'One overcompensation upwards' signal went off (it lasted 3 min 33 s)
01:23:40	EPS-S button was pressed; the EPS rods and manual control rods started to move down into the core
01:23:43	Power excursion rate emergency protection system signals on; excursion period: less than 20 s; emergency power protection system signals actuated; power exceeded 530 MW(th)
01:23:46	Disconnection of the first pair of MCPs being 'run down'
01:23:46.5	Disconnection of the second pair of MCPs being 'run down'
01:23:47	Sharp reduction in the flow rates (by 40%) of MCPs not involved in the rundown test (MCPs Nos. 11, 12, 21 and 22) and unreliable flow rate readings of the MCPs taking part in the rundown (MCPs Nos. 13, 14, 23 and 24); sharp increase of pressure and in the water level in the SDs; signals 'failures of measuring systems' from both main range automatic controllers (automatic power controllers Nos. 1 and 2)
01:23:48	Restoration of flow rates of MCPs not involved in the rundown test to values close to the initial ones; restoration of flow rates to 15% below the initial rate for the MCPs on the left side which were being 'run down'; restoration of flow rates to 10% below the initial rate for MCP No. 24; unreliable readings for MCP No. 23; further increase of pressure in die steam separator drums (left side 75.2 kg/cm2, right side 88.2 kg/cm2) and of water level in the steam separator drums; triggering of fast acting systems for dumping of steam to condensers Nos. 1 and 2
01:23:49	Emergency protection signal 'Pressure increase in reactor space (rupture of a fuel channel)'; 'No voltage — 48 V signal (no power supply to the servo-drive mechanisms of the EPS); 'Failure of the actuators of automatic power controllers Nos. 1 and 2' signals. From a note in the chief reactor control engineer's operating log: "01:24: Severe shocks; the RCPS rods stopped moving before they reached the lower limit stop switches; power switch of clutch mechanisms is off"

From the review of data and from the successive simulations it was deduced that the main causes of the accidents were the followings. The reactor, through the series of events that preceded that test, was brought to an instable point, characterized by:

- Complete extraction of most of the MCRs, with consequent reduction of the ORM
- Xenon poisoning of the core with axial flux characterized by a concave shape, with two humps, one in the bottom and one in the top of the core (see Fig. 153)
- Low level in SD
- 4 MCP per side in operation instead of two per side
- Coolant temperature close to saturation at the core inlet

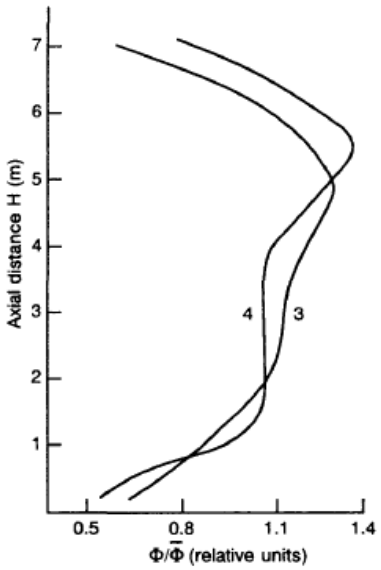

Fig. 153 – Chernobyl axial distribution of the thermal neutron flux density at h.22:00 (curve 3) and h. 00:30 (curve 4) before the accident [83]

The actuation of the scram caused a positive reactivity insertion because of the particular design of the MCR (see Fig. 152). A further positive reactivity insertion was introduced by the coolant vaporization bringing the reactor to a power excursion that was anymore possible to compensate by the CPS. The rupture of several fuel channels with a consequent cavity pressurization, top reactor plate movement and air ingress into the reactor cavity caused several violent chemical reactions (e.g., $C+O_2$, H_2+O, $C+H_2O$, see [85]) that led to an explosion and a destruction of the reactor.

6.3. Literature review

The problem of simulation of the Chernobyl-4 accident was immediately addressed in the aftermath of the event. Unfortunately, at that time, coupled codes calculations were not available because of the lack of sufficiently robust and validated codes and because of the lack of computational power for dealing with simulations of such a large system.
Therefore the analyses were focused on calculating the thermal-hydraulics phenomena with simplified 0-D neutron kinetics model. An example of these works can be found in [87]. Neutronics calculations were instead effectuated using nodal codes with simplified TH models [88], [93] or performing static analyses using Monte Carlo simulations [91].

The fields of investigation were the followings:

- Assessment of the positive scram reactivity
- Assessment of the reactivity introduced by the core voiding
- Calculations of the plant dynamics, including MCP cavitations

The outcomes from all these investigations demonstrated the positive scram effects introduced by the old design of MCR (see Fig. 152). Different axial power shapes and different burnup distribution were investigated. The burnup distribution did not affect so much the positive scram effect. What was found to be an important parameter was the flux axial shape: concave axial shape (neutronic decoupling) was found to be the main cause of the positive reactivity insertion by scram. On the other hand, convex axial shapes resulted in a negative reactivity insertion by scram [89], [90]. Reactivity insertion values were estimated to be super prompt critical (ρ> 1 β, values between 1-1.25) [91].
The core voiding, instead, was estimated to cause a greater reactivity insertion, from 2 β up to 5.6 β [95]. The causes of the core voiding, including the pump run-down effects and the eventual pumps cavitations were also investigated by several TH codes [92]. The conclusions were that the main contributions to the core voiding were given by the pump rundown and not by pumps cavitation.

6.4. Low Power analyses – the model upgrade

A transient like the Chernobyl 4 was simulated using the developed Smolensk-3 model. In order to minimize the differences between the simulation and the accident, it was decided to start the calculations from the power reduction sequence (see Tab. 59, h.23.10 of 25 April 1986). These required the upgrade of the RELAP5-3D model with the inclusion of Xenon microscopic cross sections and of a power control system for operate the reactor power descent according to the available data.

6.4.1. Xenon modeling

The capability to calculate a low power scenario could imply the code capability in handling a Xenon transient. A recent version of the RELAP5-3D code (e.g., RELAP5-3D v.2.4.2) allows modeling the microscopic cross section of Xenon and its effects on different elementary fuel cells. In order to speed up calculations it was assumed an average value of the microscopic cross section for all the fuel cell type, independently of the fuel cell burnup value.
Thus, RELAP5-3D code calculated the steady-state Xenon number densities and upgraded it during the transient calculations (e.g., see Fig. 157).

6.4.2. Power Control modeling

A simplified RBMK power control system was developed and implemented. The objective was to create a control logic able to move a CR bank and to obtain the desired power history. The system should also be able to operate a scram signal and to compensate automatically the Xenon build-up or reduction. The scheme of the control logic is given in Fig. 154.

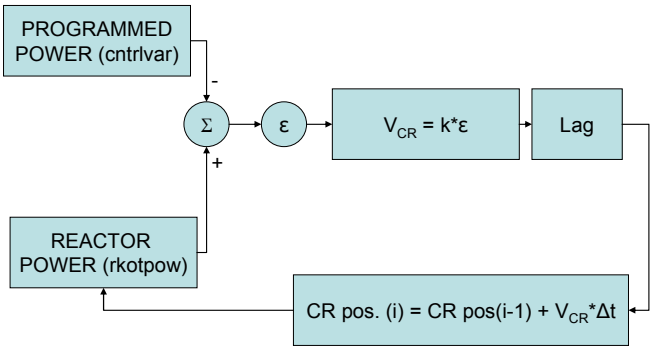

Fig. 154 – CR bank 2 actuation logic

The control logic is generating a signal operating on the CR bank velocity, with imposed limits for the minimum and maximum CR extraction as well as limits for the minimum and maximum velocity. An external general table gives as input the desired power history (power versus time). The control logic is calculating the error between the desired power and the actual reactor power and using this error for generating a proportional signal for the calculation of the velocity of the CR. A lag is used for assuring the control system stability.

Therefore the CR positions are updated at each time step calculating the obtained CR velocity (see Fig. 154).

The control logic and its interaction with Xenon build-up was thoroughly tested in several conditions and on different reactor core design (VVER-440) [96].For the Smolensk-3 reactor, the developed CR logic was applied to a group of 22 MCR, all inserted at the same depth. This assured enough reactivity for the Xenon transient.

6.5. The Power-reduction transient

In order to reproduce as well as possible the status of the Chernobyl-4 reactor before the accident, a preliminary power-reduction transient was executed, using as imposed events those reported in Tab. 59. The transient was aimed to obtain the following reactor core conditions:

- Power reduction from 1600 MWth to 200 MWth
- Xenon build-up
- 3 MCP per side running in stable conditions
- The maximum number of MCRs extracted (reduced ORM)
- A stable level in the SDs

Reactor power was reduced from 50% of Nominal Power (i.e., 1600 MWth) to roughly 500 MW in 90 minutes (see Tab. 59 and Fig. 155). Then, after a sudden power reduction to low power values (50 MWth) for 5 minutes, the reactor power was increased and stabilized around 200 MWth in half an hour.

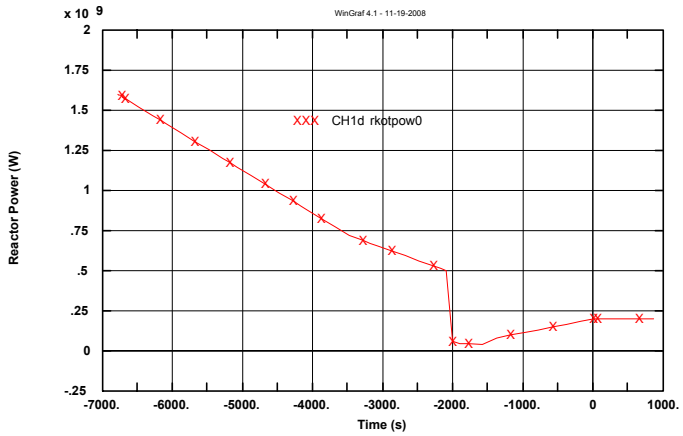

Fig. 155 – Simulation of Chernobyl event in the Smolensk NPP: Reconstructed-imposed reactor power before the event start (t = 1240 s in the scale above)

The MCRs operated by the power control system were at the beginning inserted and then slowly extracted for compensating Xenon buildup. At around time t=+4680 sec. (corresponding to the 00:30 of the 26 April 1986), they were completely inserted, together with the Safety Rods, in order to simulate the abrupt power reduction that occurred during the Chernobyl-4 accident and the further Xenon concentration increase (see Fig. 156 and Fig. 157).

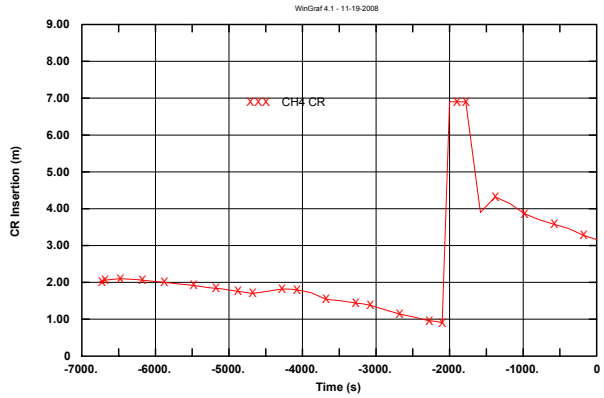

Fig. 156 – Simulation of Chernobyl event in the Smolensk NPP: MCR operated by power control logic - insertion

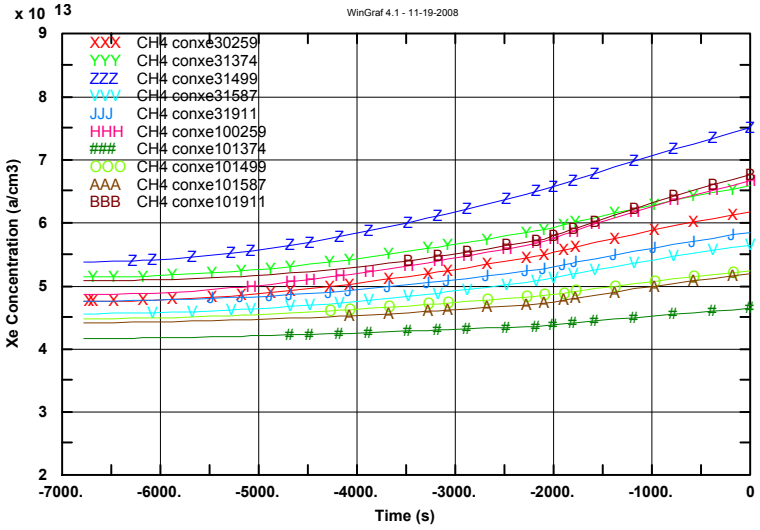

Fig. 157 – Simulation of Chernobyl event in the Smolensk NPP: Xenon buildup

The power was then stabilized at 200 MWth in half an hour by extracting again Safety Rods, the MCR operated by the power control system and other 10 MCRs already completely inserted (see Fig. 155 and Fig. 156). 3 MCP per side were in operation, in stable conditions. This was achieved by increasing the pressure losses at the MCP exit, simulating the throttling of the regulation valve (see Fig. 158).

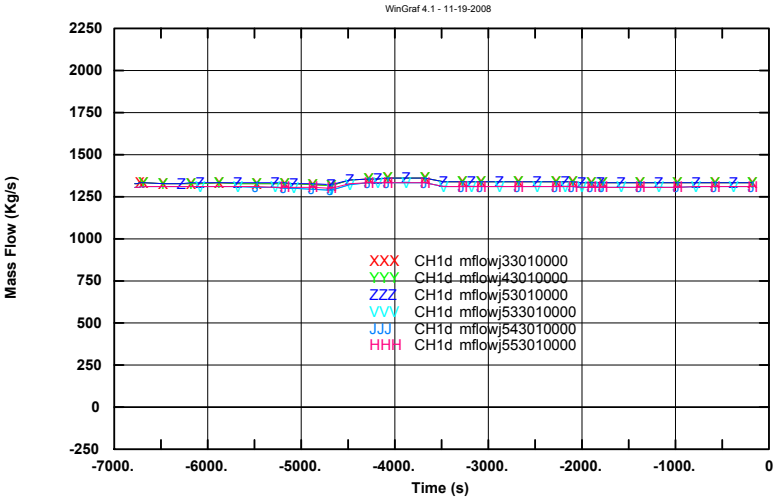

Fig. 158 – Simulation of Chernobyl event in the Smolensk NPP: MCPs mass flow, RHS and LHS

A sufficient water level in the SDs was also achieved (Fig. 159) by some manual FW injections in order to avoid the risk of MCPs cavitation (Fig. 160).

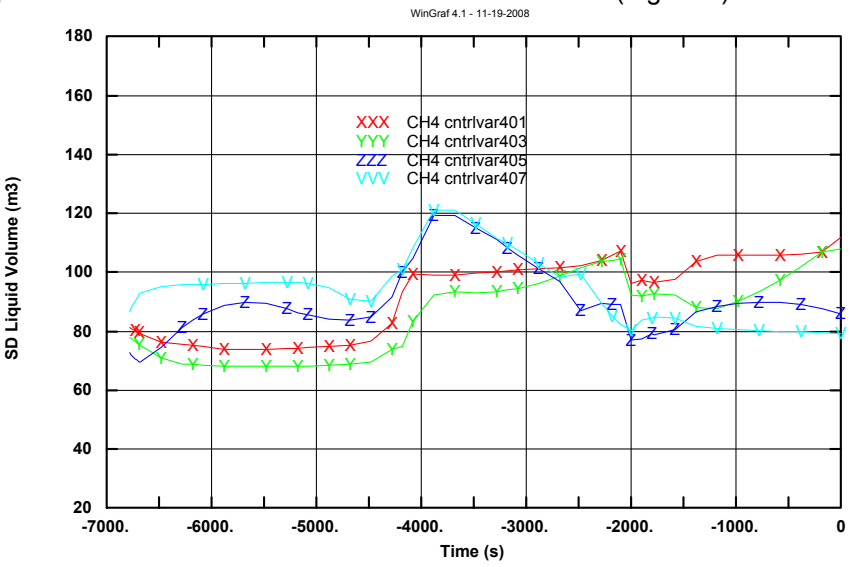

Fig. 159 – Simulation of Chernobyl event in the Smolensk NPP: SD liquid level

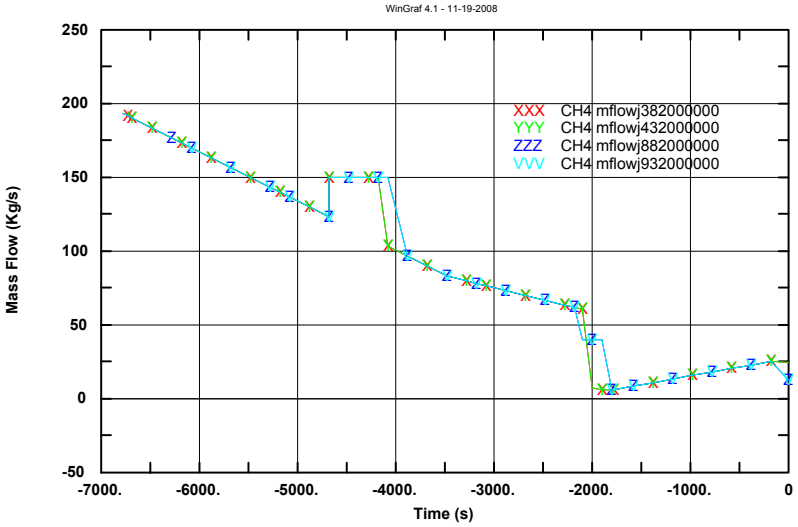

Fig. 160 – Simulation of Chernobyl event in the Smolensk NPP: FW mass flow per SD, LHS and RHS

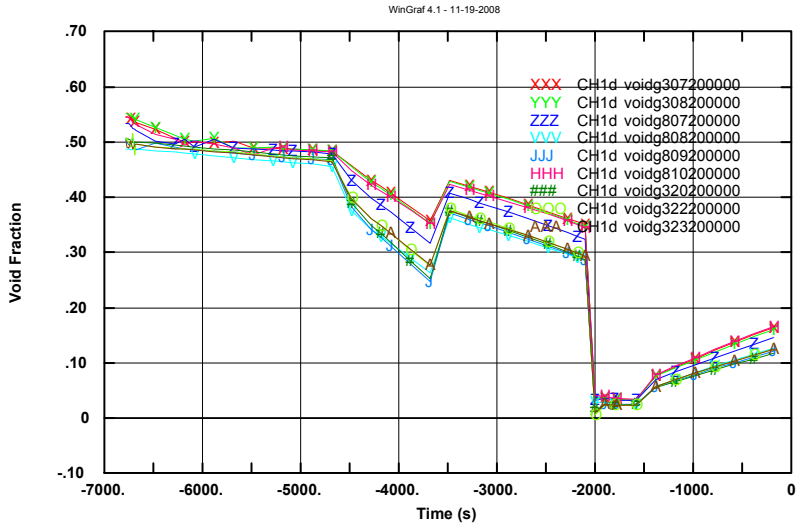

Fig. 161 – Simulation of Chernobyl event in the Smolensk NPP: Void fraction at the core outlet, right and left side

The obtained reactor state was then used for the transient Chernobyl-like accident simulation.

6.6. The "Chernobyl-like" event

The sequence of events that were implemented in the RELAP5-3D code for reproducing the Chernobyl-4 event are given in Tab. 60. The correspondence between the RELAP5-3D transient time and the accident sequence of the events is given.

Tab. 60 – Sequence of the events (actual versus reconstructed)

Time transient (26 April 1986)	Time (s) RELAP5-3D	ACCIDENT EVENTS	RELAP EVENTS
1.02.00	0.	Thermal Power Stabilized at 200 MW	Thermal Power Stabilized at 200 MW
1.03.00	60.	MCP-7 ON	Opening Isolation Valves of MCP-63
1.03.05	65.		MCP-63 ON
1.06.00	240.	FW Adjustment	N/A
1.06.55	295		Opening Isolation Valves of MCP-563
1.07.00	300	MCP-8 ON	MCP-563 ON
1.09.00	420	FW transient values (Reduction)	FW at 90 Ton/h for RHS; FW at 180 Ton/h for LHS
1.18.52	1012	*DBA Signal*	N/A
1.22.30	1230		
1.23.04	1264	**Test Beginning** Closure of SV on Right side of MCC, rundown of 4 MCP, 2 per side	SV 397 Closed; MCPs 33,43,533,543 rundown
1.23.40	1300	EPS5 Button pressed; CRs Inserted	Scram by MCR#1 and Safety CRs
1.23.43	1303		
1.23.47	1307		
1.23.48	1308		
1.23.49	1309		
1.24.00	1320	**Reactor Explosion**	
1.28.04	1564		End Of Calculation

In the following pages, the main results are reported. A couple of sensitivities were also run. In the first one a positive reactivity perturbation was introduced at the bottom of the reactor core by the extraction of the shortened CR, thus reproducing a key phenomenon of the Chernobyl transient. In the second sensitivity, no scram signal was activated in order to assess the dynamic of the plant.

6.6.1. Reference Transient

In the following figures the trends of the main parameters are reported. The reactor power before the test is kept stable at 200 MWth by the power control system. CR are compensating Xenon buildup (see Fig. 162 and Fig. 163).

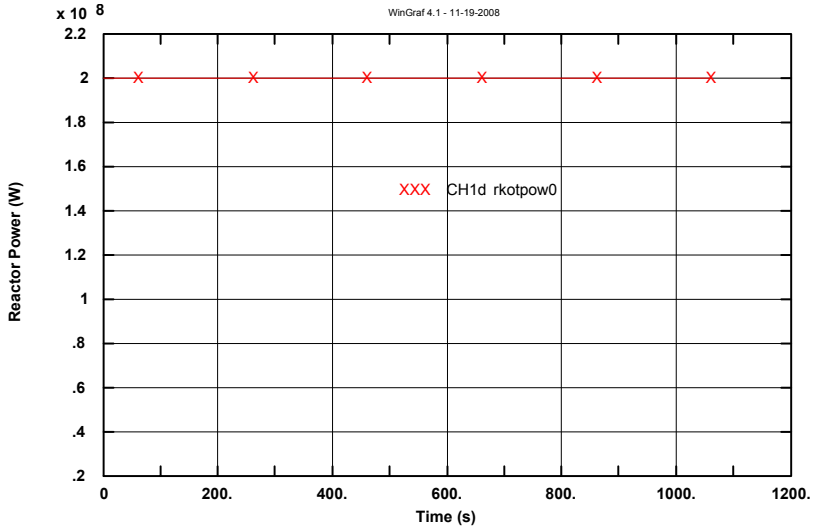

Fig. 162 – Simulation of Chernobyl event in the Smolensk NPP: Reactor Power before the Test

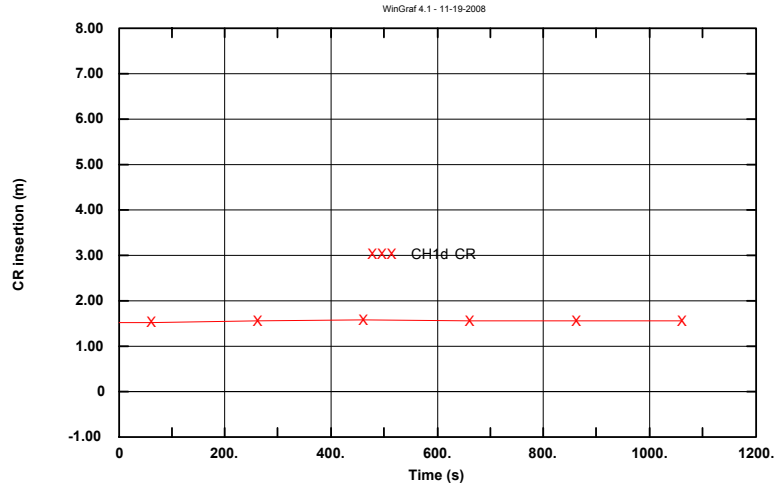

Fig. 163 – Simulation of Chernobyl event in the Smolensk NPP: CR before the test.

At 1.03.05 and 1.07.00 two MCP, one per side, are turned on (Fig. 164). This is increasing the mass flow rate per each circuit, redistributing the mass flow rate in each MCP (Fig. 164 and Fig. 165).

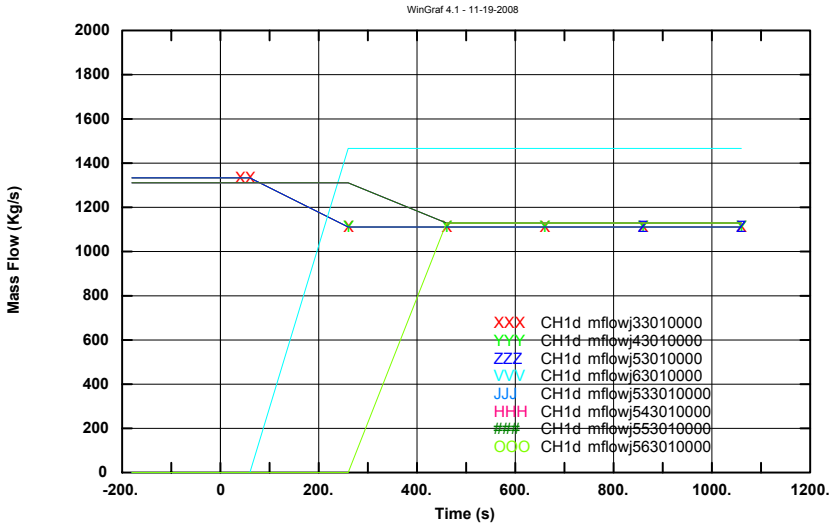

Fig. 164 - Simulation of Chernobyl event in the Smolensk NPP: MCP activation

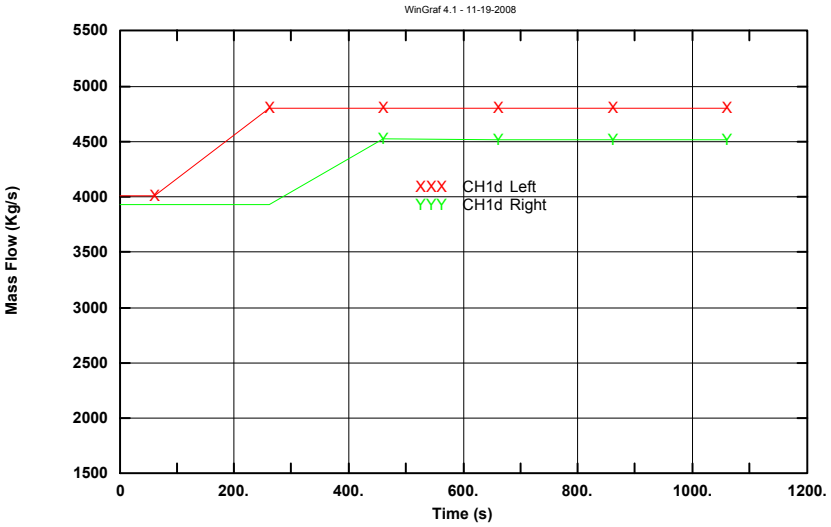

Fig. 165 – Simulation of Chernobyl event in the Smolensk NPP: Left and Right side Mass Flow (Kg/s)

At 1.09.00 a FW perturbation is operated, reducing the mass flow on the right side of the MCC (Fig. 166).

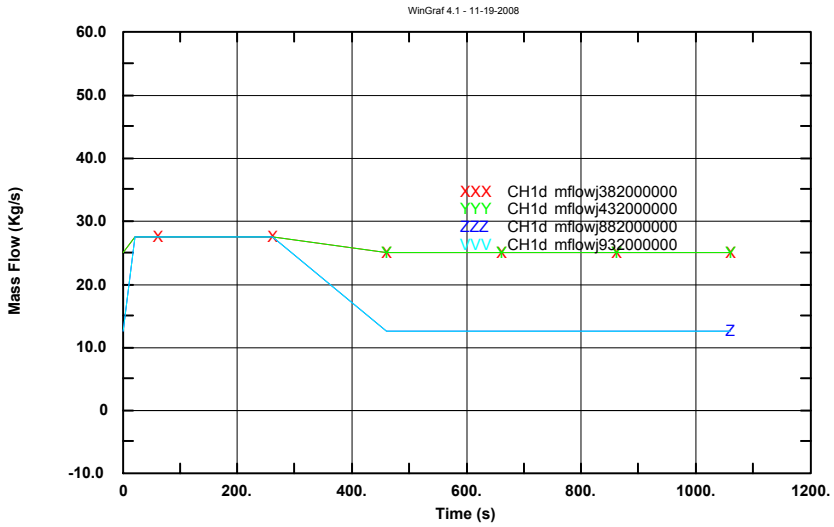

Fig. 166 – Simulation of Chernobyl event in the Smolensk NPP: FW perturbation

At 1.23.04 the test began, with the closure of stop valve for the RHS SD. Power control system is deactivated and at the same time, the rundown of two MCPs per side is operated (Fig. 167).

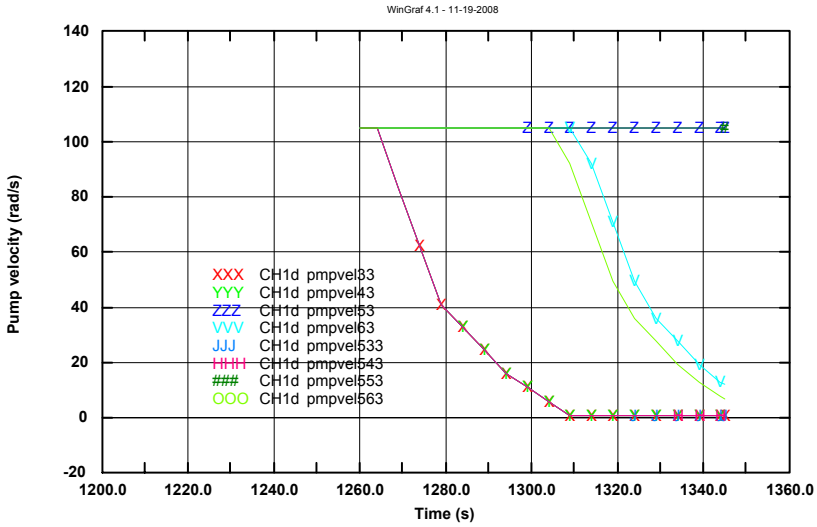

Fig. 167 – Simulation of Chernobyl event in the Smolensk NPP: MCPs speed

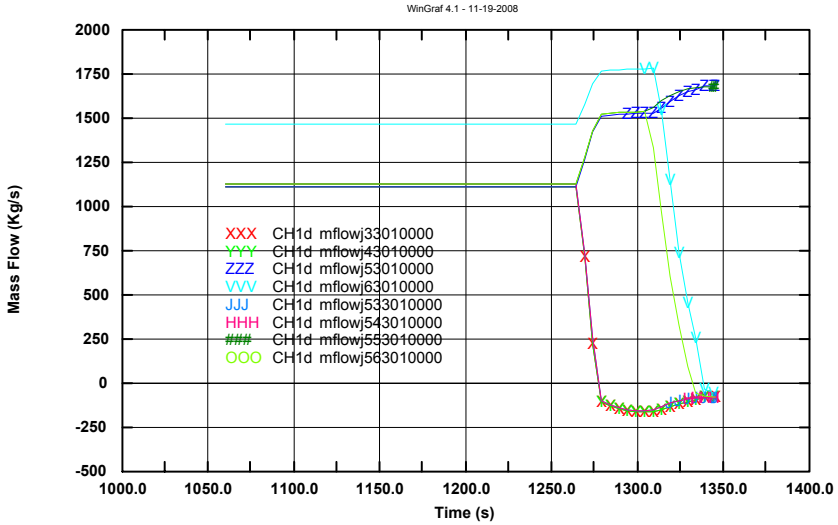

Fig. 168 – Simulation of Chernobyl event in the Smolensk NPP: MCP flow rates

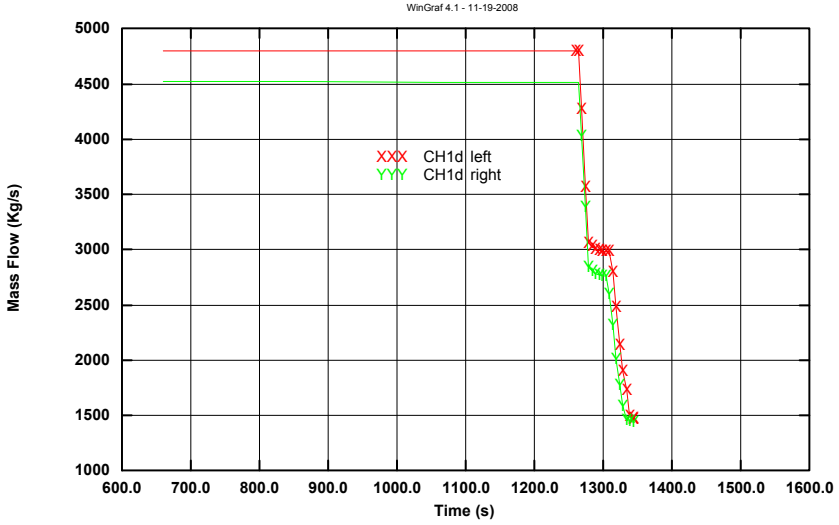

Fig. 169 – Simulation of Chernobyl event in the Smolensk NPP: Circuit Flow Rate

The reduction in the circuit mass flow rates (Fig. 168 and Fig. 169) is causing a void increase that is leading to a power reduction. This is consistent with the new neutronics characteristics of the RBMK system (see Chapter 2), because of the negative void coefficients.

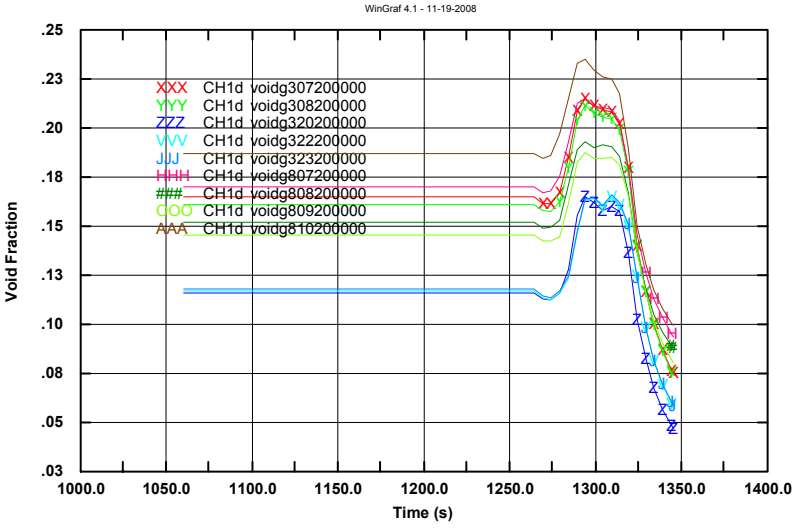

Fig. 170 – Simulation of Chernobyl event in the Smolensk NPP: Void Fraction at core exit during the transient

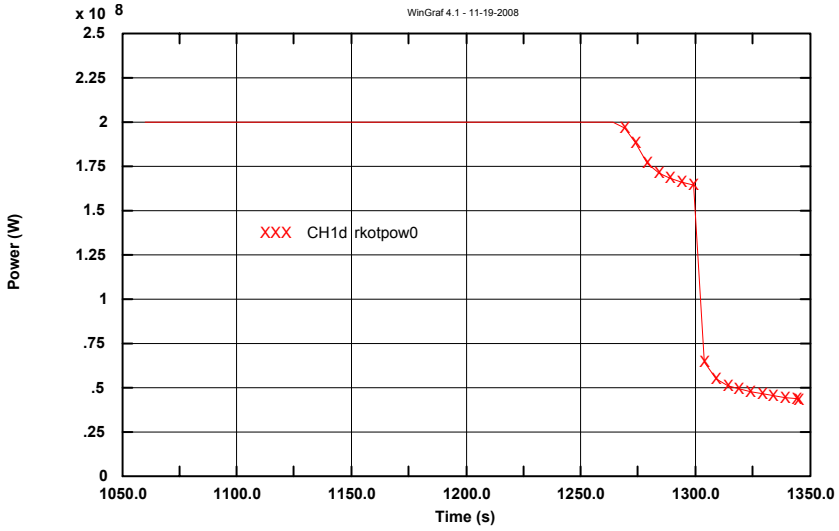

Fig. 171 – Simulation of Chernobyl event in the Smolensk NPP: Power during the transient

The transient is then terminated by the actuation of the scram signal. The new configuration of the MCR is anymore introducing any positive reactivity, thus leading the reactor in safe shutdown conditions.

6.6.1.1. Positive Reactivity Perturbation

This sensitivity was run in order to assess the effects of a positive reactivity insertion during the first phase of the test. This was caused in Chernobyl by the particular design of the MCR (see Fig. 152). In the current configuration of the RBMK, positive reactivity could be introduced in the bottom of the reactor by the Shortened CR only. These CR are not moved during any transient. Therefore, these results should be looked as a pure sensitivity test that should not happen under any circumstance during the real plant operation. Results of calculations with extraction speed of 0.5, 0.25 and 0.1 m/s are given in Fig. 172 and Fig. 173.

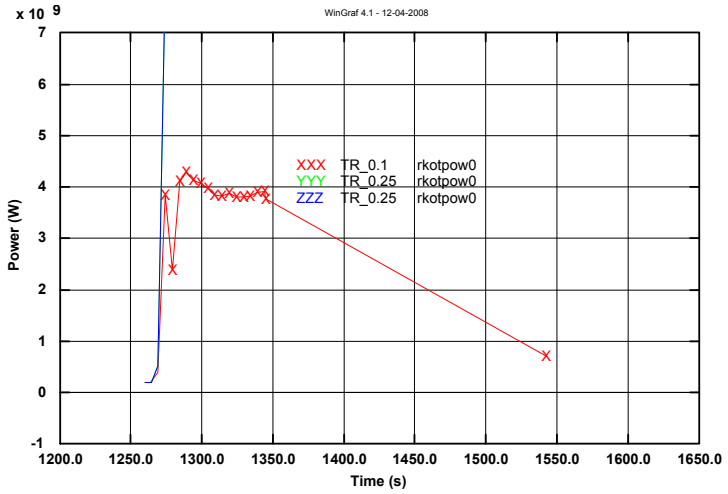

Fig. 172 – Sensitivity with introduction of additional positive reactivity: Reactor Power

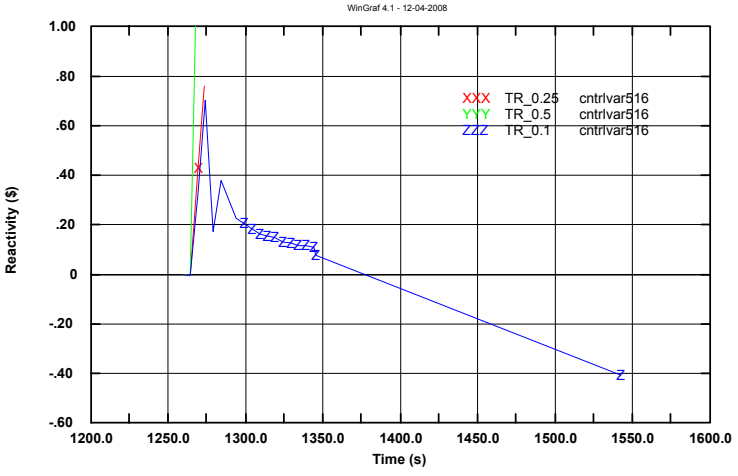

Fig. 173 – Sensitivity with introduction of additional positive reactivity: Core Reactivity

6.6.1.2. No Scram actuation

This sensitivity considered the execution of the test without the intervention of any scram signal. The power, after the reduction caused by the core voiding, was easily controlled by the power control system.

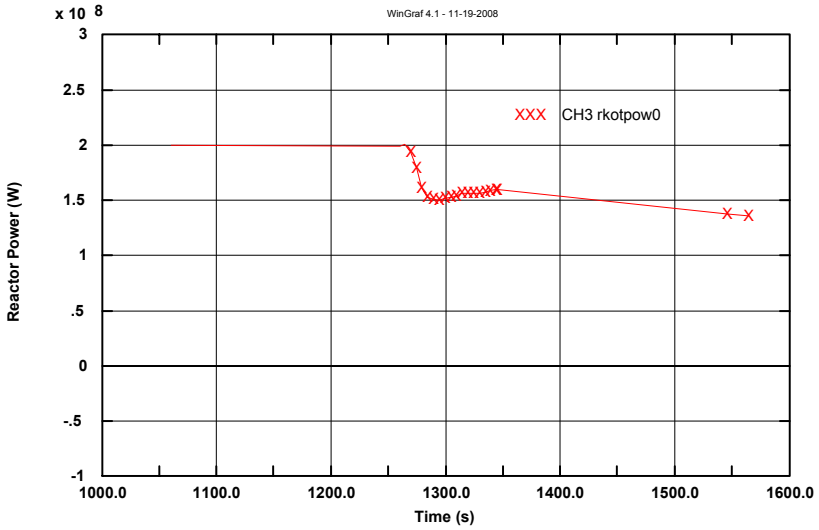

Fig. 174 – Reactor Power without scram actuation

6.6.2. Conclusions

The calculations showed that the neutronics and hardware modifications introduced after Chernobyl accident were effective in avoiding such kind of events. In particular, the two main phenomena that triggered the reactor explosion at that time were eliminated. In fact :

- the new design of MCR avoid the possibility to obtain concave flux shapes and a positive reactivity insertion during the first phase of the scram;
- the elimination of the positive void coefficients avoids the possibility to get a power excursions when operating the reactor at low power, i.e., with a reduced margin of coolant subcooling

The upgrades that were introduced during the recent years on the RBMK (e.g., the increase of U enrichment at 2.8%, the cluster MCR) and that were not present in the Smolensk-3 configuration analyzed here, are further increasing the safety levels of these type of reactors for transients like the Chernobyl-4 one.

7. CONCLUSIONS

The application of a “chain of codes” to the analysis of transients in RBMK Smolensk 3 NPP aimed at investigating coupled 3D NK TH phenomena in the core has been presented. The capabilities of the adopted codes to handle the resulting complex scenarios have been demonstrated, though it was not the purpose of the PhD activity to perform licensing calculations.

The key conclusions can be summarized as follows:

a) a pioneering application of the chain of codes RELAP5-3D-HELIOS/DRAGON-MCNP5 to the RBMK safety technology has been successfully effectuated;
b) detailed input decks for RBMK system have been developed for the coupled codes and are available to the GRNSPG/UNIPI. In the case of RELAP5-3D, the nodalization includes up to 4000 hydraulic nodes, 50000 meshes for conduction heat transfer and about 40000 meshes for the neutron kinetics model;
c) problems were founds in calculating the correct values of void coefficients using both deterministic neutron transport codes DRAGON and HELIOS. The results showed a sensible under-estimation of the void reactivity. Calculations by the Monte Carlo code MCNP5 was instead not affected by this problem. The weight of this problem on the system code calculation uncertainties should be evaluated in future works;
d) a key identified problem (confirming what found for TH analysis of Ignalina, see [97]) in case of GDH-Blockage event, was the (calculated) occurrence of inlet flow oscillations in affected FC. This caused temperature excursions in some FC bundles and can be the precursor of severe core damage;
e) mild and controllable power excursions were calculated in the case of spurious withdrawal of single and of bank-of CR (CR-withdrawal and CR-group withdrawal, respectively);
f) the CPS-LOCA event brings to scram caused by high average core power and safety functions of the system are not challenged with main concern to SD pressure and rod surface temperatures;
g) The analysis of the single FC-Blockage event confirmed that the affected rod bundle power tends to decrease following the lack of cooling event. This is due to the Doppler effect and to the increased neutron leakages that overpasses the effect of loosing coolant. Several calculations for this kind of transient were also run by the use of MCNP5 code. The influence of 3D NK in predicting the overall system performance following individual channel blockage is negligible. Namely the power generated in the affected channel does not increase, rather a decrease has been calculated;
h) A detailed simulation of the Chernobyl-type accident was performed. This kind of analyses required the integration of a suitable Xenon cross section model in RELAP5-3D and the implementation of a simplified power control

system. The results showed that the Smolensk-3 configuration of RBMK was safe also during this low power test, avoiding the positive reactivity excursion that led the Chernobyl reactor to a destruction.

REFERENCES

[1] E. Adamov et alii, *"Status and prospects for pressure-tube water-cooled graphite-moderated reactors"*, Nuclear Engineering and Design, Pages 59-66, Vol. 173, 1997.

[2] N.M. Sorokin, B.A. Gabaraev, Yu.M. Cherkashov, *"Safe operation and life extension of RBMK plants"*, Nuclear Engineering and Design, Pages 1648-1656, Vol. 236, 2006.

[3] A. Kaliatka, E. Knoglinger, M. W. Jankowski, D. Mazzini, A. M. Moskalev, S. Soloviev, E. Ušpuras, *"Review of the Safety Needs that are Related to the Project, and of the Relevant Physical Phenomena"*, TD.B.1.2-DER/1 rev 1, 27 May 2004.

[4] M. W. Jankowski, J. Misak, A. Kaliatka, E. Ušpuras, A. M. Moskalev, Ju. A. Migrov. *"Thermal Hydraulics Code for the Primary Loop and the Containment System"*, TD.B.2.1-DER/1, July 2004.

[5] C. Parisi, V. Malofeev, *"3D Space-Time Neutron Kinetics Code"*, TD.B.2.2-DER/1, 06 April 2005.

[6] Power Reactor Information System (PRIS), IAEA Website, http://www.iaea.org/programmes/a2/

[7] S. F. Hall, B. A. Gabaraev, *"Severe Transient Analysis for RBMK Reactor TACIS Project R 2.30/94" – Ultimate Design Basis Accident, October 1997* referring to *"RBMK Safety Review Final Report"* RBMK/CMC/FR Issue 1, March 1994.

[8] "*Safety assessment of design solutions and proposed improvements to Smolensk Unit 3 RBMK nuclear power plant*", IAEA, TECDOC-722, Vienna, 1993.

[9] K. Almenas, A. Kaliatka, E. Uspuras, *"Ignalina RBMK-1500 a source book",* Extended and updated version, LEI – April 1998.

[10] E. Urbonavicius, A. Kaliatka, *"Investigation of hydrogen control system effectiveness in RBMK-1500 containment"* Proceedings of ICAPP '05 Seoul, KOREA, May 15-19, 2005, Paper 5422

[11] Various, *"Control Rod Withdrawal"* TACIS Project R 2.30/94 Severe Transient Analysis for RBMK Reactors, October 1997

[12] *"Safety margins of operating reactors: Analysis of uncertainties and implications for decision making",* IAEA TECDOC 1332, Vienna, 2003.

[13] *"Accident analysis for Nuclear Power Plants with Graphite Moderated Boiling Water RBMK Reactors"* Safety Reports Series No. 43, Vienna (A) 2005.

[14] J. P. Weber, G. Bava, D. Bestion, A. Maccabee, D. Reichenbach, *"Final Report of Topic Group 1: System Engineering and Accident Progression (Appendix 11 of RBMK/CMC/FR)"* Western topic Group 1 members, March 1994.

[15] Gosatomnadzor, *"General Regulations for Nuclear Power Plant Safety (ОПБ-88/97)",* GAN Report НП-001-97, 1998г

[16] *"Basic Safety Principles for Nuclear Power Plants"* IAEA, INSAG Series No. 12, 75-INSAG-3 Rev. 1, Vienna, 1999..

[17] *"Comparison of the Russian nuclear power safety concept contained in OPB-88 and the next lower level norms/rules with the NUSS requirements"* Extra-budgetary Programme on the Safety of WWER NPP, WWER-RD-69, Vienna, 1994.

[18] Gosatomnadzor, *"Layout of nuclear stations. The basic criteria and safety requirements",* GAN Report НП-032-01, 2002 г.

[19] *"Probabilistic Safety Assessment",* Safety Series No. 75, INSAG-6, Vienna, 1992.

[20] A. Kaliatka, E. Knoglinger, M. W. Jankowski, D. Mazzini, A. M. Moskalev, S. Soloviev, E. Ušpuras, *"Review of the Safety Needs that are Related to the Project, and of the Relevant Physical Phenomena",* TD.B.1.2-DER/1 rev 1, 27 May 2004.

[21] N. Aksan, D. Bessette, I. Brittain, F. D'Auria, P. Gruber, H.L.O. Holmstrom, R. Landry, S. Naff, R. Pochard, G. Preusche, M. Reocreux, O. Sandervag, H. Staedtke, K. Wolfert, N. Zuber, *"Code Validation Matrix of Thermal-Hydraulic Codes for LWR LOCA and Transient"* OECD/CSNI 132, March 1987.

[22] N. Aksan, F. D'Auria, H. Glaeser, R. Pochard, C. Richards, A. Sjoberg, *"A Separate Effect Test Matrix for Thermal-Hydraulic Code Validation: Phenomena Characterization and Selection of Facilities and Tests"* OECD/GN (94) 82, Vols. I and II, 1993.

[23] A. Annunziato, H. Glaeser, J.N. Lillington, P. Marsili, C. Renault, A. Sjoberg *"CSNI Code Validation Matrix of Thermal-Hydraulic Codes for LWR LOCA and Transient",* OECD/CSNI 132, Rev 1, July 1996.

[24] X-5 Monte Carlo Team, "*MCNP — A General Monte Carlo N-Particle Transport Code, Version 5*", Los Alamos National Laboratory, LA-UR-03-1987, April 24, 2003 (Revised 10/3/05)

[25] "*Accident Analysis and its associated training programme for the RBMK 1000 Kursk 1 NPP*", IAEA Technical Report, Volume II, Rev. 3, July 2001, Vienna, Austria.

[26] A. Jasulevicius et al., *"Development and Validation of a Methodology for Neutron Dynamics Analysis of RBMK Reactors"*, Proceedings of the ANS M&C 2001 Conference, Salt Lake City, USA, September 9-12 (2001).

[27] L. A. Hageman and D. M. Young, "*Applied Iterative Methods*," Computer Science and Applied Mathematics, Orlando: Academic Press, 1981.

[28] K. I. Derstine, *DIF3D: A Code to Solve One-, Two-, and Three-Dimensional Finite Difference Diffusion Theory Problems*, ANL-82-84, Argonne National Laboratory, 1984.

[29] R. S. Varga, *Matirx Iterative Analysis*, Englewood Cliffs, NJ: Prentice-Hall, 1962.

[30] S. K. Zee, *Numerical Algorithms for Parallel Processors Computer Architectures with Applications to a Few-Group Neutron Diffusion Equations*, Ph. D. Dissertation, North Carolina State University, 1987.

[31] K. S. Smith, "*Nodal Method Storage Reduction By Non-Linear Iteration*", Transactions of the American Nuclear Society, Detroit, MI, June 1983, 44, pp. 265.

[32] K. S. Smith, "*QPANDA: An Advanced Nodal Method for LWR Analyses*", Transactions of the American Nuclear Society, June 1985, pp. 265.

[33] K. S. Smith and K. R. Rempe, "*Testing and Applications of the QPANDA Nodal Method*,"Proceedings of the International Topical Meeting on Advances in Reactor Physics, Pittsburgh, PA, 1987, 2, pp. 861.

[34] W. L. Weaver, "*Software Design and Implementation Document; Three Dimensional Neutron Kinetics for RELAP5/MOD3*", EGG-NRE-11021, Idaho National Engineering Laboratory, November 1993.

[35] Edenius, M., K. Ekberg, B.H. Forssen and D.G. Knott, *A Fuel Assembly Burn-up Program User's Manual*, STUDSVIK/SOA-95/01 (1995).

[36] Edenius, M. and B. Forssen, *CASMO-3, A Fuel Assembly Burn-up Program, Users Manual*, STUDSVIK/NFA-89/3.

[37] Watson, J., K. Ivanov, *et al*., "*Cross-section Generation Methodology for Three-dimensional Transient Reactor Simulations*", ANS TANSAO 77, p. 175 (1998).

[38] Watson, J. and K. Ivanov, "*Improved Cross-section Modeling Methodology for Coupled Three-dimensional Transient Calculations*", Annals of Nuclear Energy, 29, 937-966 (2002).

[39] Langenbuch, S., *et al*., "*Investigation of Modeling Aspects for Coupled Code Application in Safety Analysis*", Proc. of the Int. Conf. on Mathematics, Computation, Reactor Physics and Environmental Analysis (M&C 2001), Salt Lake City, Utah, USA, September 2001.

[40] Ivanov, K. and A. Baratta, "*Coupling Methodologies for Best Estimate Safety Analysis*", Proc. of the Int. Conf. on Mathematics, Computation, Reactor Physics and Environmental Analysis (M&C'99), Madrid, Spain, 27-30 September 1999, Vol. 1, pp. 493-502.

[41] Langenbuch, S., *et al*., "*Interface Requirements to Couple Thermal-hydraulic Codes to 3-D Neutronic Codes*", OECD/CSNI Workshop on Transient Thermal-hydraulic and Neutronics Codes Requirements, Annapolis, MD, USA, Nov. 1996.

[42] Grundmann, U., et al., "*Coupling of the Thermo-hydraulic Code ATHLET with the Neutron Kinetic Core Model Dyn3d*", Proc. of the Int. Conf. on Mathematics and Computations, Reactor Physics and Environmental Analysis (M&C'95), Portland, OR, USA 30 April-5 May 1995, Vol. 1, pp. 257-263.

[43] "*CRISSUE-S-WP2: Neutronics/Thermal-hydraulics Coupling in LWR Technolog: State-of-the-art Report (REAC-SOAR)*", OECD/NEA, 2004. ISBN 92-64-02084-5

[44] C. Parisi, M. Cherubini, W. Giannotti, B. Neykov *"Smolensk-3 NPP RELAP5 Thermal-Hydraulic Nodalization"* TD.B.2.2-DER/1, Appendix A, 06 April 2005.

[45] IAEA, *"Accident Analysis for Nuclear Power Plants",* Safety Report Series No.23, Vienna, November 2002.

[46] NRC, "*Standard Review Plan for the Review of Safety Analysis Reports for Nuclear Power Plants*", NUREG-0800, June 1996

[47] S. N. Aksan, F. D'Auria, H. Städtke, "*User effects on the thermal-hydraulic transient system code calculations*", Nuclear Engineering and Design, Volume 145, Issues 1-2, 2 November 1993, Pages 159-174

[48] D'Auria F., "*Proposal for training of thermalhydraulic system codes users*", IAEA Spec. Meet. on User Qualification and User Effects on Accident Analysis for Nuclear Power Plants - Vienna (A), Aug. 31-Sept. 4, 1998

[49] D'Auria F., Frogheri M., Marsili P., Giannotti W., "*Standardised Procedure for thermohydraulic system code assessment*", Spring 1998 CAMP Meeting, Ankara (TK); June 24-26, 1998, IAEA Spec. Meet. on User Qualification and User Effects on Accident Analysis for Nuclear Power Plants - Vienna (A); Aug. 31-Sept. 4, 1998, 2nd Int. Yugoslav Nuclear Society Conf. (YUNSC '98) – Belgrad (YU) Sept. 28, Oct. 1, 1998.

[50] "Enhancement of Lithuanian TSO`s Licensing Assistance Capability within Core Integrity, Control Systems Upgrading and Management of Equipment Ageing", Task 1 Report "*RBMK – Core Safety Surveillance*" SIP/RISKAUDIT-report No. 95684-R6, May 2004

[51] N. Alexeev et alii, "*The Monte Carlo codes MCNP and MCU for RBMK criticality calculations*", Nuclear Engineering and Design, Vol.183 (1998), pages 287-302.

[52] F. D'Auria et alii, "*Development of a Code System for Severe Accident Analysis in RBMK*" Final Technical Report for TACIS Project R2.03/97, part B, , December 2005

[53] C. Parisi, V. Malofeev, K. N. Ivanov ,"Neutron Cross Section Model", Task 2.3 Technical Report for TACIS Project R2.03/97, April 2005

[54] Studsvik™ Scandpower, "*HELIOS Methods*", 2000

[55] S. C. Frankle, "*Summary Documentation for the ENDL92 Continuous-Energy Neutron Data Library (Release 1)*" Los Alamos National Laboratory internal memorandum, XTM:96-05, and report LA-UR-96-327 (1996).

[56]G. Marleau, A. Hébert, R. Roy. "A User Guide for DRAGON 3.05D", Technical Report IGE-174 Rev. 6D. Institut de genie nucléaire, Ecole Polytechnique de Montréal, June 2006.

[57] International Atomic Energy Agency (IAEA). "Accident Analysis and its associated training programme for the RBMK 1000 Kursk 1 NPP". Technical Report. Volume II. July 2001, Vienna (Austria).

[58] International Atomic Energy Agency (IAEA). "WIMS-D Library Update. Final report of a coordinated research project". Vienna, 2006

[59] C. Parisi, F. D'Auria "RBMK Fuel Channel Blockage Reactivity Analysis by MCNP5, DRAGON and RELAP5-3D© codes", International Conference "Nuclear Energy for the New Europe", Portoroz, Slovenia, September 10-13, 2007

[60] Personal communication of V. Malofeev, June 2005.

[61] P. F. Rose, Compiler and Editor, "ENDF-201, ENDF/B-VI Summary Documentation," BNL-NCS-17541, Brookhaven National Laboratory (October 1991).

[62] R. J. Howerton, D. E. Cullen, R. C. Haight, M. H. MacGregor, S. T. Perkins, and E. F. Plechaty, "The LLL Evaluated Nuclear Data Library (ENDL): Evaluation Techniques, Reaction Index, and Descriptions of Individual Reactions," Lawrence Livermore National Laboratory report UCRL-50400, Vol. 15, Part A (September 1975).

[63] D. E. Cullen, M. H. Chen, J. H. Hubbell, S. T. Perkins, E. F. Plechaty, J. A. Rathkopf, and J. H. Scofield, "Tables and Graphs of Photon Interaction Cross Sections from 10 eV to 100 GeV Derived from the LLNL Evaluated Photon Data Library (EPDL)," Lawrence Livermore National Laboratory report UCRL-50400, Volume 6, Rev. 4, Part A: Z = 1 to 50 and Part B: Z = 51 to 100 (1989).

[64] R. E. MacFarlane and D. W. Muir, "The NJOY Nuclear Data Processing System Version 91," Los Alamos National Laboratory report LA-12740-M, (October 1994).

[65] R. E. MacFarlane, D. W. Muir, and R. M. Boicourt, "The NJOY Nuclear Data Processing System, Volume I: User's Manual," Los Alamos National Laboratory report LA-9303-M, Vol. I (ENDF-324) (May 1982).

[66] J. R. Askew, F. J. Fayers, and P. B. Kemshell, "A General Description of the Lattice Code WIMS," J. Brit. Nucl. Energy Soc., 5, 564 (1966).

[67] C. J. Taubman, The WIMS 69–Group Library Tape 166259 , Technical Report AEEW-M1324, United Kingdom Atomic Energy Establishment (1975).

[68] J. J. Kim, J. T. Lee, and H. R. Kim, "Generation and Benchmarking of a 69 Group Cross Section Library for Thermal Reactor Applications," J. Korean Nucl. Soc., 21, 245 (1989).

[69] WLUP, Final Stage of the WIMS-D Library Update Project, www-nds.iaea.org/wimsd (2005).

[70] J. V. Donnelly, WIMS-CRNL, A User's Manual for the Chalk River Version of WIMS, Technical Report AECL-8955, Atomic Energy of Canada Limited (1986).

[71] W. M. Stacey, "*Nuclear Reactor Physics*", Wiley-VCH Verlag GmbH & Co. KGaA, 2004. ISBN-13:978-0-471-39127-2

[72] Turinsky, P., et. al., 1994. NESTLE, Few-group neutron diffusion equation solver utilizing the nodal expansion method for eigenvalue, adjoint, fixed-source steady-state and transient problems. Electric Power Research Center, North Carolina State University, Raleigh, NC, USA.

[73] V. Malofeev, Personal email to C. Parisi. 31 January 2006.

[74] V. Malofeev, Personal email to C. Parisi. 31 May 2007.

[75] H. Finnemann and A. Galati, "NEACRP 3-D LWR Core Transient Benchmark – Final Specifications," NEACRP-L-335 (Revision 1), January, 1992

[76]J. L. Judd, W. L. Weaver, T. Downar, and J. G. Joo, "A Three Dimensional Nodal Neutron Kinetics Capability for RELAP5," Proceedings of the 1994

Topical Meeting on Advances in Reactor Physics, Knoxville, TN, April 11-15, 1994, Vol. II, pp 269-280

[77] E. Bubelis, A. Kaliatka, and E. Uspuras, "RELAP-3D Code Application for RBMK-1500 Reactor Core Analysis", Proceedings of ICONE-10 Conference, Arlington, VA, April 14-18 (2002).

[78] E. Uspuras, A. Kaliatka, E. Bubelis, 'Modeling of void, fast power and graphite temperature reactivity coefficients measurements for the validation of RELAP5-3D© RBMK-1500 reactor model', Nuclear Engineering and Design, Vol. 224, pgs. 293-300

[79] E. Uspuras, E. Bubelis, 'RELAP5-3D code validation in the neutron-dynamic analysis of transient proceses taking place in RBMK-1500 reactors', Nuclear Engineering and Design, Vol. 232, pgs. 29-45

[80] R. C. Little, "Neutron and Photon Multigroup Data Tables for MCNP3B," Los Alamos National Laboratory internal memorandum, X-6:RCL-87-225 (1987) (available URL: http://laws.lanl.gov/projects/data/index.html).

[81] E. Knoglinger et al., "Evaluation of the Smolensk-3 Shutdown System - Final Report – Phase II and III ", PSI Bericht Nr. 96-10, April 1996 – ISSN 1019-0643

[82] Lombardi Costa A., Cherubini M., D'Auria F., Giannotti W., Moskalev A. "*Thermal-Hydraulic Analysis of Coolant Flow Decrease in Fuel Channels of Smolensk-3 RBMK during GDH Blockage Event*", J. Science and Technology of Nuclear Installations, Vol. (2007), Art. ID 87834, pp. 1-7

[83] INSAG-7, "*The Chernobyl Accident: Updating of INSAG-1"*, Safety Series Report No. 75, IAEA, Vienna, 1992

[84] S. Lavrencic, "*Chernobyl. Anatomia di un'esplosione*", Report AT-WAA-00003, ENEA, Dipartimento Reattori Innovativi, 1991. Translation o fan article of G. L'vov, correspondent of "Nauka i Zhizn", No. 12, 1989.

[85] *"Dossier Chernobyl"*, an ANSALDO-NIRA report

[86]GIDROPROEKT, "*1st stage Smolensk nuclear power plant; 2nd stage Kursk nuclear power plant; 2nd stage Chernobyl nuclear power plant*", Technical Safety Report, Rep. 176, Moscow, 1976.

[87] G. Fruttuoso, G.M. Galassi, M. Mazzini, "*Analisi dell'incidente di Chernobyl con l'impiego del codice di calcolo RELAP 4 MOD. 6*", ENEA-DISP Seminar on Chernobyl Accident, 8 January 1987, Rome.

[88] E. O. Adamov, "*Soviet Chernobyl model highlights role of pump trip*", Nuclear Engineering International, 33 (406), 1998.

[89]P. S. W. Chan, A. R. Dastur, "*The Sensitivity of Positive Scram Reactivity to Neutronic Decoupling in the RBMK-1000*", Nuclear Science and Engineering, Vol. 103, 1989. Pages 289-293

[90] V. A. Khotylev, "*On the interpretation of a positive scram reactivity"*, Annals of Nuclear Energy, Vol. 23, No. 9, 1996. Pages 779-784.

[91] P. A. Landeyro, A. Buccafruni, "*Time-Independent Neutronic Analysis of the Chernobyl Accident*", Nuclear Science and Engineering, Vol. 108, 1991. Pages 126-149.

[92] H. Mochizuki, "*Analysis of the Chernobyl accident from 1:19:00 to the first power excursion*", Nuclear Engineering and Design, Vol. 237, 2007. Pages 300-307.

[93] A. D'Angelo, "*Sensitivity study of the positive scram effect relevant to the Chernobyl accident simulation*", Nuclear Science and Engineering, Vol. 125, 1997. Pages 93-100.

[94] S. Lavrencic, translation of: A. V. Krayushkin et alii, "*Neutron-Physical Investigation of the DBA of RBMK-1000*", on Atomnaya Energiya, Vol. 71, No. 6, December 1991. ENEA Report, AT-WAA-00009, 1998.

[95] J. Chao et alii, "*An analysis of the Chernobyl accident using RETRAN-02/mod3*", Nuclear Technology, Vol. 83, 1988. Pages 289-301.

[96] C. Parisi, F. D'Auria, "*Calculation of Xenon transients and implementation of an automatic power control system on a RELAP5-3D VVER-440 model*", Technical Note of DIMNP, 2008.

[97] E. Uspuras, A. Kaliatka, V. Vileiniskis, "*Implementation of weak heat conduction mechanism model for analysis of long-term transients using RELAP5-3D code"*, The 7th International Information Exchange Forum on "Safety Analysis for Nuclear Power Plants of VVER and RBMK types" (FORUM-7), 28-30 October 2003, Piestany, Slovakia.

[98] P. Bayless, J. Fisher, "*INSP IRUG-related Activities in FY-2001*", RELAP5 Users Seminar, Elkhorn Resort, Sun Valley, Idaho, 5-7 September 2001

[99] M. Clemente, S. Langenbuch, K. Velkov, P. Kusnetzov, I. A. Steinbock, *"Application of the coupled code system ATHLET and QUABOX/CUBBOX to an ATWS Transient 'Total Loss-of-Feedwater' in RBMK"*, International Conference on the Physics of Nuclear Science and Technology, Islandia Marriott, Long Island, USA, October 5-8, 1998.

[100] A. Petry, H. Wolff, S. Langenbuch, M. Clemente *"Analysen von RBMK-Reaktoren,Gesellschaft für Anlagen- und Reaktorsicherheit (GRS) mbH"* Report GRS – A – 2483, June 1997 (in German)